

PB 269 655

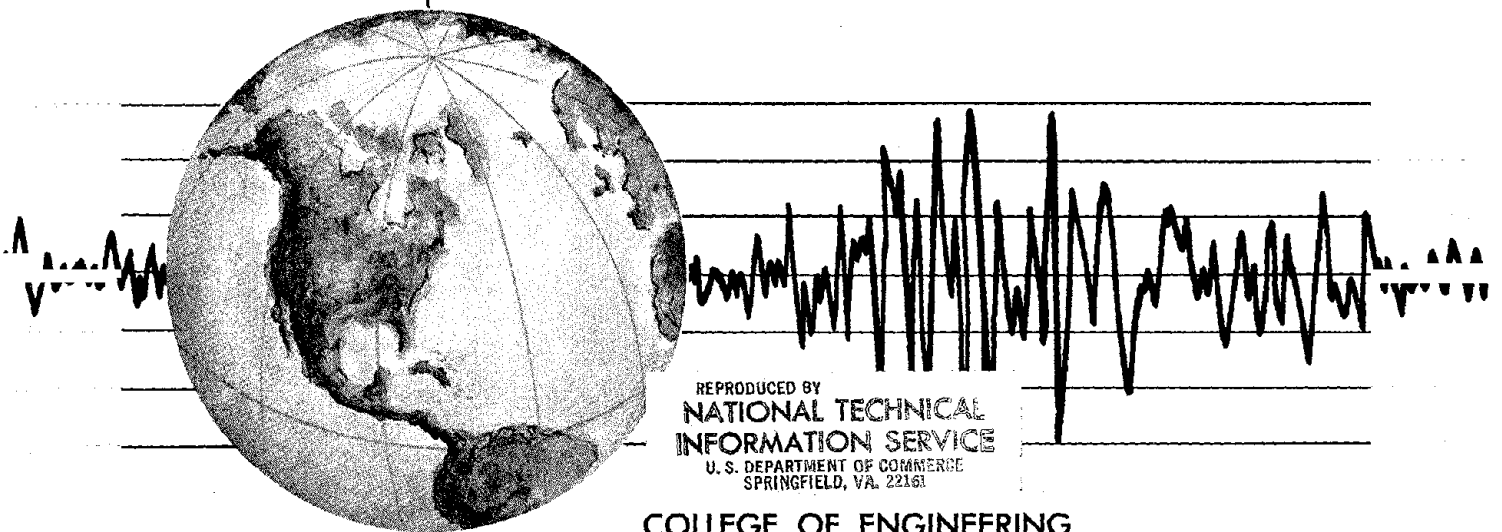
REPORT NO.
UCB/EERC-77/04
JANUARY 1977

EARTHQUAKE ENGINEERING RESEARCH CENTER

SEISMOLOGICAL STUDIES OF STRONG MOTION RECORDS

by

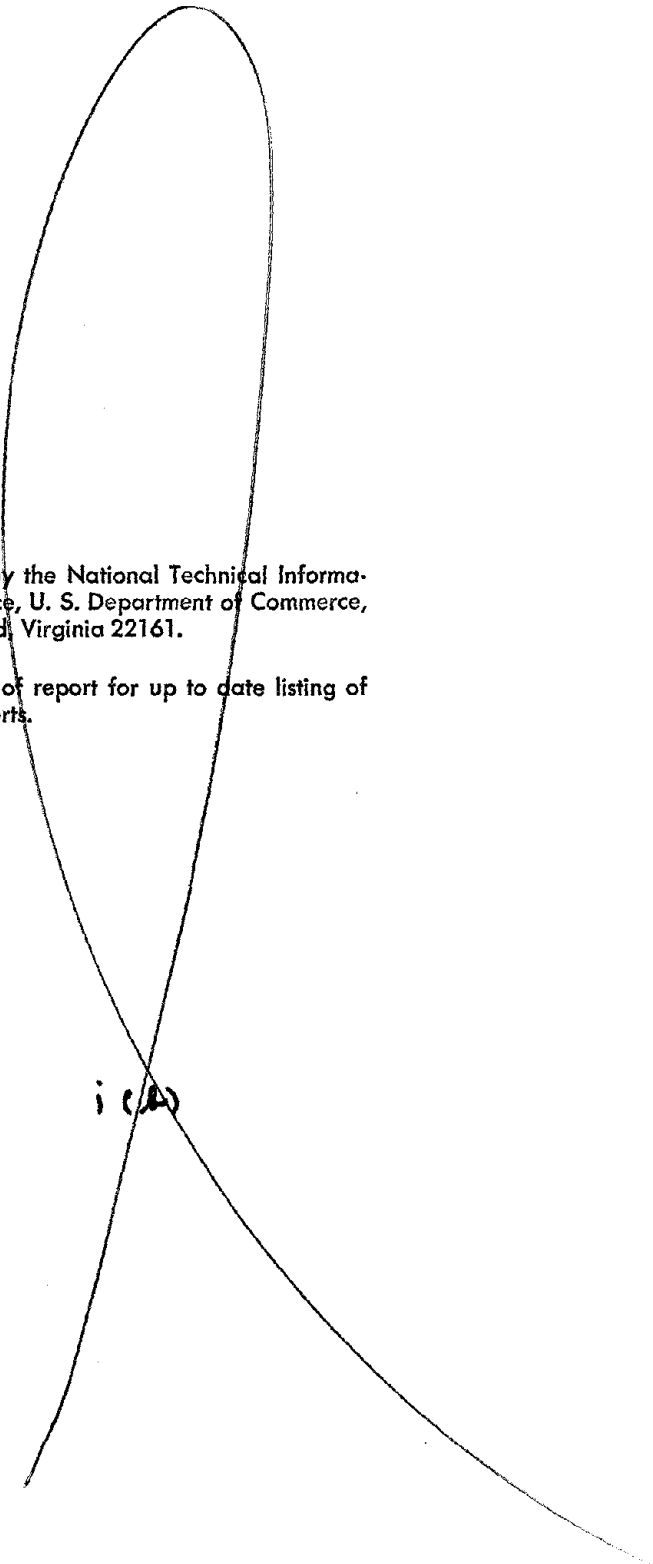
JAFAR SHOJA-TAHERI



REPRODUCED BY
NATIONAL TECHNICAL
INFORMATION SERVICE
U. S. DEPARTMENT OF COMMERCE
SPRINGFIELD, VA. 22161

COLLEGE OF ENGINEERING

UNIVERSITY OF CALIFORNIA • Berkeley, California



For sale by the National Technical Information Service, U. S. Department of Commerce, Springfield, Virginia 22161.

See back of report for up to date listing of EERC reports.

i (A)

NOTICE

THIS DOCUMENT HAS BEEN REPRODUCED FROM THE BEST COPY FURNISHED US BY THE SPONSORING AGENCY. ALTHOUGH IT IS RECOGNIZED THAT CERTAIN PORTIONS ARE ILLEGIBLE, IT IS BEING RELEASED IN THE INTEREST OF MAKING AVAILABLE AS MUCH INFORMATION AS POSSIBLE.



BIOGRAPHIC DATA SHEET		1. Report No. UCB/EERC-77/04	2.	3. Recipient's Accession No.
4. Title and Subtitle Seismological Studies of Strong Motion Records			5. Report Date January 1977	6.
7. Author(s) Jafar Shoja-Taheri			8. Performing Organization Rept. No. 77/04	
9. Performing Organization Name and Address Earthquake Engineering Research Center University of California, Berkeley 1301 South 46th Street Richmond, California 94804			10. Project/Task/Work Unit No.	
			11. Contract/Grant No. AEN 74-21548	
12. Sponsoring Organization Name and Address National Science Foundation 1800 G Street, N.W. Washington, D.C. 20550			13. Type of Report & Period Covered	
			14.	
15. Supplementary Notes				
<p>16. Abstracts</p> <p>A number of problems pertinent to seismological and engineering interpretations of strong ground motions in earthquakes are studied. The main new results are as follows:</p> <p>1) A new form of strong motion accelerogram (Spectrally Maximized Records or "SMR") and its associated generalized spectrum are proposed for earthquake engineering use. Parameters (e.g., spectral, duration, peak amplitude) of horizontal-component strong-motion records at a given site generally depend significantly on the (arbitrary) azimuthal direction, often resulting in a crucially deficient description of these parameters if only a single component is used. Combination of horizontal components using spectral maximization is shown to be effective in minimizing the difficulty. The spectra of the two horizontal components at each site are combined to maximize the resultant spectrum, independently of azimuthal orientation. SMRs of thirty-three important strong-motion accelerograms (including twelve New Guinea records) are then calculated from their corresponding spectra. In only sixty percent of cases is the peak acceleration from a maximized spectrum greater than that of the single components, the bracketed duration from the maximized spectrum is always greater. After filtering to provide records in ten frequency bands (0-1 H₂, 1-2 H₂, . . . 9-10 H₂), correlations for each band are made between acceleration peaks, spectral energy, magnitudes, and source distances. More stable estimates of these strong motion parameters appear to be provided by spectrally maximized accelerations compared with single component estimates.</p> <p>2) Statistical analysis of all accelerograms of the 1966 Parkfield earthquake, California and the 1952 Taft earthquake, California indicates that the usable long period of ground displacements obtained from double integration of accelerogram records are limited by two major sources of errors--human reading and base-line corrections. Usable long period limits are estimated to vary between 7 to 14 seconds depending on the individual earthquake.</p> <p>3) It is shown that the integration of ragged functions such as strong motion accelerograms, by regular quadrature formulas, leads to significant errors. The conventional method of frequency domain integration also leads to indeterminacy of zero frequency information and distortion of the shape of the resulting integral. A modification of the conventional method of frequency domain integration was developed to avoid these deficiencies. The new technique extrapolates the integrand by joining its mirror image to the end of reflection. The zero frequency information is also determined by this technique. (continued on second page)</p>				
18. Availability Statement Release unlimited			19. Security Class (This Report) UNCLASSIFIED	
			20. Security Class (This Page) UNCLASSIFIED	
			22. Price PCA 10 MFA 01	

INSTRUCTIONS FOR COMPLETING FORM NTIS-35 (10-70) (Bibliographic Data Sheet based on COSATI Guidelines to Format Standards for Scientific and Technical Reports Prepared by or for the Federal Government, PB-180 600).

1. **Report Number.** Each individually bound report shall carry a unique alphanumeric designation selected by the performing organization or provided by the sponsoring organization. Use uppercase letters and Arabic numerals only. Examples FASEB-NS-87 and FAA-RD-68-09.
2. Leave blank.
3. **Recipient's Accession Number.** Reserved for use by each report recipient.
4. **Title and Subtitle.** Title should indicate clearly and briefly the subject coverage of the report, and be displayed prominently. Set subtitle, if used, in smaller type or otherwise subordinate it to main title. When a report is prepared in more than one volume, repeat the primary title, add volume number and include subtitle for the specific volume.
5. **Report Date.** Each report shall carry a date indicating at least month and year. Indicate the basis on which it was selected (e.g., date of issue, date of approval, date of preparation).
6. **Performing Organization Code.** Leave blank.
7. **Author(s).** Give name(s) in conventional order (e.g., John R. Doe, or J. Robert Doe). List author's affiliation if it differs from the performing organization.
8. **Performing Organization Report Number.** Insert if performing organization wishes to assign this number.
9. **Performing Organization Name and Address.** Give name, street, city, state, and zip code. List no more than two levels of an organizational hierarchy. Display the name of the organization exactly as it should appear in Government indexes such as USGRDR-I.
10. **Project/Task/Work Unit Number.** Use the project, task and work unit numbers under which the report was prepared.
11. **Contract/Grant Number.** Insert contract or grant number under which report was prepared.
12. **Sponsoring Agency Name and Address.** Include zip code.
13. **Type of Report and Period Covered.** Indicate interim, final, etc., and, if applicable, dates covered.
14. **Sponsoring Agency Code.** Leave blank.
15. **Supplementary Notes.** Enter information not included elsewhere but useful, such as: Prepared in cooperation with . . . Translation of . . . Presented at conference of . . . To be published in . . . Supersedes . . . Supplements . . .
16. **Abstract.** Include a brief (200 words or less) factual summary of the most significant information contained in the report. If the report contains a significant bibliography or literature survey, mention it here.
17. **Key Words and Document Analysis.** (a). **Descriptors.** Select from the Thesaurus of Engineering and Scientific Terms the proper authorized terms that identify the major concept of the research and are sufficiently specific and precise to be used as index entries for cataloging.
 (b). **Identifiers and Open-Ended Terms.** Use identifiers for project names, code names, equipment designators, etc. Use open-ended terms written in descriptor form for those subjects for which no descriptor exists.
 (c). **COSATI Field/Group.** Field and Group assignments are to be taken from the 1965 COSATI Subject Category List. Since the majority of documents are multidisciplinary in nature, the primary Field/Group assignment(s) will be the specific discipline, area of human endeavor, or type of physical object. The application(s) will be cross-referenced with secondary Field/Group assignments that will follow the primary posting(s).
18. **Distribution Statement.** Denote releasability to the public or limitation for reasons other than security for example "Release unlimited". Cite any availability to the public, with address and price.
- 19 & 20. **Security Classification.** Do not submit classified reports to the National Technical
21. **Number of Pages.** Insert the total number of pages, including this one and unnumbered pages, but excluding distribution list, if any.
22. **Price.** Insert the price set by the National Technical Information Service or the Government Printing Office, if known.

BIBLIOGRAPHIC DATA SHEET	1. Report No. UCB/EERC-77/04	2.	3. Recipient's Accession No.
4. Title and Subtitle Seismological Studies of Strong Motion Records		5. Report Date	
7. Author(s) Jafar Shoja-Taheri		6.	
9. Performing Organization Name and Address		8. Performing Organization Rept. No.	
12. Sponsoring Organization Name and Address		10. Project/Task/Work Unit No.	
15. Supplementary Notes		11. Contract/Grant No.	
16. Abstracts (CONTINUED FROM FIRST PAGE)		13. Type of Report & Period Covered	
<p>4) A detailed seismological interpretation of the strong motion records was attempted for the 1966 Parkfield earthquake, California. Velocity and displacement traces integrated from the corresponding recorded accelerograms were found most valuable in studying the earthquake mechanism and wave forms. A double-couple right-lateral strike-slip mechanism (along the San Andreas fault) is consistent with the recorded direct S waves originating from the hypocenter. High energy arrivals observed on the velocity traces are interpreted as S waves ("stopping phases") that originated at the termination of the rupture towards the southeast of the San Andreas fault.</p> <p>From particle velocity diagrams of the stopping phases in the horizontal plane, the rupture length was between 20 to 28 km. Corresponding rupture velocities are estimated to be 2.5 ± 0.1 km/sec and 3.1 ± 0.5 km/sec. The inference from the strong motion records is that Love waves were more excited at the southwestern than the northeastern side of the fault, whereas the Rayleigh waves were more energetic at the northeastern than the southeastern side of the fault. The late arrivals of both Love and Rayleigh waves of long period (about 6 sec) together with the observed reversed dispersion of Rayleigh waves observed at the Temblor station all indicate a low velocity zone within the crust.</p>		14.	
17b. Identifiers/Open-Ended Terms		15. Supplementary Notes	
17c. COSATI Field/Group		16. Abstracts (CONTINUED FROM FIRST PAGE)	
18. Availability Statement		19. Security Class (This Report) UNCLASSIFIED	
18. Availability Statement		20. Security Class (This Page) UNCLASSIFIED	
18. Availability Statement		21. No. of Pages	
18. Availability Statement		22. Price	

INSTRUCTIONS FOR COMPLETING FORM NTIS-35

(Bibliographic Data Sheet based on COSATI

Guidelines to Format Standards for Scientific and Technical Reports Prepared by or for the Federal Government, PB-180 600).

1. **Report Number.** Each individually bound report shall carry a unique alphanumeric designation selected by the performing organization or provided by the sponsoring organization. Use uppercase letters and Arabic numerals only. Examples FASEB-NS-73-87 and FAA-RD-73-09.
2. Leave blank.
3. **Recipient's Accession Number.** Reserved for use by each report recipient.
4. **Title and Subtitle.** Title should indicate clearly and briefly the subject coverage of the report, subordinate subtitle to the main title. When a report is prepared in more than one volume, repeat the primary title, add volume number and include subtitle for the specific volume.
5. **Report Date.** Each report shall carry a date indicating at least month and year. Indicate the basis on which it was selected (e.g., date of issue, date of approval, date of preparation, date published).
6. **Performing Organization Code.** Leave blank.
7. **Author(s).** Give name(s) in conventional order (e.g., John R. Doe, or J. Robert Doe). List author's affiliation if it differs from the performing organization.
8. **Performing Organization Report Number.** Insert if performing organization wishes to assign this number.
9. **Performing Organization Name and Mailing Address.** Give name, street, city, state, and zip code. List no more than two levels of an organizational hierarchy. Display the name of the organization exactly as it should appear in Government indexes such as Government Reports Index (GRI).
10. **Project/Task/Work Unit Number.** Use the project, task and work unit numbers under which the report was prepared.
11. **Contract/Grant Number.** Insert contract or grant number under which report was prepared.
12. **Sponsoring Agency Name and Mailing Address.** Include zip code. Cite main sponsors.
13. **Type of Report and Period Covered.** State interim, final, etc., and, if applicable, inclusive dates.
14. **Sponsoring Agency Code.** Leave blank.
15. **Supplementary Notes.** Enter information not included elsewhere but useful, such as: Prepared in cooperation with . . . Translation of . . . Presented at conference of . . . To be published in . . . Supersedes . . . Supplements . . . Cite availability of related parts, volumes, phases, etc. with report number.
16. **Abstract.** Include a brief (200 words or less) factual summary of the most significant information contained in the report. If the report contains a significant bibliography or literature survey, mention it here.
17. **Key Words and Document Analysis.** (a). **Descriptors.** Select from the Thesaurus of Engineering and Scientific Terms the proper authorized terms that identify the major concept of the research and are sufficiently specific and precise to be used as index entries for cataloging.
(b). **Identifiers and Open-Ended Terms.** Use identifiers for project names, code names, equipment designators, etc. Use open-ended terms written in descriptor form for those subjects for which no descriptor exists.
(c). **COSATI Field/Group.** Field and Group assignments are to be taken from the 1964 COSATI Subject Category List. Since the majority of documents are multidisciplinary in nature, the primary Field/Group assignment(s) will be the specific discipline, area of human endeavor, or type of physical object. The application(s) will be cross-referenced with secondary Field/Group assignments that will follow the primary posting(s).
18. **Distribution Statement.** Denote public releasability, for example "Release unlimited", or limitation for reasons other than security. Cite any availability to the public, other than NTIS, with address, order number and price, if known.
- 19 & 20. **Security Classification.** Do not submit classified reports to the National Technical Information Service.
21. **Number of Pages.** Insert the total number of pages, including introductory pages, but excluding distribution list, if any.
22. **NTIS Price.** Leave blank.

SEISMOLOGICAL STUDIES OF STRONG MOTION RECORDS

by

Jafar Shoja-Taheri

Report No. UCE/EERC-77/04
Earthquake Engineering Research Center
College of Engineering
University of California
Berkeley, California

January 1977

ib

SEISMOLOGICAL STUDIES OF STRONG MOTION RECORDS

ABSTRACT

by

Jafar Shoja-Taheri

A number of problems pertinent to seismological and engineering interpretations of strong ground motions in earthquakes are studied.

The main new results are as follows:

- 1) A new form of strong motion accelerogram (Spectrally Maximized Records or "SMR") and its associated generalized spectrum are proposed for earthquake engineering use. Parameters (e.g., spectral, duration, peak amplitude) of horizontal-component strong-motion records at a given site generally depend significantly on the (arbitrary) azimuthal direction, often resulting in a crucially deficient description of these parameters if only a single component is used. Combination of horizontal components using spectral maximization is shown to be effective in minimizing the difficulty. The spectra of the two horizontal components at each site are combined to maximize the resultant spectrum, independently of azimuthal orientation. SMRs of thirty-three important strong-motion accelerograms (including twelve New Guinea records) are then calculated from their corresponding spectra. In only sixty percent of cases is the peak acceleration from a maximized spectrum greater than that of the single components, the bracketed duration from the maximized spectrum is always greater. After filtering to provide records in ten frequency bands (0-1 HZ, 1-2 HZ, . . . 9-10 HZ), correlations for each band are

made between acceleration peaks, spectral energy, magnitudes, and source distances. More stable estimates of these strong motion parameters appear to be provided by spectrally maximized accelerations compared with single component estimates.

2) Statistical analysis of all accelerograms of the 1966 Parkfield earthquake, California and the 1952 Taft earthquake, California indicates that the usable long period of ground displacements obtained from double integration of accelerogram records are limited by two major sources of errors--human reading and base-line corrections. Usable long period limits are estimated to vary between 7 to 14 seconds depending on the individual earthquake.

3) It is shown that the integration of ragged functions such as strong motion accelerograms, by regular quadrature formulas, leads to significant errors. The conventional method of frequency domain integration also leads to indeterminacy of zero frequency information and distortion of the shape of the resulting integral. A modification of the conventional method of frequency domain integration was developed to avoid these deficiencies. The new technique extrapolates the integrand by joining its mirror image to the end of reflection. The zero frequency information is also determined by this technique.

4) A detailed seismological interpretation of the strong motion records was attempted for the 1966 Parkfield earthquake, California. Velocity and displacement traces integrated from the corresponding recorded accelerograms were found most valuable in studying the earthquake mechanism and wave forms. A double-couple right-lateral strike-slip mechanism (along the San Andreas fault) is consistent with the recorded direct S waves originating from the hypocenter. High energy

arrivals observed on the velocity traces are interpreted as S waves ("stopping phases") that originated at the termination of the rupture towards the southeast of the San Andreas fault.

From particle velocity diagrams of the stopping phases in the horizontal plane, the rupture length was between 20 to 28 km. Corresponding rupture velocities are estimated to be 2.5 ± 0.1 km/sec and 3.1 ± 0.5 km/sec. The inference from the strong motion records is that Love waves were more excited at the southwestern than the northeastern side of the fault, whereas the Rayleigh waves were more energetic at the northeastern than the southeastern side of the fault. The late arrivals of both Love and Rayleigh waves of long period (about 6 sec) together with the observed reversed dispersion of Rayleigh waves observed at the Temblor station all indicate a low velocity zone within the crust.



ACKNOWLEDGMENTS

I am indebted to Dr. Bruce A. Bolt for the initial suggestion of this program and for his guidance and constructive criticism during its investigation. I thank Dr. Lane R. Johnson for enlightening discussions. I also thank Dr. H. Bolton Seed for his carefully reading the manuscript and his comments. I am very grateful to my wife Sholeh for her understanding and patient encouragement. Finally I thank my fellow graduate students and Seismographic Stations personnel for making my stay at Berkeley an enjoyable experience.

This work has been supported by the National Science Foundation Grant AEN 74-21548, and the Seismographic Stations of the University of California, Berkeley.

During the course of this study I was on educational leave from the Department of Geophysics, Ferdowsi University, Mashad, Iran. The financial support of Ferdowsi University and Iran's Ministry of Sciences and Higher Education is gratefully recognized.

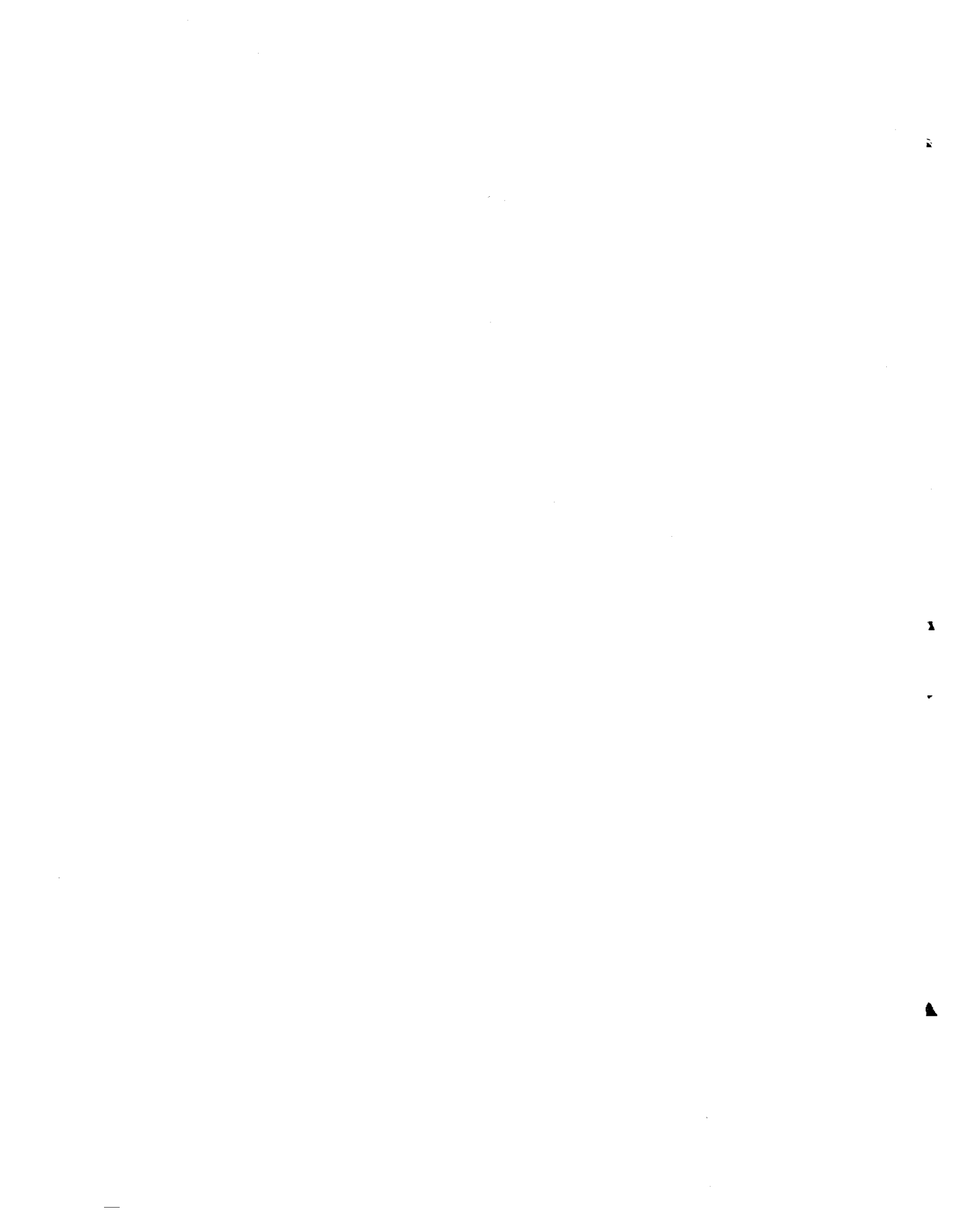
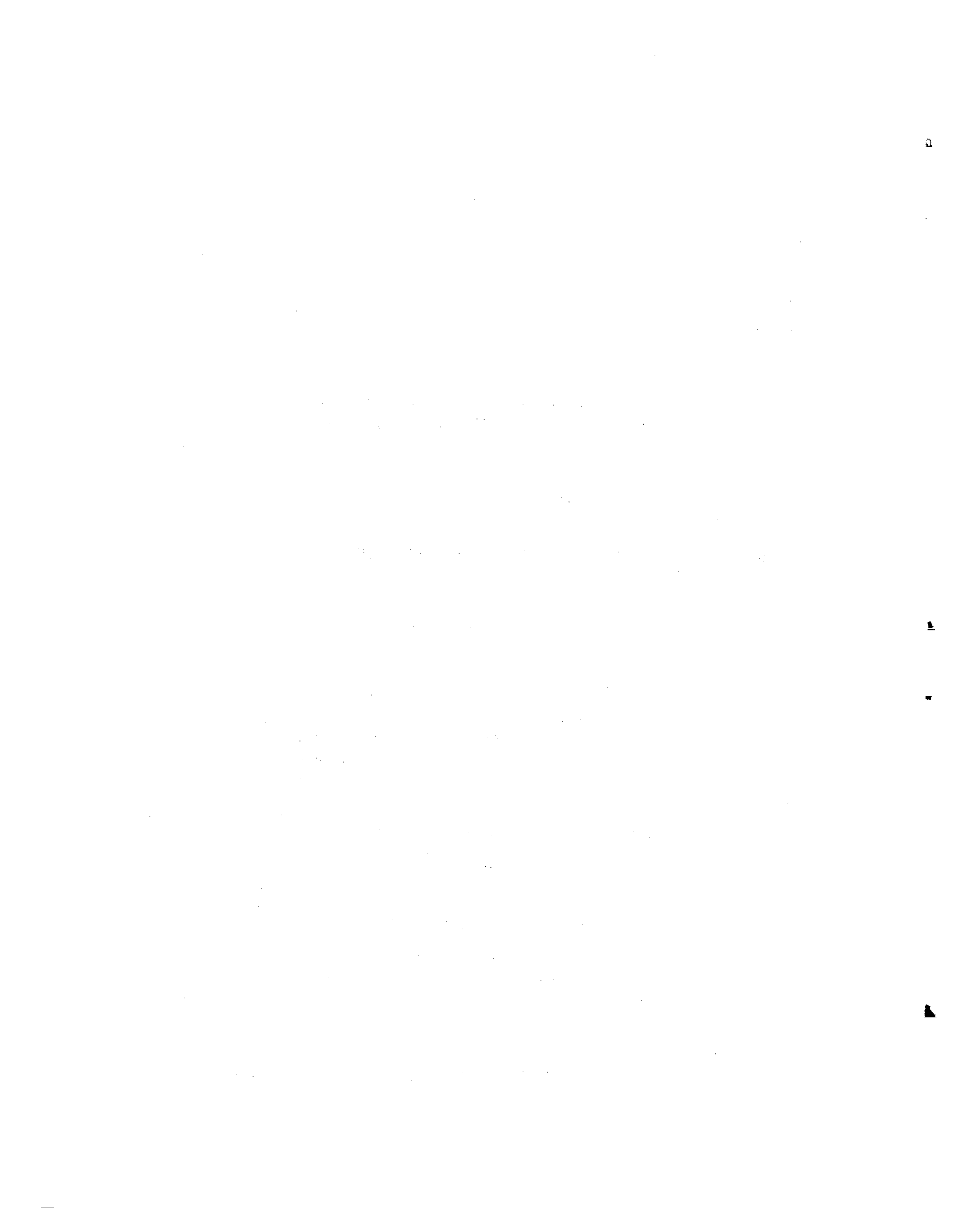


TABLE OF CONTENTS

	<u>Page</u>
ACKNOWLEDGMENTS.	v
CHAPTER	
I INTRODUCTION	1
II A GENERALIZED STRONG MOTION ACCELEROGRAM BASED ON SPECTRAL MAXIMIZATION FROM TWO HORIZONTAL COMPONENTS	5
2.1 Introduction.	5
2.2 Spectral Maximization	6
2.3 Estimates of Strong Motion Parameters	20
III ASSESSMENT OF DIGITIZATION AND BASE-LINE CORRECTION ERRORS	96
3.1 Introduction.	96
3.2 Reading Errors Due to Human Eyes.	99
3.3 Errors Due to Base-Line Correction.	102
3.4 Combined Errors of Reading and Base-Line Correction.	107
IV TIME INTEGRATION OF STRONG MOTION ACCELEROGRAMS BOTH IN THE TIME AND FREQUENCY DOMAIN. A NEW METHOD OF ACCURATE TIME INTEGRATION IN THE FREQUENCY DOMAIN	125
4.1 Introduction.	125
4.2 Integration of Strong Motion Accelerograms in the Time Domain	126
4.3 Integration of Strong Motion Accelerograms in the Frequency Domain.	136
4.4 Accurate Time Integration and Differentiation of a Function in Frequency Domain	141
V PARKFIELD, CALIFORNIA, EARTHQUAKE OF JUNE 1966: SEISMOLOGICAL INTERPRETATION OF THE STRONG MOTION RECORDS.	143
5.1 Introduction.	143
5.2 Background.	144
5.3 Interpretation of the Strong Motion Recordings.	147



	<u>Page</u>
CHAPTER	
VI CONCLUSIONS	178
REFERENCES	184



CHAPTER I

INTRODUCTION

The current increased demand for greater knowledge regarding the problems of earthquake hazards and the design of earthquake resistant structures as well as the increased availability of strong motion records have prompted much effort into detailed seismological analysis of strong ground motions. The ground motion produced in the near field is generally more complicated than the ground motion recorded in the far field. At a near site, the source parameters (e.g., fault dimension, rupture velocity, and dislocation amplitude) as well as detailed geological complexities are significantly influential.

Considerable progress has recently been made in the development of theoretical models for computing the strong ground motion (e.g., Aki, 1968; Haskell, 1969; Haskell and Thomson, 1972; Trifunac, 1974a; Trifunac *et al.*, 1974b). These models have assisted the understanding of gross features of strong ground motions in terms of source mechanism, but because of limitations imposed by the mathematical formulation, one or more relevant physical parameters (e.g., boundary conditions) defining the strong motions are generally neglected.

Interpretation of the seismograms themselves ("time histories") of recorded strong motions in terms of elastic wave theory has proved to be useful in explaining the mechanism of energy release and generation of elastic waves. For example, Bolt (1972) and Hanks (1974)

2.

analyzed the Pacoima strong motion recording of the February 9, 1971, San Fernando earthquake and they showed that several features occurring during the first 10 seconds of recording could be explained in terms of a mechanical model of faulting. Hanks (1975) made an extensive analysis of 234 components of the strong ground displacement recorded during the 1971 San Fernando earthquake. He indicated that the variations of gross amplitude and frequency content observed among the recorded displacements can be used to infer source parameters such as the seismic moment, source dimension, rupture velocity, rupture propagation, as well as the development of surface waves and subsequent dispersion.

Determination and definition of strong motion parameters (e.g., peak acceleration, duration) as functions of magnitude, intensity, source distance, and so on are essential for both engineering design and seismological purposes (e.g., Housner, 1970; Newmark and Rosenblueth, 1971; Bolt, 1972; Algermissen and Perkins, 1976). Schnabel and Seed (1973) have analyzed the strong ground motion records of the Western United States in order to estimate some relations between peak accelerations in rock and magnitudes. Trifunac and Brady (1975) have studied the duration of strong earthquake ground motion, recorded at different geological site conditions, in terms of magnitude and intensity.

As a contribution to the present efforts towards a deeper understanding of both seismological and engineering aspects of strong ground motion, a number of prominent problems are considered in this thesis. The main results achieved are fourfold.

First, a method that allows more robust estimation of earthquake design parameters (peak acceleration, duration, etc.) has been devised.

As discussed in chapter 2, the development combines individual recorded components of strong ground motions in the frequency domain by choosing a maximum amplitude at each frequency. The maximized spectra and corresponding accelerograms (Spectrally Maximized Records or SMR) are calculated from the earthquake recordings of 33 strong motion instruments around the world. The SMRs are then used to introduce the pertinent statistical correlations among such key strong motion parameters as peak acceleration, magnitude, and attenuation as functions of source distance and frequency. Further it is shown that the method of spectral maximization allows the prediction of an expected maximum acceleration for any given acceleration amplitude spectrum.

Secondly, quantitative interpretations of strong motion records require careful definition of the frequency within which the recording and processing of the ground motion meets a given precision of measurement. For example, in chapter 5 of this thesis, the source mechanism of the June 27, 1966 Parkfield earthquake, California is analyzed based on velocity and displacement components which are calculated by integrating accelerograms recorded at different sites. In order to provide an adequate numerical basis for such studies, a full statistical analysis of errors due to data processing of strong motion accelerograms is carried through (chapter 3). This study leads to an estimate of a usable frequency band of displacement components.

Thirdly, the general problem of time integration of strong motion records in time domain and frequency domain is studied, in chapter 4. Use of regular quadrature formulas to integrate the class of ragged functions represented by strong motion accelerograms produces significant errors. An alternative procedure using the frequency domain representation

4.

has been devised. This construction appears to be new and successfully provides more precise results of integration than previously used in strong motion seismology. This technique is employed in chapter 5 to integrate strong motion accelerograms before analysis.

Fourthly, the Parkfield earthquake of 1966 is analyzed by interpreting the velocity and displacement traces integrated from the recorded accelerograms. It is shown that these records provide invaluable seismological information on the faulting and the source of energy release during the earthquake.

The results presented in this thesis demonstrate overall that detailed seismological interpretation of strong motion seismograms, while difficult, is not an impossible art. The necessary insights and skills will require more specific research effort but in time are likely to be developed for more-or-less routine work.

CHAPTER II

A GENERALIZED STRONG MOTION ACCELEROGRAM BASED ON SPECTRAL MAXIMIZATION FROM TWO HORIZONTAL COMPONENTS2.1--Introduction

Major seismological work on determining and defining strong motion parameters that are stable, i.e., are not seriously dependent on abnormal values, is still much needed. Such robust parameters are required for not only purely seismological purposes on understanding earthquake waves (e.g., Bolt, 1972), risk mapping (e.g., Algermissen and Perkins, 1976) and so on, but are vital for engineering design purposes (e.g., Housner, 1970; Newmark and Rosenblueth, 1971). The aim of the present chapter is to report some pertinent results of analysis of a variety of strong motion records. In this search for stable parameters, a new procedure of combining ground motions has been found that may have wide application.

In practice, even in some of the most recent work (e.g., Cloud and Perez, 1969; Schnable and Seed, 1973; Trifunac and Brady, 1975), generally raw measurements of such parameters as peak acceleration have been used for correlations with intensity, magnitude and distance. The question is whether mean parameters would be more robust if spectral characteristics such as frequency and phase were involved. An affirmative answer is likely because the responses of both complex geological and man-made structures are dominated by seismic wave characteristics in restricted bands of frequencies. Overall, therefore, the work is

directed towards determining the functional dependence of the kinematical parameters on frequency as an independent variable. More specifically, a review of published analyses of strong motion records and their engineering use shows that the usual procedure is to work separately with wave amplitudes or spectra from just one horizontal component (or the vertical component) of the ground motion. Because three components are recorded, the problem is to develop a physically acceptable method whereby optimum use is made of all components of strong motion acceleration, velocity and so on. The second purpose here, therefore, is to demonstrate the effectiveness of one technique of combining the two horizontal components before parameterization begins. It is suggested that the method, called spectral maximization, might be adopted generally with advantage by seismologists and earthquake engineers.

2.2--Spectral Maximization

Consider the two orthogonal horizontal components of acceleration recorded at small distances from the earthquake source. These are generally made up of the superposition of many wave types radiating from an areally distributed and moving source--not a single point. The examples shown at the top of Figure 2.1 (this figure is repeated in Figure 2.19b) are the horizontal components (S69E and N21E) recorded at Taft in the 1952 Kern County earthquake (magnitude 7.7). The directions of instrumental orientation are not related to the strike of the rupturing fault and have no seismological significance. The peak accelerations on the two components are 0.19g and 0.16g, respectively. As the seismograms show, these maximum amplitudes occur at quite different times during the motion and give little idea of the result of

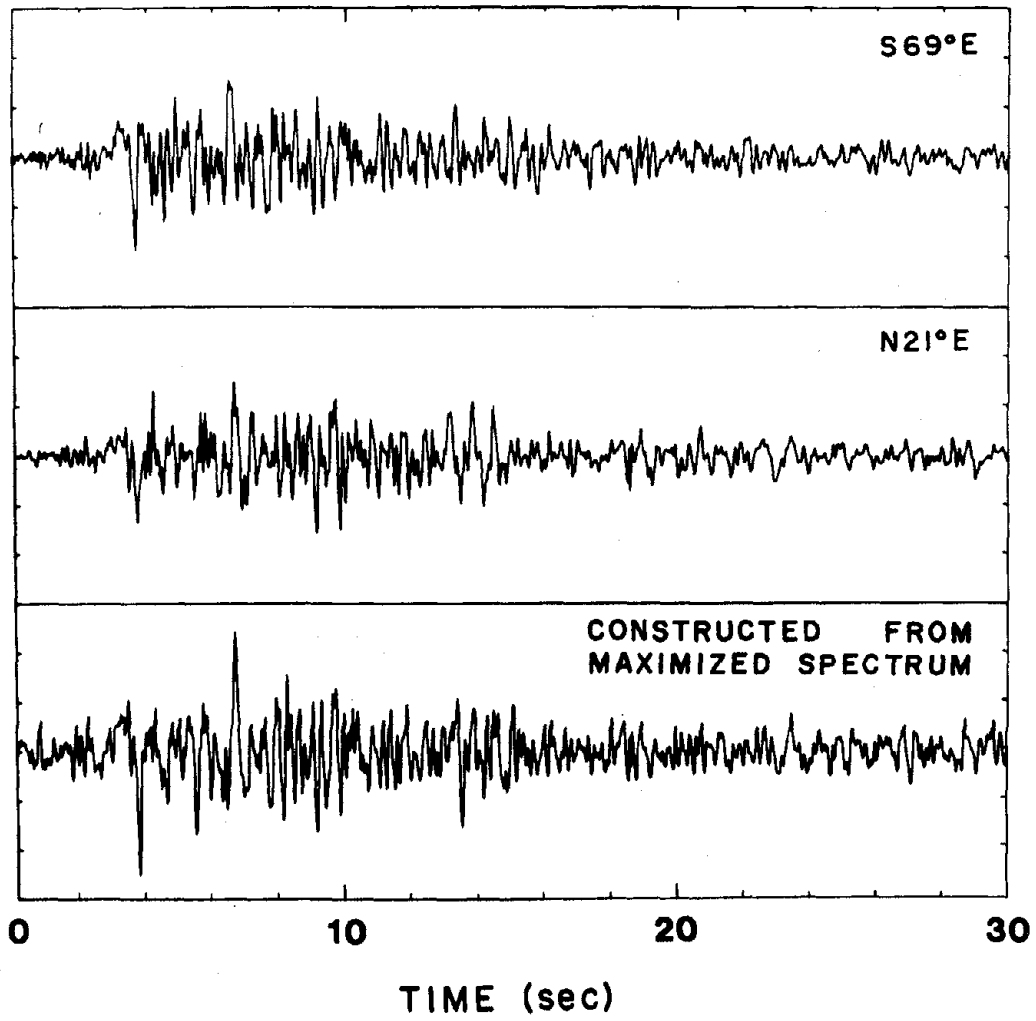


Fig. 2.1

8.

any vectorial combination.

From the point of view of representing an average earthquake excitation, it is not usually appropriate, at least in the near field of an earthquake, to resolve the motions in a particular direction. At a site near an earthquake source, such as a rupturing fault, seismic waves of various types, from various foci, travelling various paths in the crustal rocks, are superimposed in a complicated way. Penzien and Watabe (1975) deal with this problem completely in the time domain by defining a set of orthogonal directions (for 3 components) for which the variances of the component ground motions have stationary values.

The solution is approached quite differently in the present chapter. After numerical trials with many records, it is found that one particular combination of the separate frequency spectra of the two (horizontal) components leads to a spectrum which represents closely the overall variation in motion actually occurring at the site. This is named here the maximized (horizontal) spectrum of acceleration for the site and, by an inverse Fourier transform, produces the corresponding time history--or spectrally maximized record (SMR). The method differs from that of Penzien and Watabe in the use of the frequency domain and non-stochastic formulation (although statistical interpretation can be given to it).

The method of spectral combination is shown schematically in Figure 2.2.

Consider the combination of the single frequency component ω of each of the two horizontal accelerograms orthogonally oriented in the X and Y directions. A vectorial combination of amplitudes (A and B) and phases (ψ_x and ψ_y) can be numerically made so as to produce an

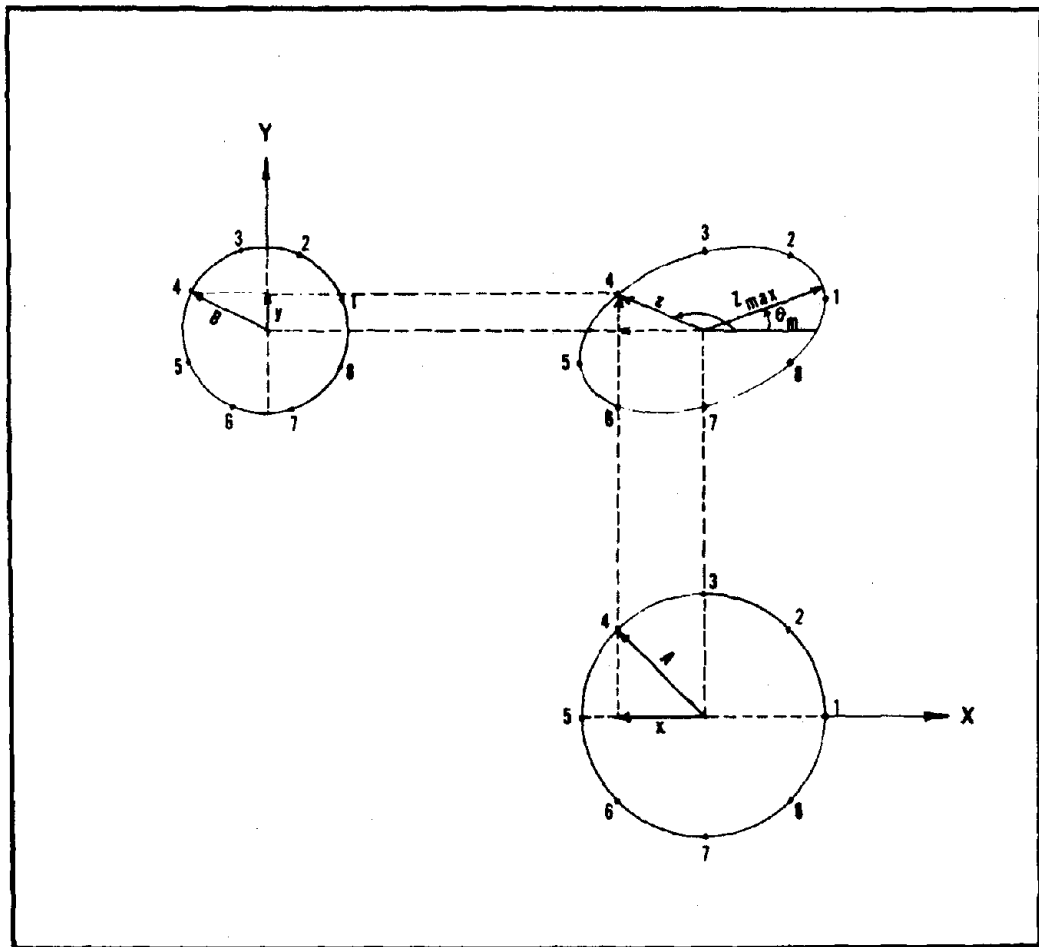


Fig. 2.2

10.

elliptical Lissajous figure in the normal way as on an oscilloscope.

The combined acceleration z for a given azimuthal angle θ , from the plus direction, is given by

$$\begin{aligned} z &= x \cos\theta + y \sin\theta \\ &= Z \cos(\omega t + \phi), \end{aligned} \quad (2.1)$$

where

$$x = A \cos(\omega t + \psi_x), \quad (2.2)$$

$$y = B \cos(\omega t + \psi_y). \quad (2.3)$$

A, ψ_x and B, ψ_y are respectively the amplitude and phase of the frequency component ω in the X and Y directions, and Z, ϕ are respectively the combined amplitude and phase in the θ direction. The combined accelerations, given by (2.1), define in general an ellipse.

It follows that an angle θ_m can always be found (for the specific frequency ω) such that θ_m is the azimuthal direction of the major axis of the ellipse with respect to the X axis. The combined spectrum given in (2.1) has maximum amplitude Z_{\max} equal to the half-length of the major axis of the ellipse. θ_m is calculated from

$$\theta_m = \frac{1}{2} \tan^{-1} \left(\frac{2AB \cos(\psi_x - \psi_y)}{A^2 - B^2} \right). \quad (2.4)$$

Substitution of (2.4) into (2.1) yields the maximized spectrum as follows:

$$Z_{\max}(\omega) = x \cos\theta_m + y \sin\theta_m = Z_{\max} \cos(\omega t + \phi_{\max}). \quad (2.5)$$

The value of Z_{\max} is calculated in a computer for each harmonic ω_n , $n = 0, 1, \dots, N$ (N corresponds in the present work to a Nyquist

frequency of 25 Hz), and the corresponding modulus $|Z_{\max}(\omega_n)|$ is plotted.

As an example, Figure 2.3 (this figure is repeated in Figure 2.19a) compares the maximized spectrum with the two spectra for the orthogonal horizontal components of the original Taft accelerograms shown in Figure 2.1. The spectral shape and energy partition with frequency of the original components differ significantly; the maximum energy of the two components clearly occurs in two different frequency bands. It follows that selection of one or other component to describe the motion of the site gives an unrepresentative sample. Similarly, simple vectorial addition of the two component seismograms towards a specified azimuth would, by introducing an arbitrary parameter, also produce an unrepresentative spectrum. The shape of the maximized spectrum obtained using equation (2.5) and plotted at the top of Figure 2.3 is clearly a more satisfactory overall spectral representation of the ground motion.

Let us now examine the spectrally maximized records (SMR "time histories") obtained by transforming the phases and amplitudes of the maximized spectra to the time domain. Figure 2.1 compares the actual strong motion accelerogram from the Taft site in the 1952 earthquake with the corresponding generalized accelerograms (SMR). The SMR for Taft has a peak (horizontal) acceleration of 0.26g. This illustration is rather typical of the thirty-three strong motion records which have been analyzed for the present chapter. Consider as a further illustration the acceleration spectra calculated from the two horizontal strong motion records at Castaic Dam in the 1971 San Fernando mainshock (Richter magnitude 6.5 and source-to-site distance 20 km). The spectral shapes in Figure 2.4 (this figure is repeated in Figure 2.26a) are strikingly

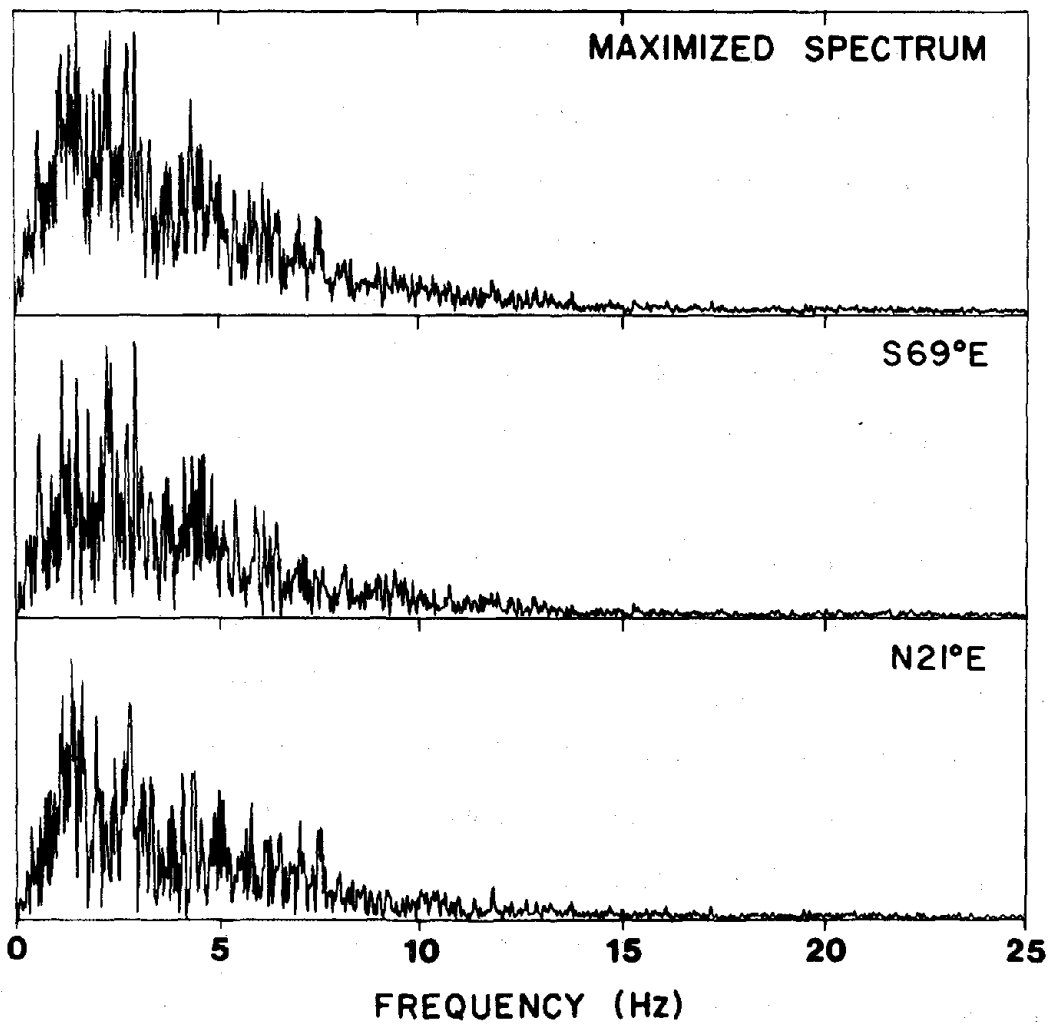


Fig. 2.3

different for the two components, with much more energy between 1 and 3 Hz on the N21E component. Indeed, selection for structural testing of the S69E component would significantly underestimate the shaking at the lower frequencies. In contrast, the maximized spectrum calculated for this site appears to sample without bias the stronger motion on both components.

Fourier transformation of the maximized spectrum at the top of Figure 2.4 yields the spectrally maximized record (SMR) at the bottom of Figure 2.5 (this figure is repeated in Figure 2.26b). Cross correlation by eye of the three accelerograms in Figure 2.5 suggests at once that the individual records are contained in a general way in the SMR. The latter appears more uniform with less modulation and, on average, with higher amplitudes throughout the shaking. The SMR is certainly not a simple superposition of the individual components, however; some peaks in the latter are reduced while some are enhanced in the SMR.

The calculation of maximized spectra and SMR have been carried out for many sites around the world, of which thirty-three are referred to in this analysis (see Table 2.1). These records come from California, Washington, Japan, Peru and New Guinea (Denham et al., 1973). Figures 2.9a through 2.41a and Figures 2.9b through 2.41b illustrate respectively the spectra and the corresponding accelerograms of these records. At the top of Figures 2.9a through 2.41a the azimuthal means of every 20 harmonics are plotted. An error bar represents the standard error of one measurement. The scatter of θ_m is generally large, as shown by the standard errors. This implies that the maximum spectral energy of different harmonics is not generally confined to a particular direction. An overall comparison between the original accelerograms

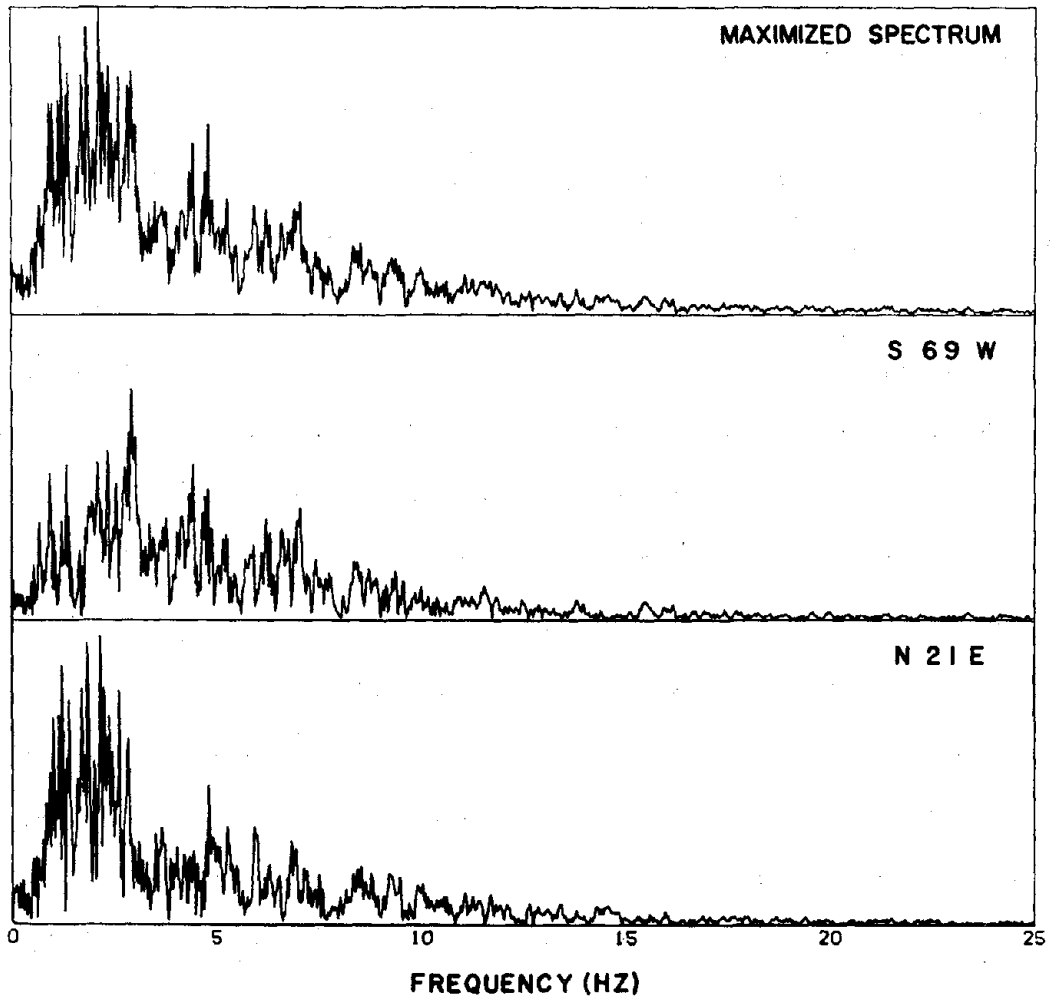


Fig. 2.4

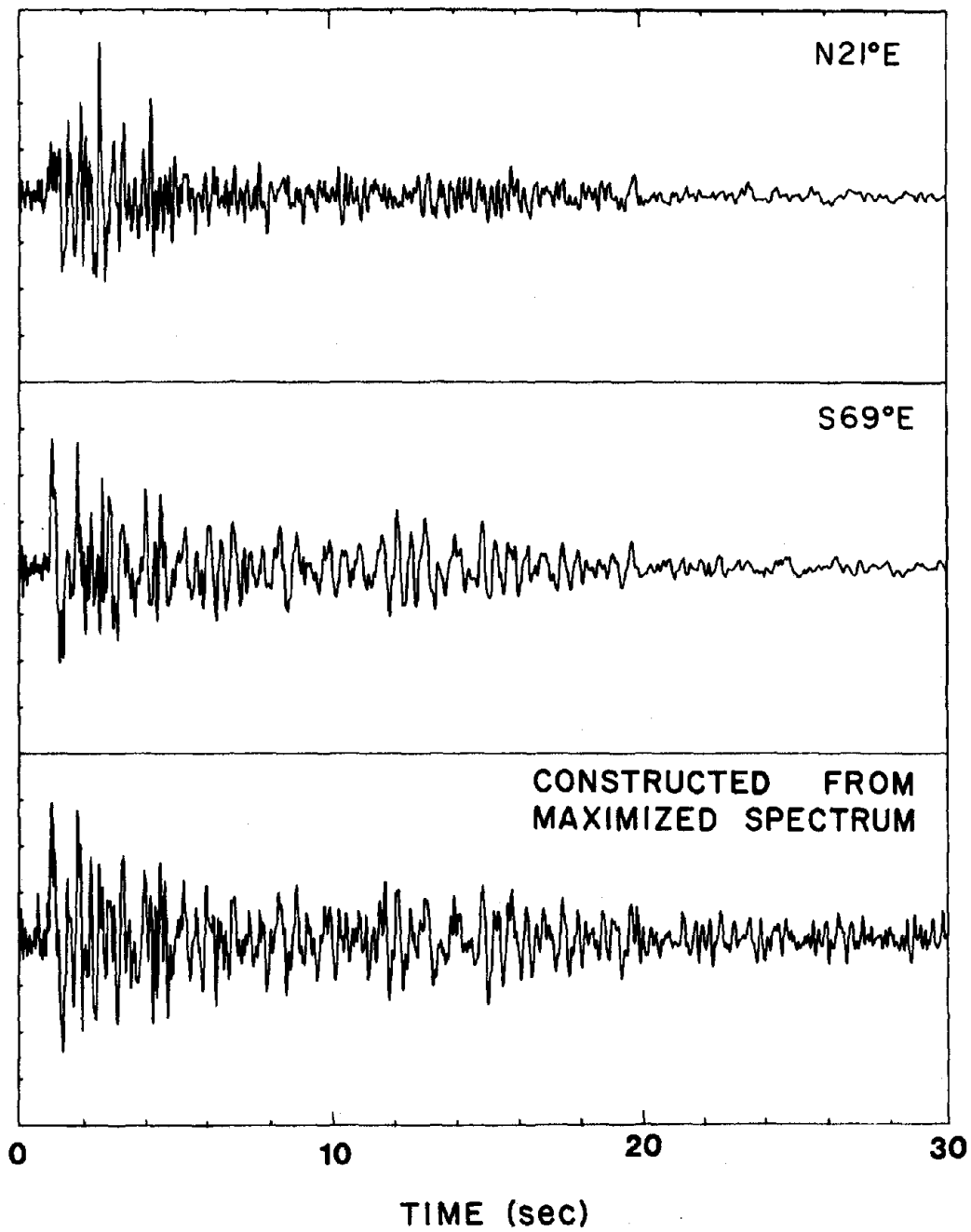


Fig. 2.5

and the corresponding SMR reveals several general properties.

First, in many cases the transformation does not remove the seismic wave pattern on the original components. It is often feasible still to identify certain seismic phases such as P and S. For example, the onset of the S wave trains can be seen on all records plotted in Figures 2.9b through 2.41b.

Secondly, SMR amplitudes are generally, but not always, greater than the amplitudes at the same epoch on the separate components. In Table 2.1, peak accelerations of thirty-three sets of horizontal components and peak accelerations of corresponding generalized records are shown. The peaks of the generalized SMR are higher, in a majority of cases (60 percent), than the peaks of original components. The greatest enhancement of a peak acceleration occurs for the Taft accelerograms (Figures 2.1 and 2.19b) where it amounts to 35 percent. Of special interest, because of their wide use for engineering design, the two horizontal components at El Centro in the May 18, 1940 Imperial Valley earthquake yield an SMR with a peak acceleration of 0.32g, which is slightly but not significantly less than the peak of the observed south component.

Thirdly, there is a uniform pattern in the duration of the spectrally maximized records. Let us consider the bracketed duration (Bolt, 1973), i.e., the elapsed time (for a specified frequency range) between the first and last acceleration excursions on the record greater than a given amplitude level (say, 0.05g). It is found that, as might be expected, for all thirty-three cases analyzed, the bracketed durations of the SMRs are greater than those of the components. The increase ranges up to 10 percent. It is concluded that, when considering the

TABLE 2.1. STRONG MOTION RECORDS ANALYZED

No.	Recording Site	Δ (km)	Mag.	Comp.	Peak Acceleration Original	cm/sec ² Generalized
1	Vernon, Calif., 3/10/33	16	6.3	N82W S08W	151.2 131.3	185.5
2	El Centro, Calif., 5/18/40	6	6.5	West South	215.4 345.8	313.6
3	Ferndale, Calif., 9/11/38	57	5.5	SE NE	89.8 156.3	134.0
4	Ferndale, Calif., 2/9/41	100	6.4	SE NE	40.7 65.0	56.8
5	Ferndale, Calif., 10/7/51	56	5.7	S44W N46W	117.7 114.8	147.9
6	Ferndale, Calif., 10/22/52	53	5.5	N44E S46E	57.5 75.2	101.8
7	Ferndale, Calif., 12/21/54	40	6.6	N44E N46W	162.1 203.7	227.8
8	Seattle, Wash., 4/13/49	61	7.1	S02W N88E	68.2 67.4	83.7
9	Olympia, Wash., 4/13/49	29	7.1	S86W S04E	284.9 175.0	281.7
10	Eureka, Calif., 12/21/54	24	6.6	N79E N11W	271.0 164.7	294.2
11	Taft, Calif., 7/21/52	40	7.7	S69E N21E	185.2 154.6	251.4
12	Golden Gate, Calif., 3/22/57	11.2	5.3	S80E N10E	102.2 103.5	116.4

TABLE 2.1--continued

No.	Recording Site	Δ (km)	Mag.	Comp.	Peak Acceleration Original	cm/sec ² Generalized
13	Olympia, Wash., 4/29/65	29.5	7.1	S04E S86W	146.0 199.2	204.8
14	Temblor, Calif., 6/27/66	6.4	5.6	S25W N65W	363.4 269.4	385.2
15	Cholame-Shandon, Calif., No. 5, 6/27/66	5.3	5.6	N05W N85E	370.8 424.5	296.0
16	Cholame-Shandon, Calif., No. 8, 6/27/66	9.2	5.6	N50E N40W	219.3 260.6	231.7
17	Cholame-Shandon, Calif., No. 12, 6/27/66	14.8	5.6	N50E N40W	61.2 64.9	77.0
18	Castaic Old Ridge, Calif., 2/9/71	29	6.5	N21E S69E	324.0 274.0	294.6
19	Itajima, Japan, 1968	32	6.6	N74E N16W	437.9 361.2	400.4
20	Hiroo, Japan, 1970	35	6.8	NS EW	399.2 419.2	467.4
21	Lima, Peru, 3/31/70	320	7.8	N13W N103W	122.4 126.1	150.9
22	Yonki, New Guinea, 11/14/67	253	6.4	HA* HB	46.4 46.2	47.3
23	Rabaul, New Guinea, 10/01/71	-	-	HA HB	61.0 68.0	69.0
24	Yonki, New Guinea, 6/17/68	131	6.0	HA HB	30.0 38.2	34.8

TABLE 2.1--continued

No.	Recording Site	Δ (km)	Mag.	Comp.	Peak Acceleration Original	Peak Acceleration Generalized ² cm/sec ²
25	Yonki, New Guinea, 3/10/69	259	6.8	HA HB	38.8 30.3	33.2
26	Yonki, New Guinea, 5/13/70	152	5.6	HA HB	25.5 30.3	32.2
27	Yonki, New Guinea, 2/12/71	128	6.1	HA HB	157.3 162.7	197.0
28	Yonki, New Guinea, 2/13/71	-	-	HA HB	78.2 46.5	54.2
29	Yonki, New Guinea, 1/19/72	-	-	HA HB	16.5 19.8	21.7
30	Panaguna, New Guinea, 9/7/69	178	5.6	HA HB	58.3 42.7	61.5
31	Panaguna, New Guinea, 3/28/70	114	6.1	HA HB	81.2 119.8	136.1
32	Panaguna, New Guinea, 7/26/71	302	8.0	HA HB	36.3 58.5	63.5
33	Panaguna, New Guinea, 3/10/69	-	-	HA HB	26.5 19.2	23.8

* See Denham et al., 1973.

overall shaking at a site, maximum duration should be measured from the spectrally maximized record rather than from the individual components.

2.3--Estimates of Strong Motion Parameters

In this section, all measurements will be made from the frequency spectra and accelerograms derived by the spectrally maximized method outlined above. The aim is to investigate significant tendencies of strong ground motion when the motion is represented by the SMR at each site rather than separate orthogonal components.

It has already been pointed out in numerous studies (e.g., Bolt, 1973; Trifunac and Brady, 1975) that the characterization of energetic seismic waves near the source is strongly dependent on the wave frequency. In order to examine the matter further, the thirty-three SMR for sites listed in Table 2.1 were filtered through ten sequential frequency bands 0-1 Hz, 1-2 Hz, . . . , 9-10 Hz, using a Butterworth filter with eight poles (Gold and Rader, 1969; see Figures 2.9b to 2.41b). These filters provide suitably narrow passbands with, of course, some phase shifts. As is often the case, the peak acceleration at different frequencies occurs at different epochs. The implication is that the peak acceleration of an unfiltered strong motion record does not necessarily represent the peak acceleration in all frequency bands.

The important inference therefore emerges that correlations of peak acceleration with other variables (such as intensity and source-to-site distance) might be more stable if they were made as a function of frequency. Let us first consider the outstanding problem of correlations of maximum acceleration with the total intensity of shaking

at a site. By Parseval's theorem (Jeffreys and Jeffreys, 1946) the total energy in the time domain equals the integral of the squared amplitude in the frequency domain. (The physical interpretation of the theorem is that the total energy in the traveling waves is the sum of the energies in the normal modes at the site.)

For any band-passed accelerogram $a(t)$, such as those shown in Figures 2.9b to 2.41b, we can therefore write

$$g = \int_0^T a^2(t) dt = \int_{f_1}^{f_2} |F(f)|^2 df, \quad (2.6)$$

where $F(f)$ is the amplitude spectrum and f_1 and f_2 are the lower and upper frequency limits of $a(t)$. If we identify the right-hand side of (2.6) with the total "site intensity," then this can be calculated using the right-hand side from the maximized spectra for each site.

The normalized peak acceleration, NPA, for each site is then defined as

$$\text{NPA} = \text{Peak Acceleration}/g^{\frac{1}{2}} \quad (2.7)$$

From (2.6) and (2.7), normalized peak accelerations for 29 United States and New Guinea records were calculated for each of the ten frequency bands from 1 to 10 Hz. (Japan, Seattle 1949, and Peru records were omitted at this step.) For each frequency band the mean of the 29 normalized peak accelerations was calculated and plotted on Figure 2.6, together with the standard error of each measurement (not the standard error of the mean).

Figure 2.6 shows that the variation of the normalized peak accelerations is relatively small, ranging from 0.7 at the lower frequencies to 1.2 at the higher frequencies. Further, from 4 to 7 Hz,

the ratio is stable and not significantly different from unity. Two results of value emerge. First, at least for these observations, there is a close correlation between peak acceleration, as measured by the SMR, and the total intensity of shaking, as defined in (2.6).

Secondly, we have obtained an algorithm which permits the estimation of peak acceleration expected for a proposed time history or spectrum of strong ground shaking. Suppose, for example, that several synthetic spectra of ground acceleration are considered for design purposes at a site. The question then may be: What is the maximum ground acceleration to be expected to correspond to each of them, in a specified frequency range? This mean value can be estimated by calculating g from (2.6) and then substituting it into (2.7) together with the appropriate NPA read from Figure 2.6.

The results of this procedure using the data set of Table 2.1 is illustrated in Figure 2.7. For each site, a calculated peak acceleration was obtained for each pass band by multiplying the mean NPA by the appropriate g . These calculated values were then plotted against the peak acceleration actually measured on the filtered SMR. As expected, this reverse process for the present data produces a linear regression with generally small scatter. The outlying points marked 1 and 3 on all pass bands of Figure 2.7 correspond to the 1966 Temblor and 1957 Golden Gate records. At these sites the foundations are rock, which might explain why the predicted values are lower than the observed peak values. On the other hand, point 2 corresponds to the Castaic record also made on rock and its prediction is normal. Prediction for the Peru site is also close.

Finally, we now consider the problem of estimation of attenuation

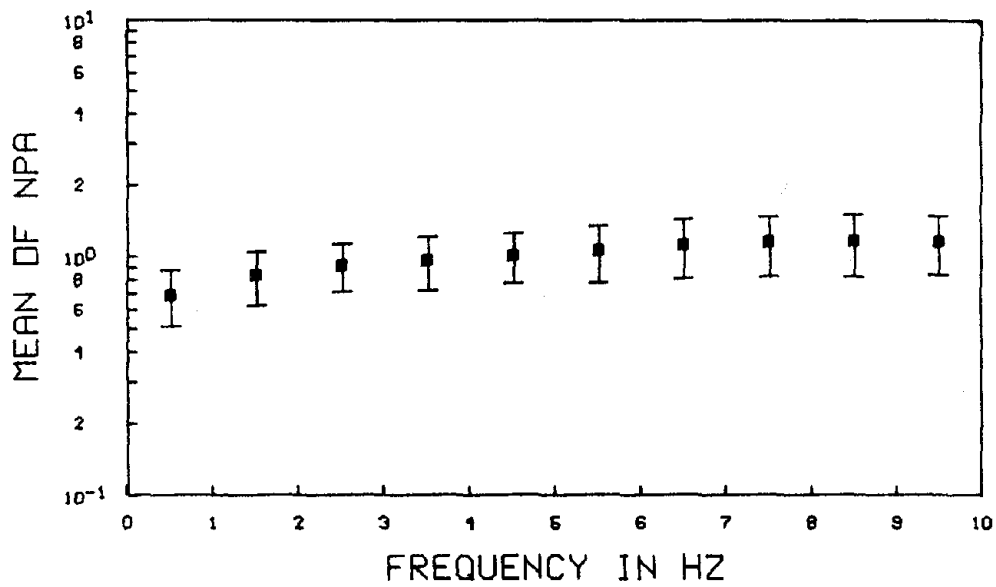


Fig. 2.6

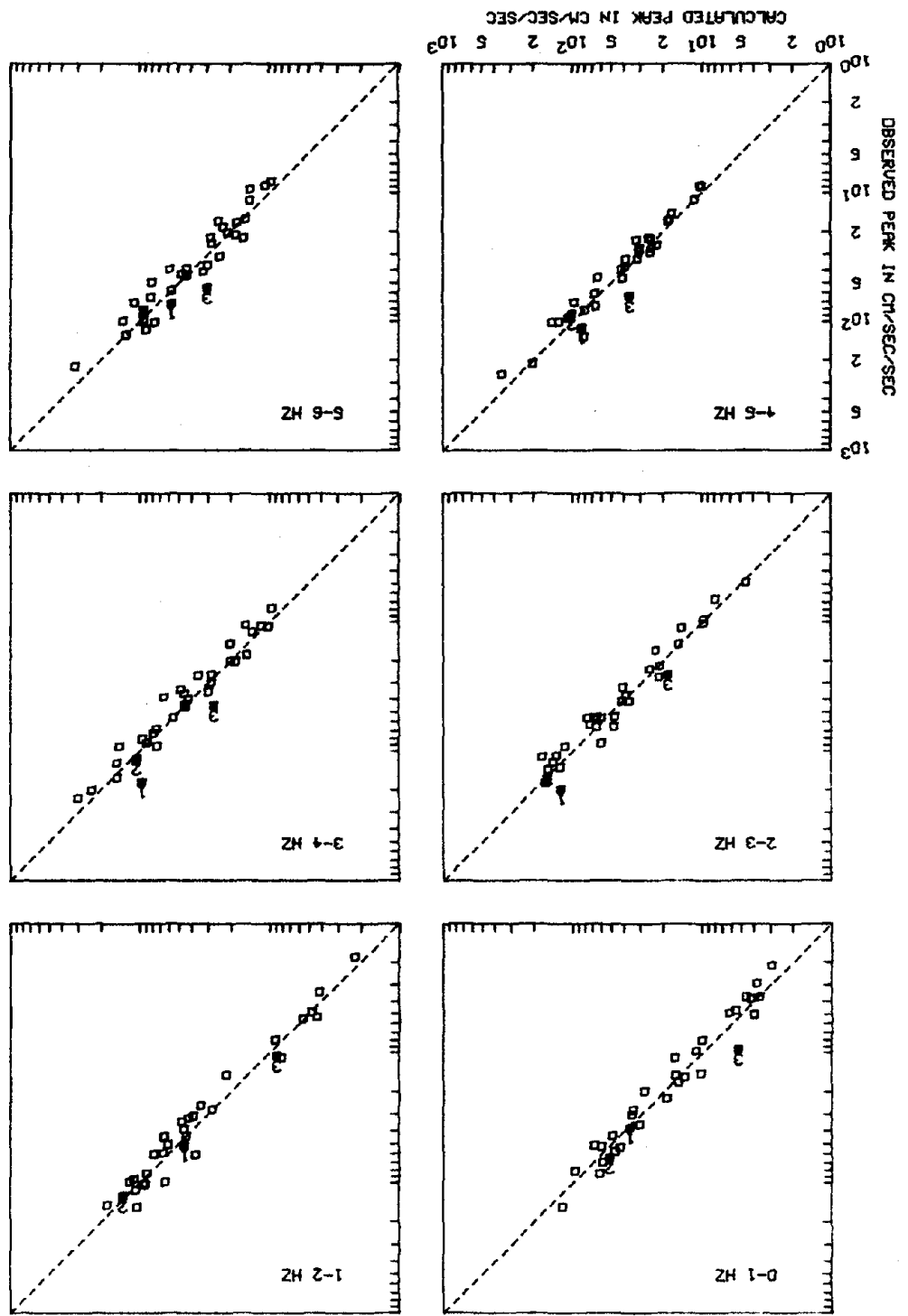


Fig. 2.7

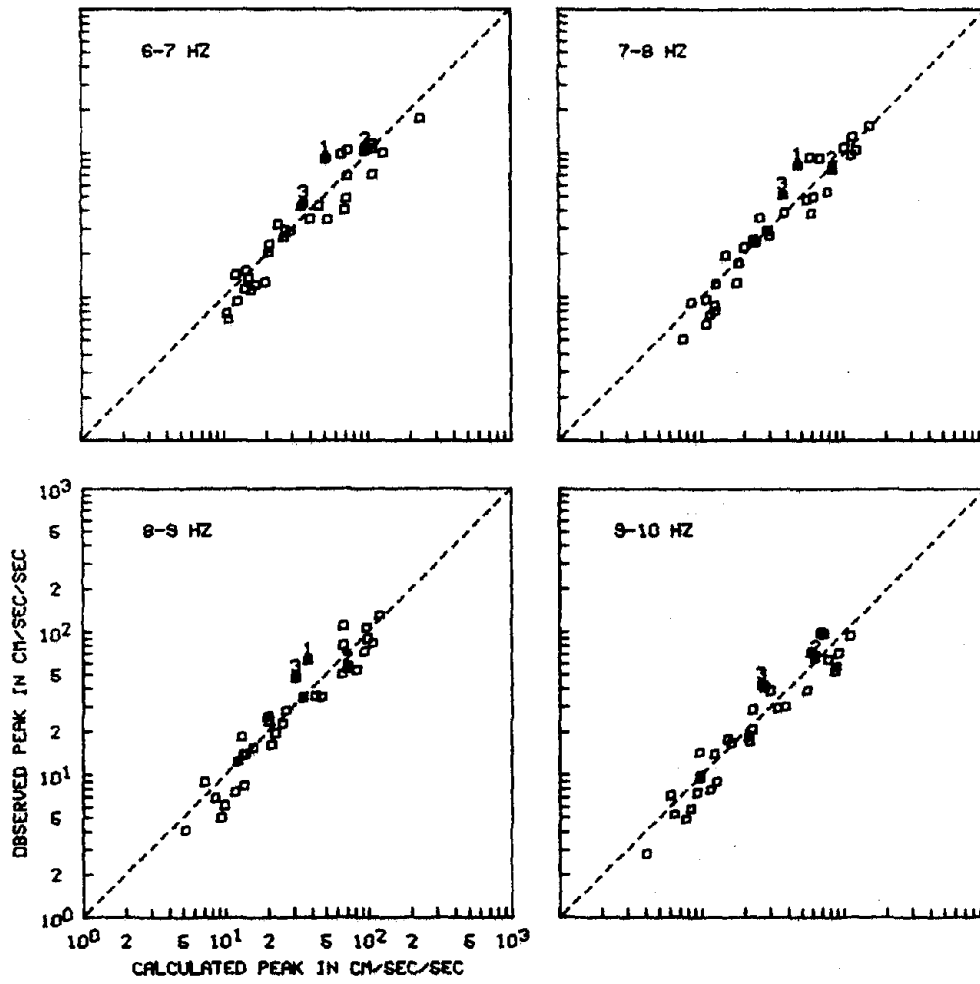


Fig. 2.7 continued

of peak acceleration with distance as a function of frequency. The procedure was to plot the peak accelerations measured from the filtered SMR for each site against the distance between the site and the source. (The nearest point on the offset fault was taken when this was known; otherwise the epicentral distance was adopted.) The results of the regression are shown for different pass bands in Figure 2.8. The Richter magnitudes of the earthquakes involved are denoted by different symbols.

As indicated in Figure 2.8, the overall result was a significant tendency for decreased peak acceleration with distance for each frequency band. While the trend is clear, there is some variation at each site from frequency band to frequency band. Many correlations of peak acceleration against source distance have been previously published and some have achieved considerable use in estimation of site parameters and seismic risk (e.g., Cloud and Perez, 1969; Schnabel and Seed, 1973; Donovan, 1974; Algermissen and Perkins, 1976). Most, however, do not consider frequency dependence and use records of the separate components of horizontal ground motion. All published correlations show a high degree of scatter and the fitted mean curves have high uncertainties. The correlation made in this study also shows the usual scatter, presumably from source path and site effects. An additional feature in the present analysis is that in the separate frequency bands, the plotted points do not clearly separate with large magnitude (e.g., $M > 6.5$). This is evident on Figure 2.8, where Richter magnitudes range from 5.3 to 8.0. The same result was pointed out previously (e.g., Donovan, 1973) and is an expected consequence of the modern seismological model of earthquake genesis (Bolt, 1972).

For the sake of comparison with other studies, logarithmic forms $PA = a\Delta^{-b}$ were fitted to attenuation plots, where PA is the peak acceleration and Δ the distance. The least-square estimates of b have large standard errors when no weighting of observations is used and no clear dependence of b on the frequency band is apparent from the estimations, at least for the sites of strong motion used in this paper, mainly California. Overall, a reasonable fit to the sample points is provided by the attenuation law $PA = a\Delta^{-0.5}$, for $10 < \Delta < 200$ km, and frequencies from 1 to 8 Hz.

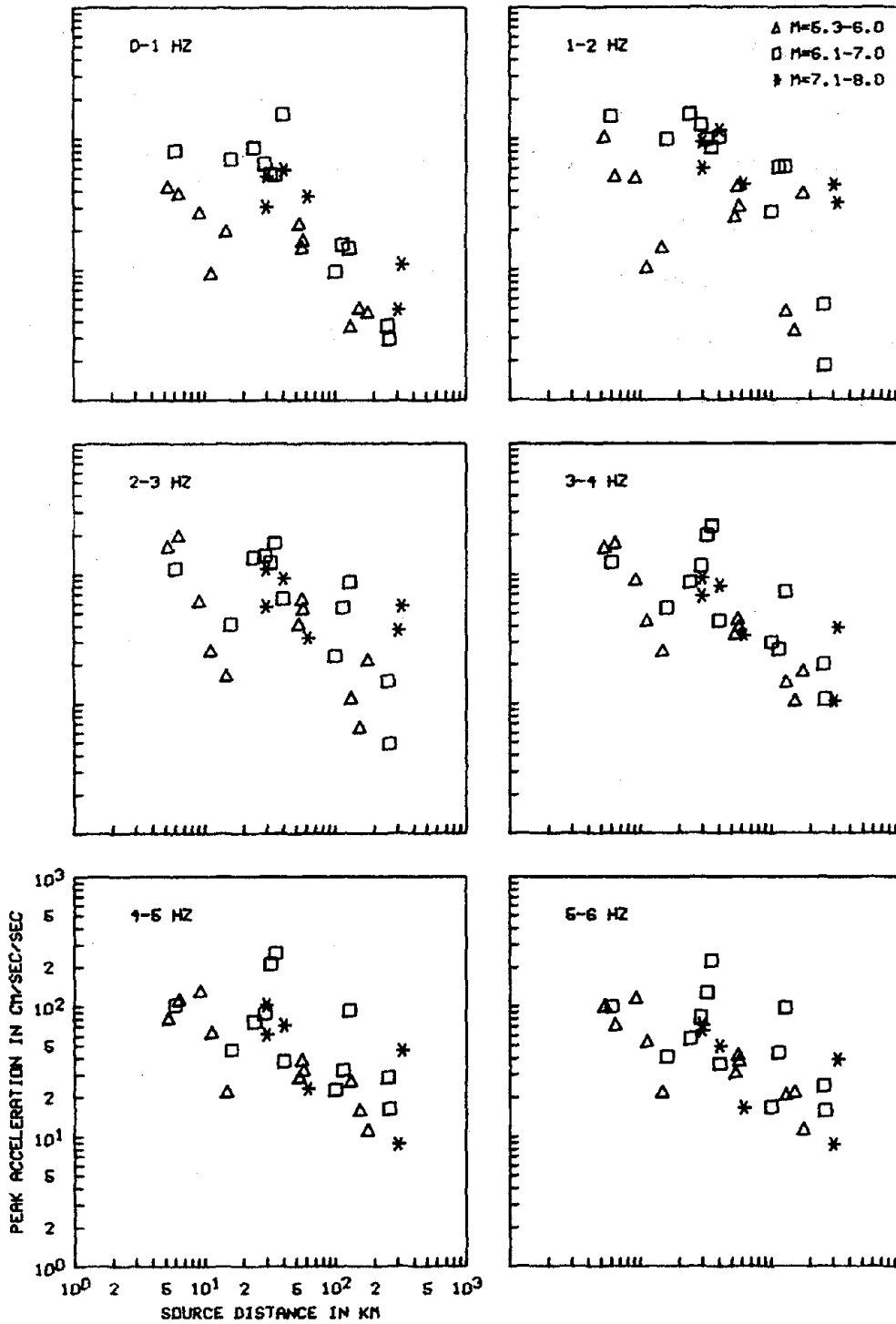


Fig. 2.8

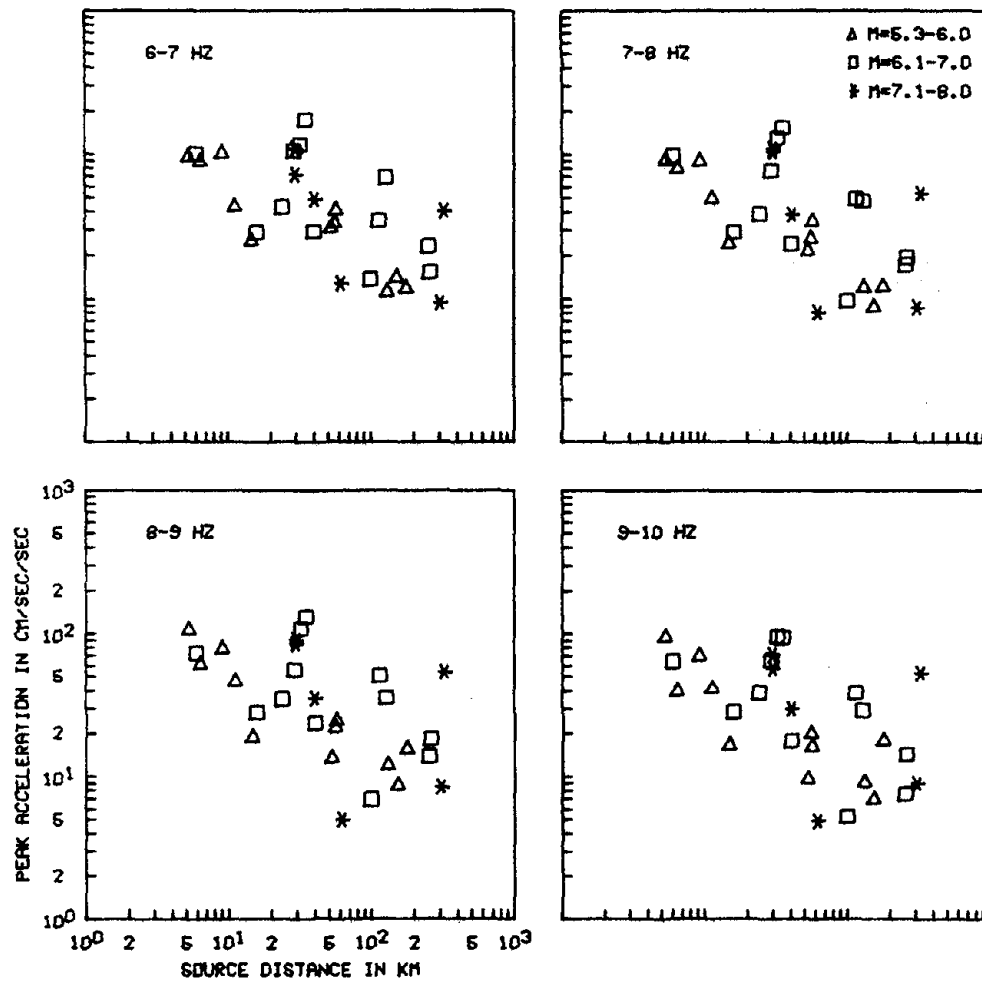


Fig. 2.8 continued

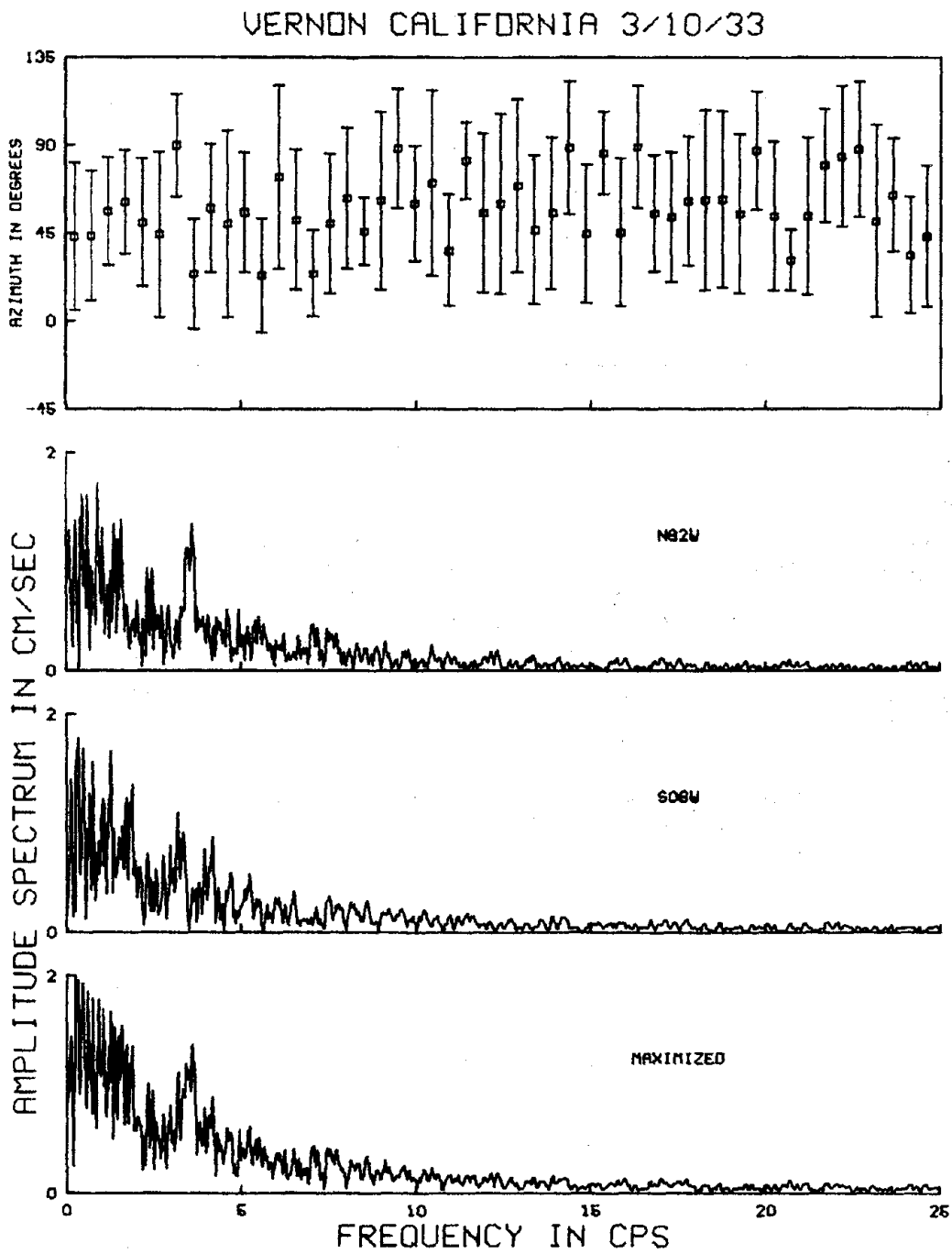


Fig. 2.9a

VERNON CALIFORNIA 3/10/33

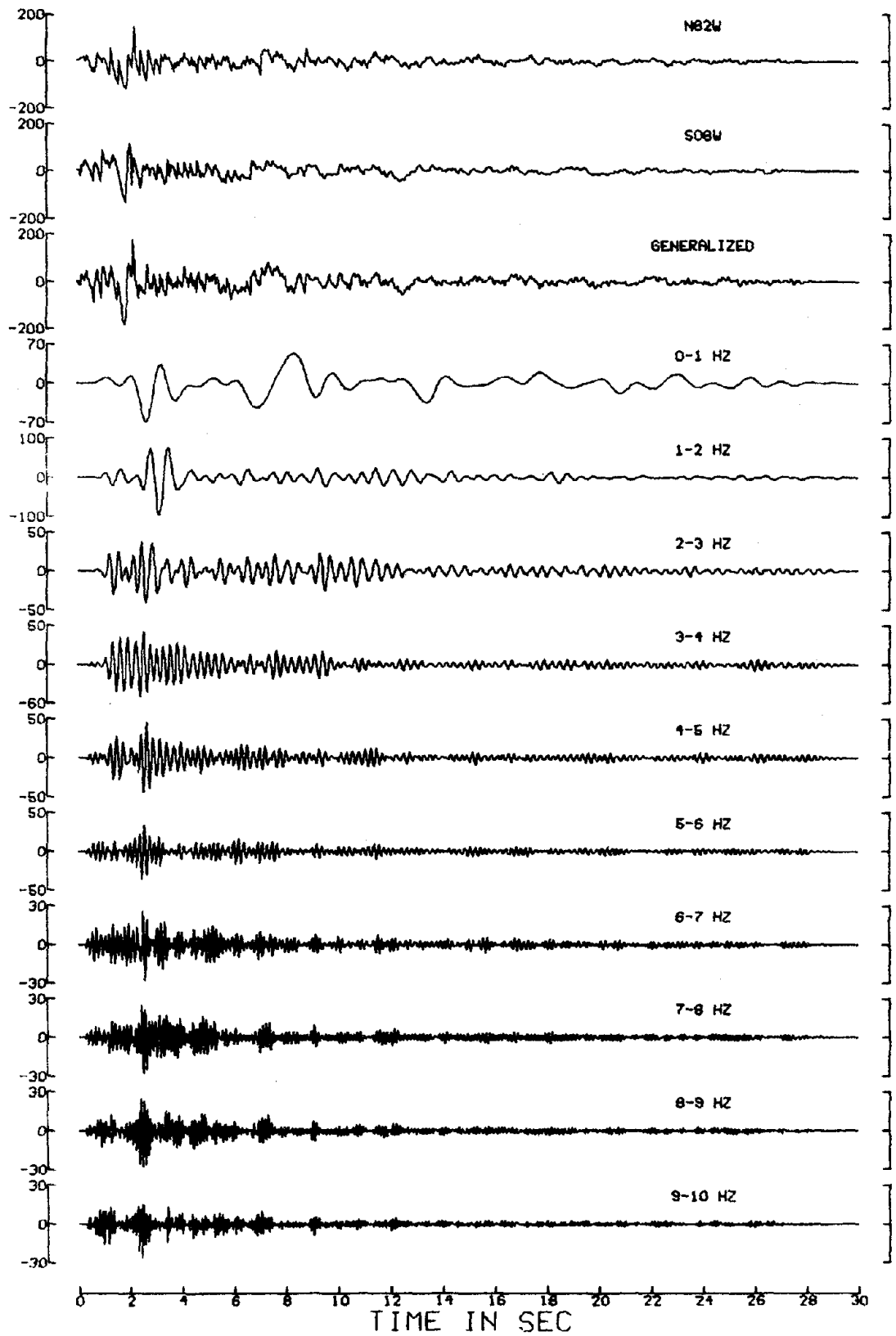


Fig. 2.9b

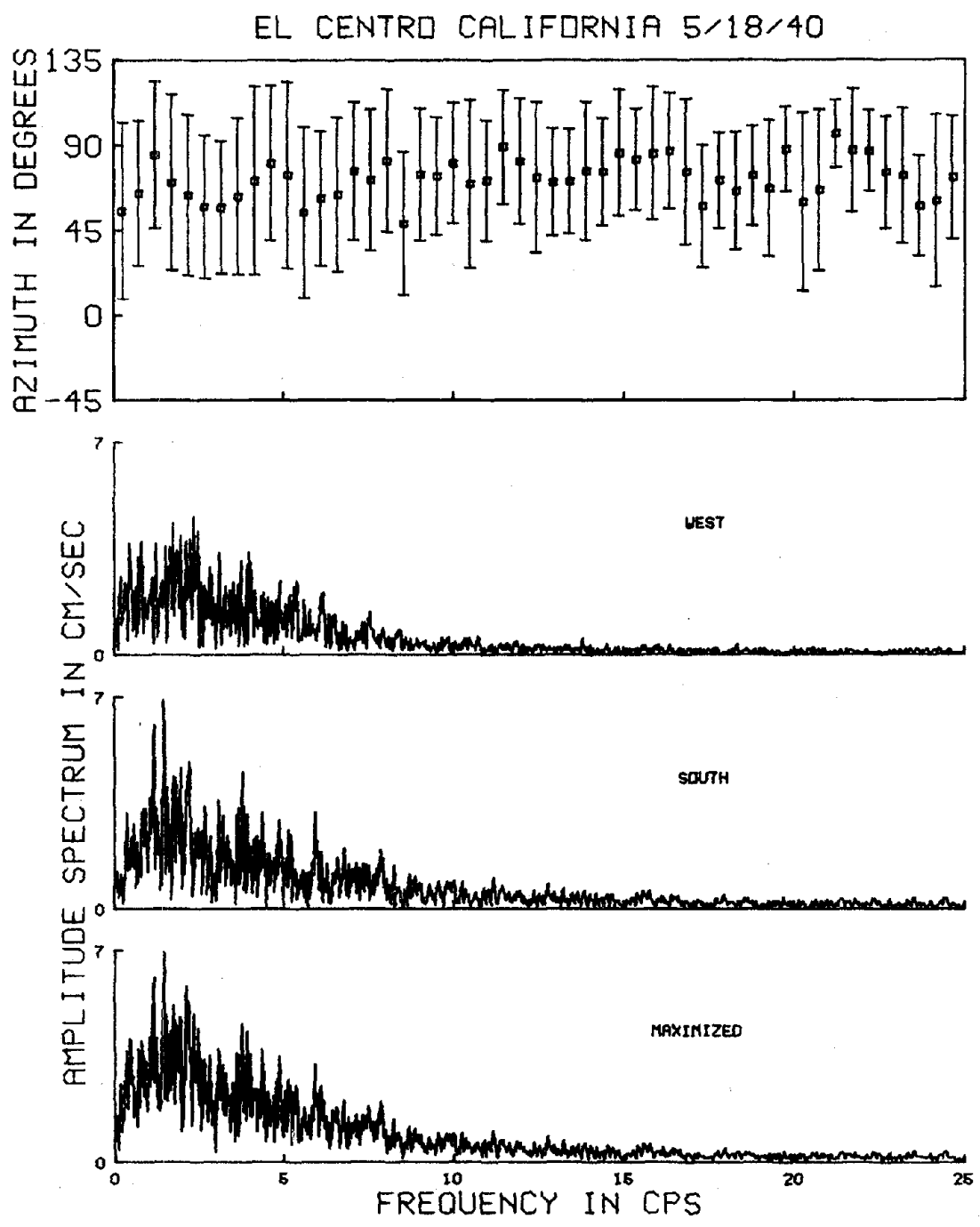


Fig. 2.10a

EL CENTRO CALIFORNIA 5/18/40

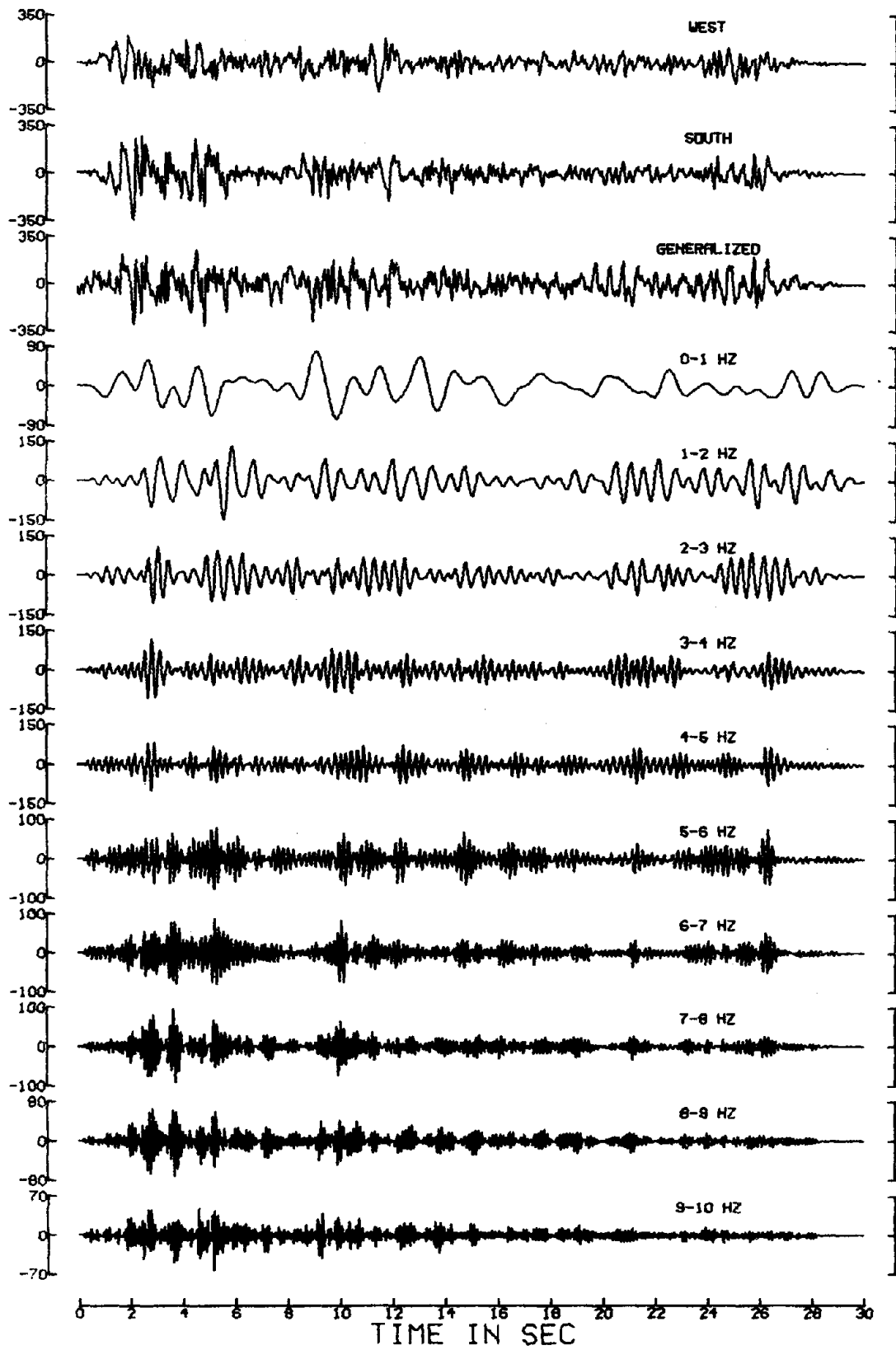


Fig. 2.10b

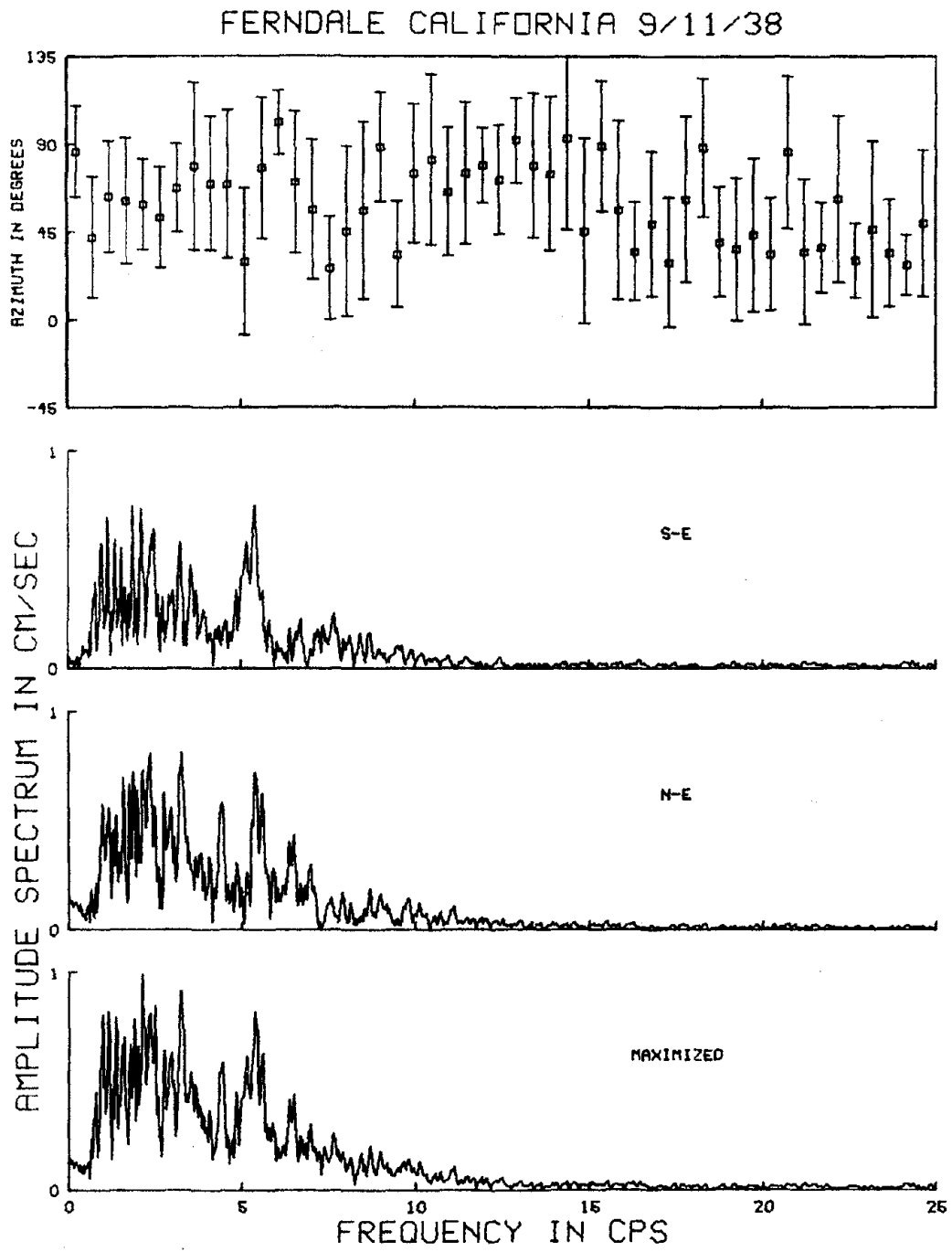


Fig. 2.11a

FERNDALE CALIFORNIA 9/11/38

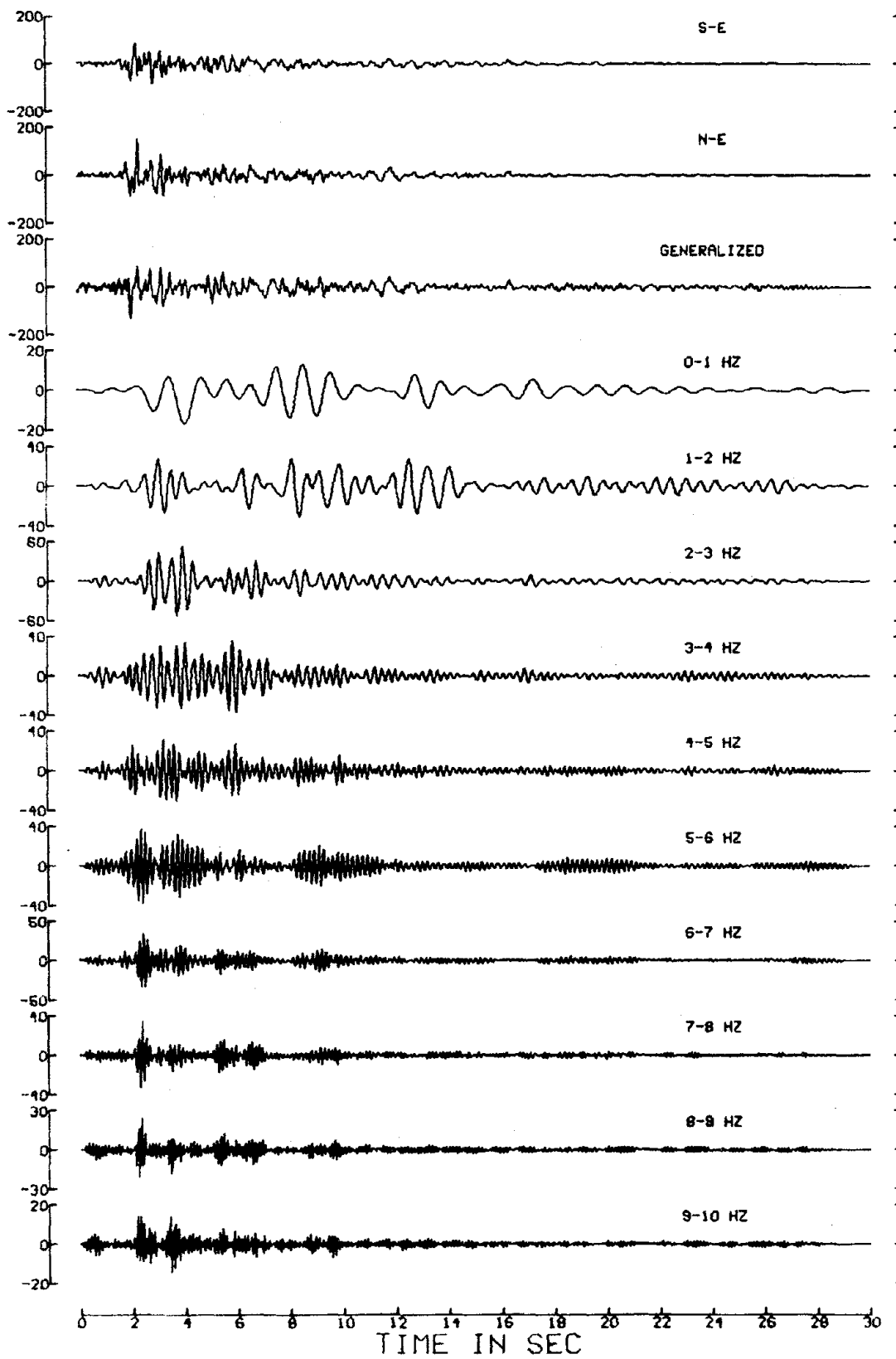


Fig. 2.11b

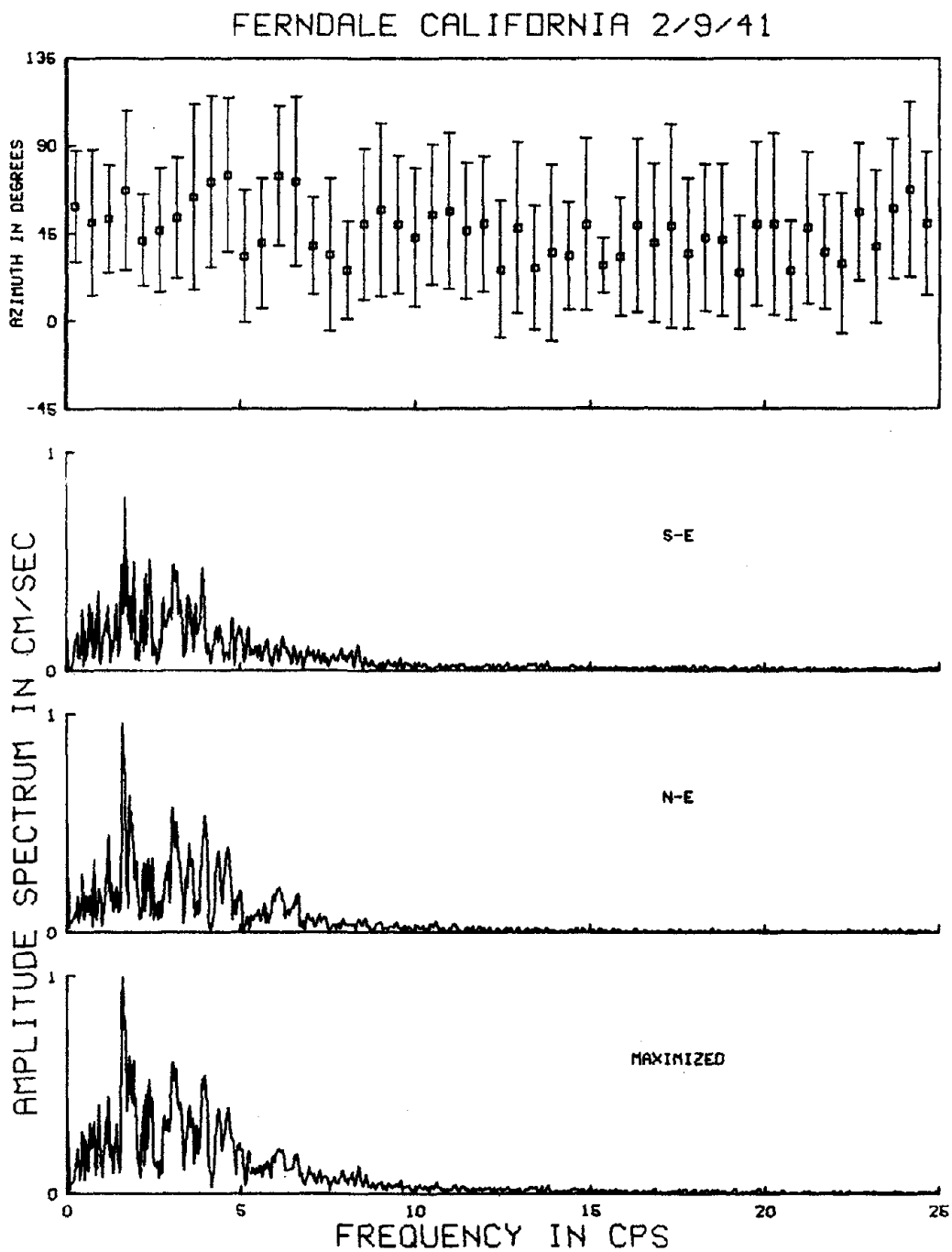


Fig. 2.12a

FERNDALE CALIFORNIA 2/9/41

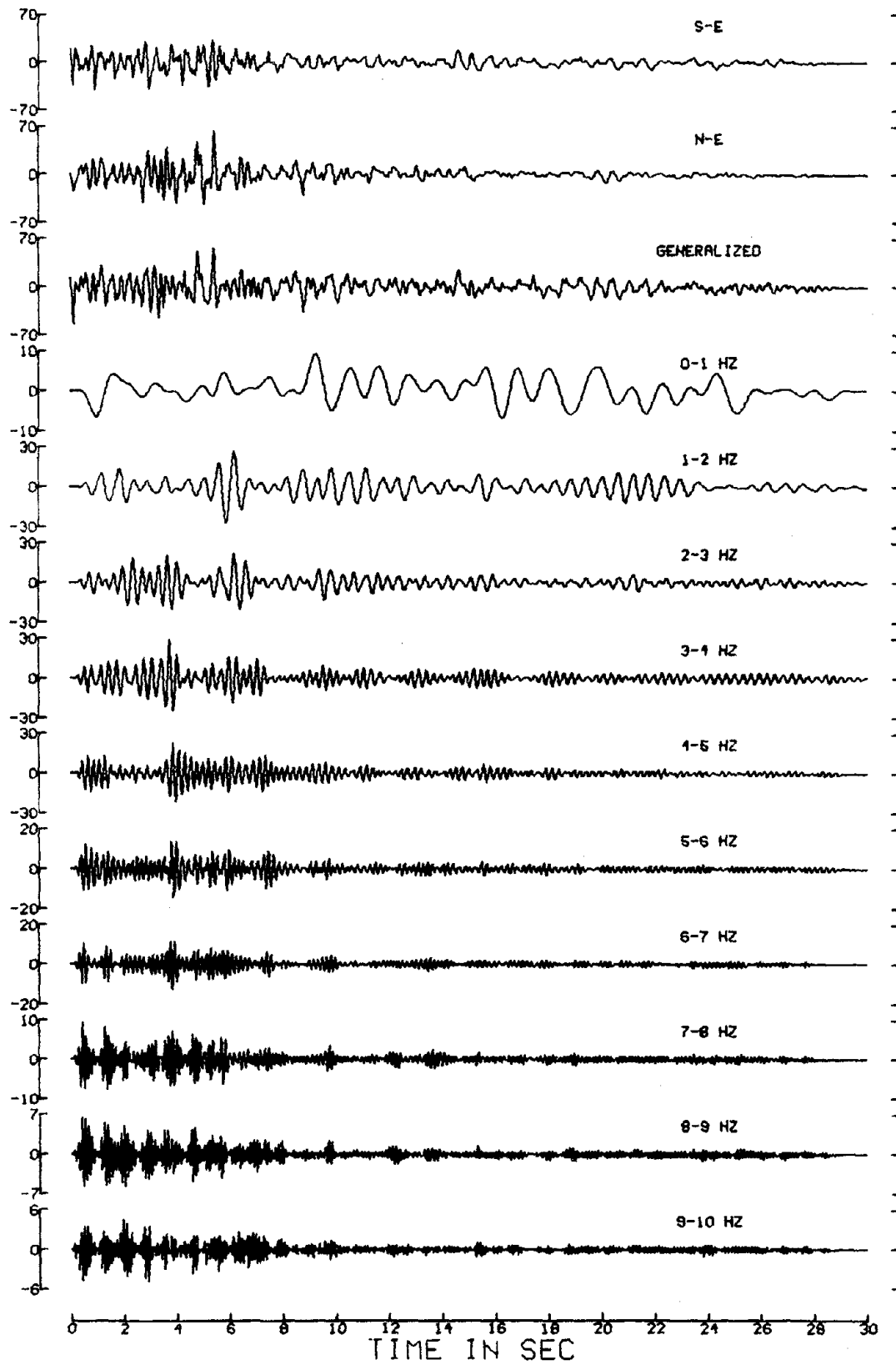


Fig. 2.12b

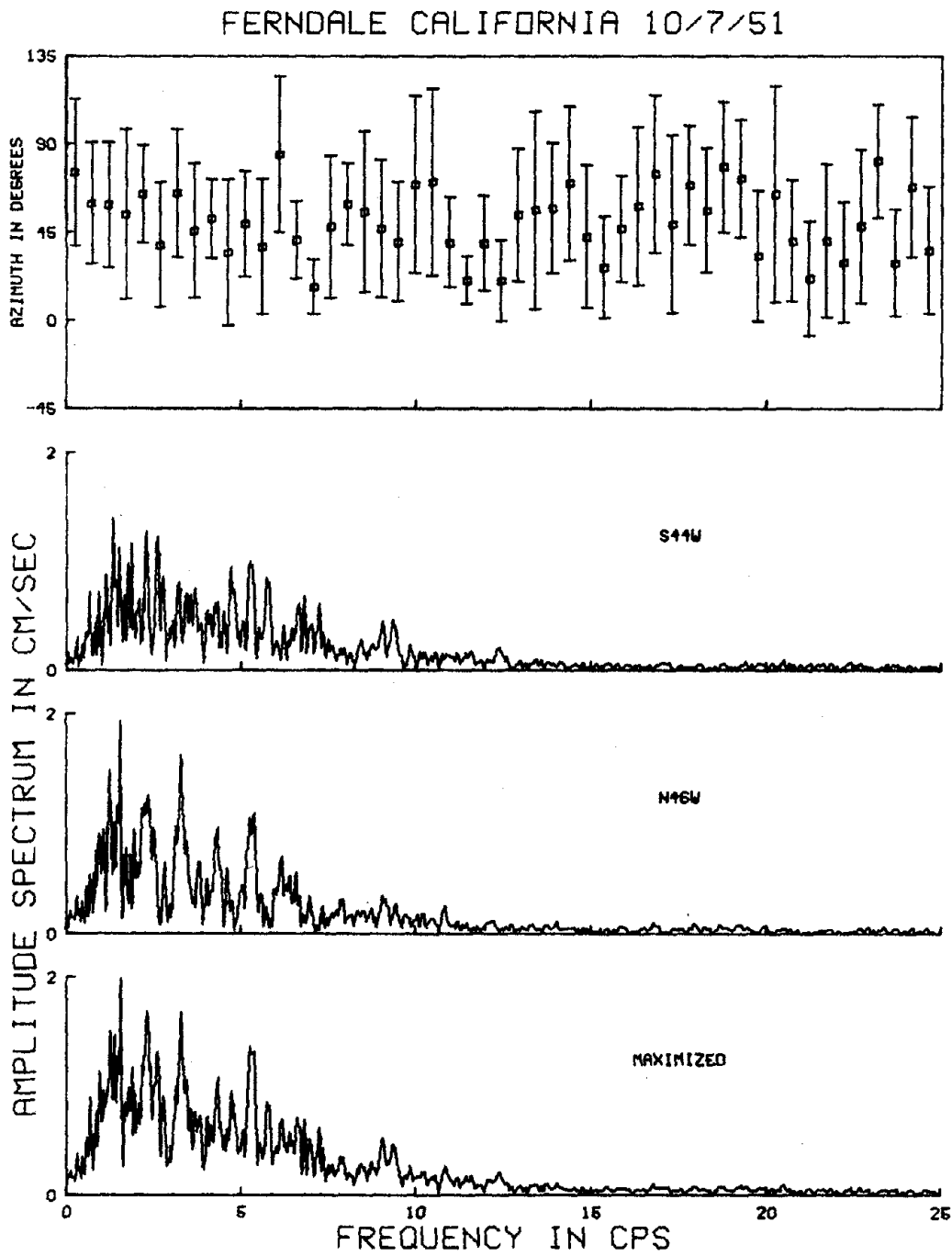


Fig. 2.13a

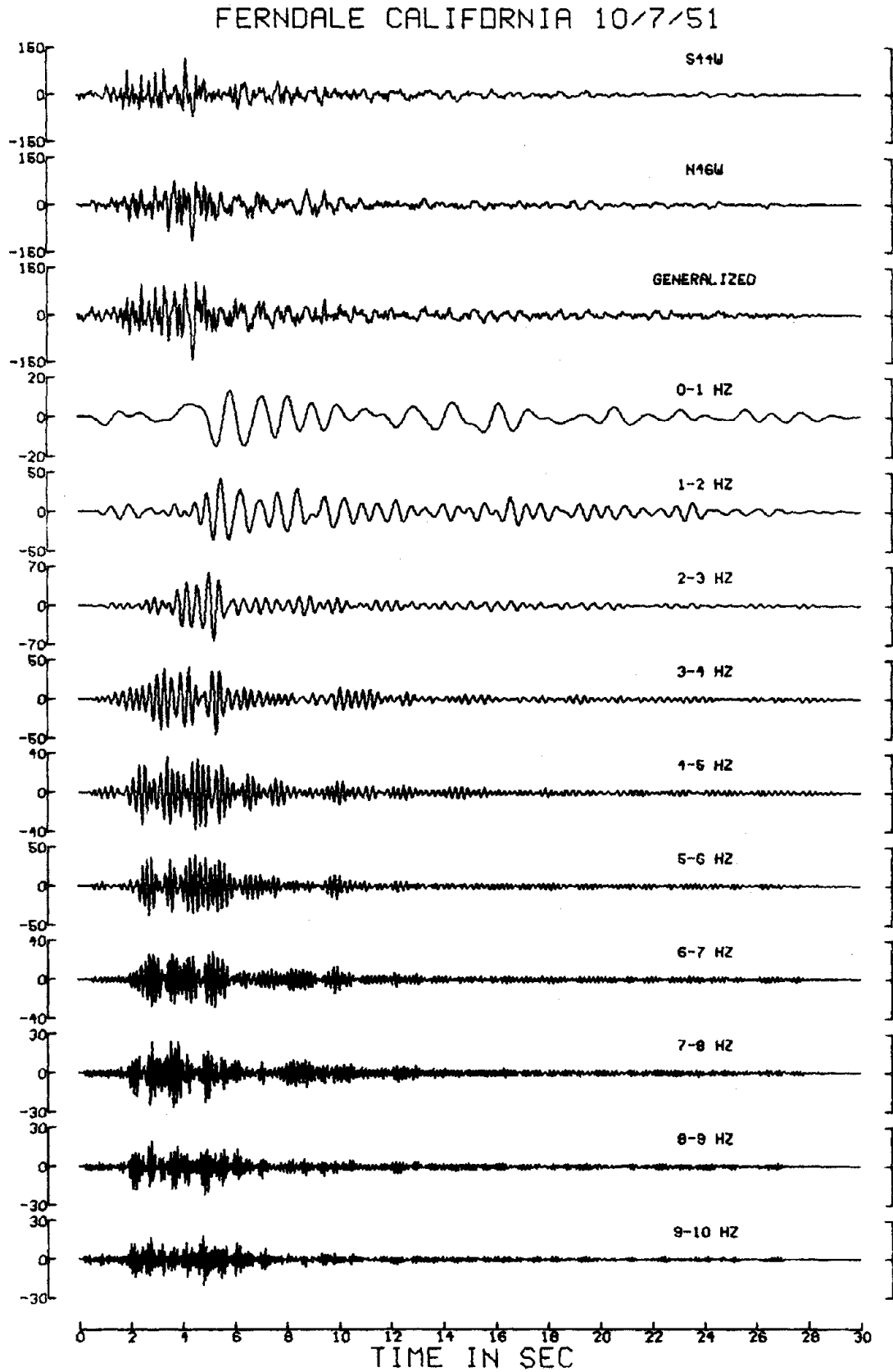


Fig. 2.13b

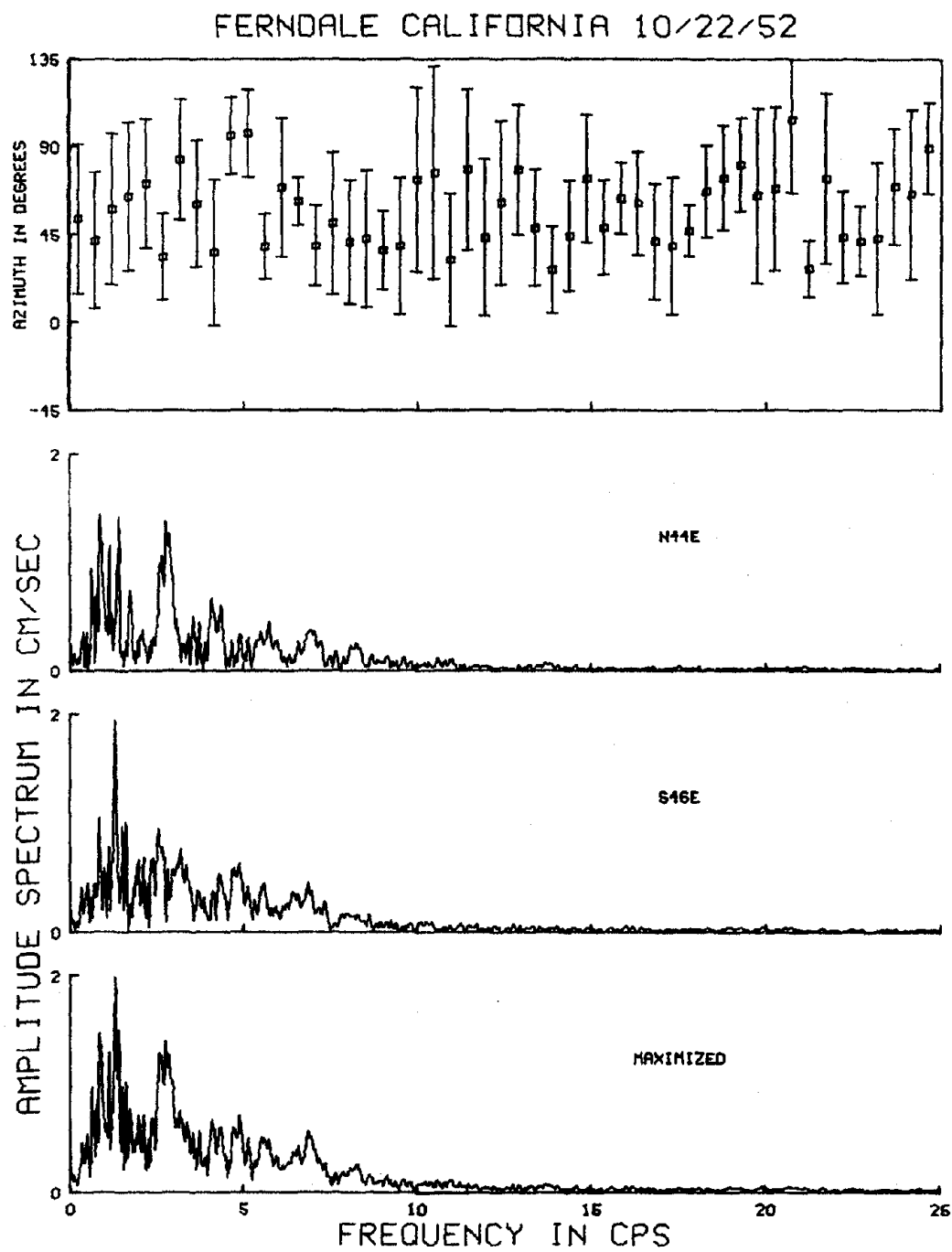


Fig. 2.14a

FERNDALE CALIFORNIA 10/22/52

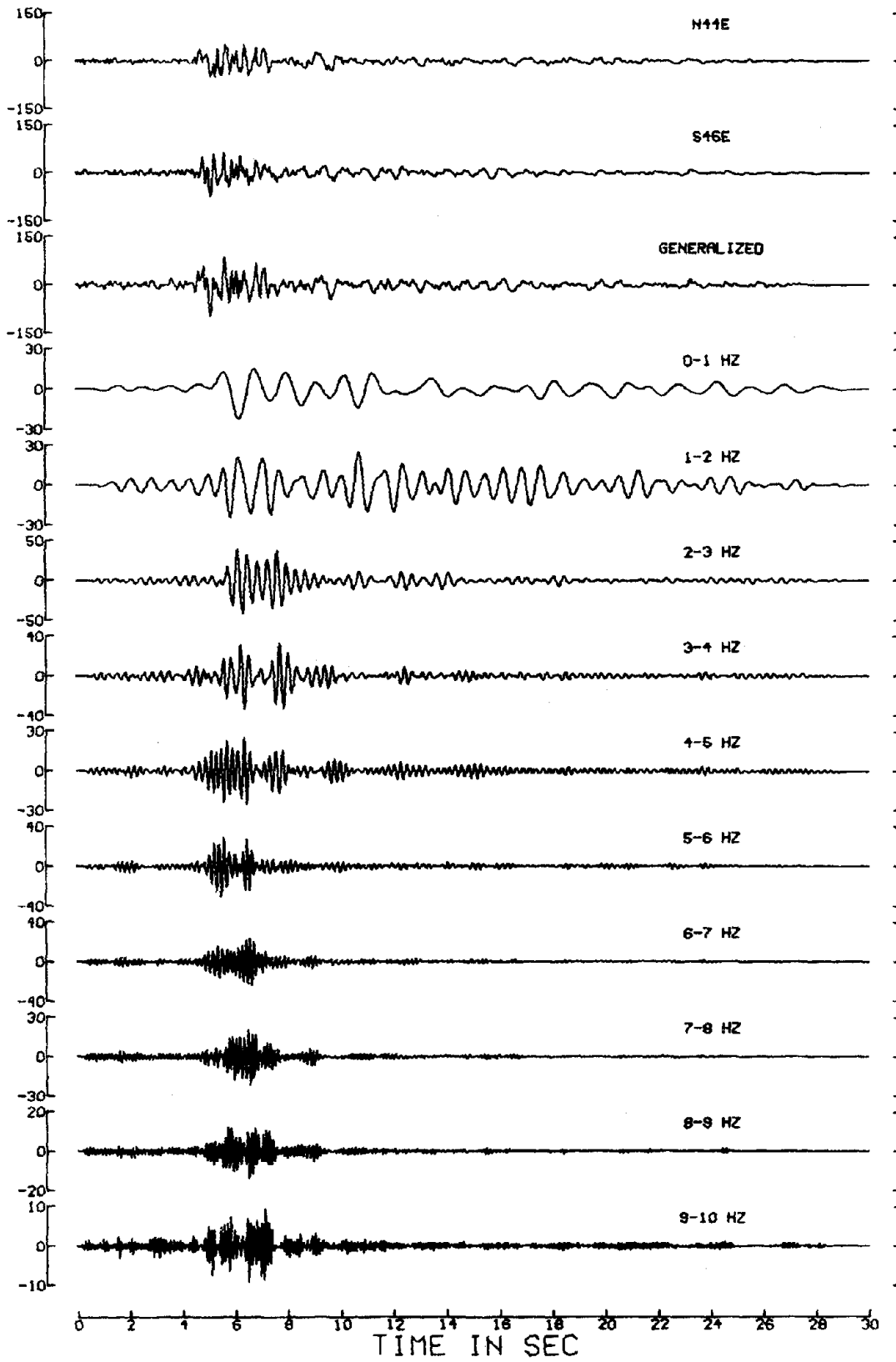


Fig. 2.14b

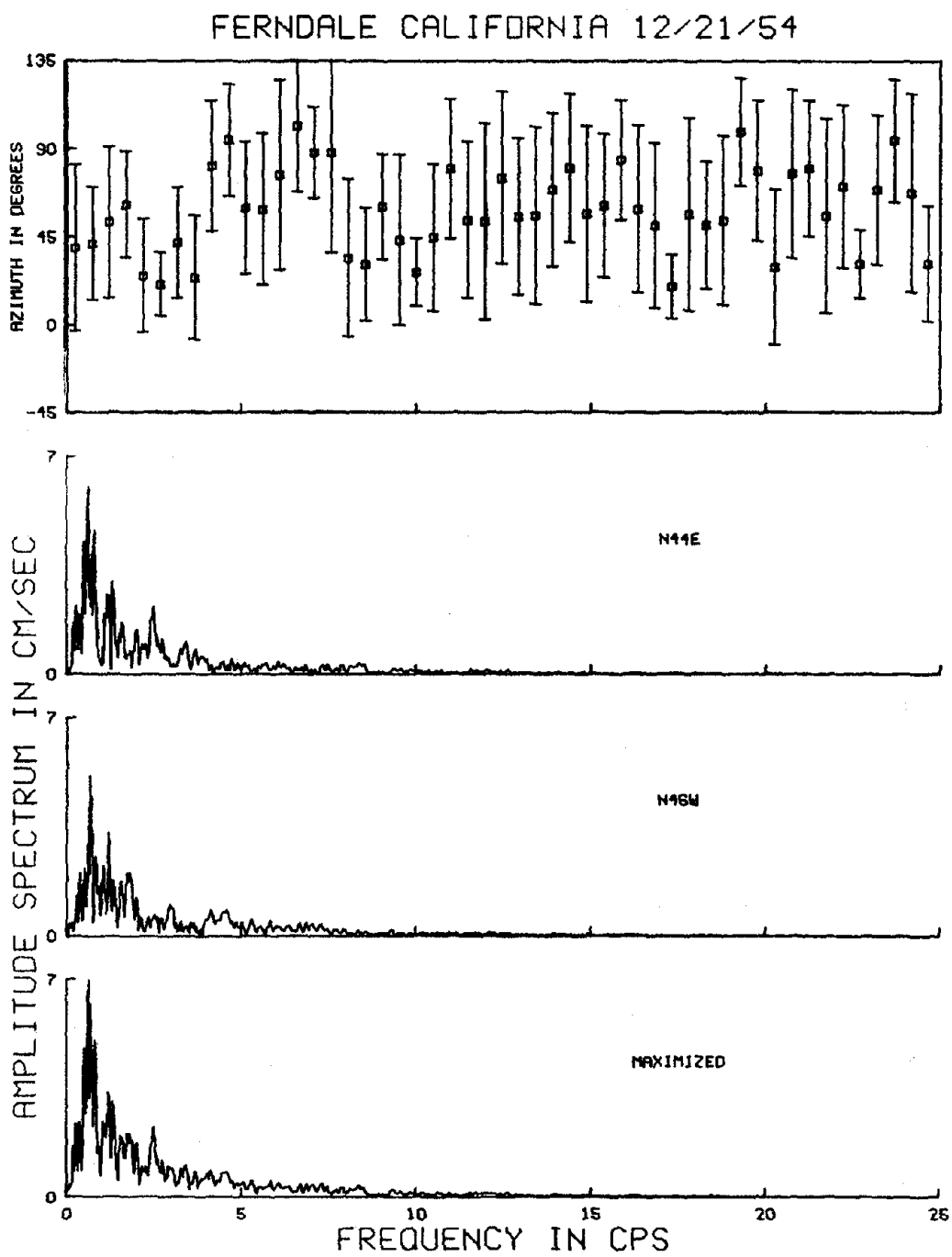


Fig. 2.15a

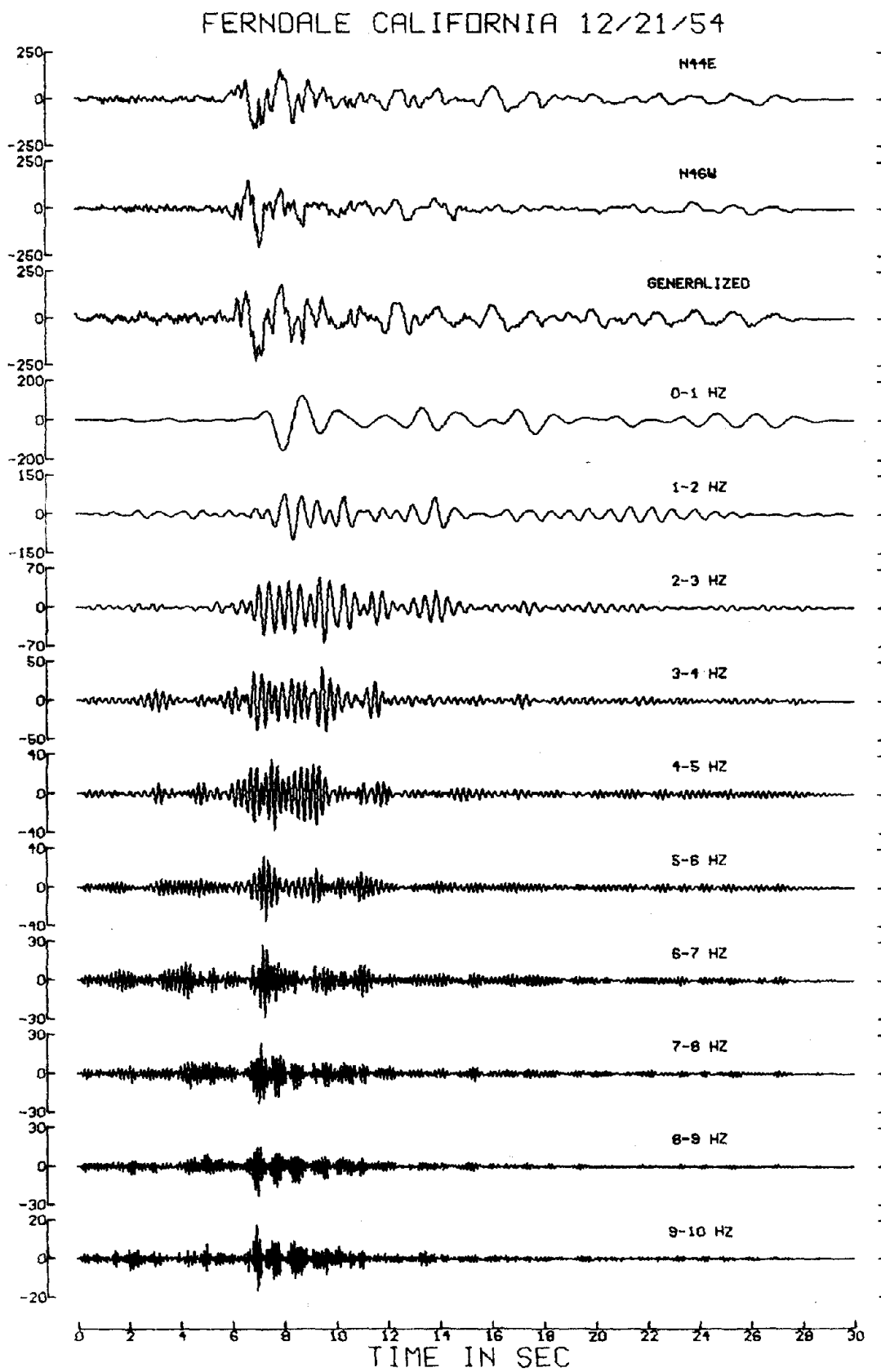


Fig. 2.15b

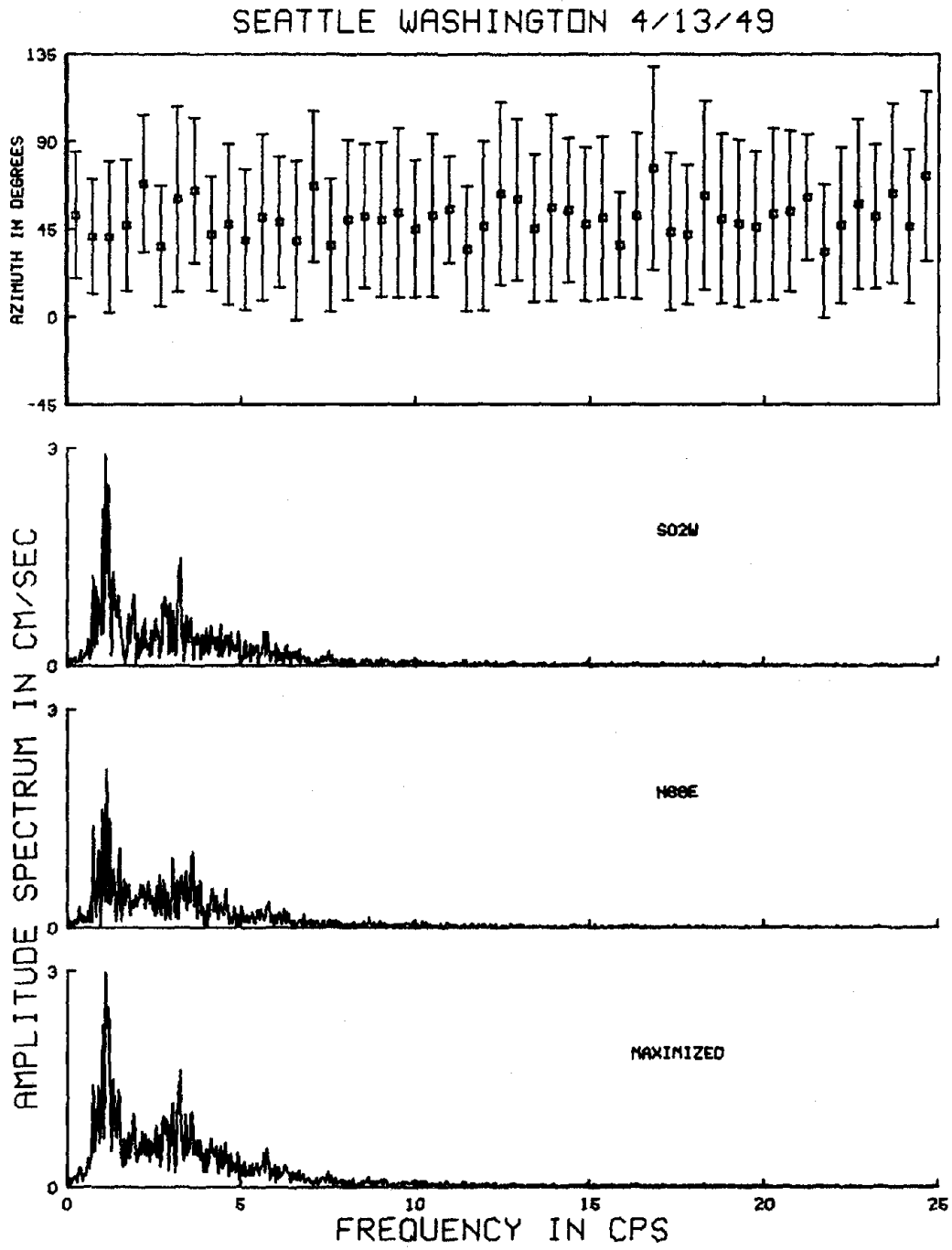


Fig. 2.16a

SEATTLE WASHINGTON 4/13/49

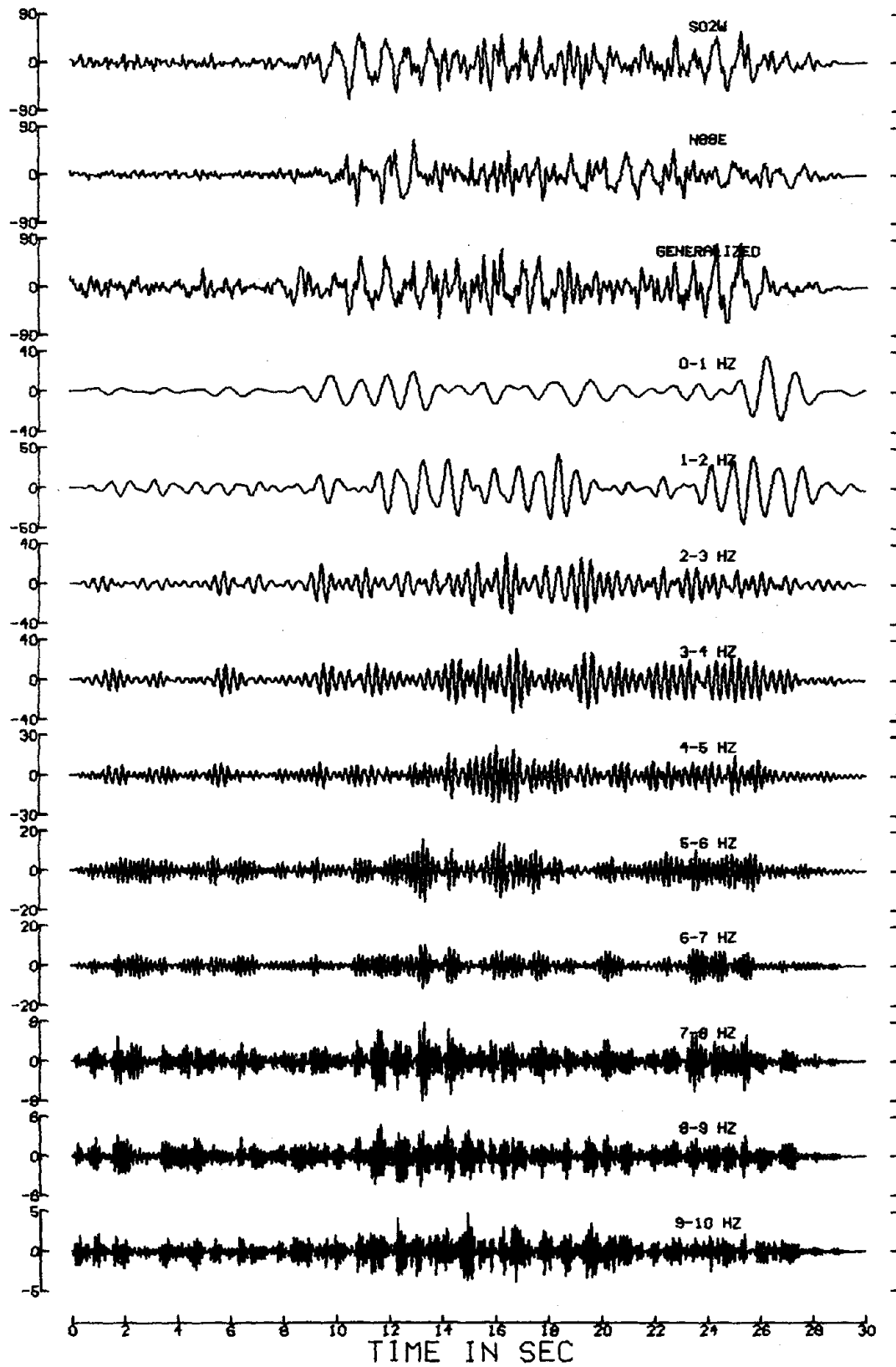


Fig. 2.16b

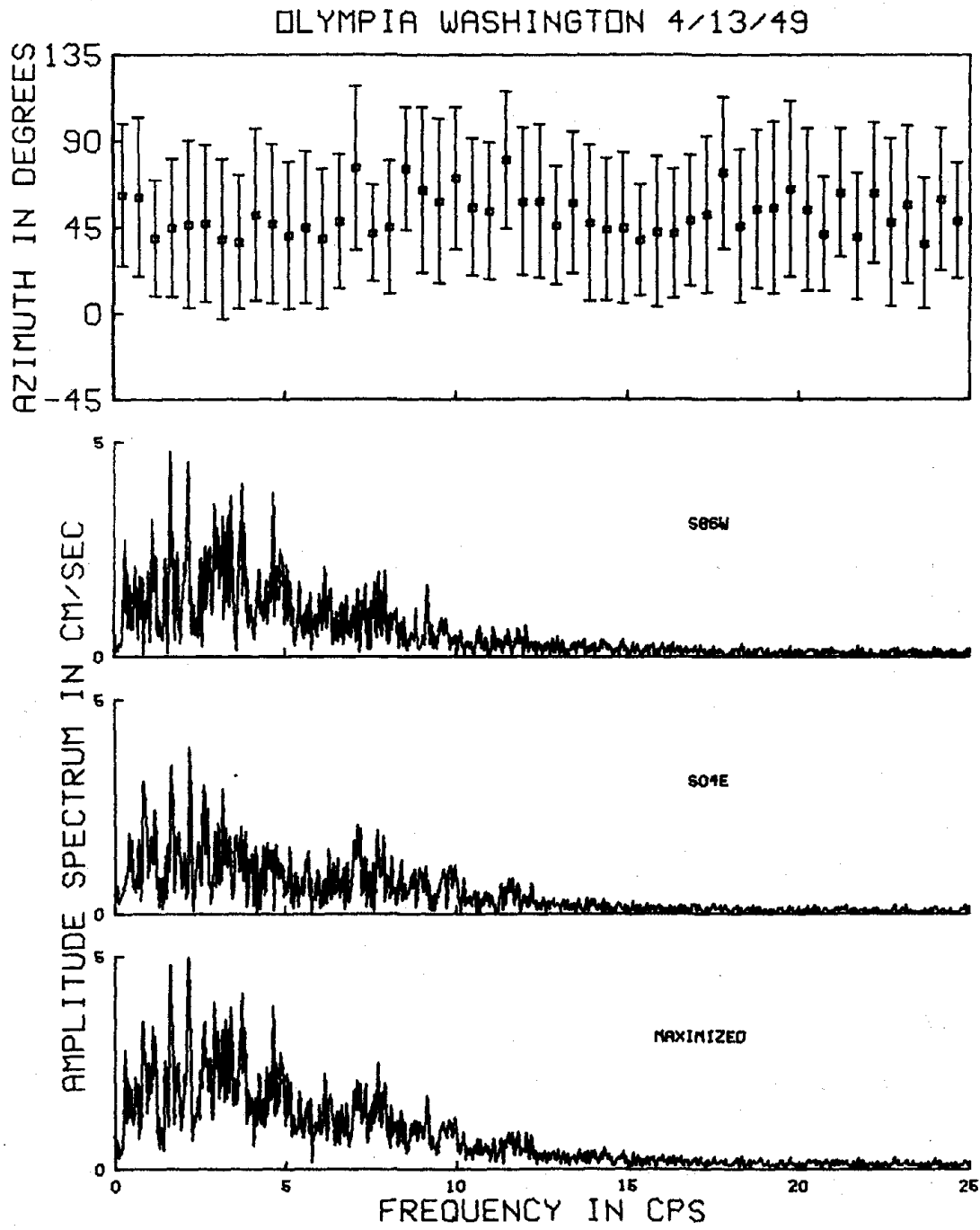


Fig. 2.17a

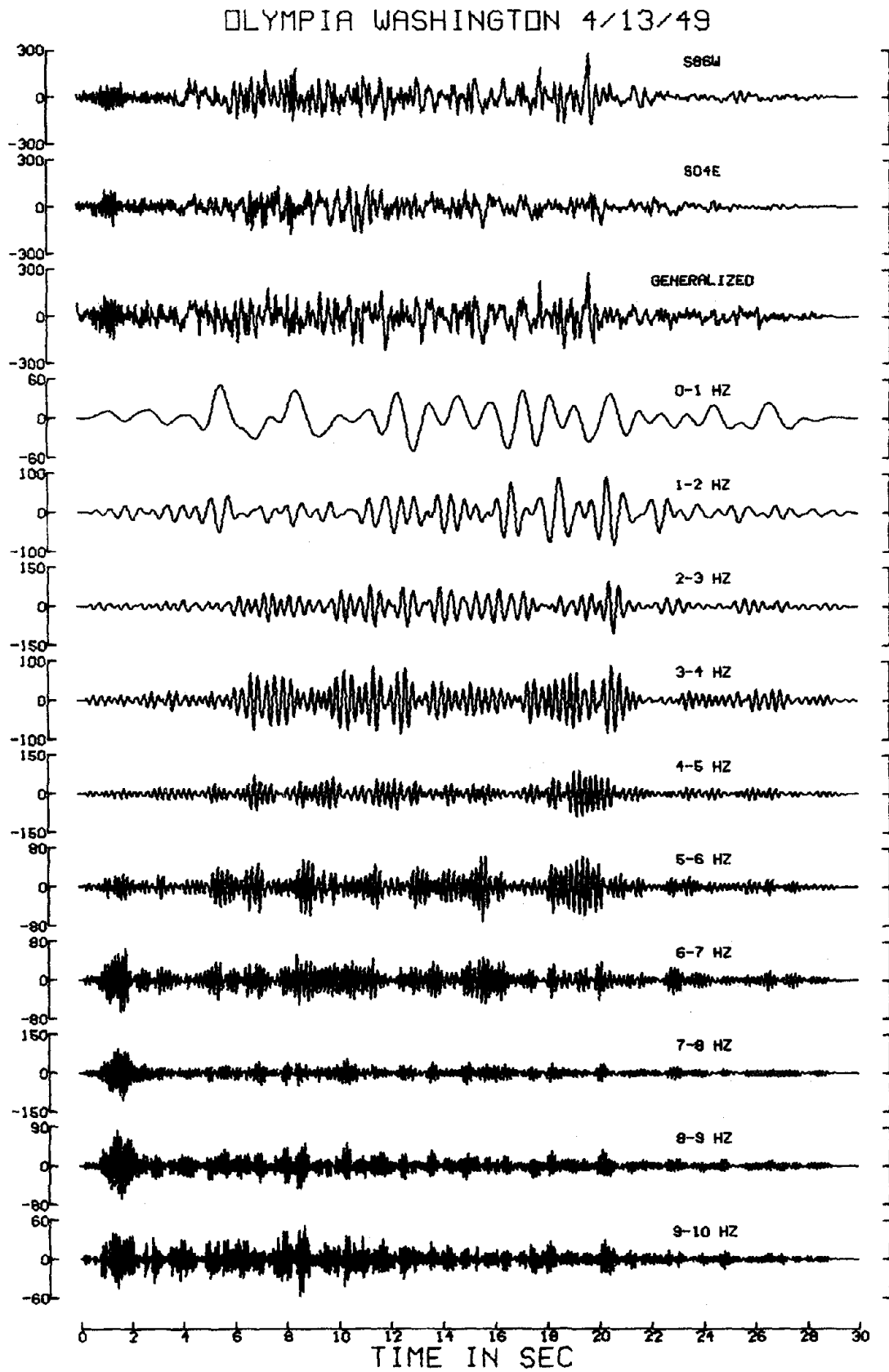


Fig. 2.17b

EUREKA CALIFORNIA 12/21/54

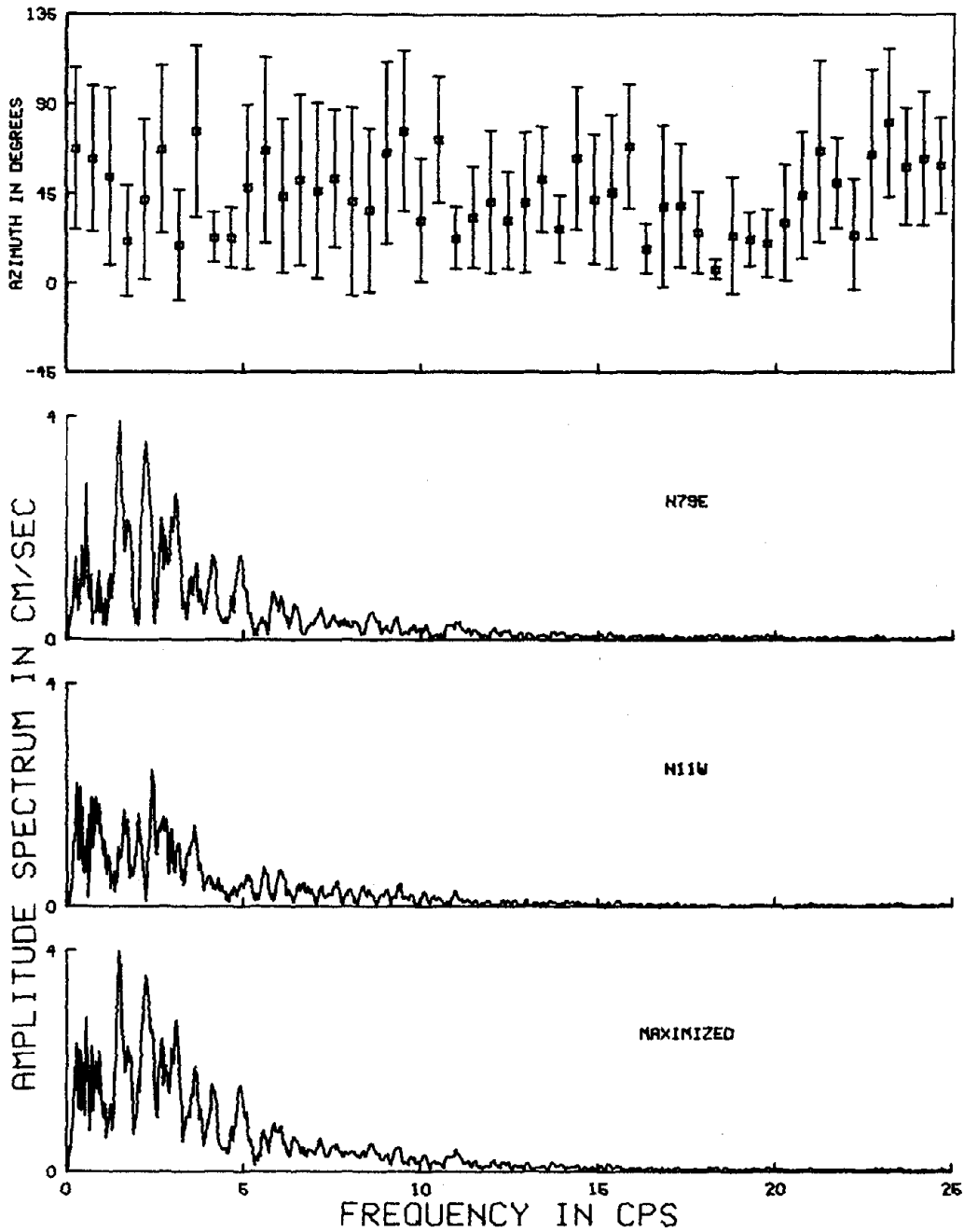


Fig. 2.18a

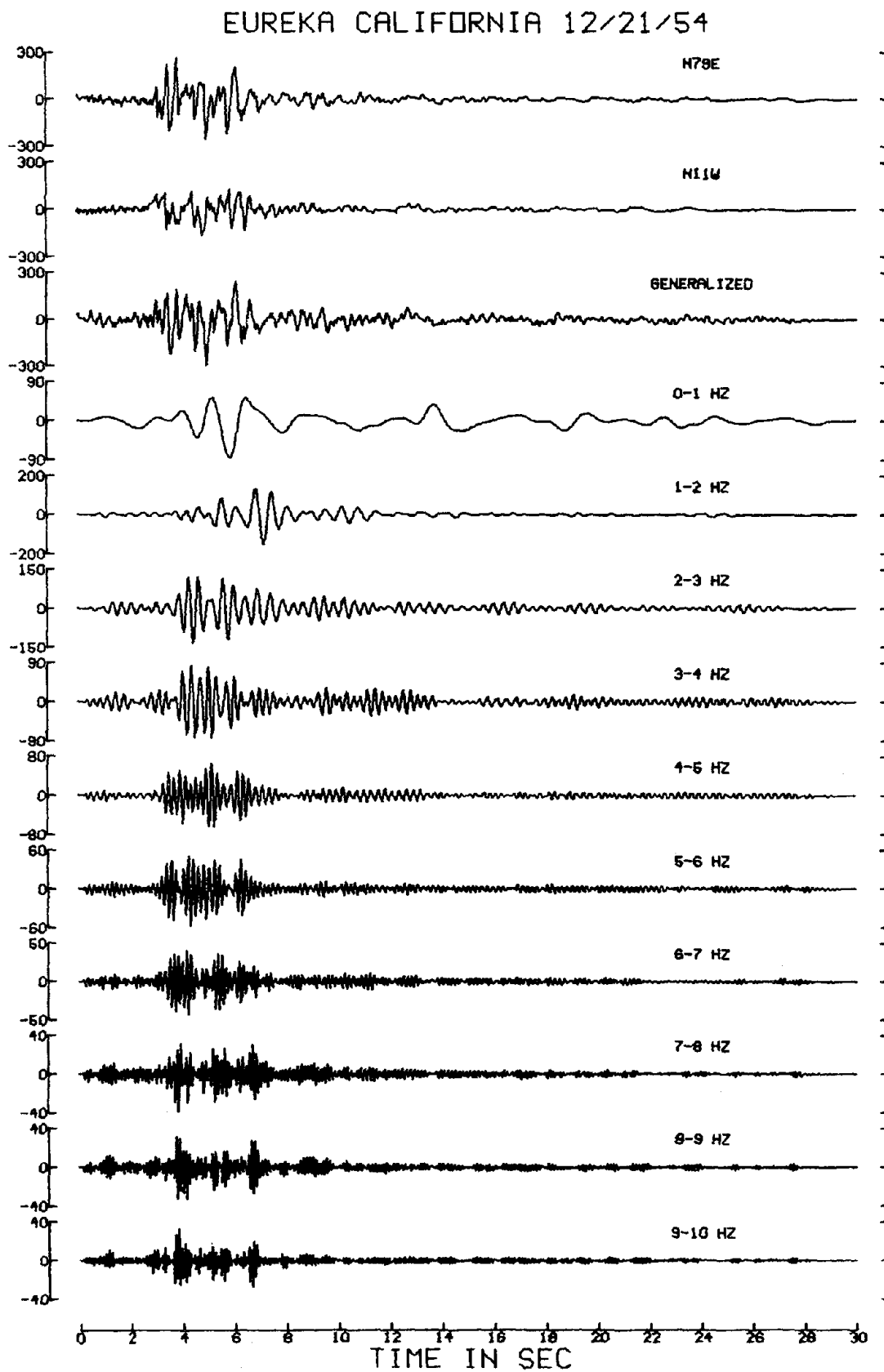


Fig. 2.18b

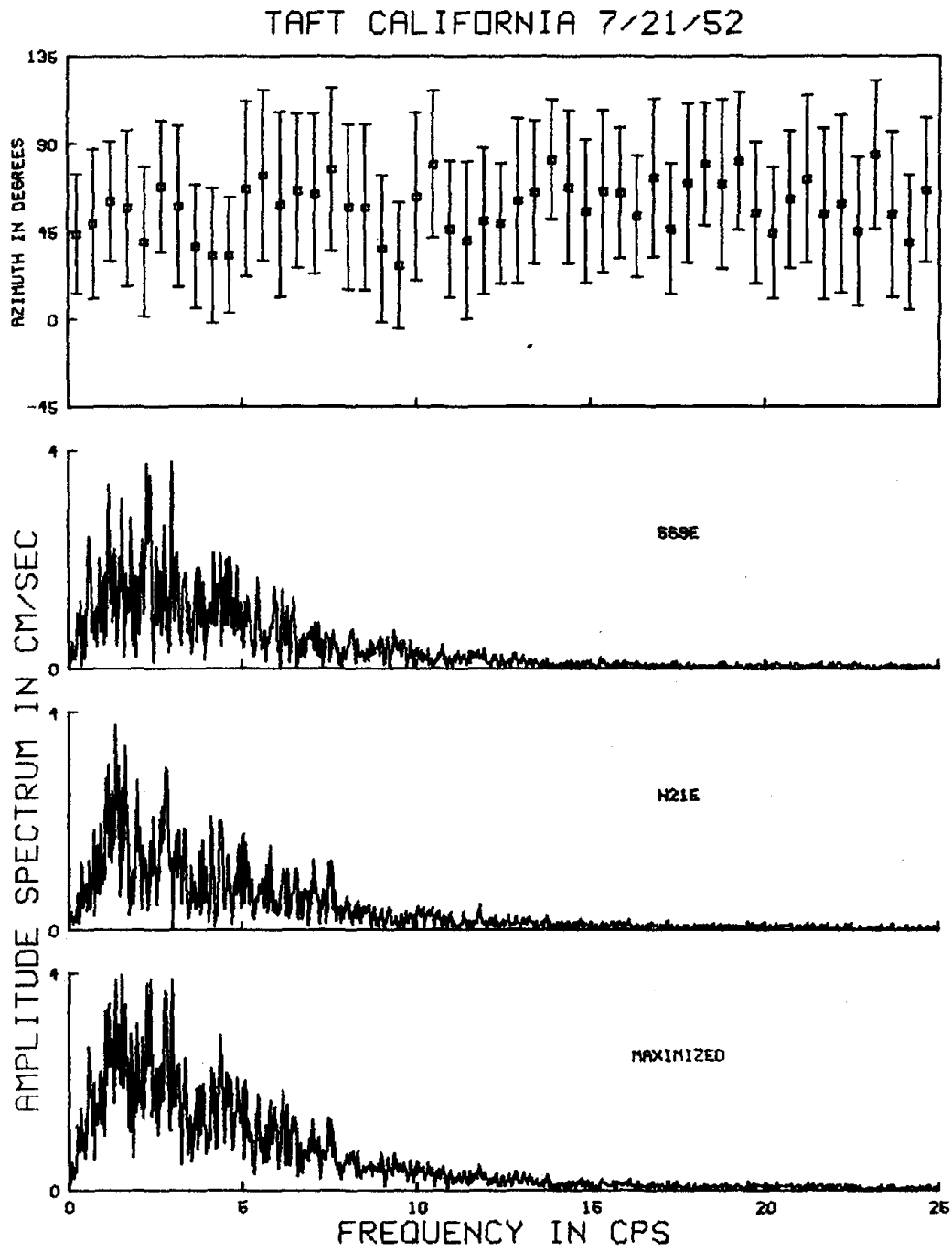


Fig. 2.19a

TAFT CALIFORNIA 7/21/52

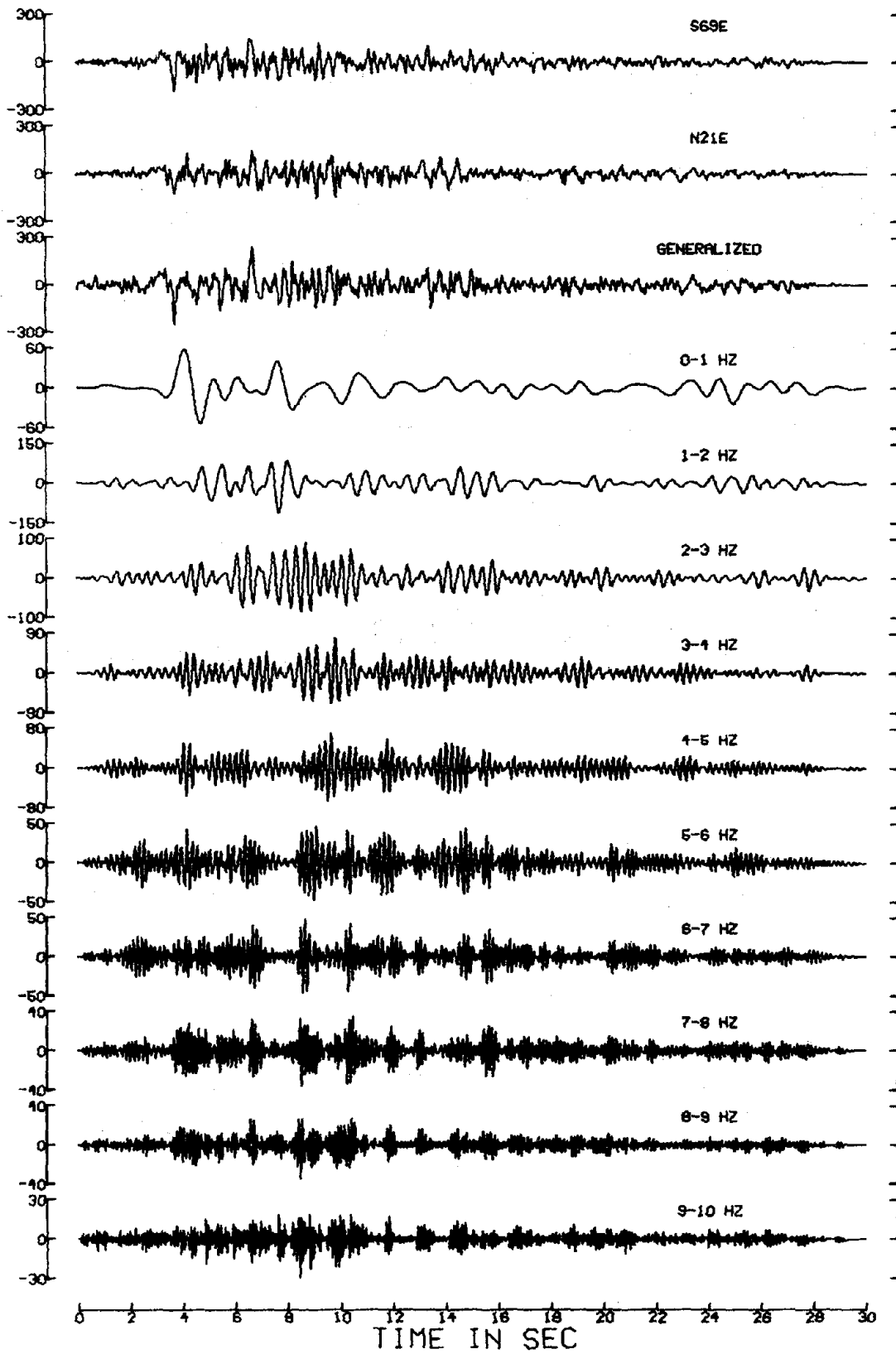


Fig. 2.19b

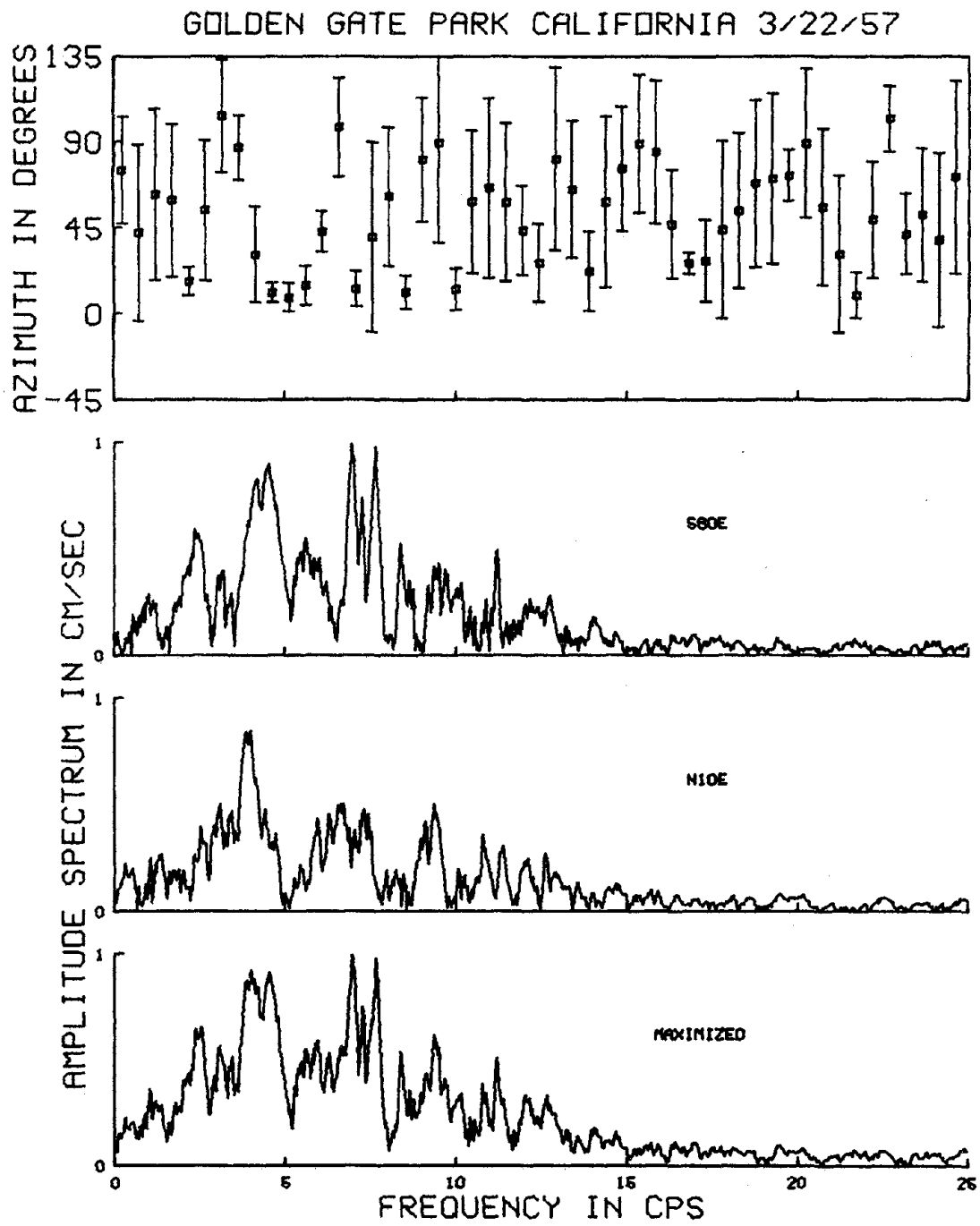


Fig. 2.20a

GOLDEN GATE PARK CALIFORNIA 3/22/57

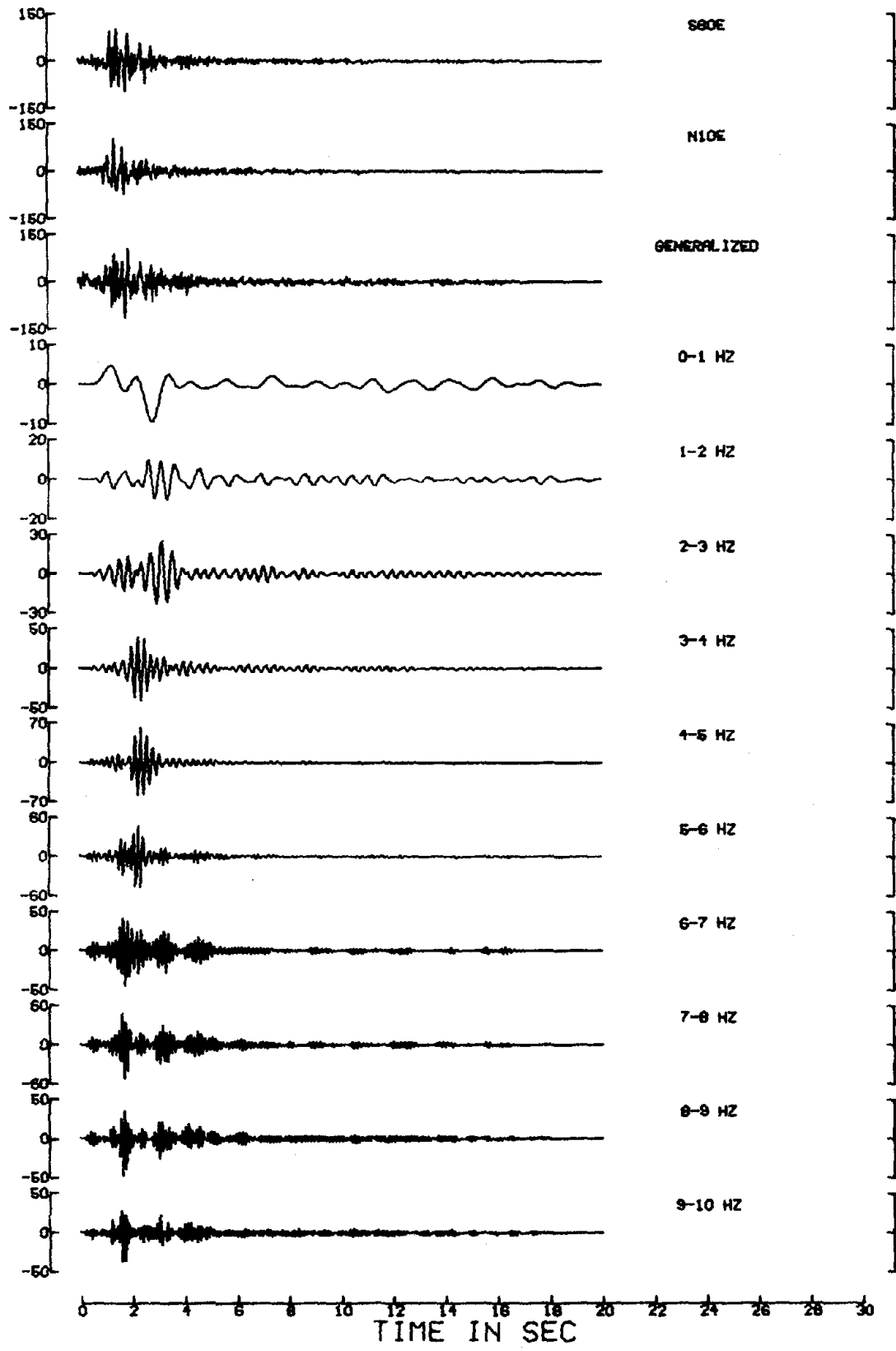


Fig. 2.20b

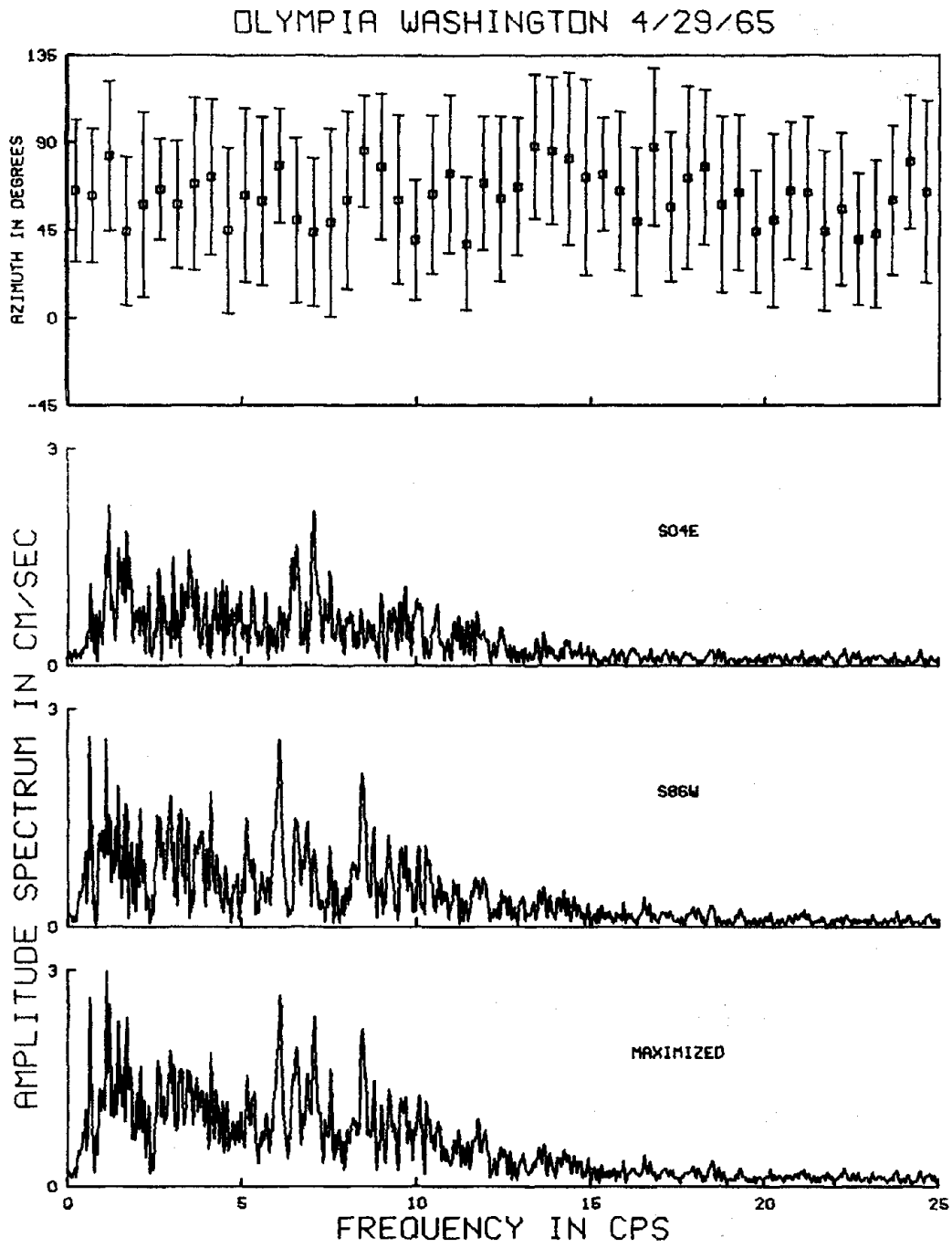


Fig. 2.21a

OLYMPIA WASHINGTON 4/29/65

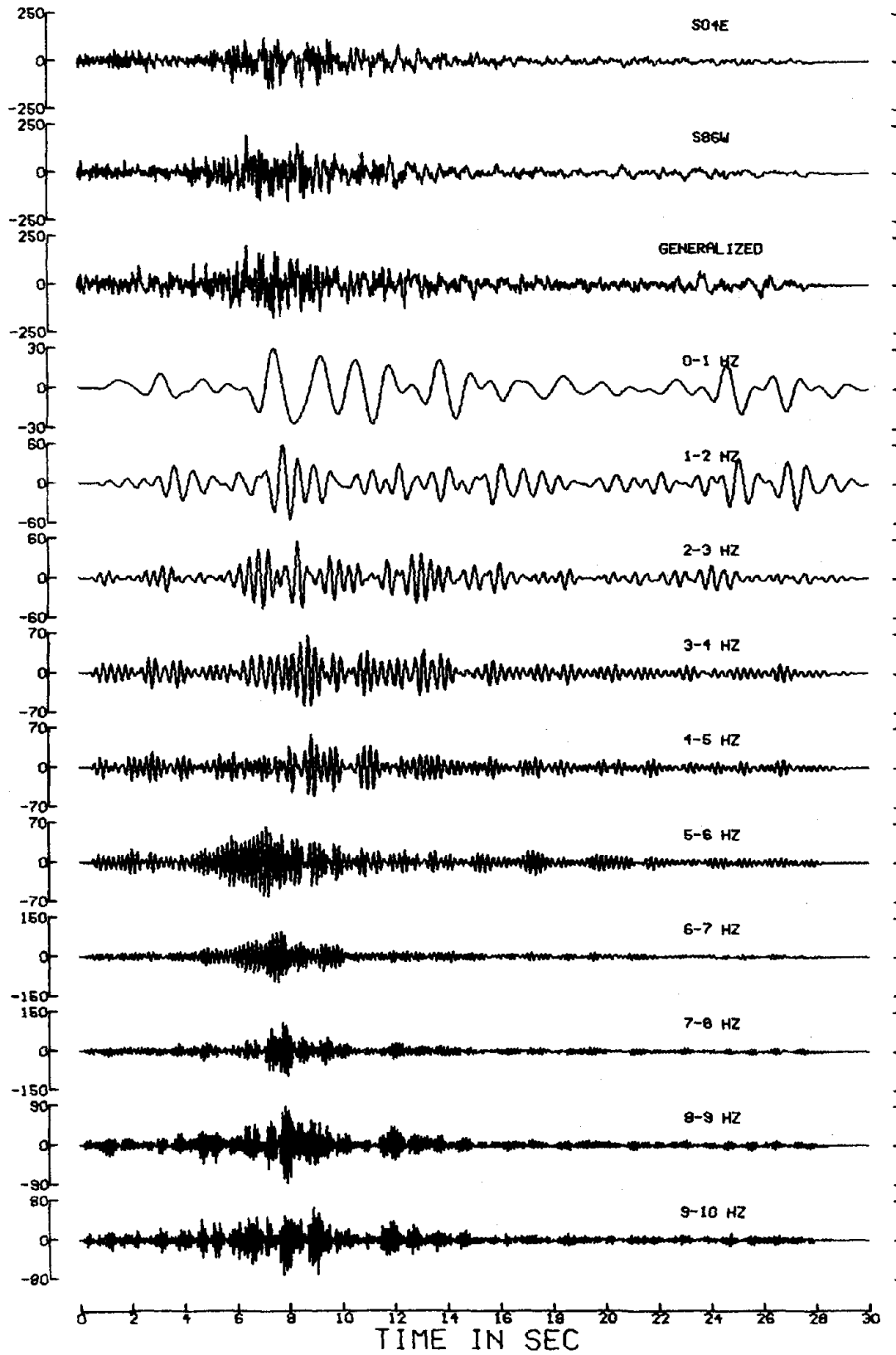


Fig. 2.21b

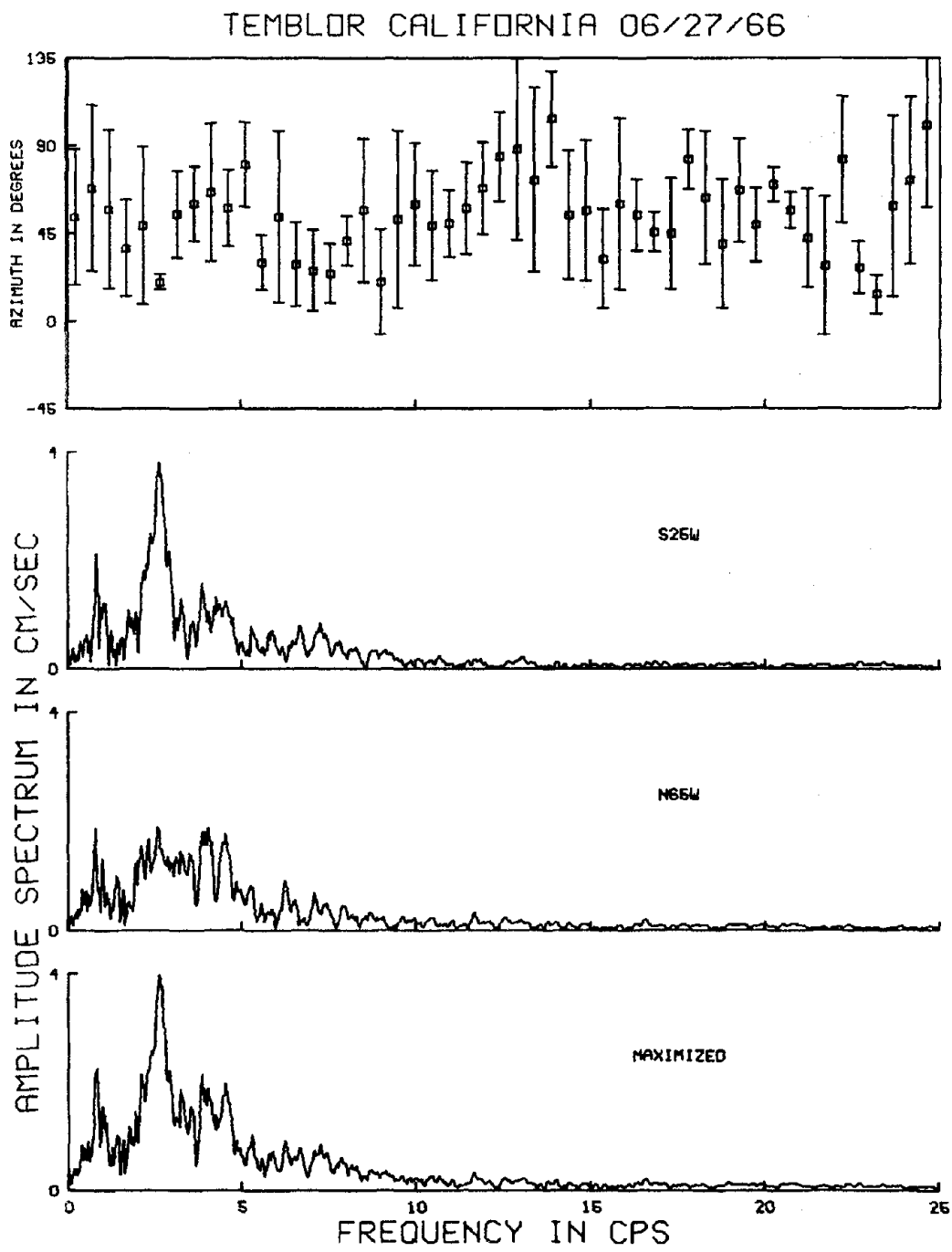


Fig. 2.22a

TEMBLOR CALIFORNIA 06/27/66

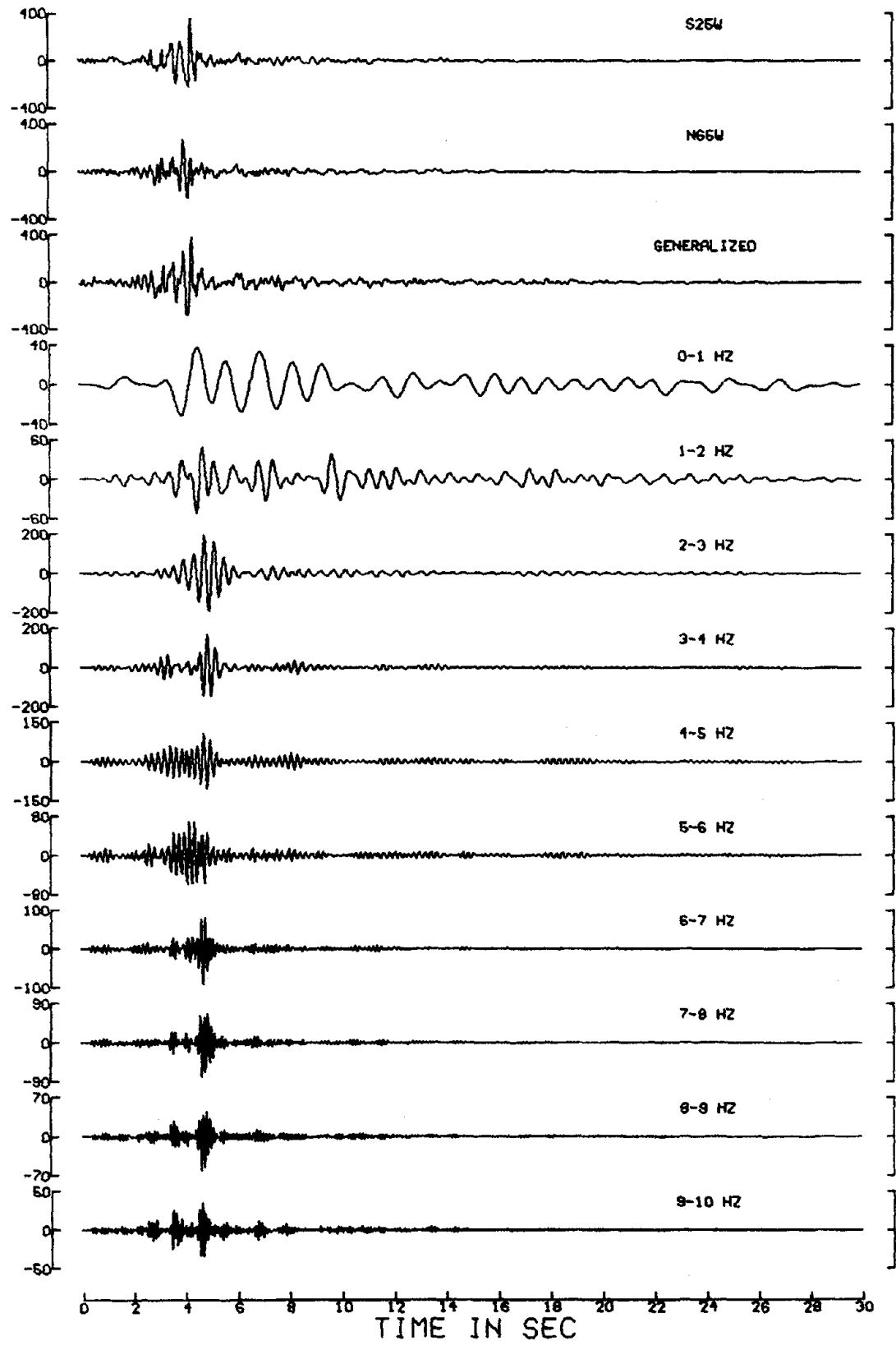


Fig. 2.22b

CH NO 5 PARKFIELD CALIFORNIA 06/27/66

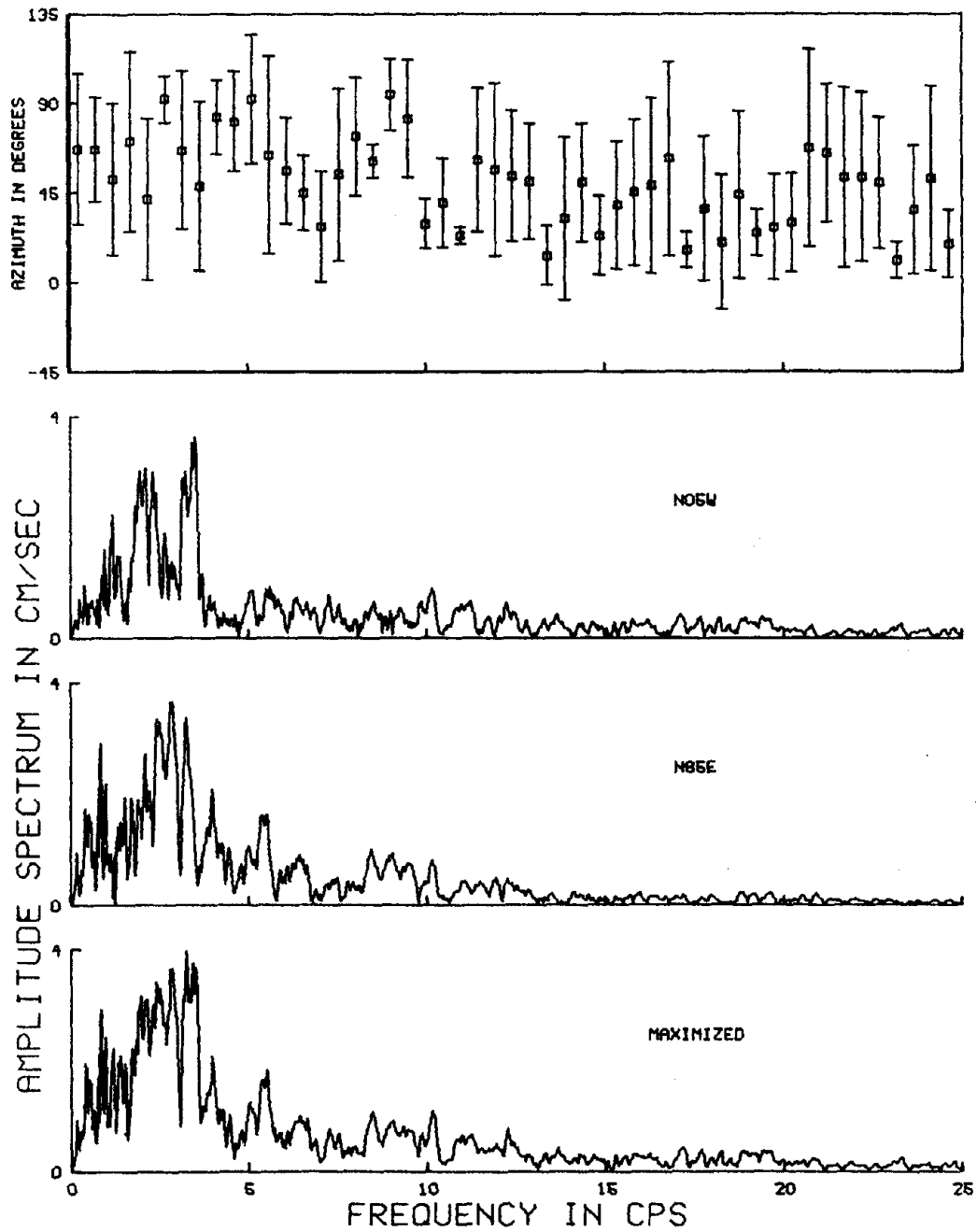


Fig. 2.23a

CH NO 5 PARKFIELD CALIFORNIA 06/27/66

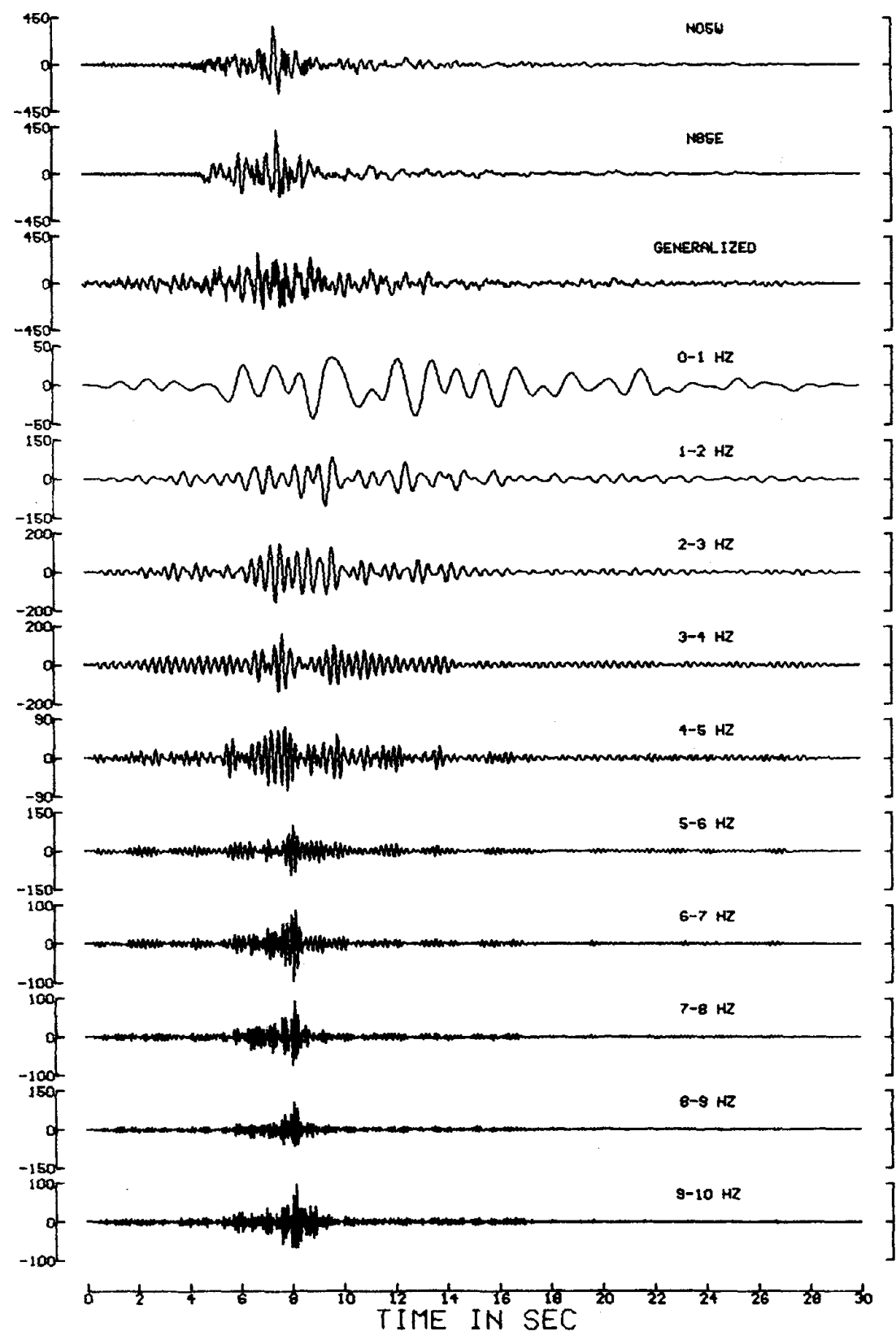


Fig. 2.23b

CH NO 8 PARKFIELD CALIFORNIA 06/27/66

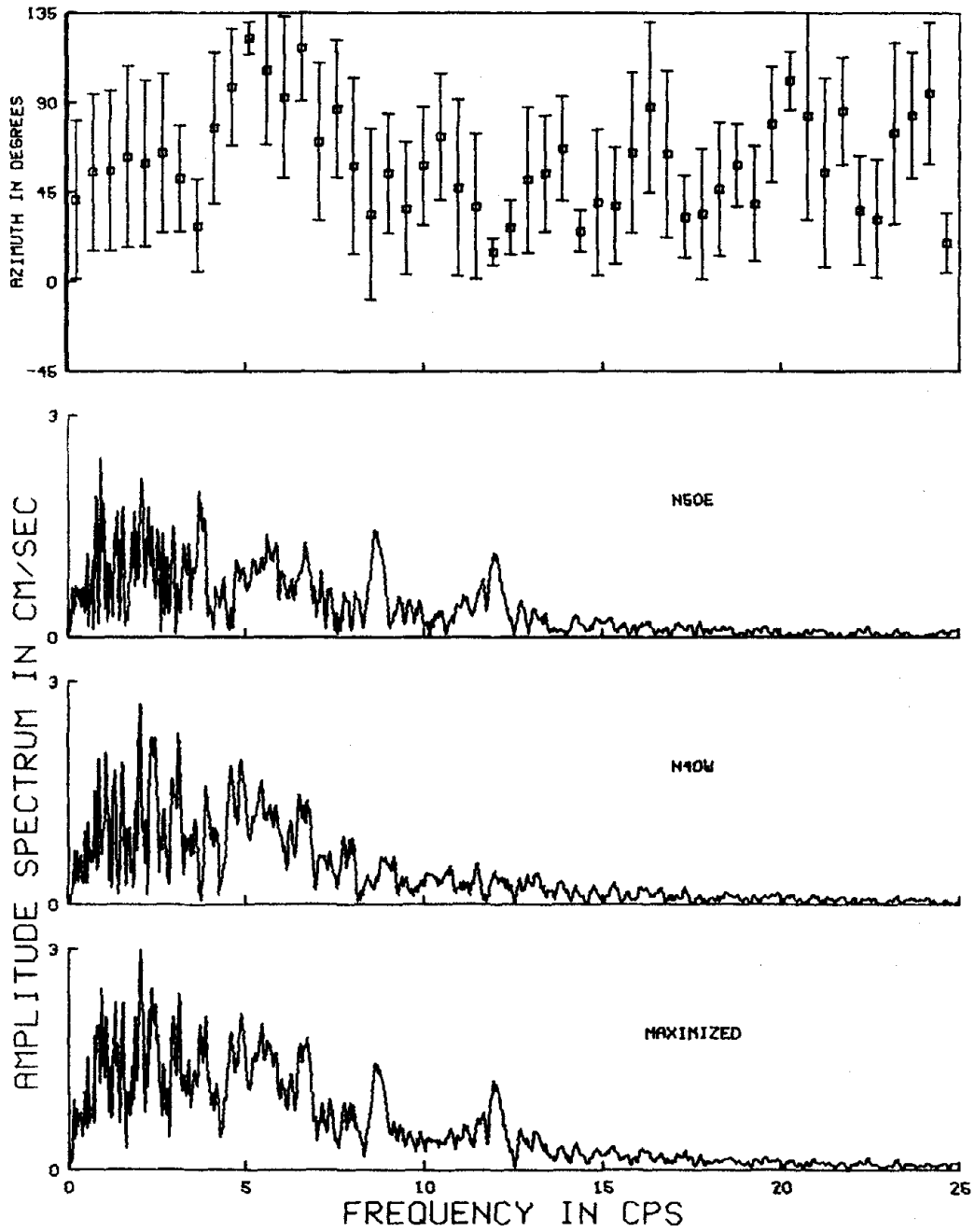


Fig. 2.24a

CH NO 8 PARKFIELD CALIFORNIA 06/27/66

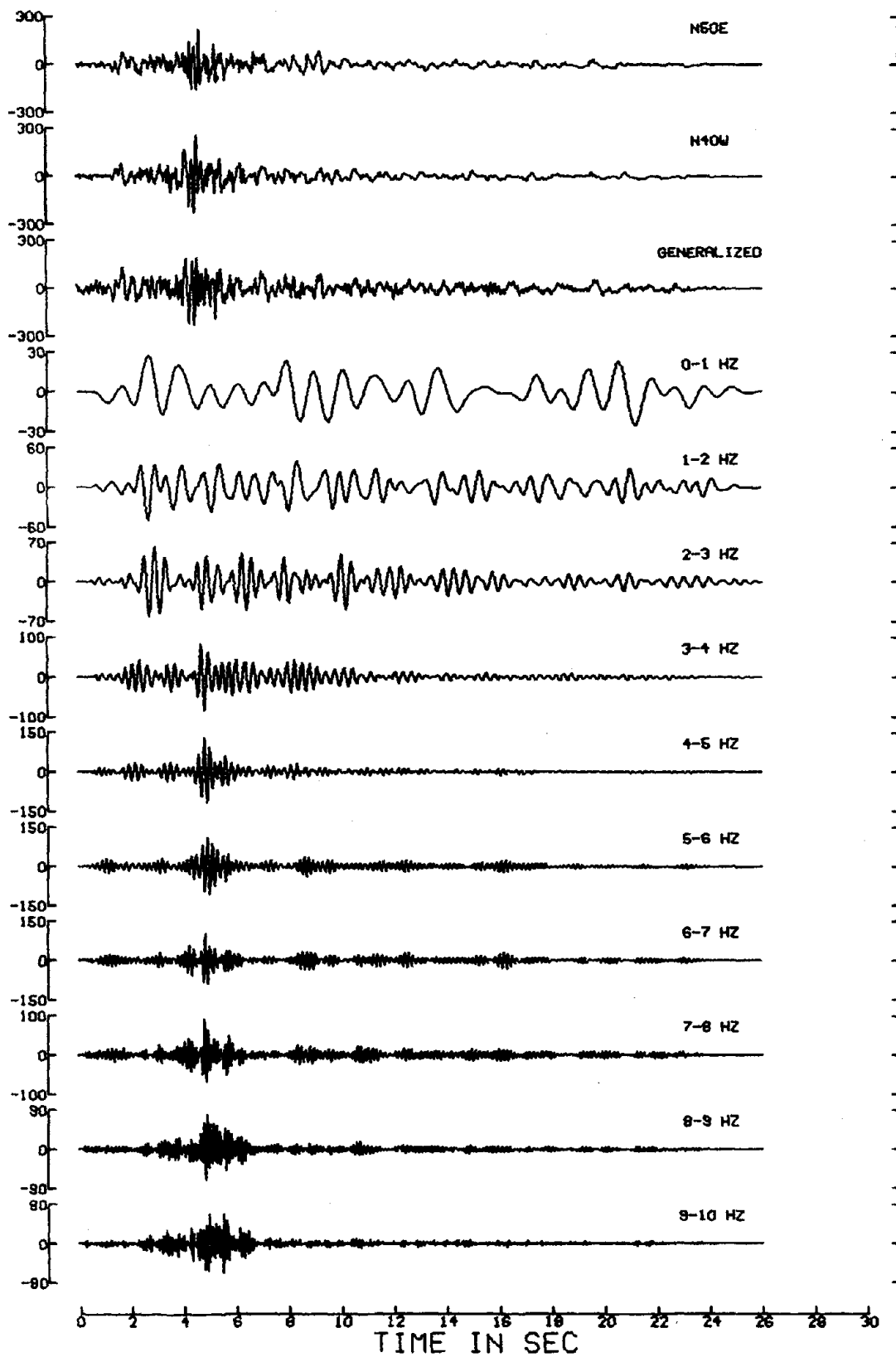


Fig. 2.24b

CH NO 12 PARKFIELD CALIFORNIA 06/27/66

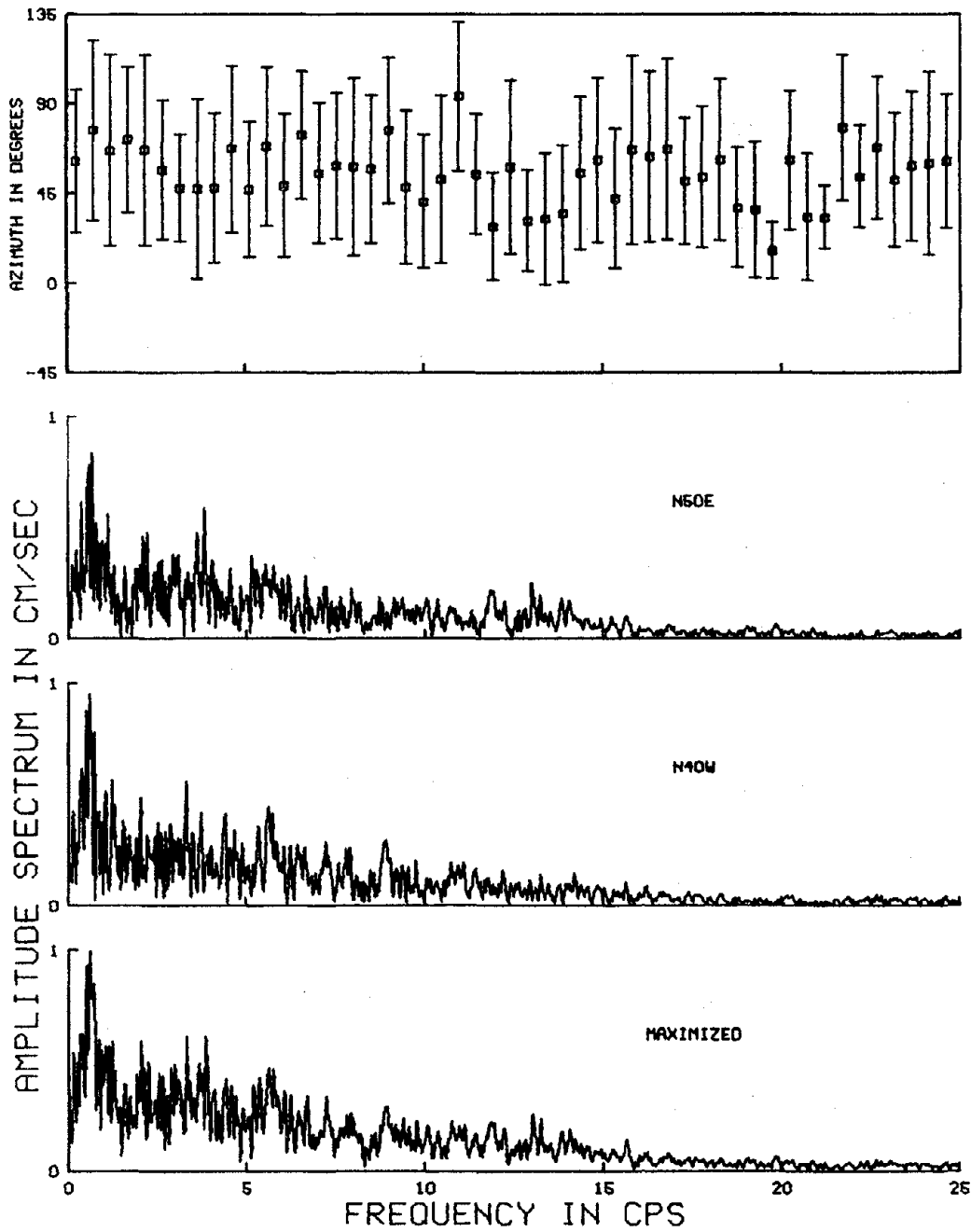


Fig. 2.25a

CH NO 12 PARKFIELD CALIFORNIA 06/27/66

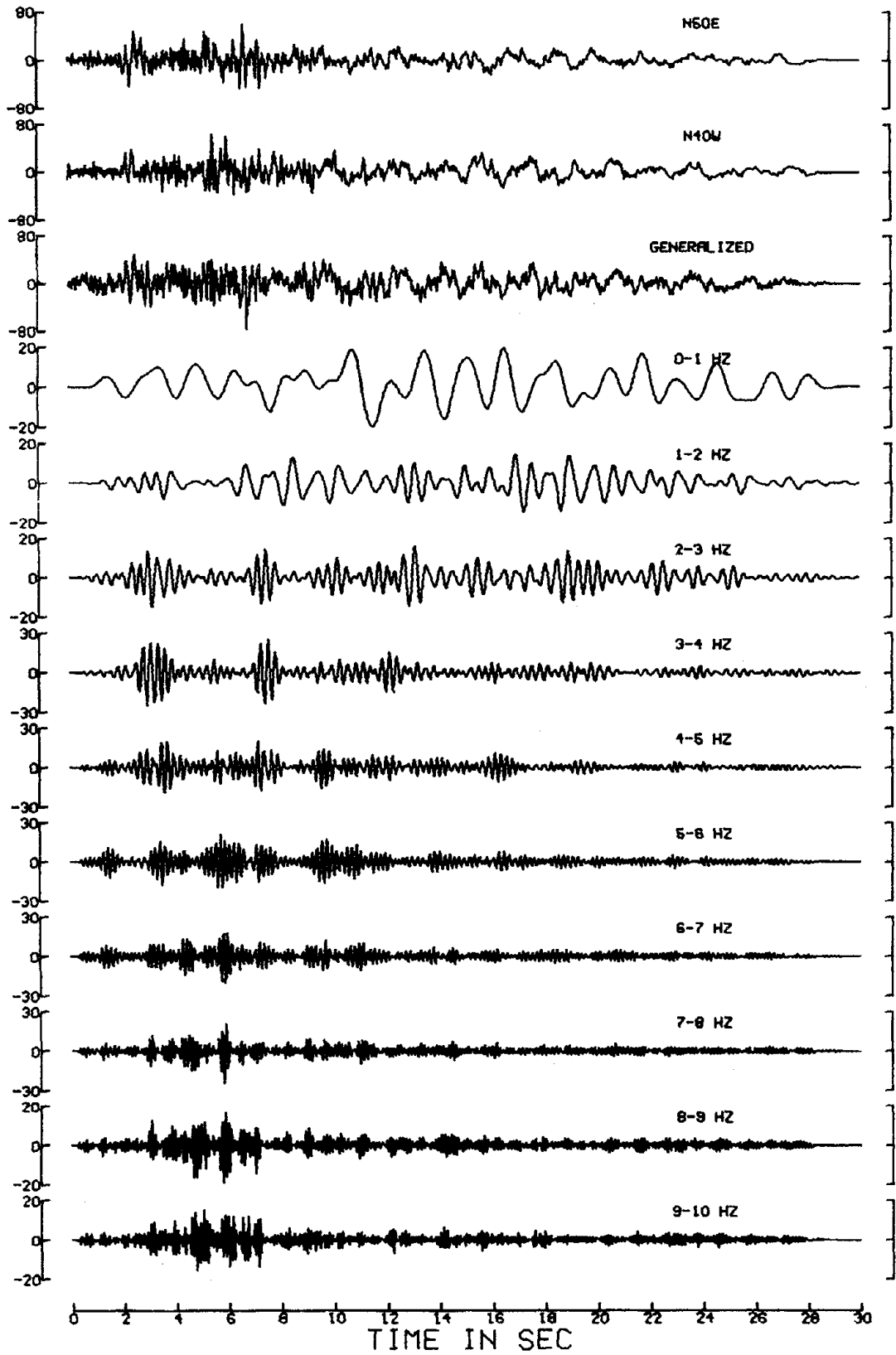


Fig. 2.25b

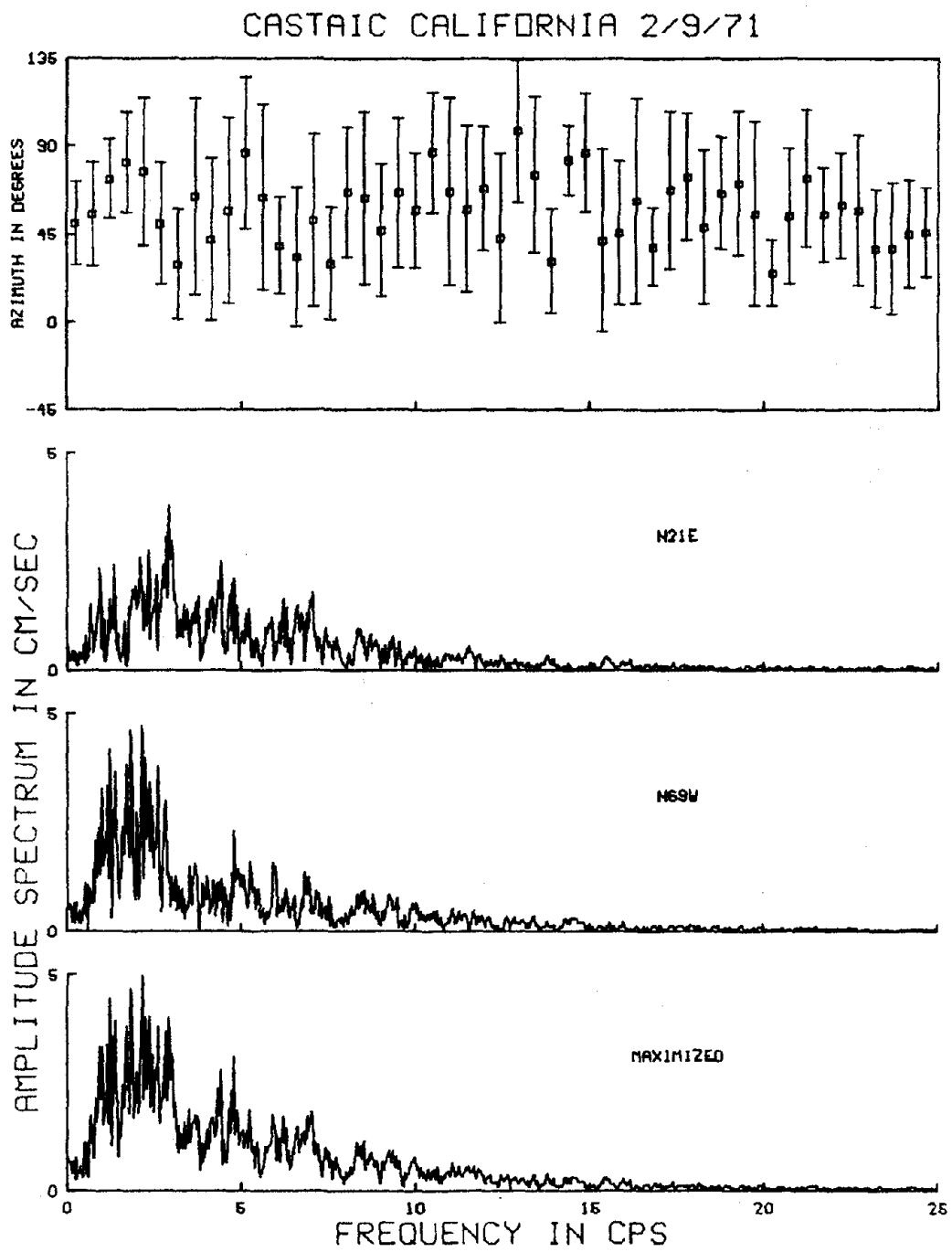


Fig. 2.26a

CASTAIC CALIFORNIA 2/9/71

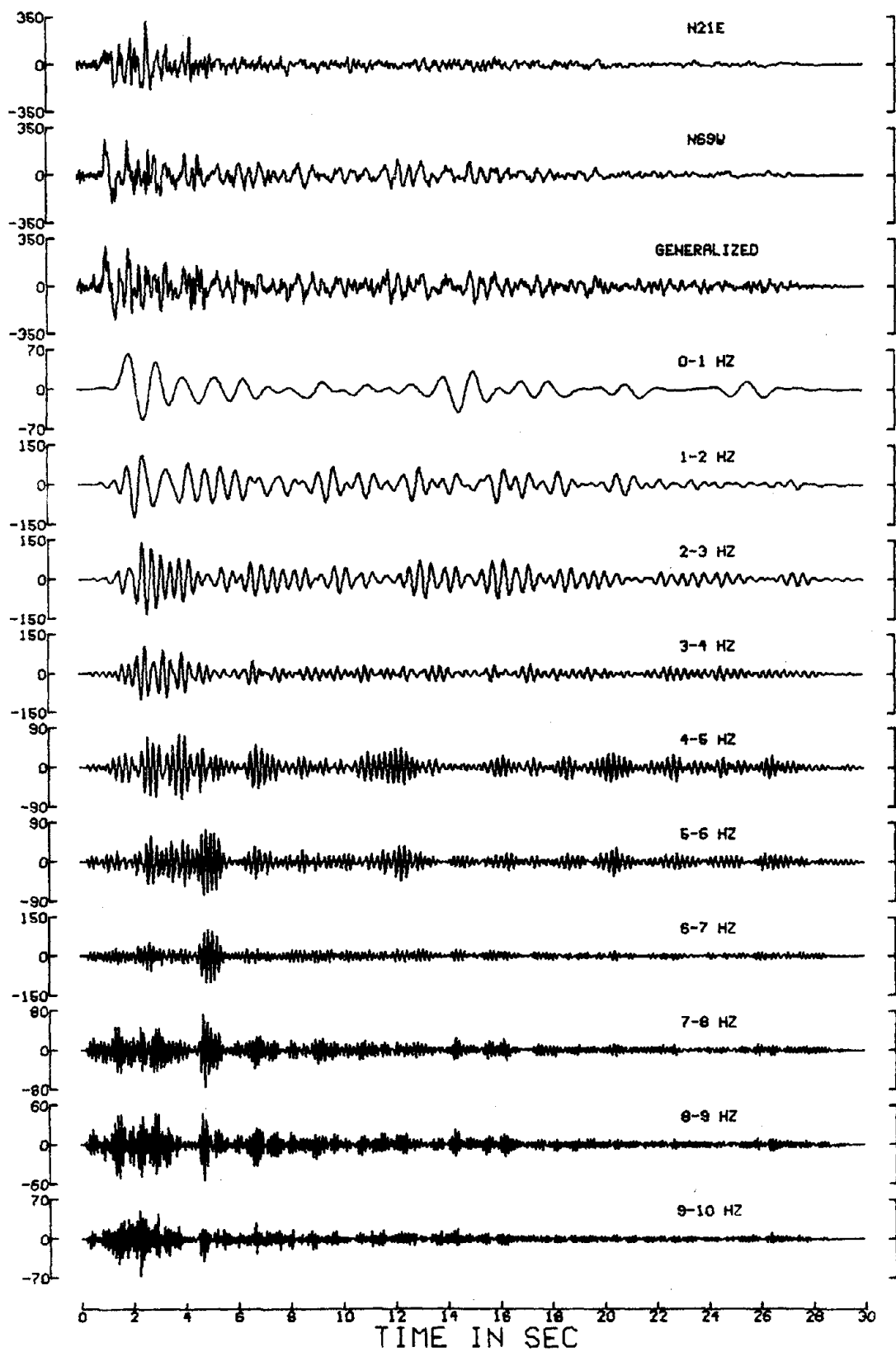


Fig. 2.26b

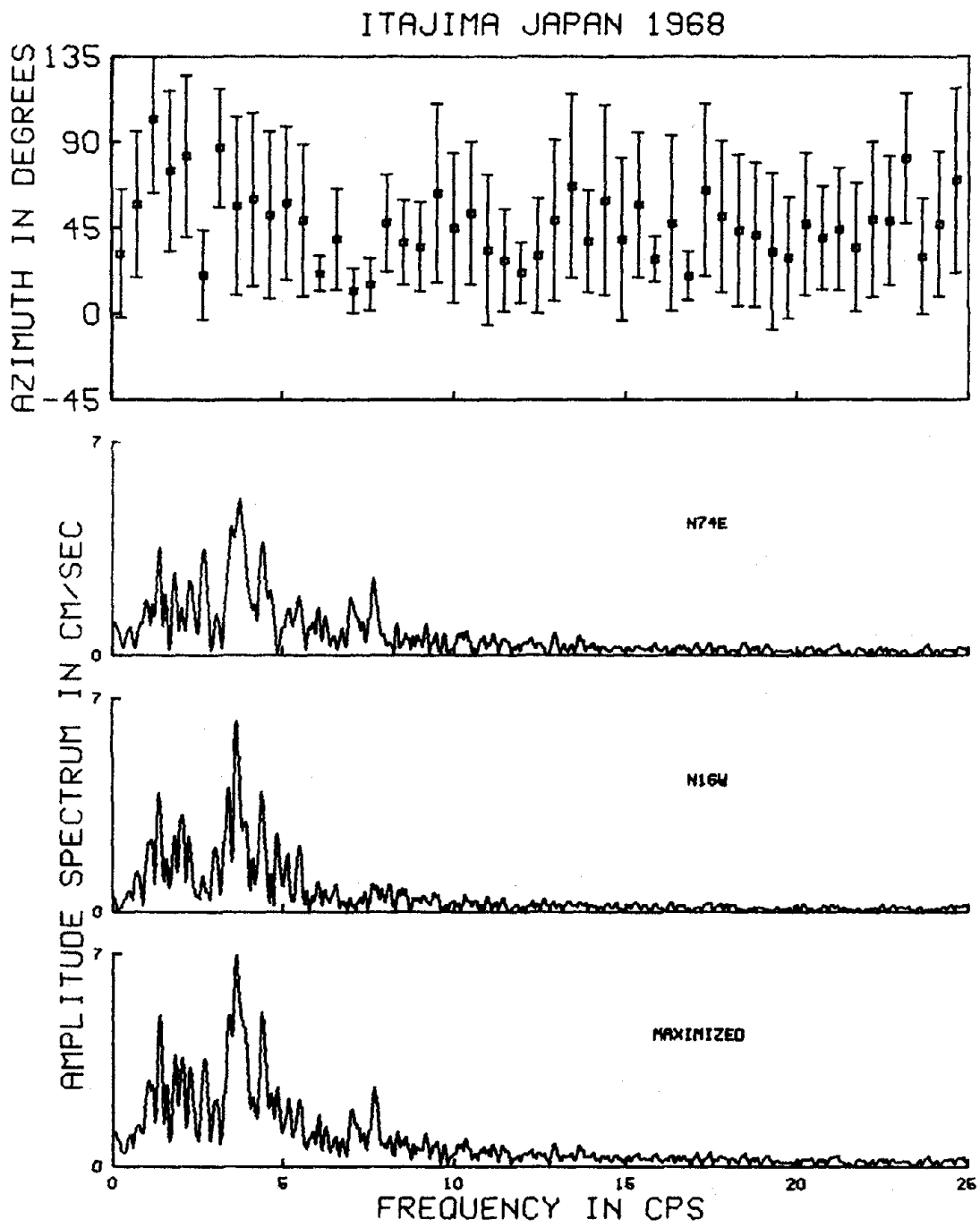


Fig. 2.27a

ITAJIMA JAPAN 1968

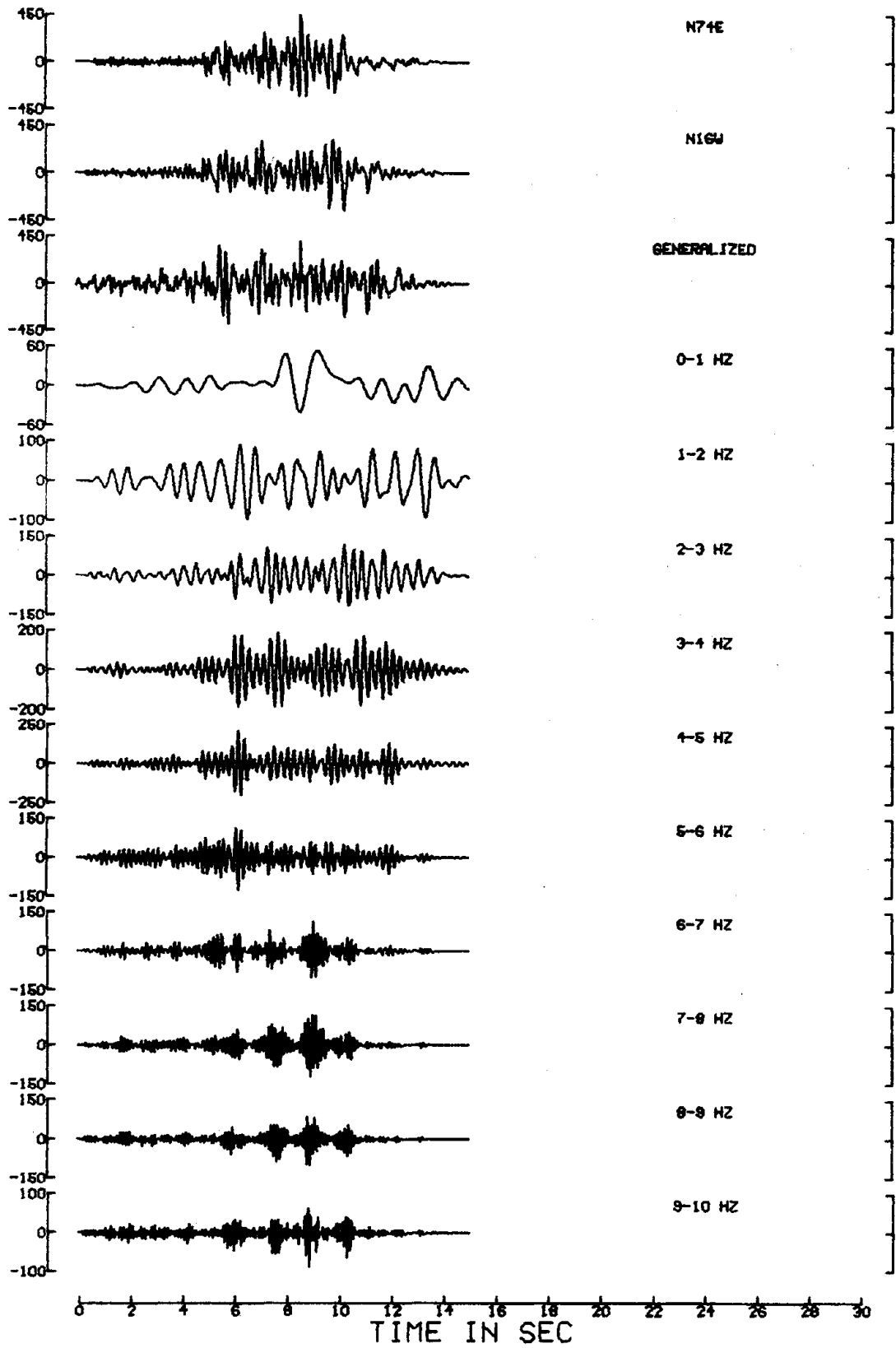


Fig. 2.27b

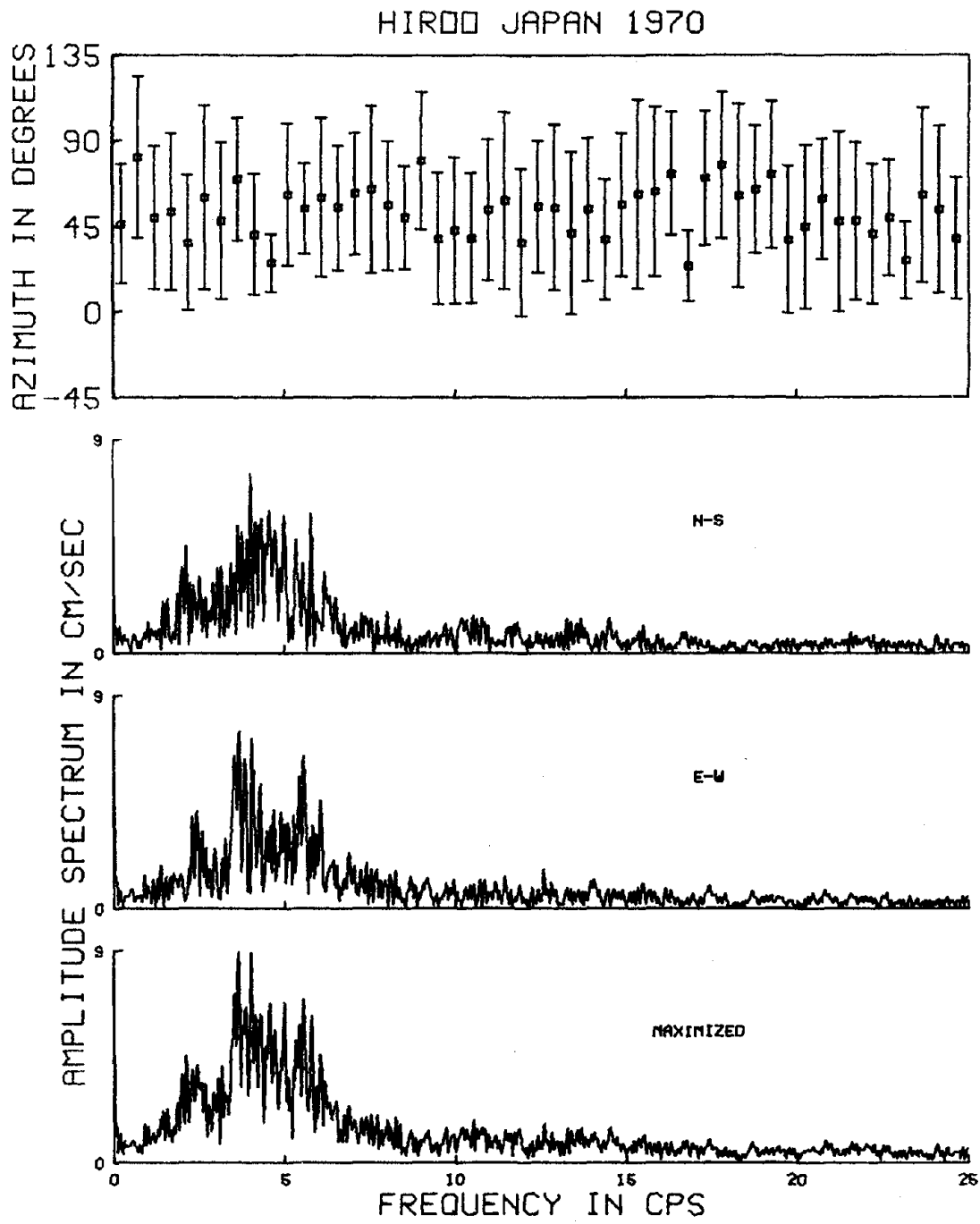


Fig. 2.28a

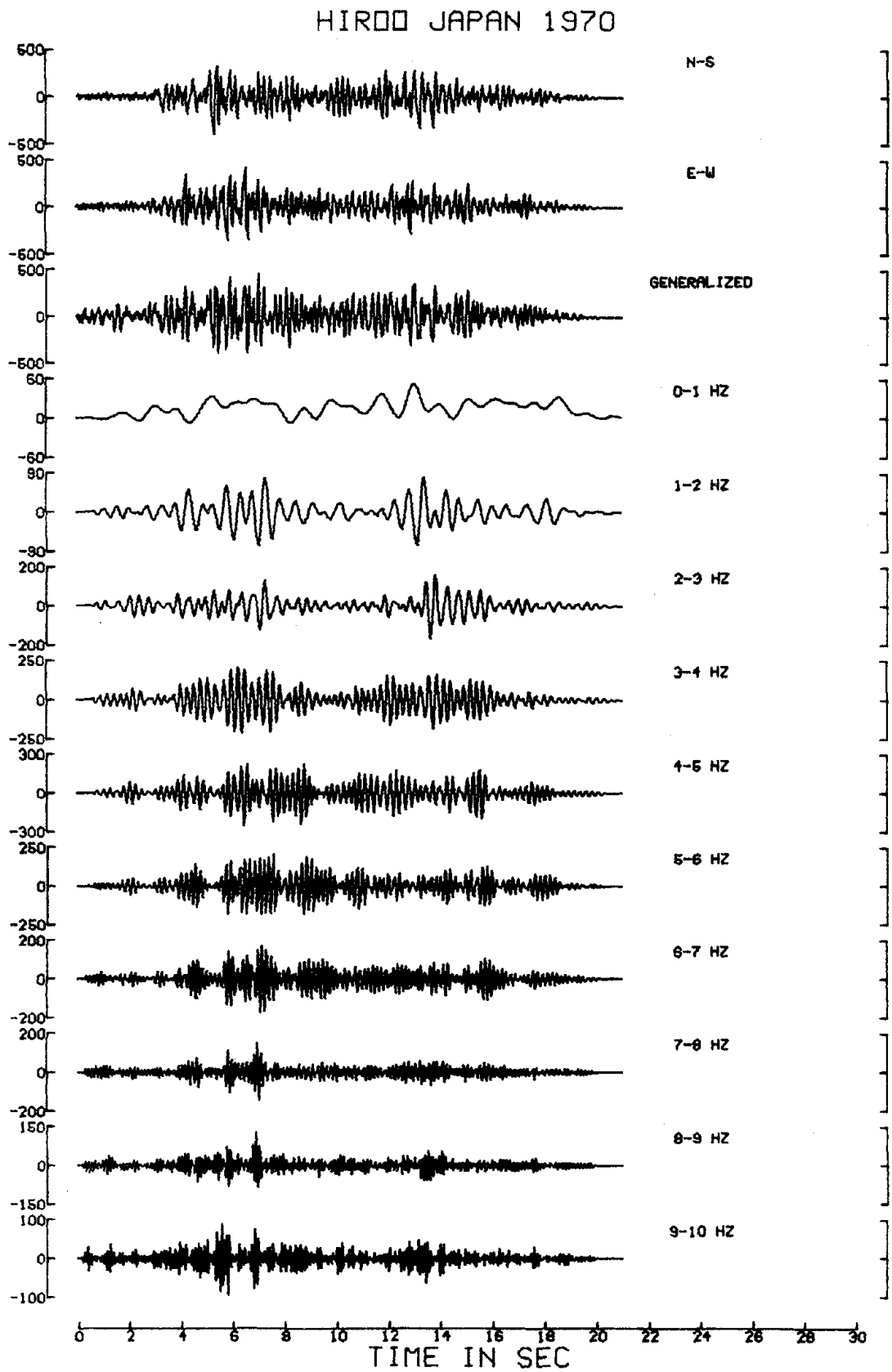


Fig. 2.28b

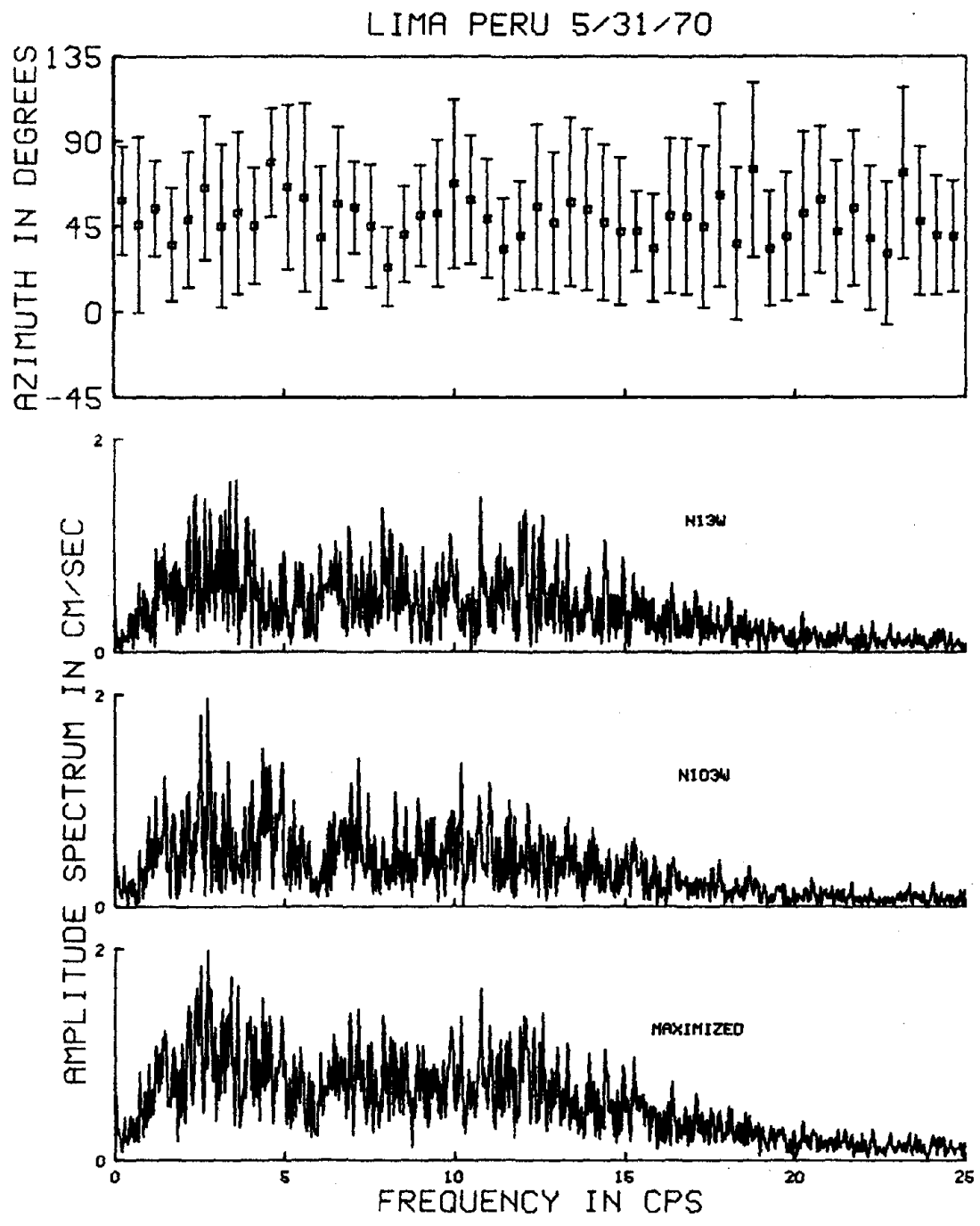


Fig. 2.29a

LIMA PERU 5/31/70

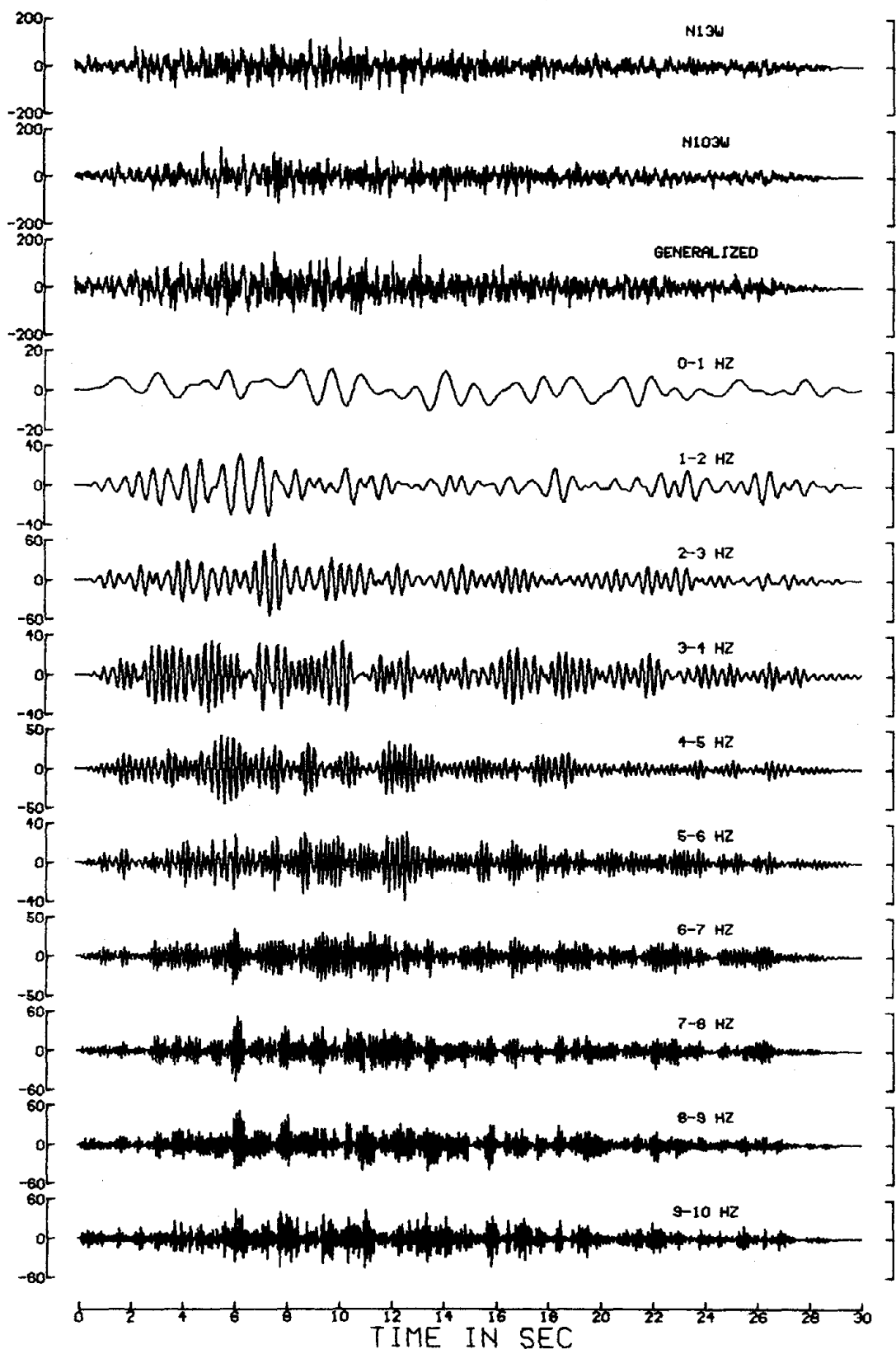


Fig. 2.29b

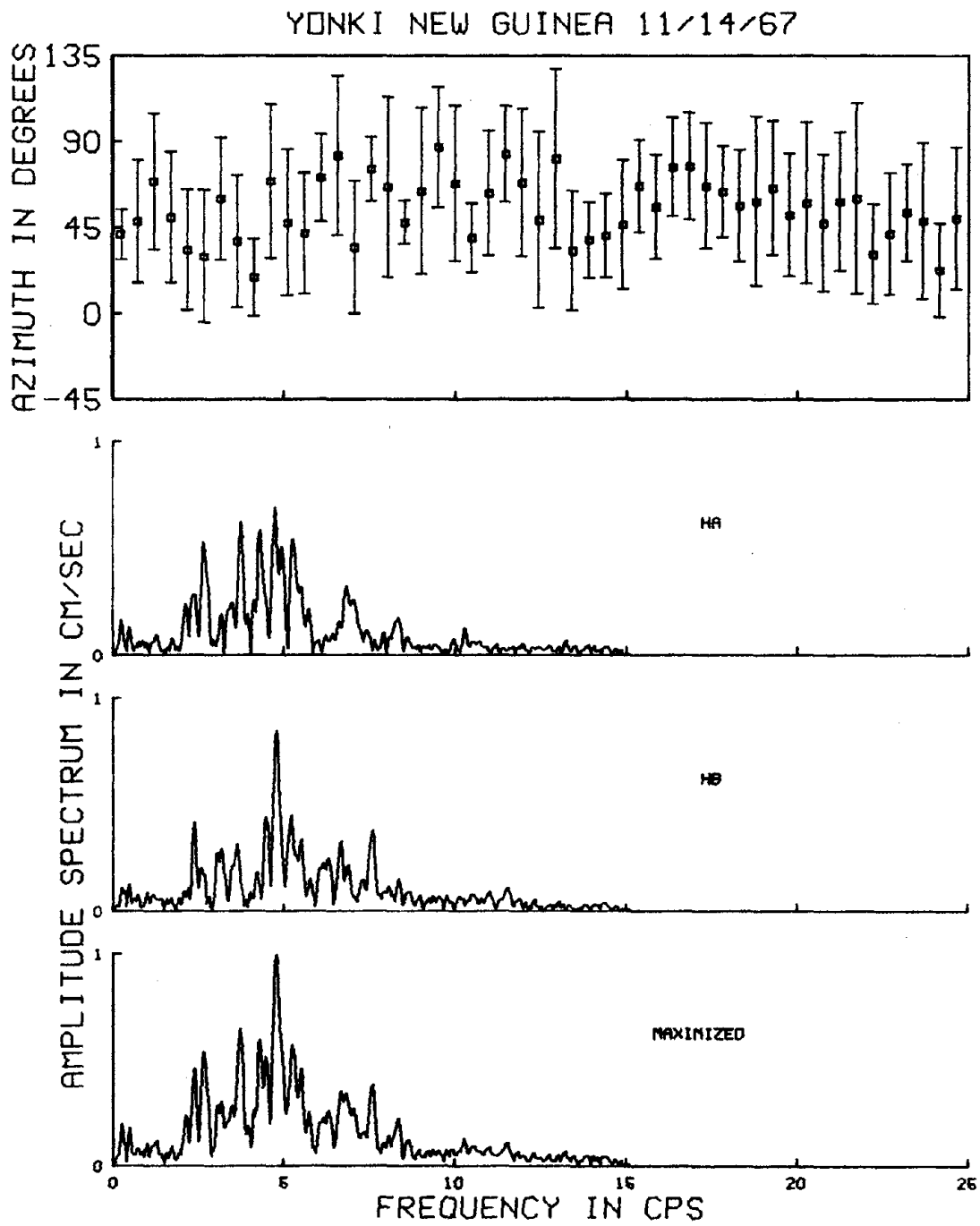


Fig. 2.30a

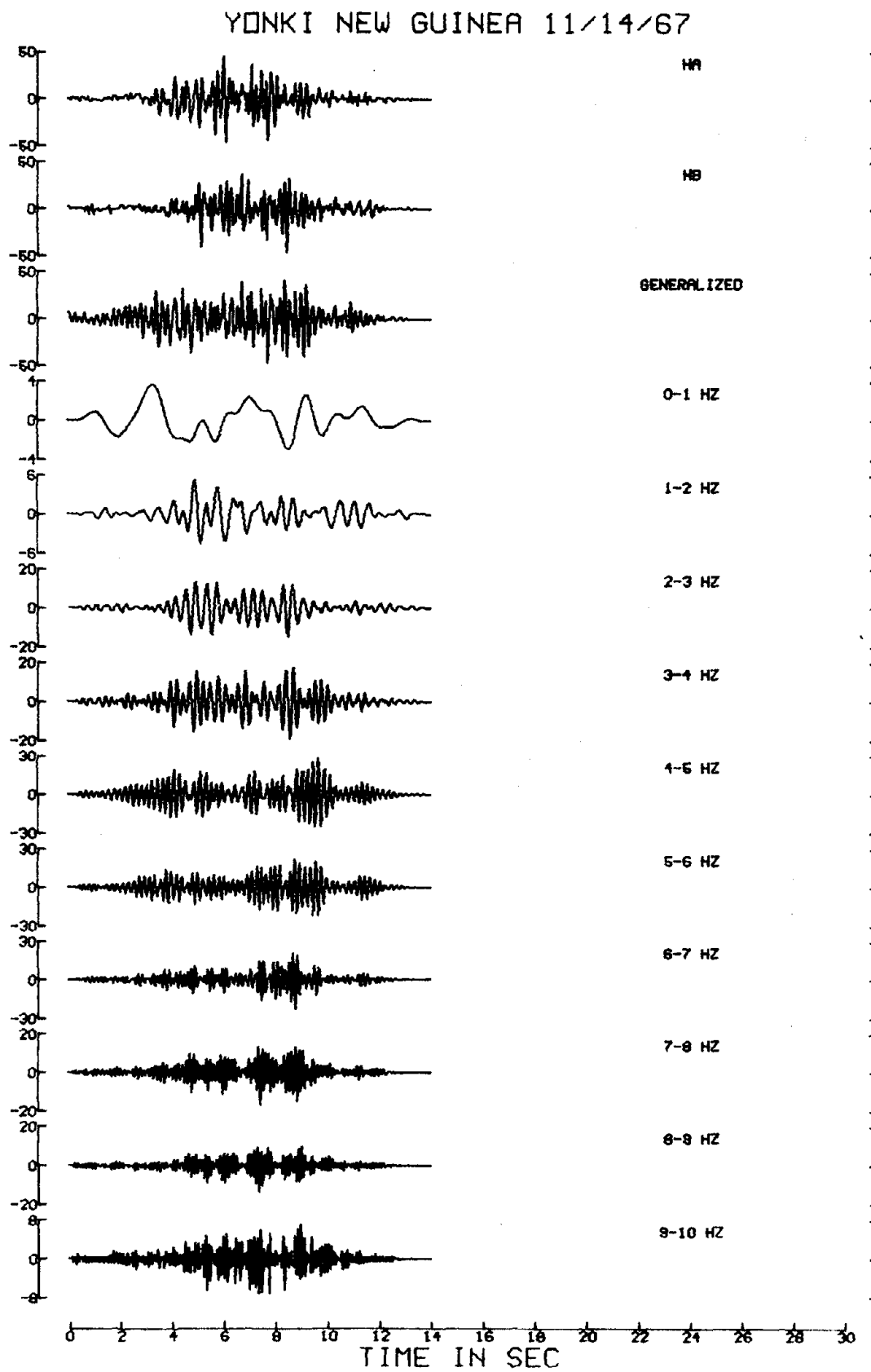


Fig. 2.30b

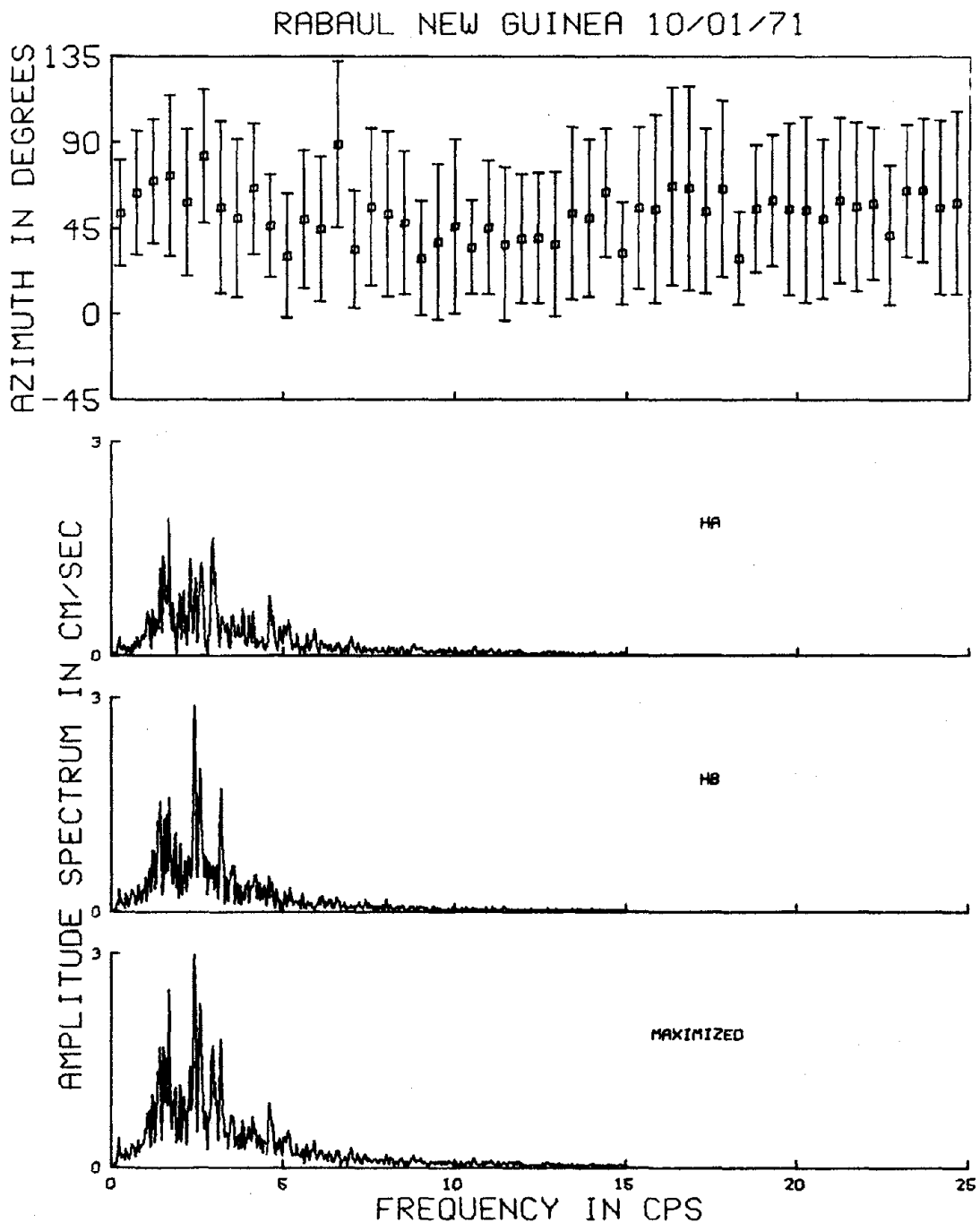


Fig. 2.31a

RABAU NEW GUINEA 10/01/71

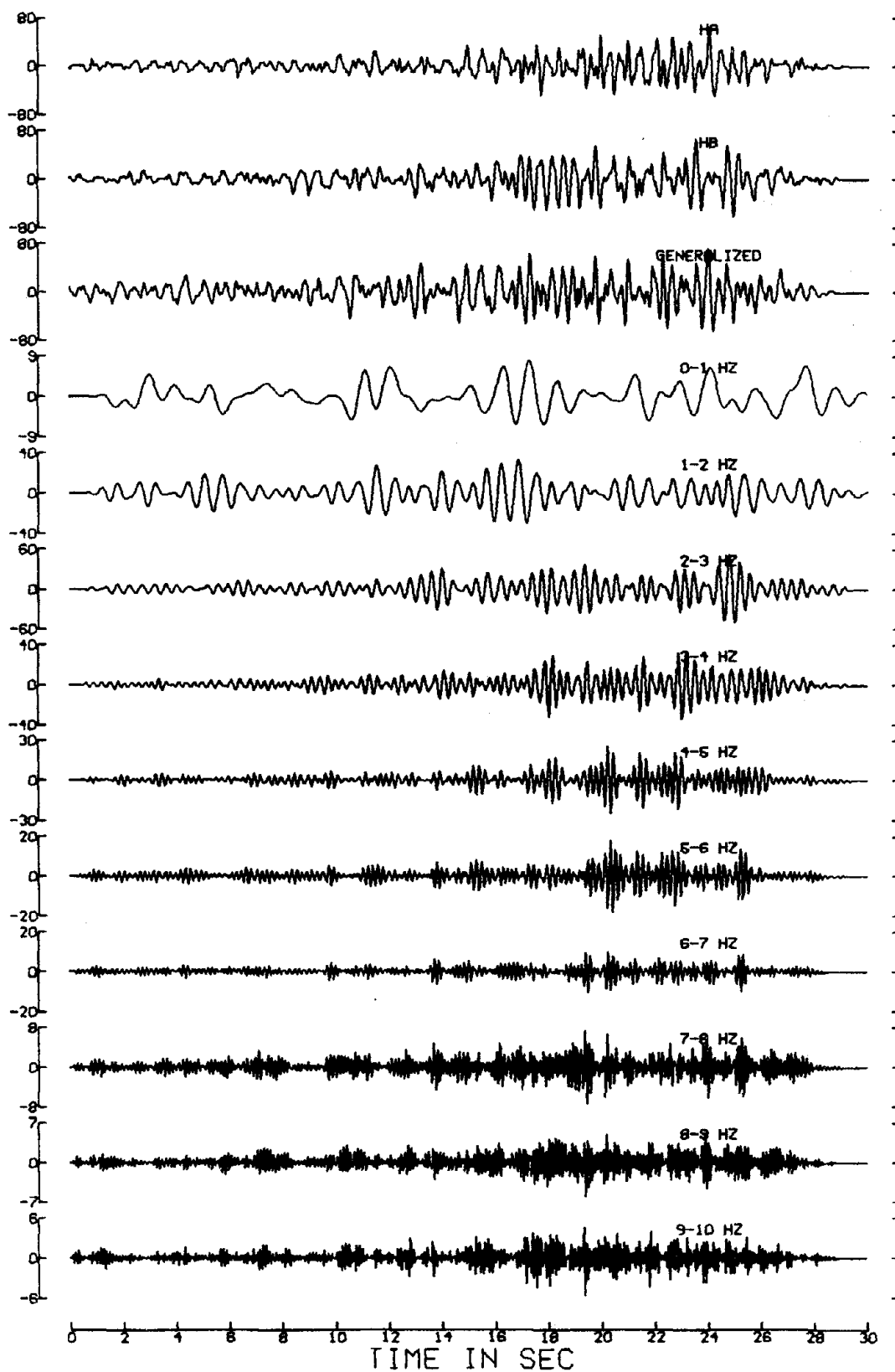


Fig. 2.31b

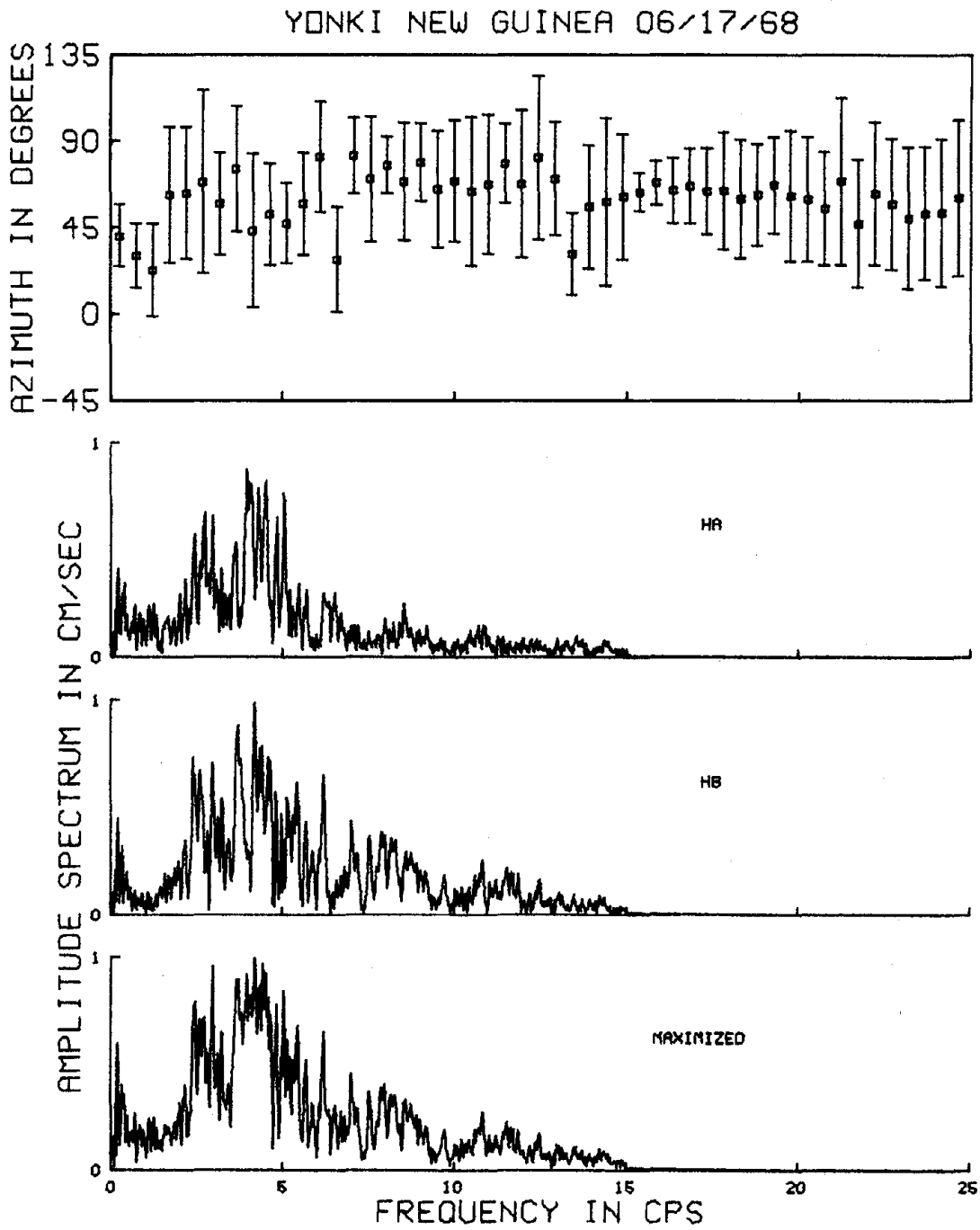


Fig. 2.32a

YONKI NEW GUINEA 06/17/68

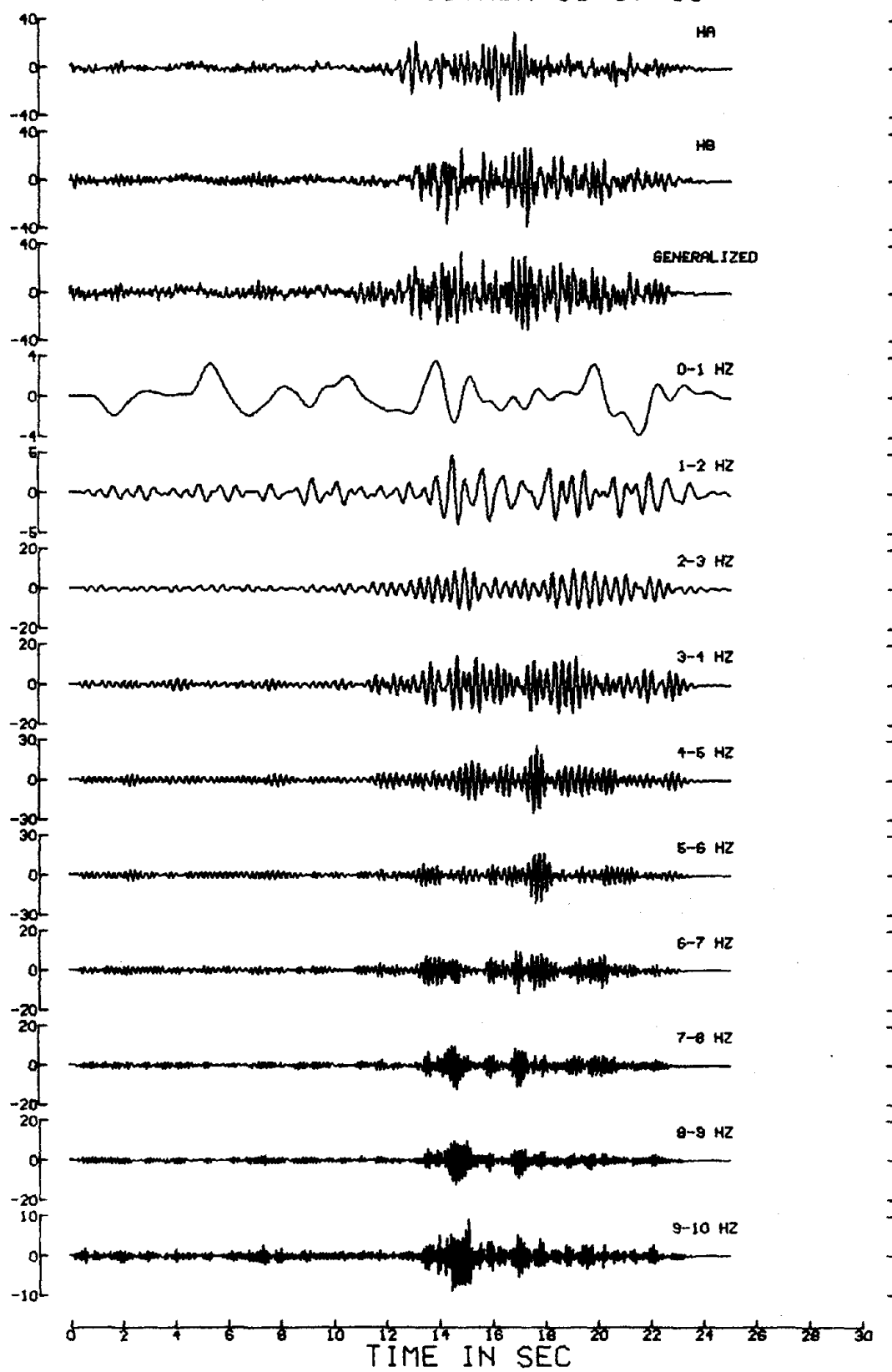


Fig. 2.32b

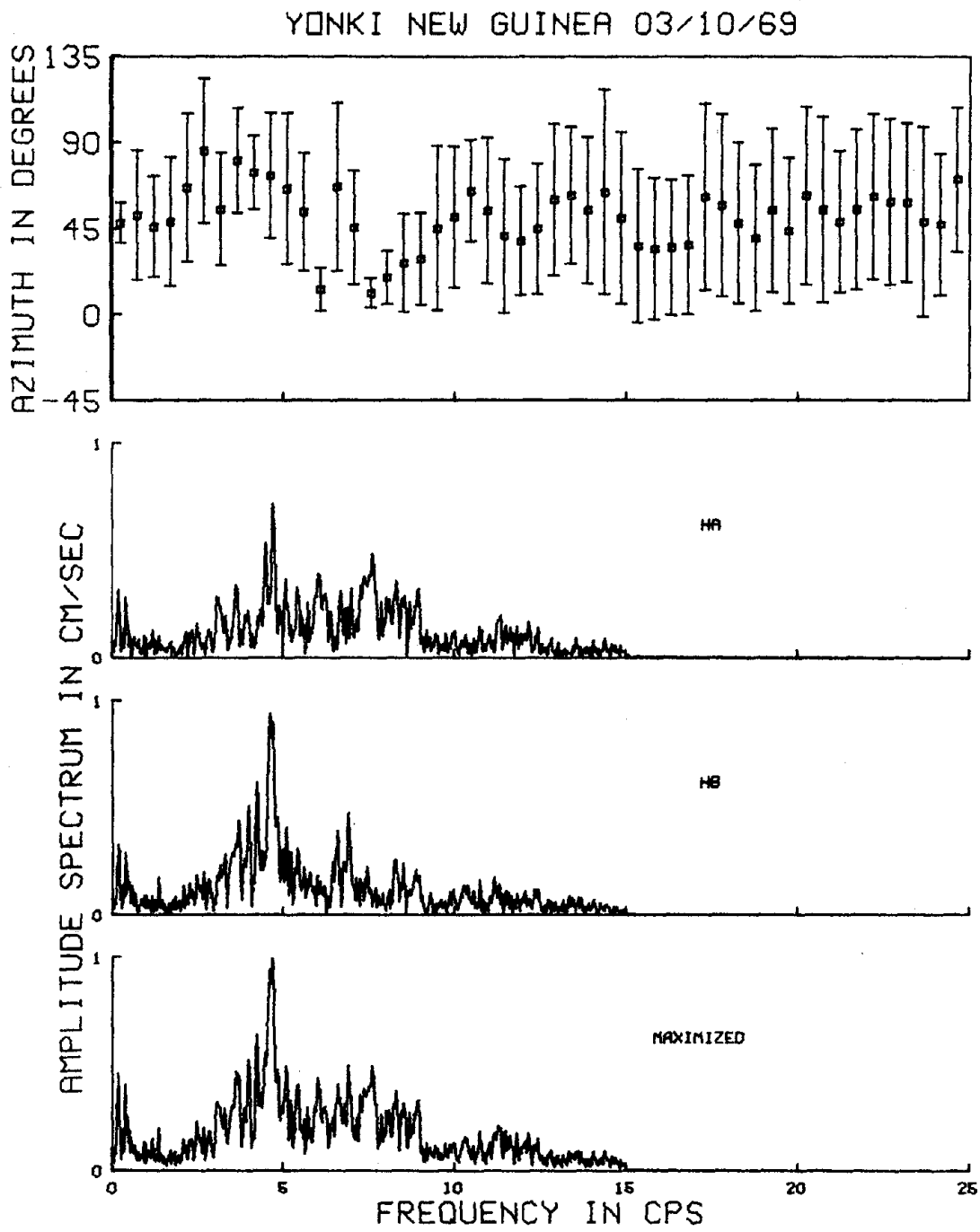


Fig. 2.33a

YONKI NEW GUINEA 03/10/69

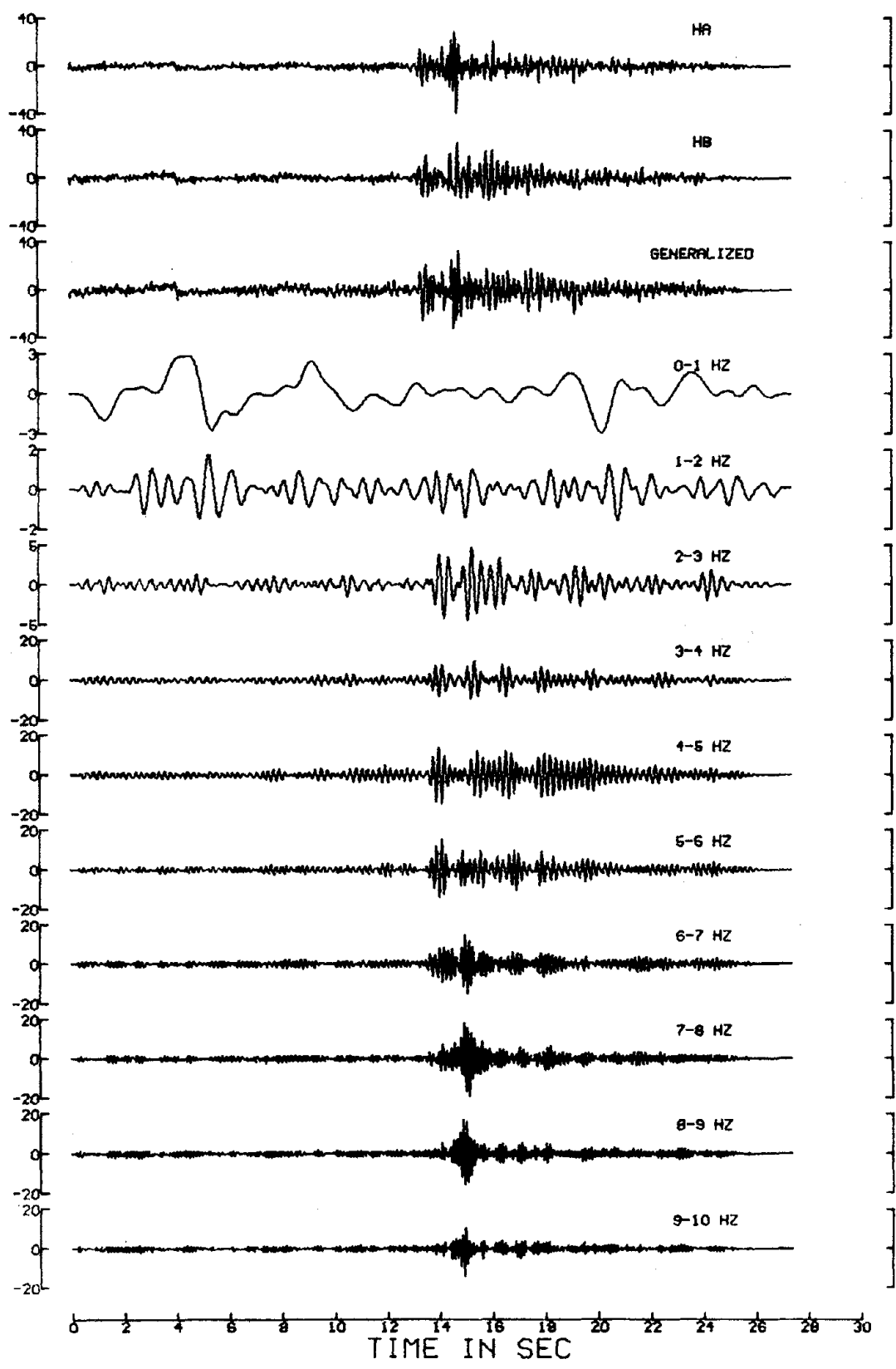


Fig. 2.33b

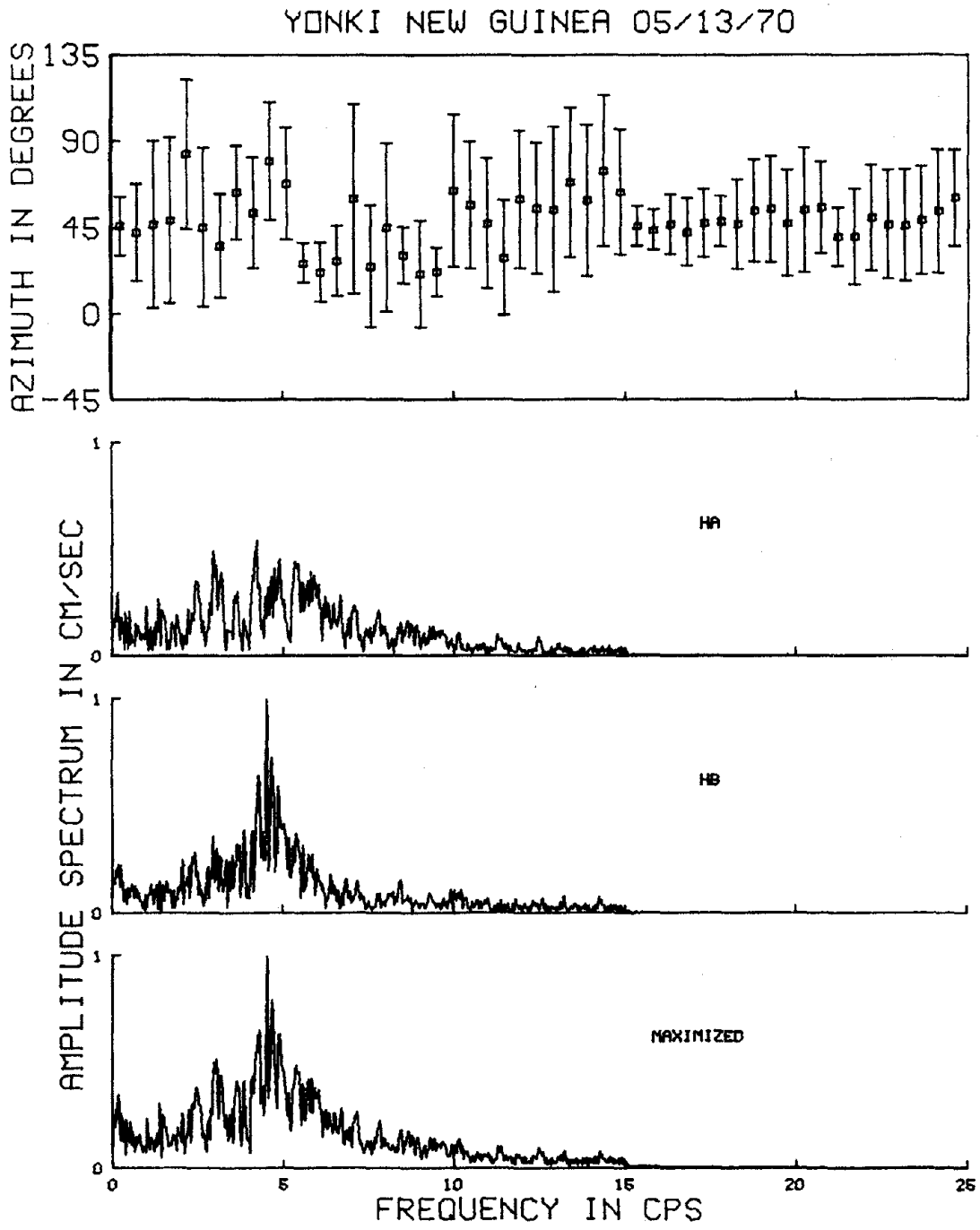


Fig. 2.34a

YONKI NEW GUINEA 05/13/70

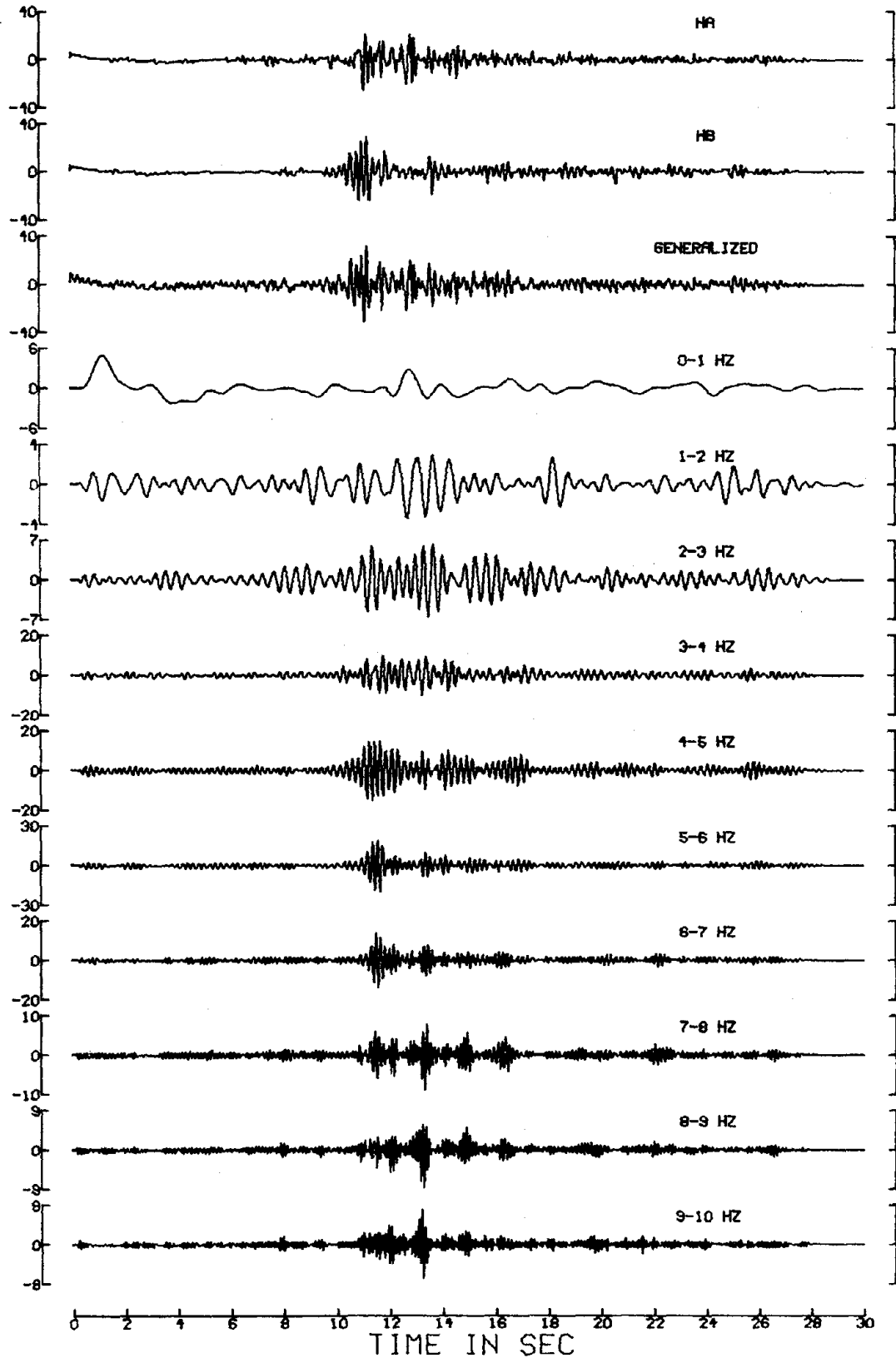


Fig. 2.34b

YONKI NEW GUINEA 02/12/71

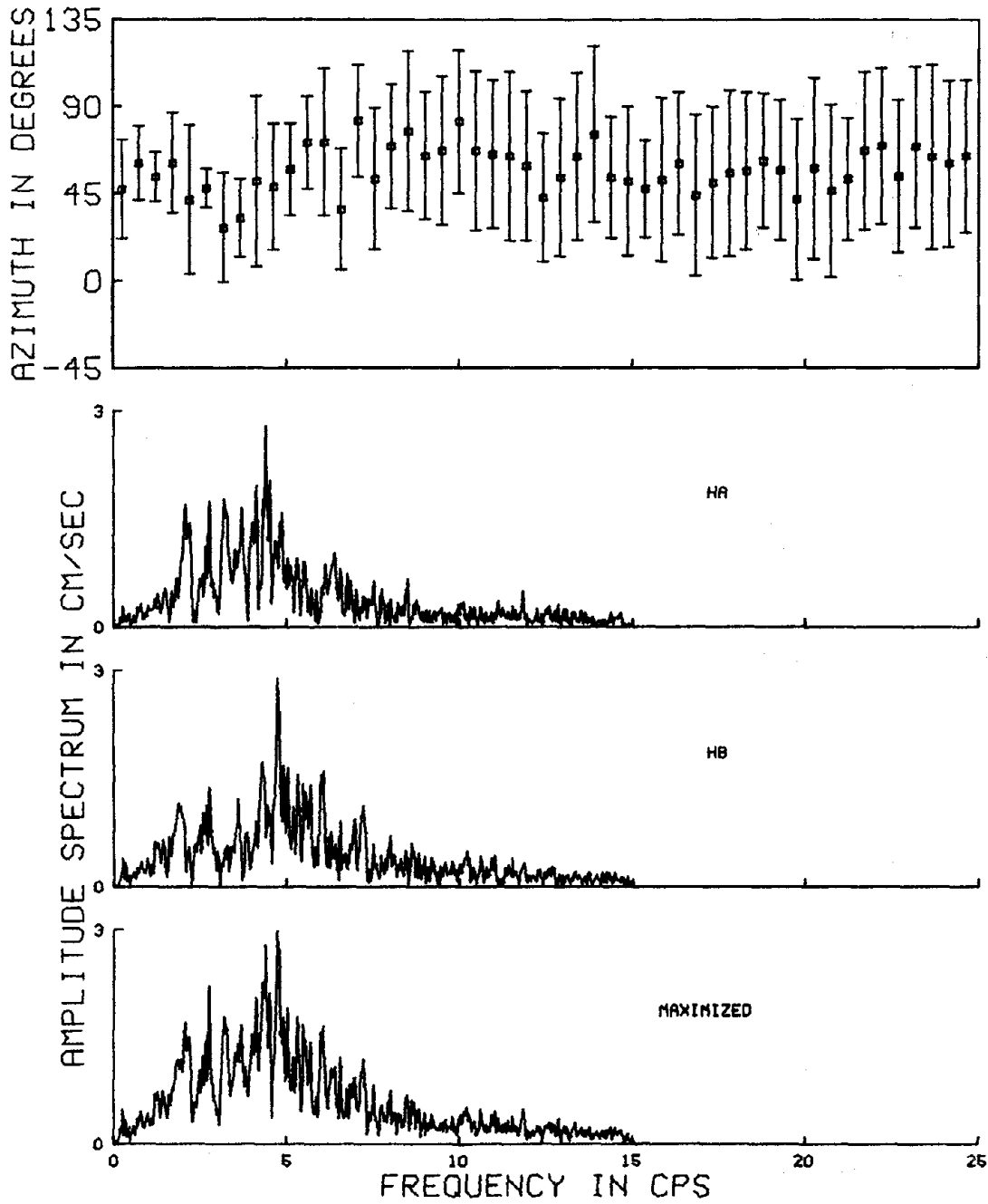


Fig. 2.35a

YONKI NEW GUINEA 02/12/71

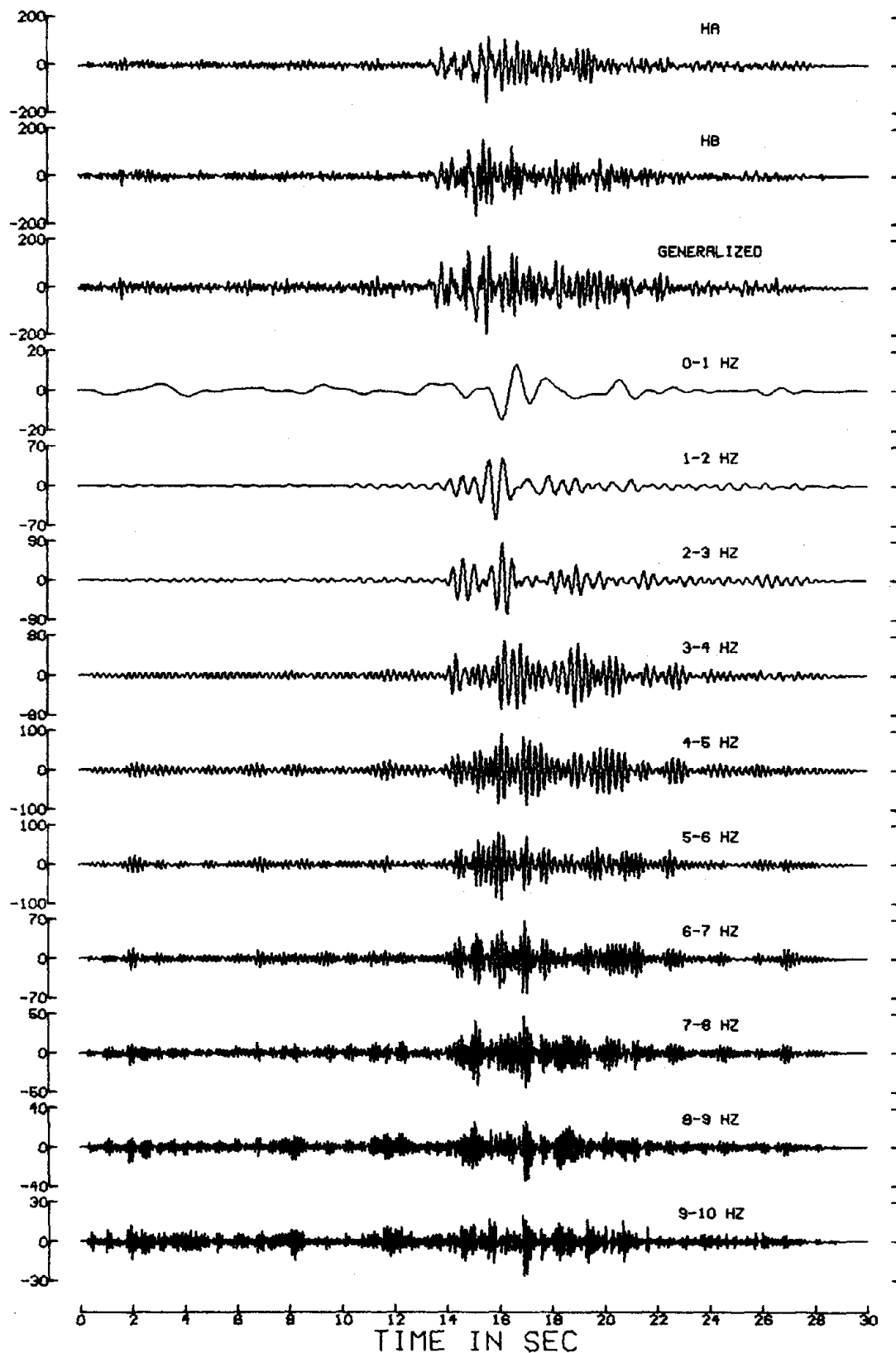


Fig. 2.35b

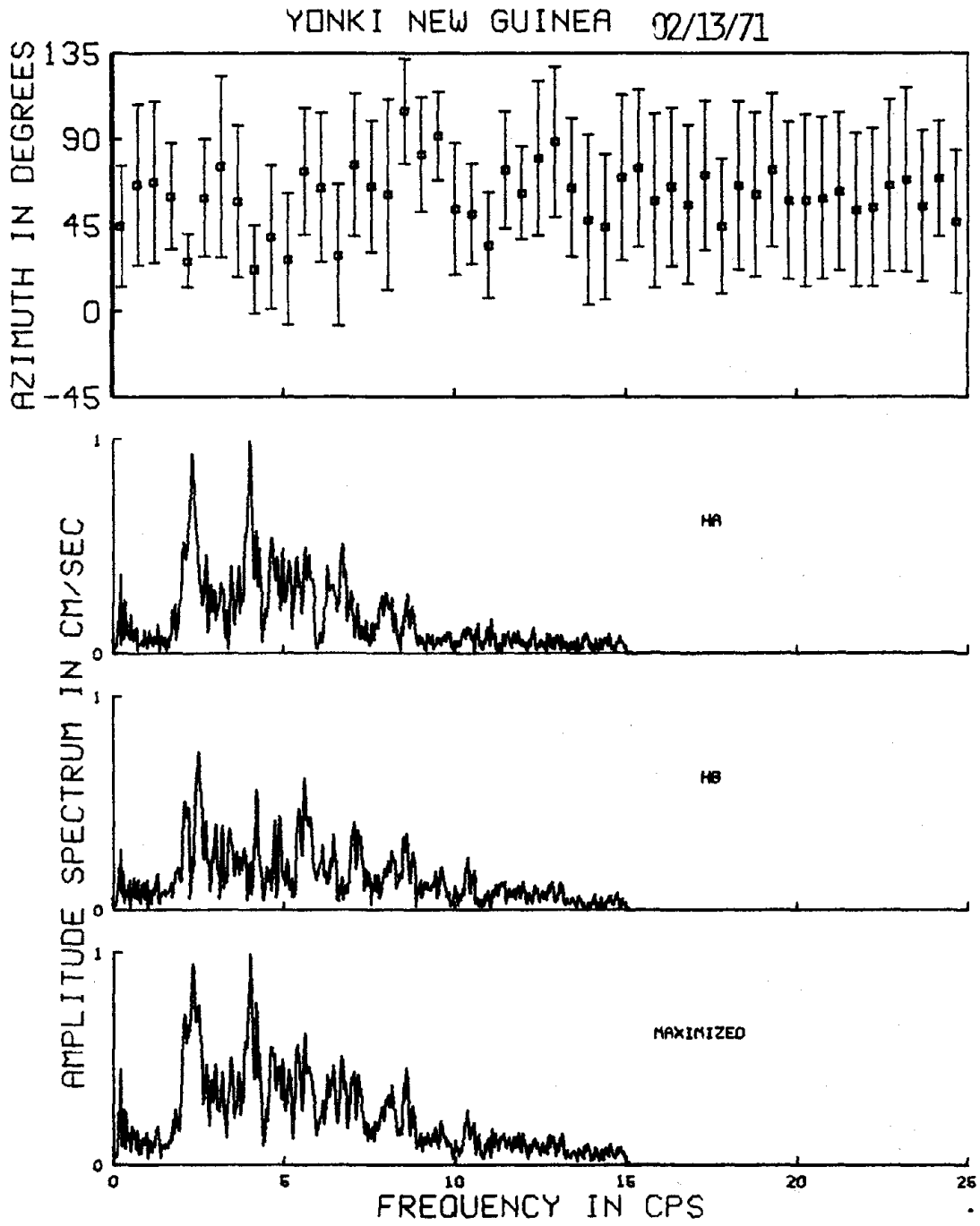


Fig. 2.36a

YONKI NEW GUINEA 02/13/71

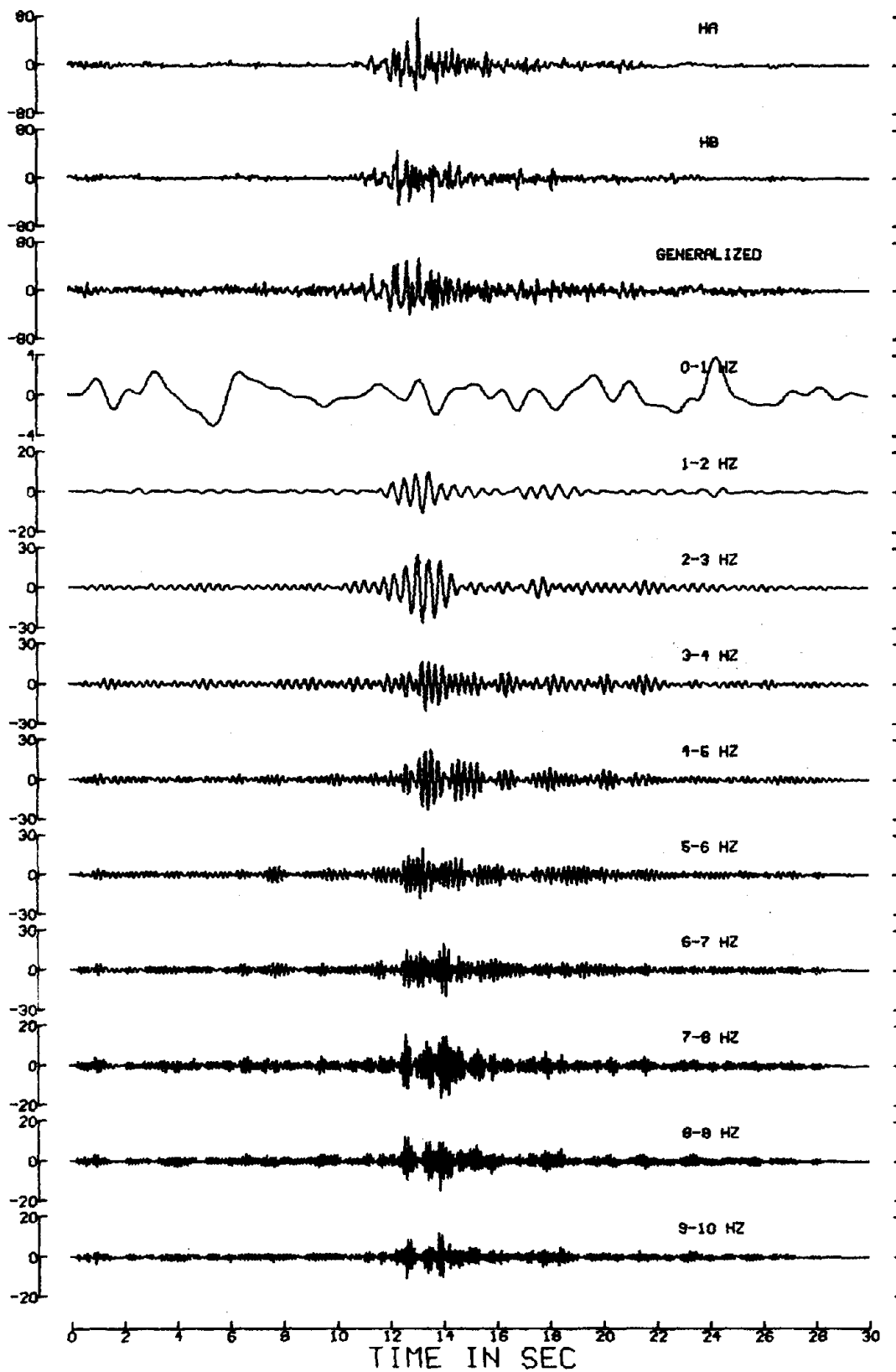


Fig. 2.36b

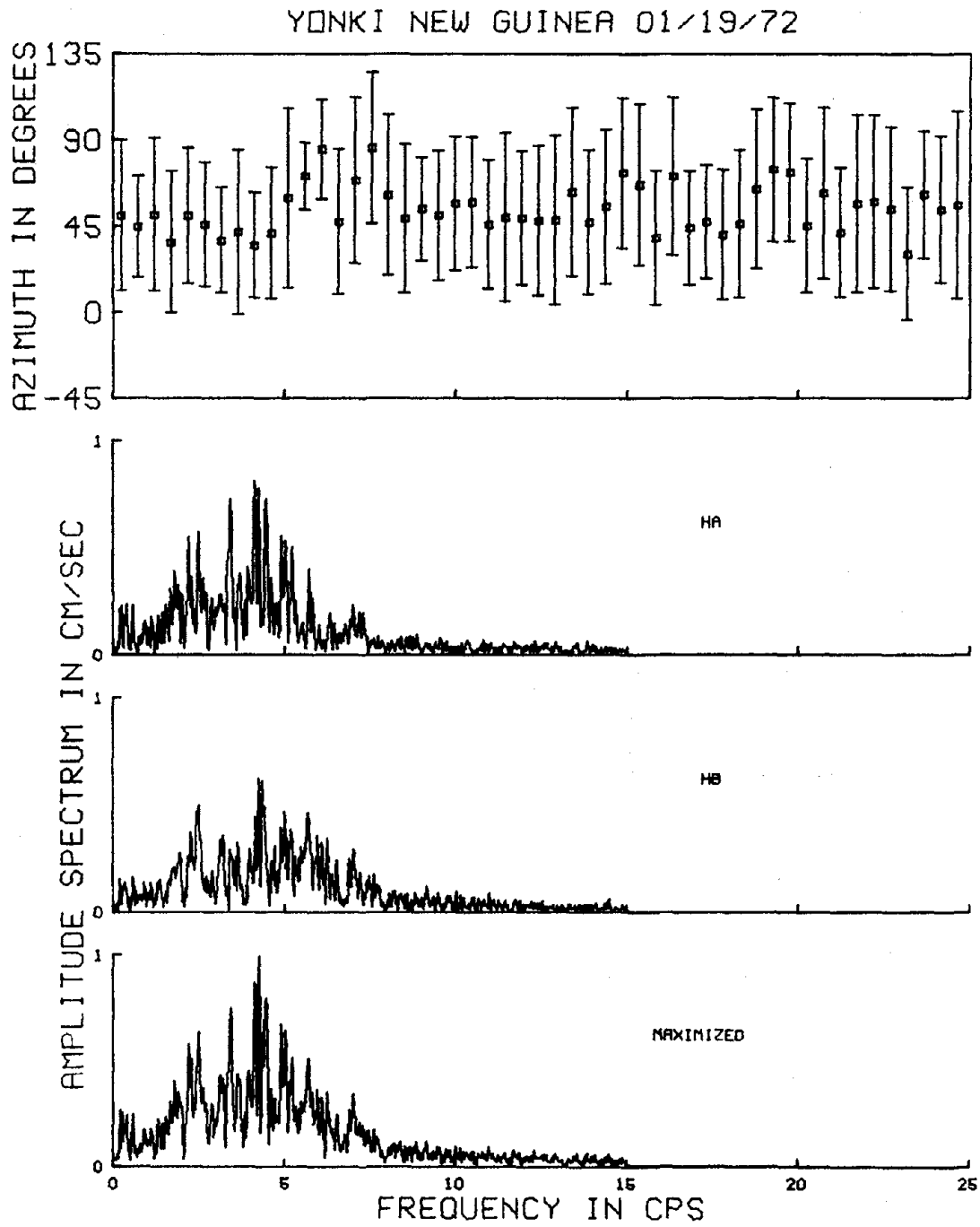


Fig. 2.37a

YONKI NEW GUINEA 01/19/72

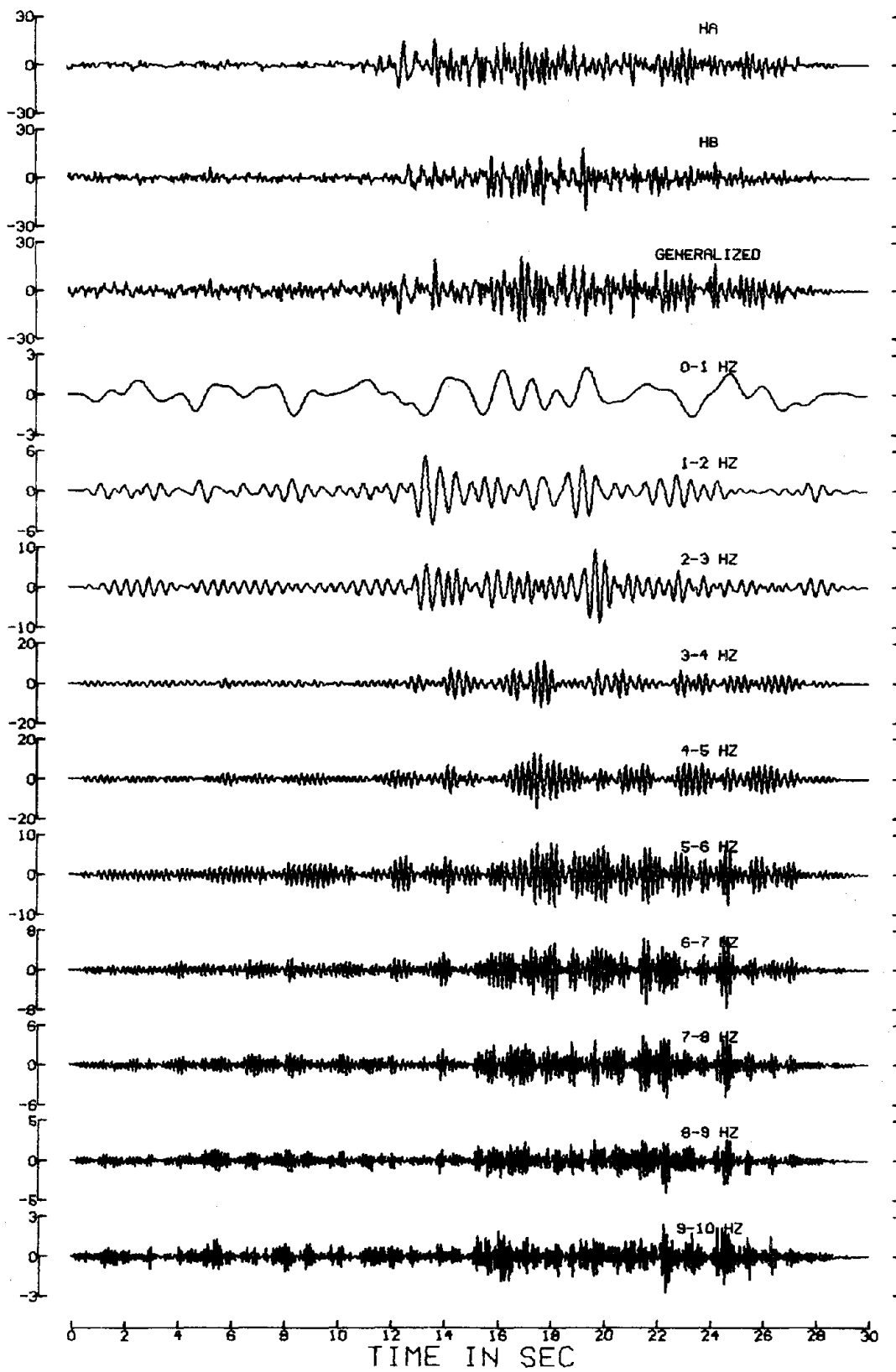


Fig. 2.37b

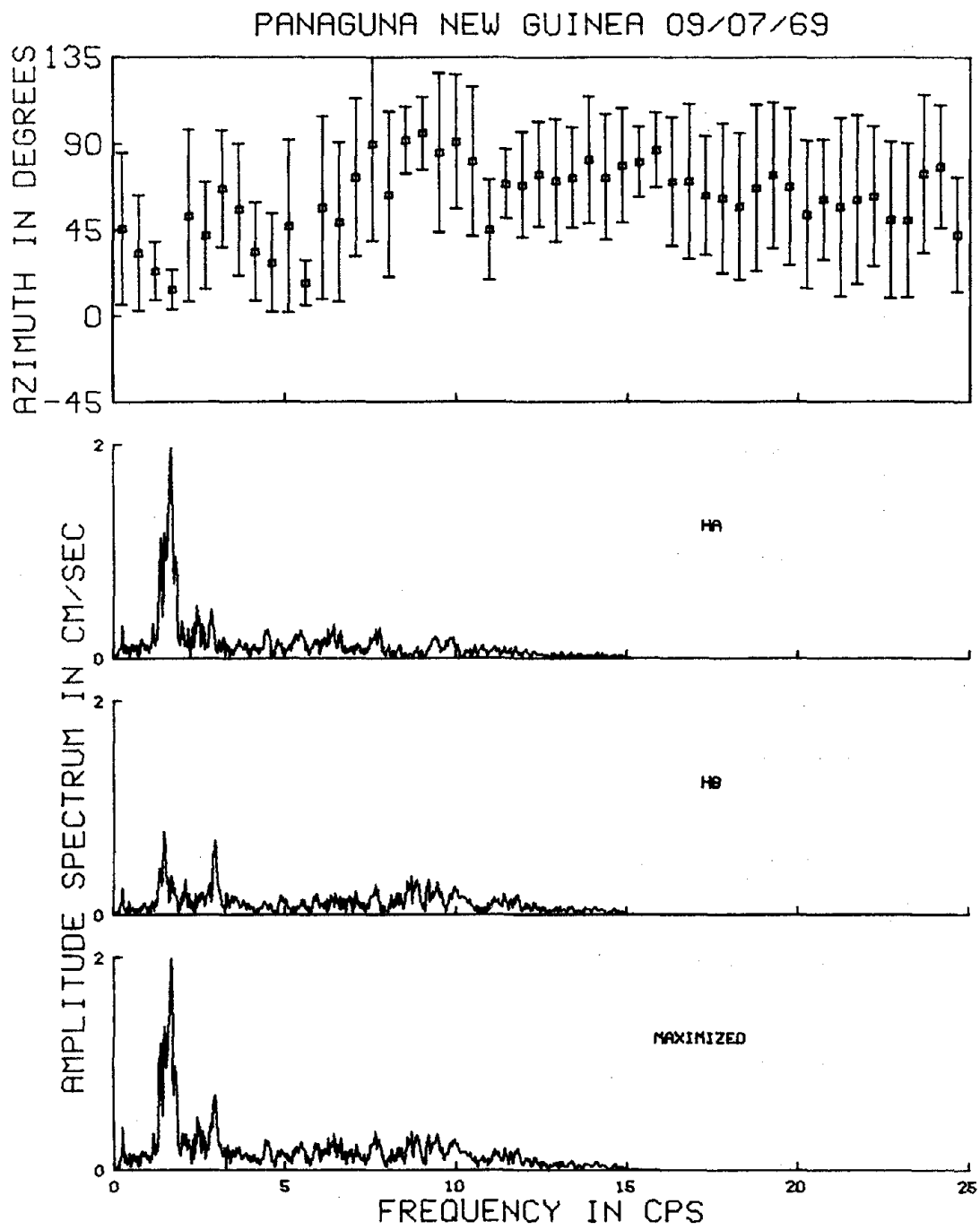


Fig. 2.38a

PANAGUNA NEW GUINEA 09/07/69

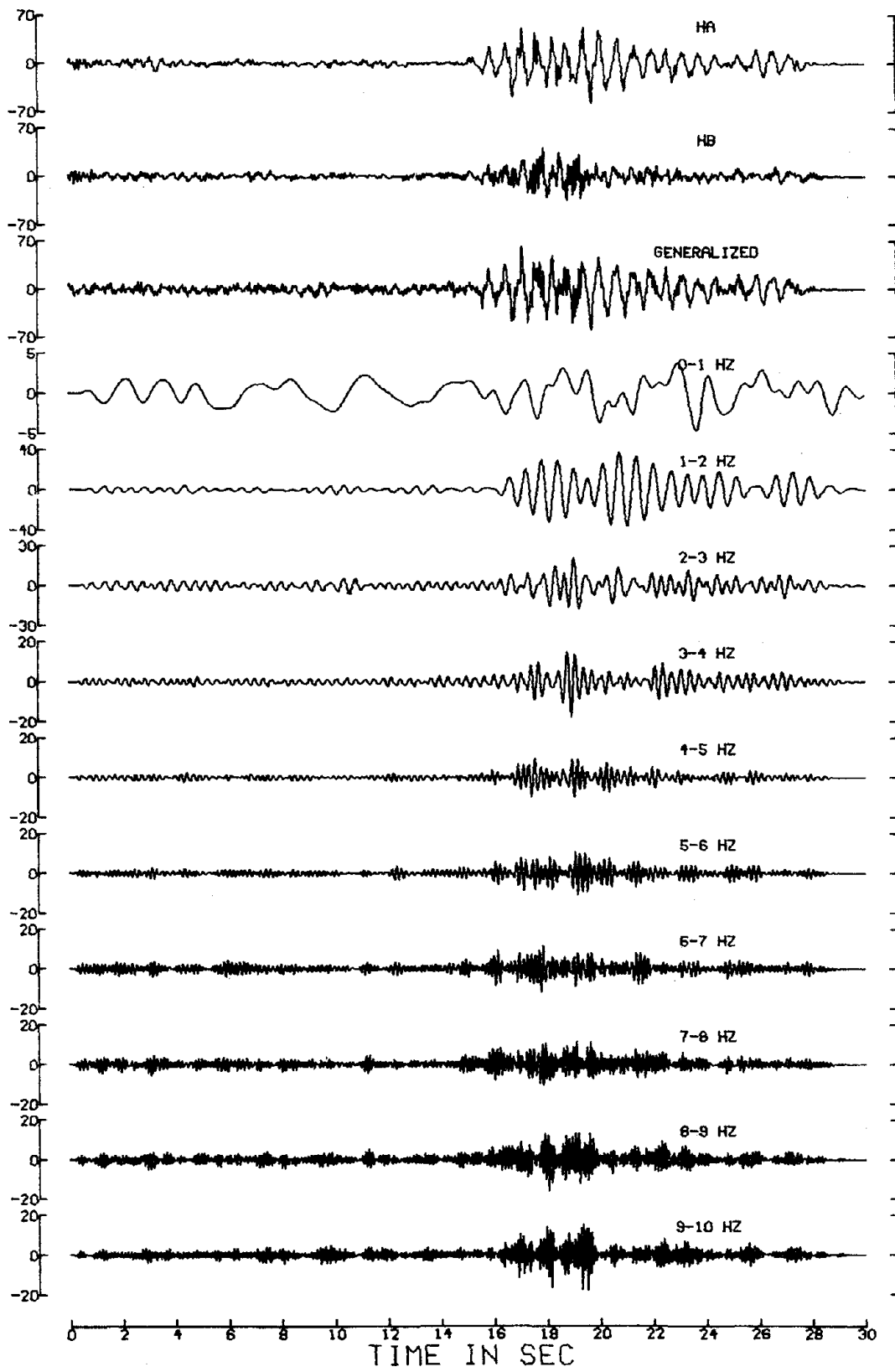


Fig. 2.38b

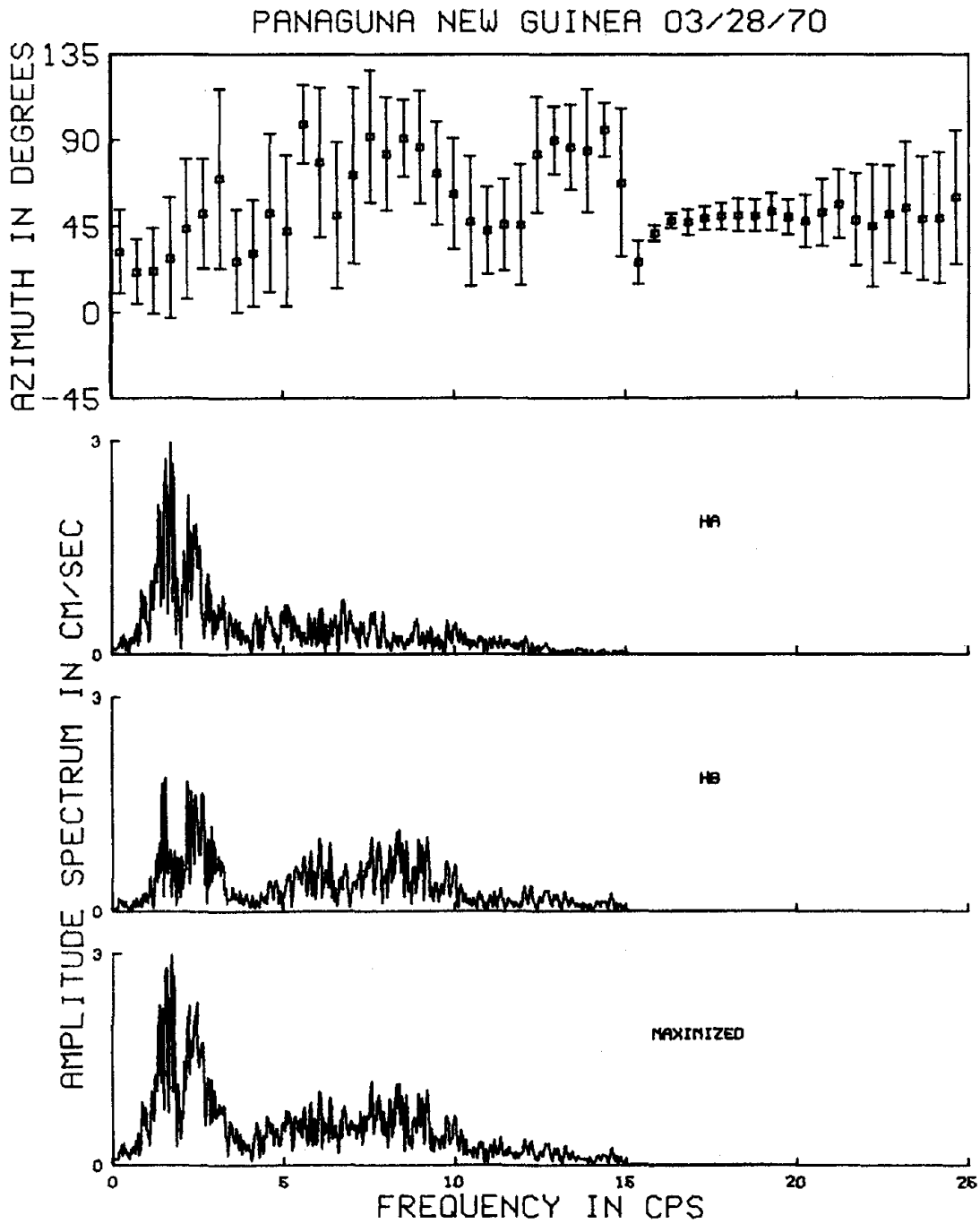


Fig. 2.39a

PANAGUNA NEW GUINEA 03/28/70

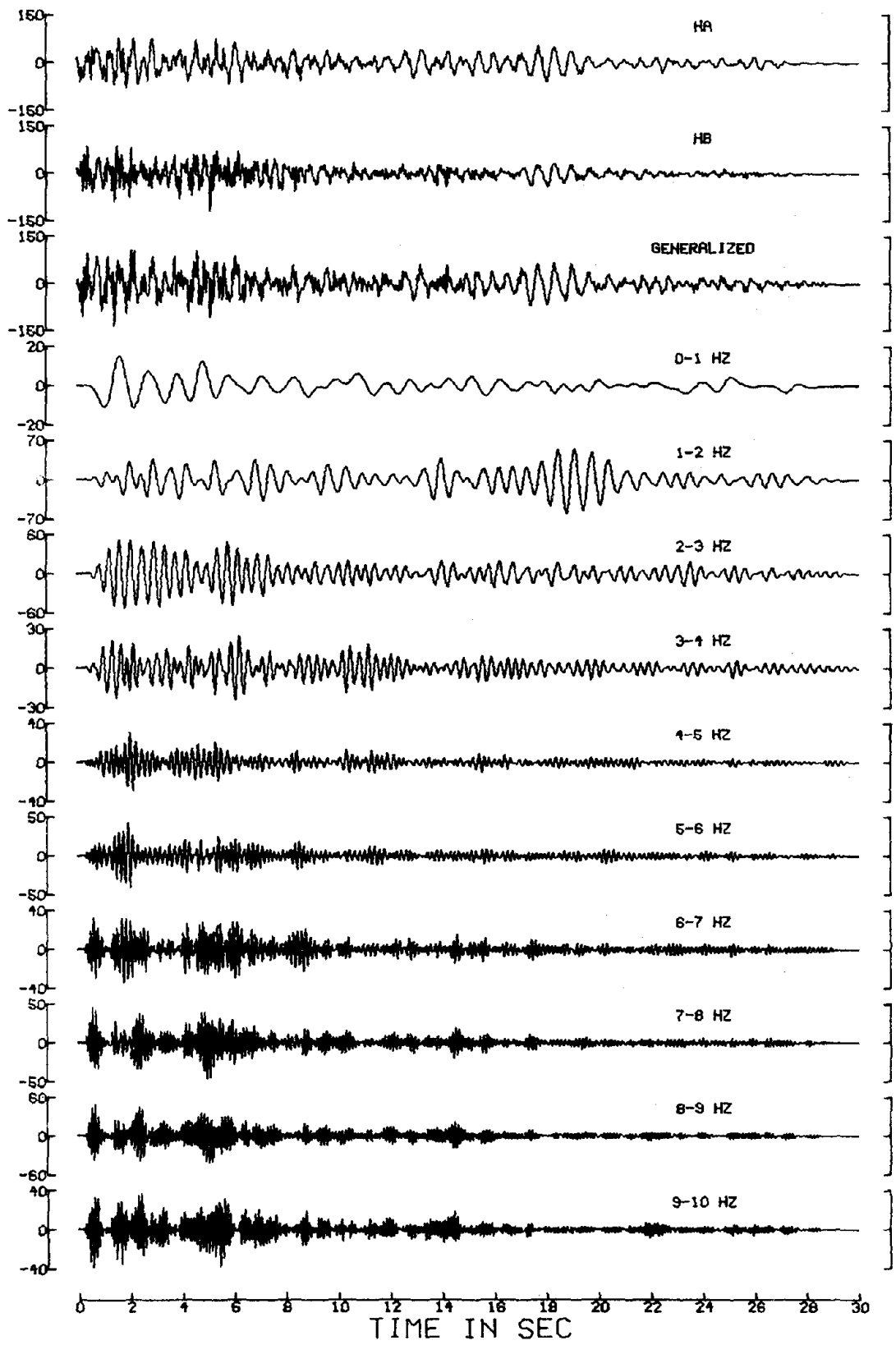


Fig. 2.39b

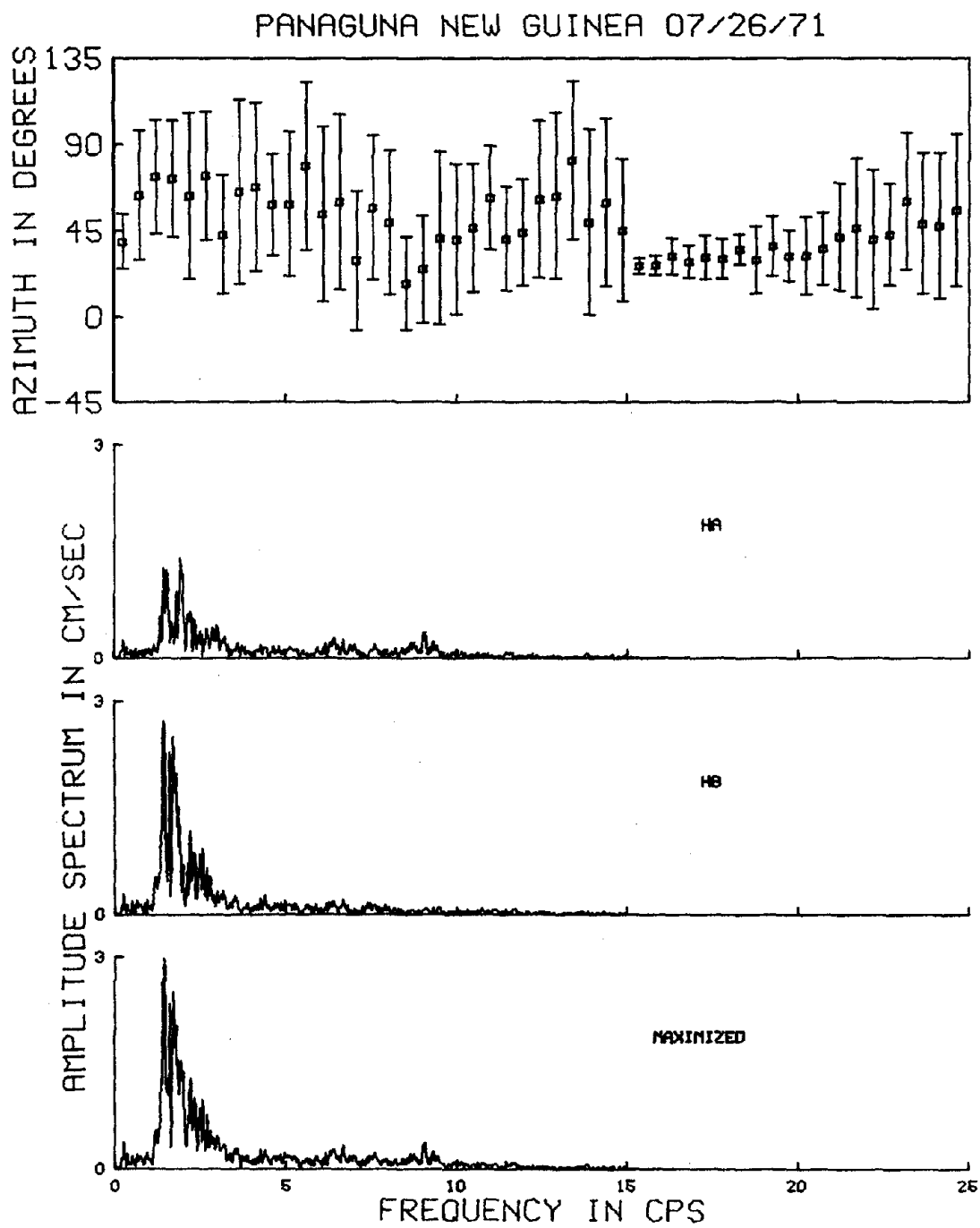


Fig. 2.40a

PANAGUNA NEW GUINEA 07/26/71

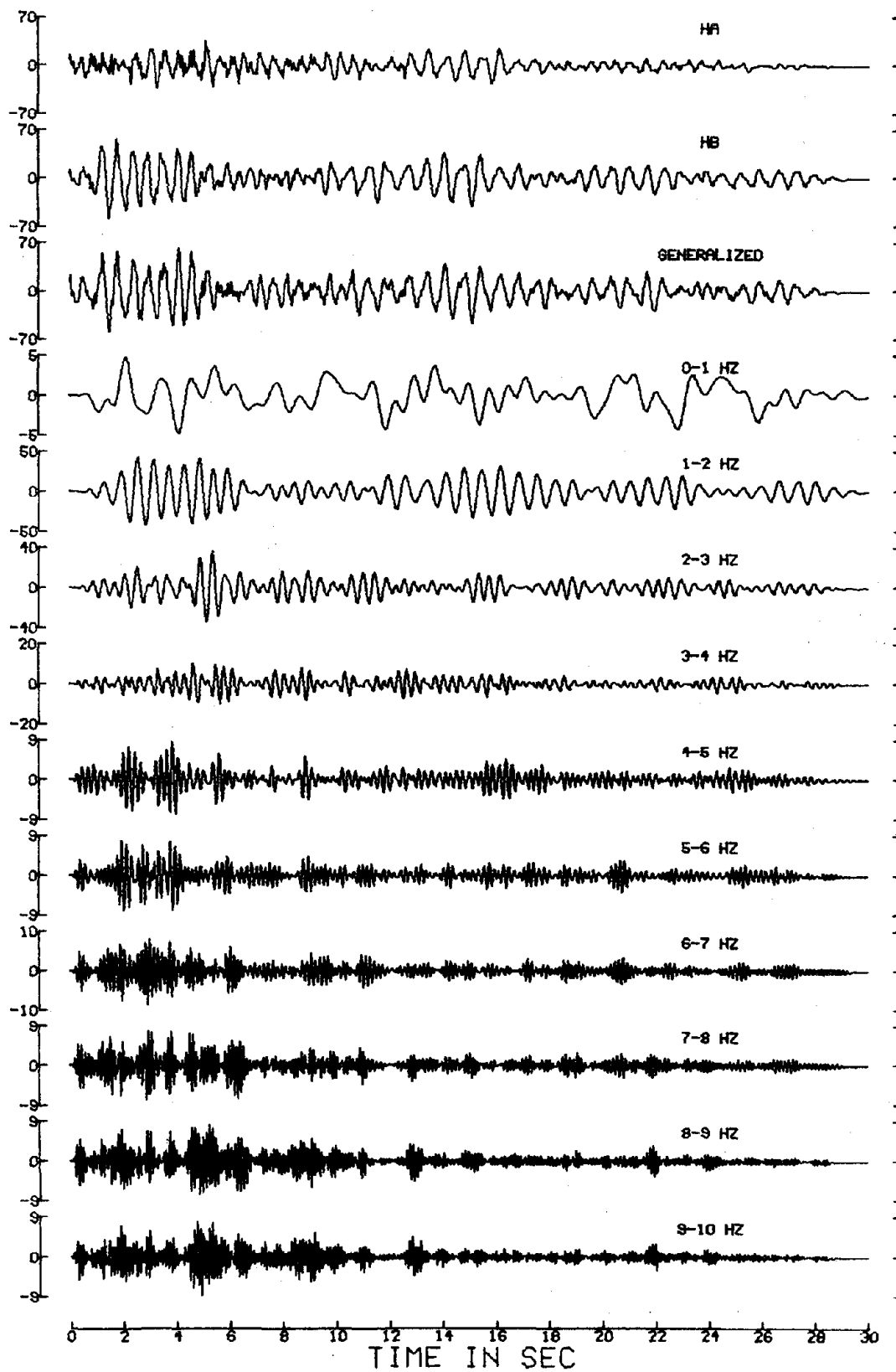


Fig. 2.40b

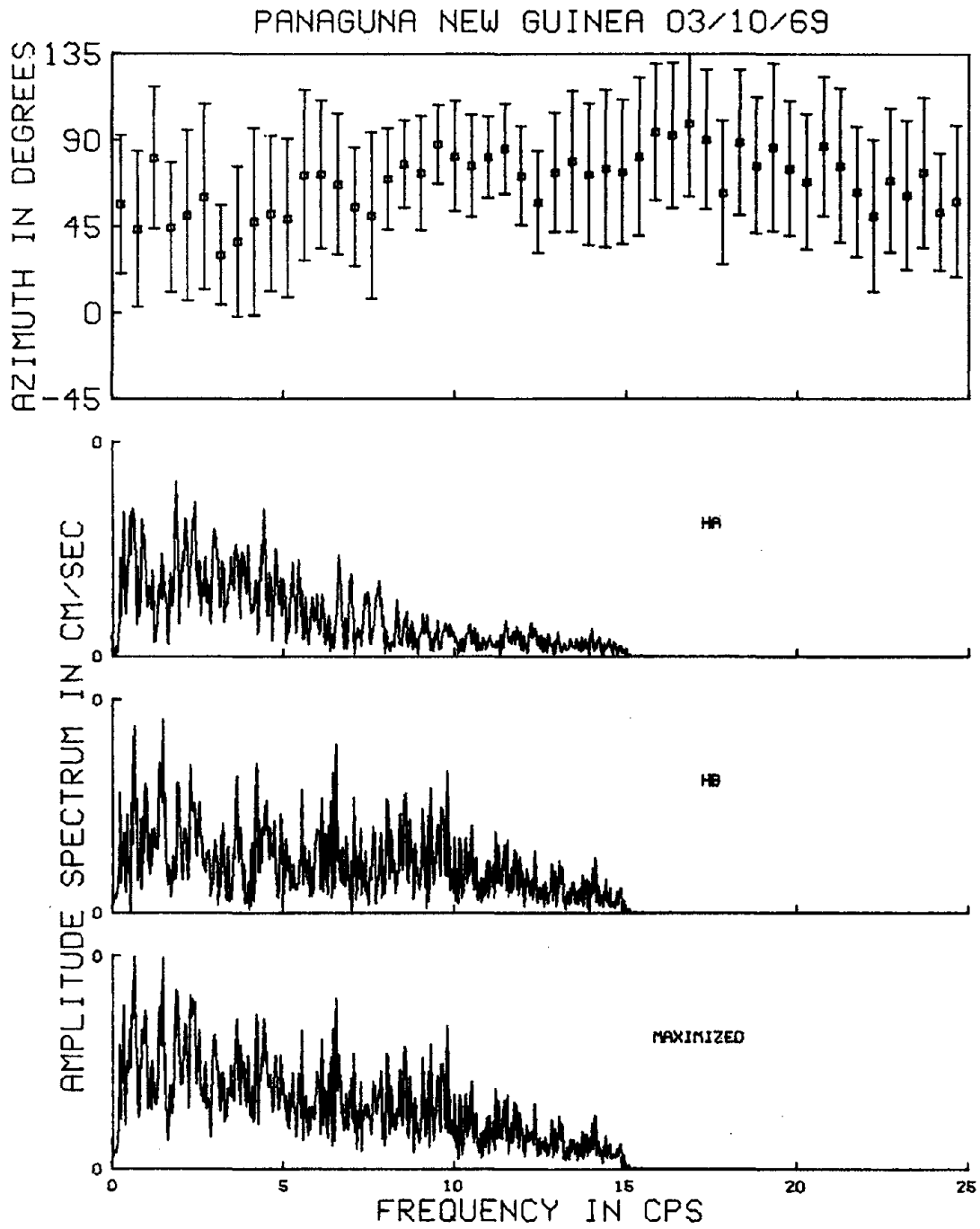


Fig. 2.41a

PANAGUNA NEW GUINEA 03/10/69

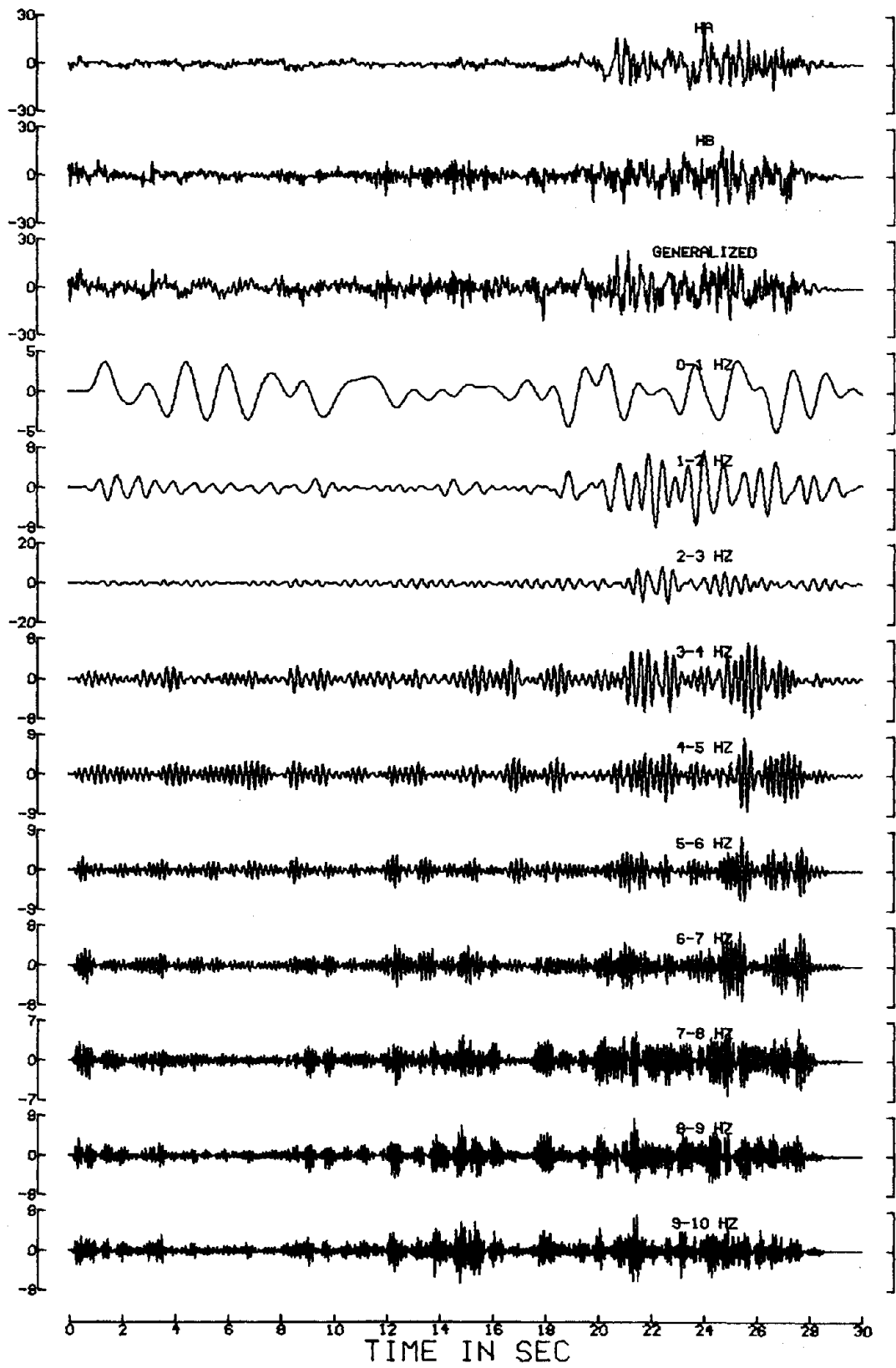


Fig. 2.41b

CHAPTER III

ASSESSMENT OF DIGITIZATION AND BASE-LINE CORRECTION ERRORS3.1--Introduction

Detailed quantitative information on the nature of ground motions close to the source of an earthquake comes from strong motion accelerographs. Quantitative interpretations of seismological and engineering characteristics of strong motion records require careful estimation of the frequency band within which the recording and processing of the ground motion meets a given precision of measurement.

An accelerograph transducer for recording strong ground motion is usually a single-degree-of-freedom oscillator with a high natural frequency of 12 to 25 Hz and with 60 percent damping. The instrumental recording closely approximates acceleration of the ground up to about 5 to 10 Hz. It therefore provides direct information needed for calculations of structural response to ground shaking. In many applications, however, when information on the intermediate and long-period spectrum is required, data on ground velocity or displacement may be preferred. In source mechanism studies, for example, in order to avoid the complicating effects of propagation path and geological complexities near the recording site, it is often more satisfactory to use ground velocities or ground displacements. These depend more upon the low-frequency components of ground motion that are not as sensitive to propagation path and recording site effects.

The usable frequency band of a strong motion record is inherently restricted by the combined noise from all the procedures involved in the record processing. The limits of this band may be determined by not only estimating the signal-to-noise ratio at each frequency harmonic, but also considering the fraction of total spectral energy which is contributed by the processing noise at each harmonic. For a harmonic with frequency ω (within the acceleration response of the instrument) recorded acceleration $\ddot{y} = A \sin \omega t$ corresponds to ground displacement $y = -\frac{A}{\omega^2} \sin \omega t$. Because the recorded amplitude, A , is contaminated with recording and processing noise, at some long period ($\omega \rightarrow 0$), the energy of the errors contributed to the calculated ground displacement, $\frac{A}{\omega^2}$, becomes so large that inclusion of this harmonic may significantly distort the actual displacement. It follows that any study based on analysis of velocity and displacement components requires an estimate of the frequency limit at which the noise energy can be neglected.

In Chapter V of this thesis, the source mechanism of the Parkfield earthquake of 1966 is studied; the analysis is based on velocity and displacement components which are calculated by integrating the accelerograms recorded at different sites. Therefore, to provide an adequate numerical basis, the present chapter is devoted to statistical analysis of the errors due to data processing of strong motion accelerograms and also to the establishment of an estimate of the usable frequency band of displacement components.

The problem of the effect of data processing on strong motion records has been extensively studied by many investigators (McComb, Ruge and Neumann, 1943; Housner, 1947; Hershberger, 1955; Berg and Housner, 1961; Berg, 1963; Amin and Ang, 1966; Brady, 1966; Schiff and

Bogdanoff, 1967; Poppitz, 1968; Hudson, Nigam and Trifunac, 1969; Boyce, 1970; Trifunac, 1971; Trifunac, Udwadia and Brady, 1973a; and Trifunac and Lee, 1974).

In general, there are two different opinions on whether digitized "uncorrected" accelerograms (i.e., no base-line or instrument corrections or adjustments) are accurate enough to calculate precise displacements by double integration. One view (e.g., Schiff and Bogdanoff, 1967) is that the accuracy of digitized uncorrected accelerograms is too limited for the double-integrated displacement curves to preserve a meaningful form. The contrary opinion (e.g., Trifunac et al., 1973) is that under normal conditions of recording and data processing, uncorrected accelerograms can yield displacement curves of usable precision up to some long-period (low-frequency) limit.

In an attempt to estimate errors in digitized strong motion accelerograms, Trifunac et al. (1973) made a statistical analysis of errors of a straight thin line, independently digitized by four different operators. They showed that among all errors of recording, record processing and digitizing, human reading error is the main contributing factor to the variance of the total errors. They concluded that this error limits the usable long periods of double-integrated digitized data at about 16 seconds.

It is, however, important to note that any estimate of recording errors based on a digitized straight line may not be an unbiased representation of the errors for actual accelerograms. Unlike the straight line which is uniformly thin (see Trifunac et al., 1973), the trace thickness of an accelerogram varies with amplitude of the record.

In addition to reading errors due to human eyes, there is

another significant and, up to the present, overlooked error which is introduced into the data during base-line correction processing. This error originates mainly from the uncertainties in the parameters by which a base-line is defined. The base-line of a given accelerogram record is usually determined by fitting the "closest" curve (straight line or higher order polynomial) to the data by the least-squares method. In this case, for a given accelerogram, values of the base-line parameters strongly depend on the particular selection of digitized data points along the length of record.

The following sections of this chapter examine these two prominent errors (reading and base-line correction) in some detail and establish a statistical basis for estimating the long-period limits introduced in computed displacements by these errors.

3.2--Reading Errors Due to Human Eyes

A direct assessment of reading errors of digitized accelerograms can be made by analyzing a group of records which are obtained from digitizing, repeatedly, the same record by a number of operators. The meaningful long-period limit of displacement can then be estimated from the variance of the displacement amplitude spectrum at low frequencies. In the absence of such information it is, nevertheless, possible to make a reliable estimate of reading errors because for each accelerogram, the sources involved with generating these errors, such as the thicknesses of accelerogram trace, the fixed trace, and cross hairs used in the typical digitizing machine, are generally well known. The trace thickness of an accelerogram on the Mylar translucent films varies between 0.2 or 0.3 mm to about 1 mm. In a typical strong motion record,

the high-energy (large-amplitude) episode occupies only a small portion of the total length. It follows that the trace thickness of a significant part of the length of a record stays at 1mm. The fixed trace is produced by a fixed mirror which is rigidly attached to the accelerograph frame. To eliminate the effect of the systematic errors introduced by the digitizing machine, this trace is digitized and subtracted from the accelerometer trace (Trifunac et al., 1973). This trace is 0.5 mm to 1 mm. The cross hairs have finite thickness of 0.1 mm to 0.2 mm.

It is reasonable to assume that the combined errors from the thicknesses of the accelerogram trace, the fixed trace, and the cross hairs are randomly distributed within bounds of at least ± 0.2 mm.

For an accelerogram recorded with sensitivity of about 8 cm/g, for example, extreme bounds of ± 0.2 mm are equivalent to values of about ± 2.45 cm/sec². In the present research, a total of 2048 pseudo-random numbers with acceleration values uniformly distributed between ± 1.225 cm/sec² were generated by computer to resemble recording errors with arbitrary bounds of ± 0.1 mm. The amplitude spectra of the corresponding displacement were then computed for frequencies between 0 and 25 Hz (the Nyquist frequency) and plotted in Figure 3.1.

The lowest straight dashed line in this figure is the least-square fitted line to the displacement amplitude spectrum. The two upper dashed lines show the fitted lines to the displacement amplitude spectra corresponding to reading errors of ± 0.2 mm and ± 0.4 mm respectively. Conveniently, therefore, the middle one of these lines will be utilized in the remainder of the present chapter to represent the effect of reading errors of accelerograms in corresponding displacement records.

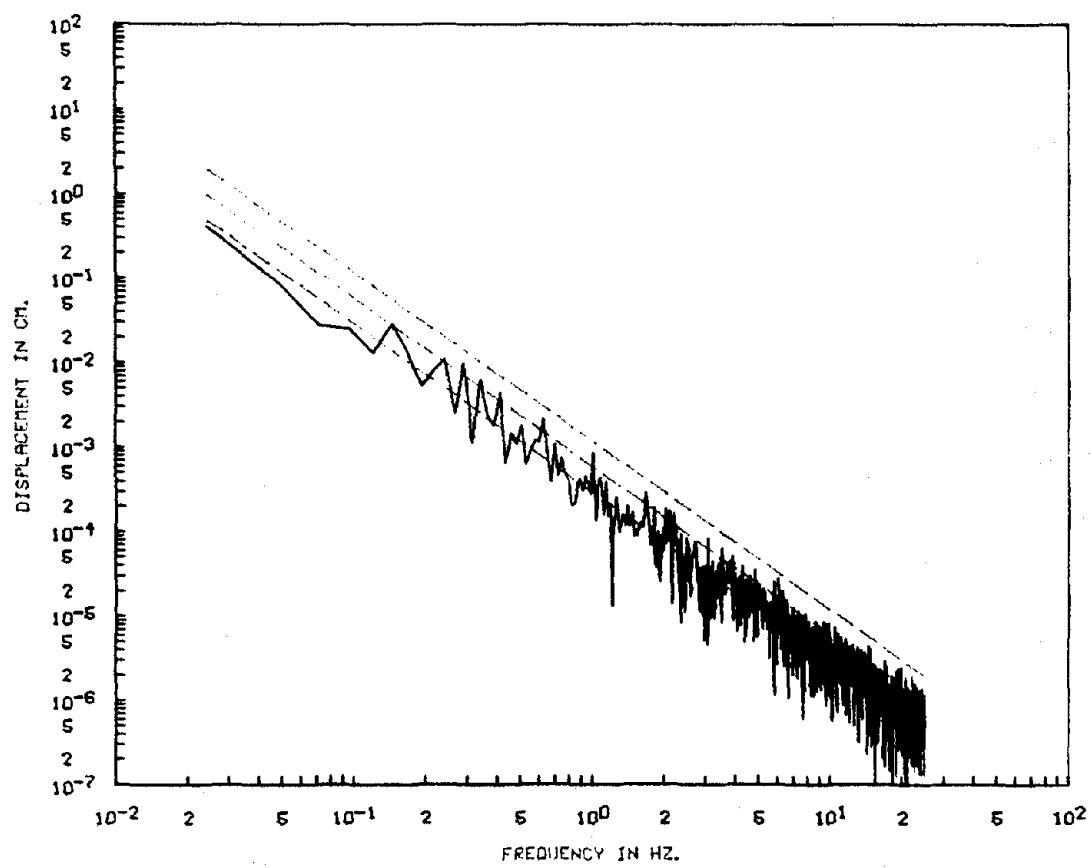


Fig. 3.1

3.3--Errors Due to Base-Line Correction

As mentioned previously, for a given accelerogram the values of the base-line parameters depend strongly on the selection of the positions of the data points along the time axis. Variations in the base-line parameters have pronounced effects on low-frequency components of the displacement records. During digitization of accelerograms, the time positions of the majority of points (with the possible exception of points corresponding to peaks and troughs) are selected more or less arbitrarily. Therefore, redigitization of the same record is likely to produce data points the majority of which have different time positions. An important question is to what extent deviation of the time positions affects the base-line parameters.

To investigate this question, we make use of the powerful statistical method called the "jack-knife technique" (Tukey, 1958; Brillinger, 1964; Brillinger, 1966). The jack-knife method entails dividing the sample into a number of different sub-samples (chosen in a particular way) and calculating the desired values from all the sub-groups, except one, to produce what are known as "pseudo-values." The procedure is repeated over and over, omitting a different sub-group each time. The variance of the population is then estimated directly from these "pseudo-values."

Suppose an accelerogram consists of N data points. Let A and B define the base-line $A + Bt$ (t is time) that may be calculated from these data points. Separate these points into r groups such that the data points of each group are selected randomly from the total N points. Let A_i and B_i be the parameters of the base-line based on all but the i th group. A_i, B_i ($i = 1, \dots, r$) are used to determine the variances

of A and B respectively.

The unbiased estimates of the variances of A and B can be determined simply from

$$\sigma_A^2 = \frac{1}{r} \sum_{i=1}^r (A - A_i)^2 / (r - 1) \quad (3.1a)$$

$$\sigma_B^2 = \frac{1}{r} \sum_{i=1}^r (B - B_i)^2 / (r - 1) \quad (3.1b)$$

Determination of base-line parameters and their corresponding variances were carried out for all strong motion accelerogram records obtained during the 1966 Parkfield earthquake. These records form the basis of the analysis of this earthquake in Chapter V. For comparison, the parameters and related variances of the Taft 1952 records were also calculated.

For all records, except CH #8 and Temblor, a length of 40 seconds ($N = 2,000$ points with equi-interval $\Delta t = 0.02$ sec) was selected. For CH #8 and Temblor, which are shorter than 40 seconds, lengths of 26 seconds ($N = 1,300$ points) and 30 seconds ($N = 1,500$ points) were selected, respectively. A straight base-line $A + Bt$ was fitted for each record to the data points by least squares.

For the jack-knife procedure, A_i and B_i were calculated based on all but the i th group (the i th group was chosen (sampled) randomly from the N data points). In the present analysis, each record was separated into 10 groups, each of which consisted of $N/10$ data points. Brillinger (1966) indicated that values of r between 10 and 20 are reasonable.

In order to examine how the estimated variance may vary with

r , standard errors σ_A and σ_B of the vertical component of CH #2 were calculated. The resulting parameters for these records were $A = 2.398$, $B = -0.1076$. (The values of data are in terms of cm/sec^2 .) For $r = 10$, $\sigma_A = 0.61000$ and $\sigma_B = 0.02208$, and for $r = 20$, $\sigma_A = 0.49120$ and $\sigma_B = 0.01767$. It should be noticed that selection of 20 groups gives slightly smaller variances.

Because under normal conditions of digitization the gross effects of the variances do not appear to be overestimated by selection of 10 groups, the data points of all records were therefore separated into 10 groups. The values of A , B , σ_A , and σ_B for CH #2, #5, #8, #12, Temblor and Taft 1952 are given in Table 3.1.

At this stage, let us examine the effects of the base-line parameters and their variations on the spectrum of displacement which are calculated from the accelerograms. The upper plots of Figure 3.2 through 3.18 illustrate the displacement amplitude spectra calculated from:

1. accelerograms with uncorrected base-line (shown by solid line)
2. accelerograms with corrected base-line, $A + Bt$ (shown by small dashed line)
3. accelerograms with corrected base-line, $A + \sigma_A + (B + \sigma_B)t$ (shown by intermediate dashed line)
4. accelerograms with corrected base-line, $A - \sigma_A + (B - \sigma_B)t$ (shown by large dashed line).

The phase variation of displacement spectra, due to variation of the base-line parameters, is as important as amplitude variation in controlling the long-period limits of displacement records; the analysis of base-line correction errors should, therefore, incorporate

this variation with amplitude variation. The middle plots show the phase variation introduced by incorporating σ_A and σ_B into the baseline corrections.

These plots, as well as the values of σ_A and σ_B shown in Table 3.1, indicate that for some records (e.g., CH #12 N50E and N40W) variation

TABLE 3.1

	A	σ_A	B	σ_B	T_b^* (sec)	T_c^{**} (sec)
CH #2, Down	2.398	0.610	-0.108	0.022	12.5	11.0
CH #2, N65E	0.475	0.982	-0.023	0.034	13.0	12.5
CH #5, Down	1.529	0.476	-0.070	0.016	12.0	8.0
CH #5, N85E	0.164	0.969	-0.008	0.031	12.0	10.0
CH #5, N05W	-0.739	0.760	0.032	0.024	11.0	10.0
Temblor, Down	0.813	0.290	-0.052	0.014	10.0	7.5
Temblor, S25W	1.514	1.012	-0.096	0.046	8.0	7.0
Temblor, N65W	0.353	0.491	-0.023	0.023	12.0	10.0
CH #8, Down	-0.133	0.444	0.009	0.023	9.0	7.5
CH #8, N50E	0.413	0.890	-0.032	0.044	9.0	7.5
CH #8, N40W	0.487	0.680	-0.037	0.036	9.5	9.0
CH #12, Down	1.634	0.292	-0.076	0.011	12.5	9.5
CH #12, N50E	1.818	0.207	-0.081	0.007	14.5	10.5
CH #12, N40W	3.007	0.138	-0.133	0.005	no limit	13.0
Taft, Down	-0.042	0.286	0.004	0.010	19.0	14.0
Taft, 869F	-0.065	0.623	0.002	0.022	13.0	12.0
Taft, N21E	0.261	0.660	-0.020	0.022	12.5	11.0

* T_b = long-period limit due to base-line corrections

** T_c = long-period limit due to combined errors of base-line and reading

of the base-line parameters are less pronounced than those of others. The possible explanation of this difference lies in variation of the gross amplitude along the length of an accelerogram; for a record along which the gross amplitude is more uniform, the σ_A and σ_B are expected to be smaller.

As it can be seen from the plots, variation of the base-line parameters affect significantly the low-frequency components of the amplitude as well as phase spectra of displacements up to about 0.1 Hz. Displacement spectral energy is mainly contributed by the few lowest frequency components and hence the significant variations observed in amplitude and phase of these components will mask the characteristics of displacement records.

In order to make an estimation of the long-period limits (longest usable periods), the following method was developed and the results depicted in the lower plots of Figure 3.2 through Figure 3.18.

The method is, simply, to compare, at a given frequency ω_i , the absolute value of amplitude variation, $|\Delta D(\omega_i)|$, (due to σ_A and σ_B) with some fraction (i.e., 5 percent) of the accumulative displacement amplitude spectra, $\sum_{j=N}^{i-1} |D(\omega_j)|$, corresponding to the subsequent frequency ω_{i-1} (N corresponds to Nyquist frequency and is equal to 1024 in this analysis). In the lower plots of Figure 3.2 through 3.18, the accumulative amplitude spectra are shown by the upper solid lines. The dashed lines parallel to these solid lines show the 5 percent fraction of the accumulative displacement spectra; a fraction of 5 percent is selected arbitrarily as the basis for estimating the usable long-period limits of displacement records. The amplitude variations $|\Delta D(\omega_i)|$ are plotted by the oscillatory solid lines. For each record,

the crossing point of the $|\Delta D(\omega_i)|$ line with the 5 percent fraction line defines the long-period limits introduced during base-line correction. These periods are listed in Table 3.1.

3.4--Combined Errors of Reading and Base-Line Correction

The combined errors of reading and base-line correction for each record were obtained simply by adding, at each frequency, the value given by the middle dashed line in Figure 3.1 (this line resembles the reading errors bounded by ± 0.2 mm) to the value given by the $|\Delta D(\omega_i)|$ curve. The combined errors are shown in the lower plots of Figure 3.2 through Figure 3.18 by the short dashed lines. Now the long-period limits due to the combined errors can be readily found from the points where the lines of combined errors cross the lines corresponding to 5 percent fraction of the accumulative displacements. The results are also given in Table 3.1.

The long-period limits introduced by the combined errors are very much controlled by the degree of fluctuation in both amplitude and phase at long periods. The long-period limits, as shown in the figures and Table 3.1, vary between 7.0 to 14.0 seconds. This result, therefore, indicates that the long-period limit of 16 seconds inferred by Trifunac et al. (1973) is probably too great. The large variation of the long-period limits of the 17 strong motion records analyzed in the present chapter suggests that the usable long-period limit of each record should be determined independently, case by case. A more representative average value to the long-period limit of actual ground displacement appears to be 12 seconds.

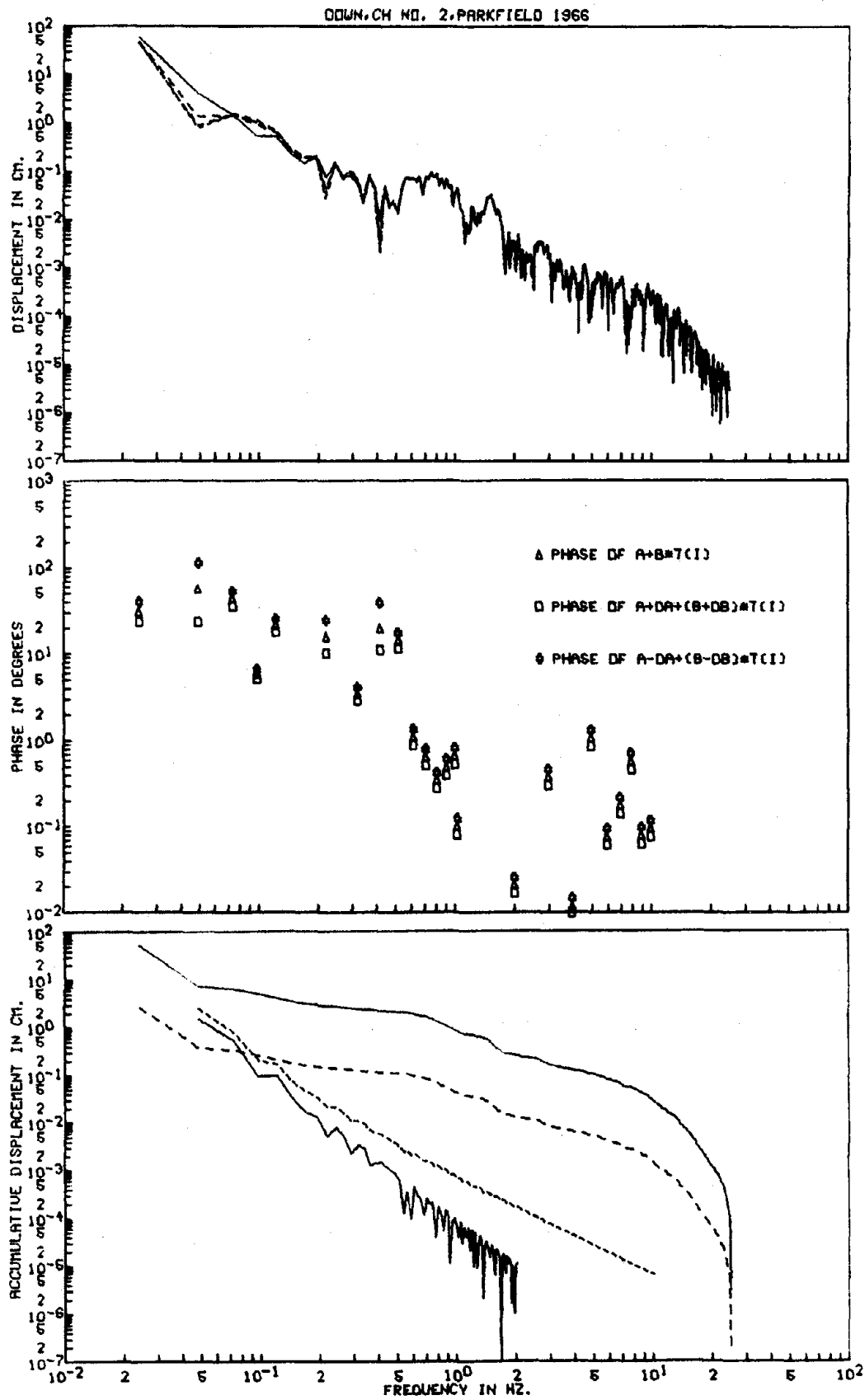


Fig. 3.2

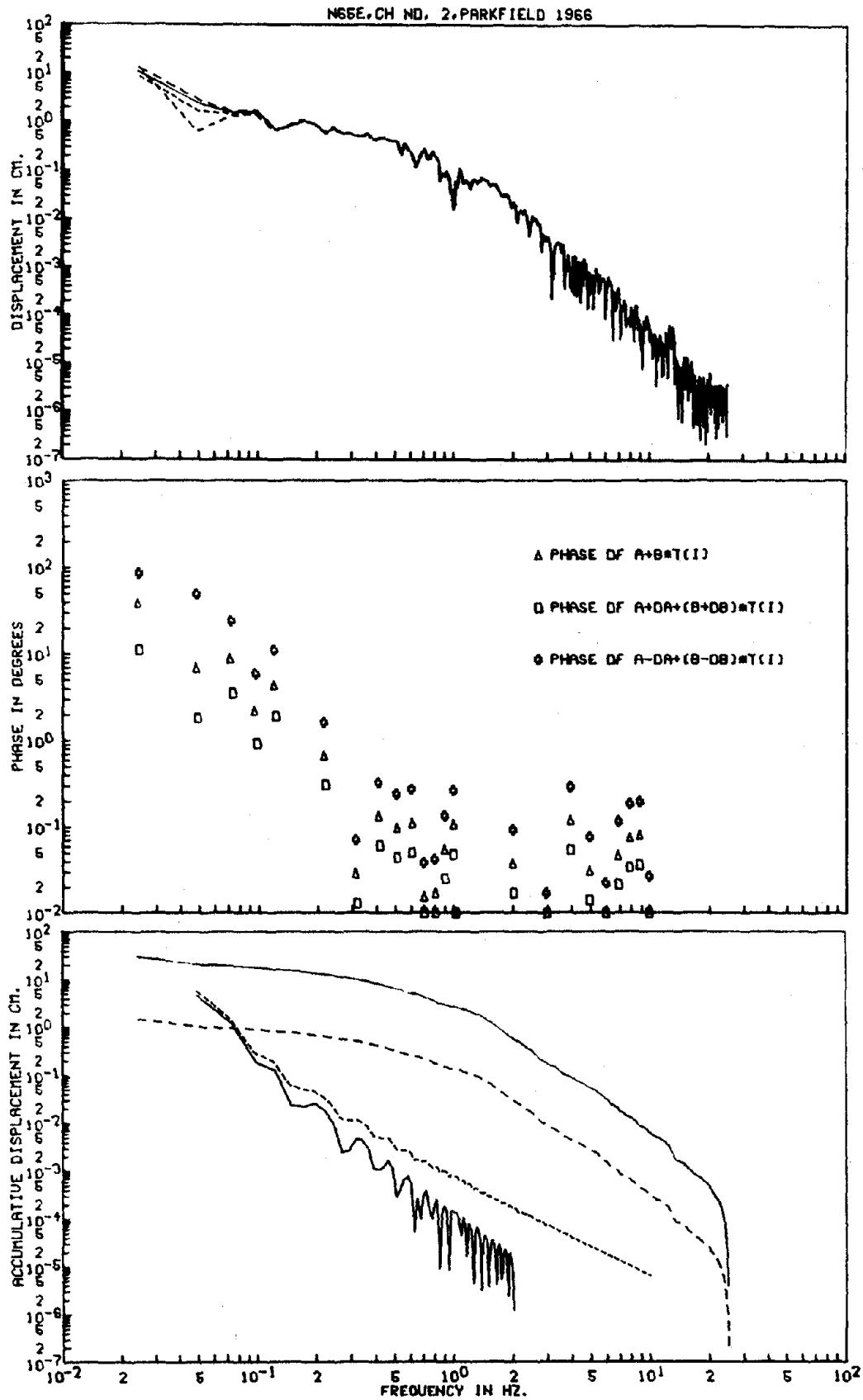


Fig. 3.3

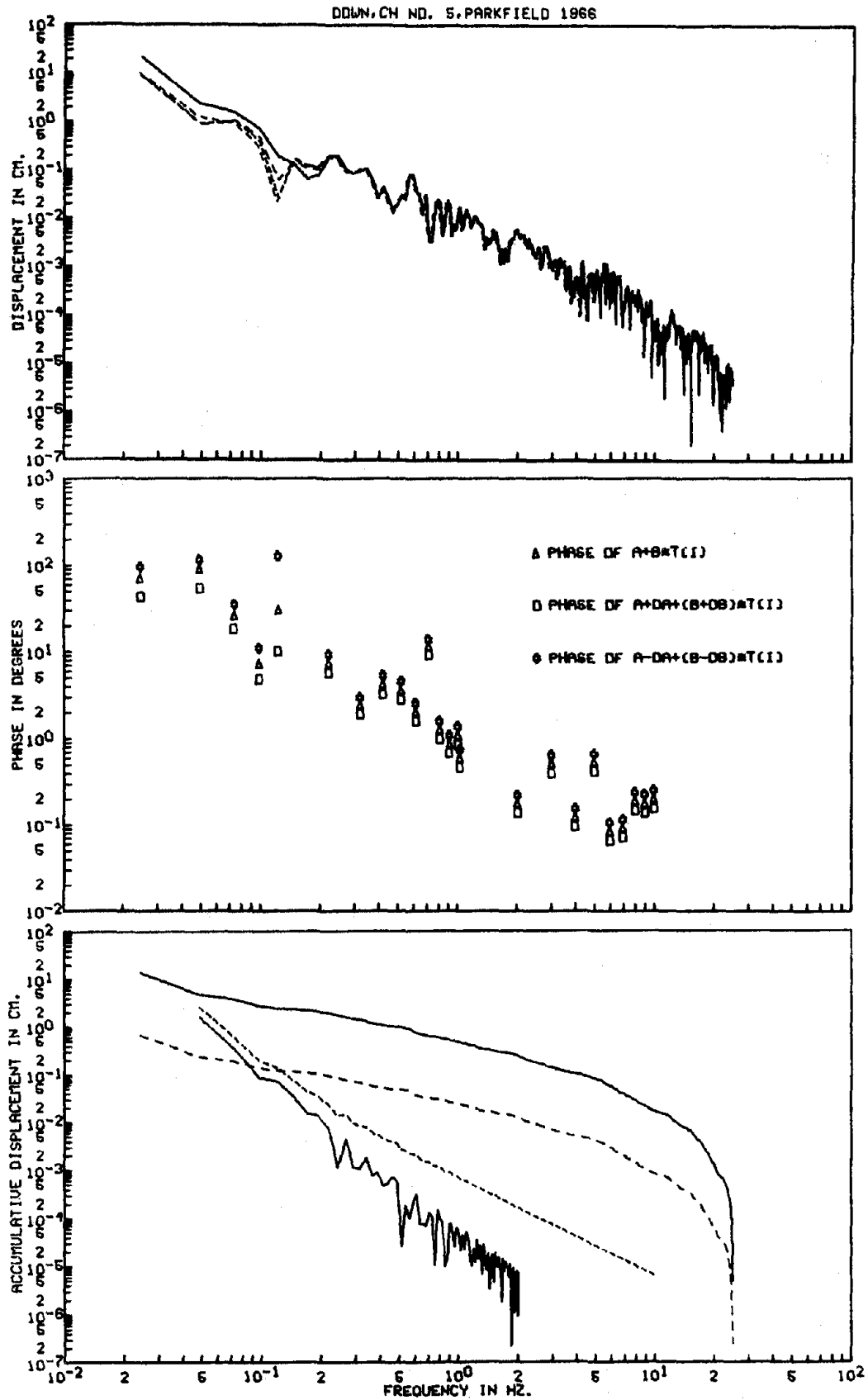


Fig. 3.4

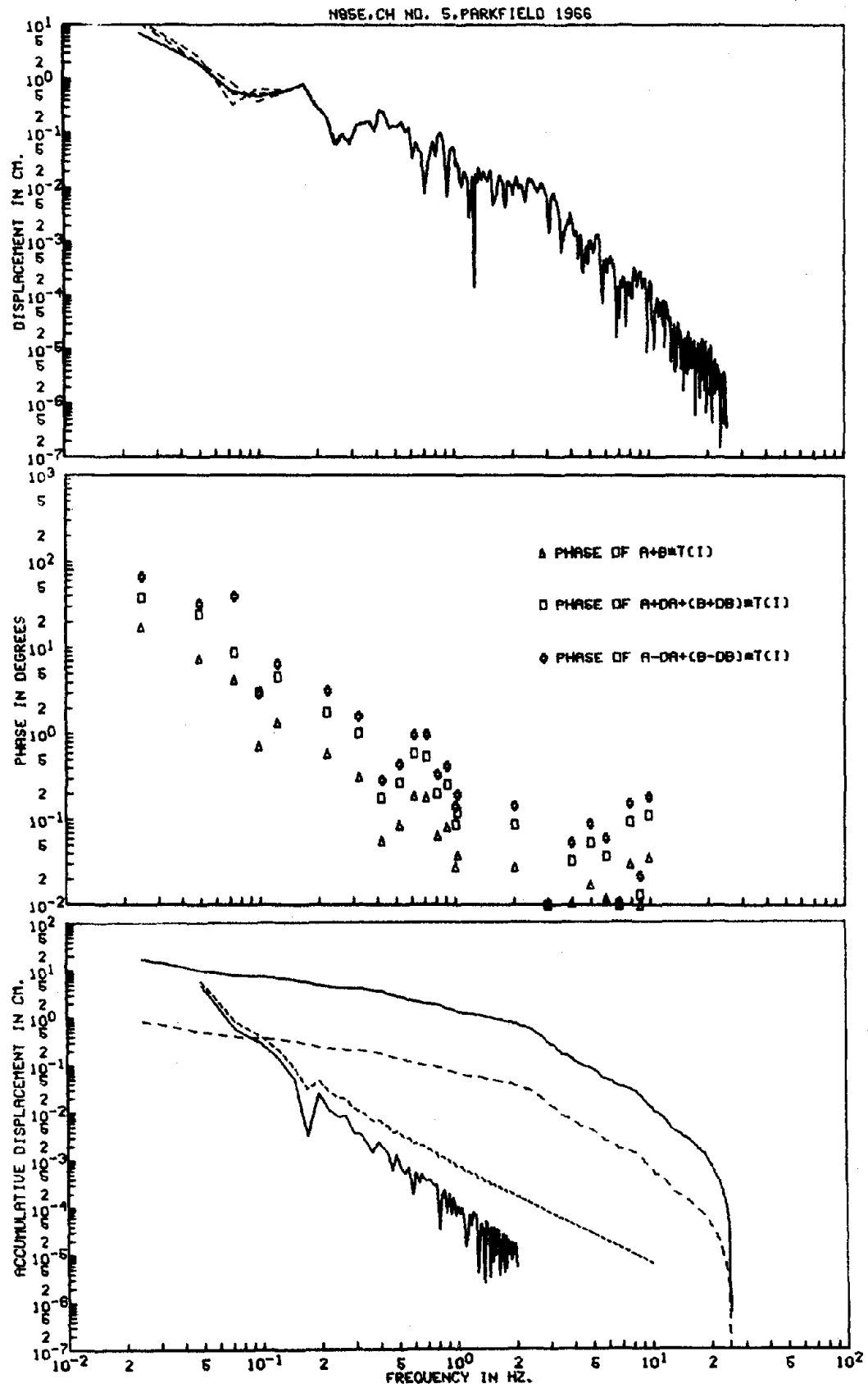


Fig. 3.5

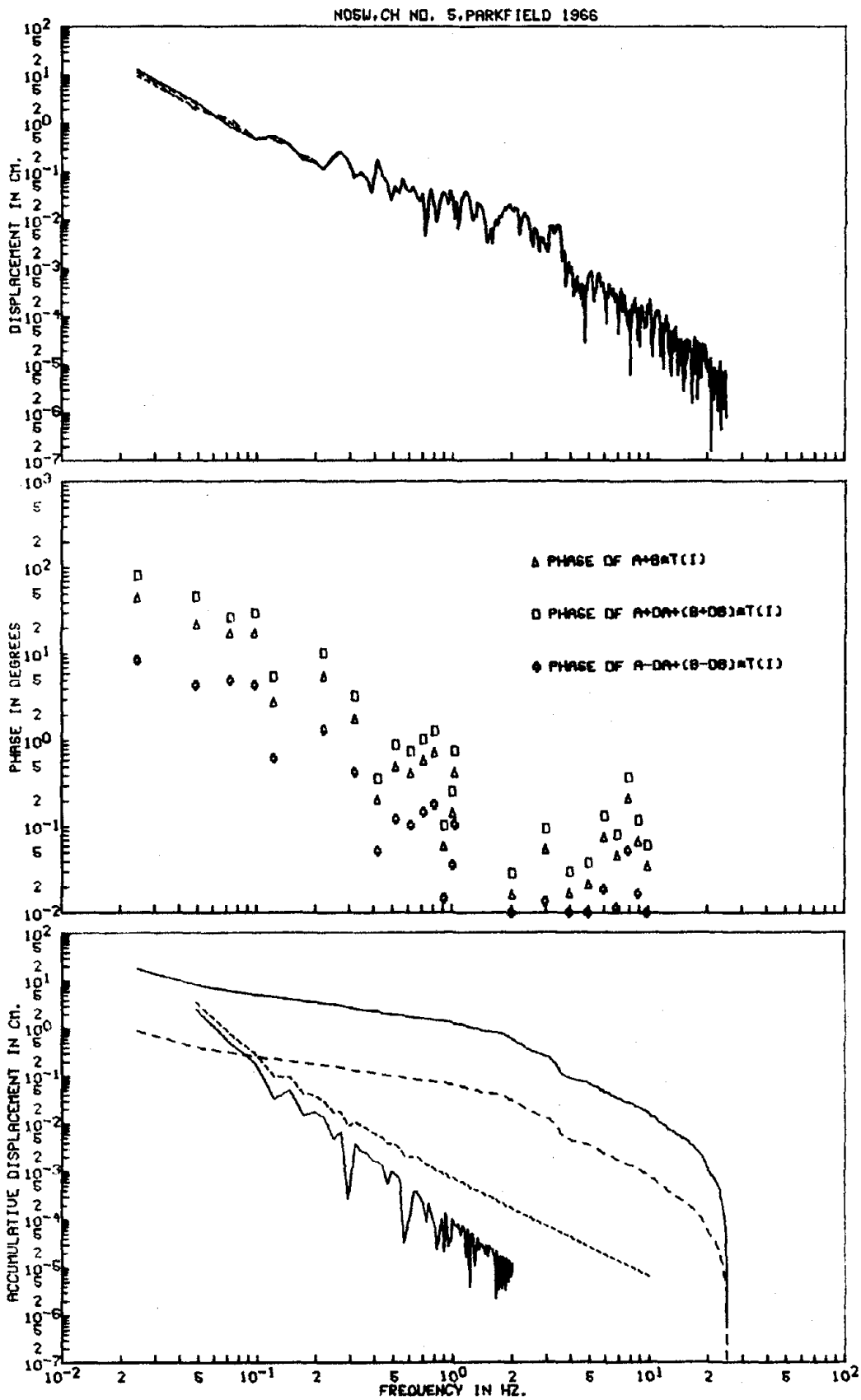


Fig. 3.6

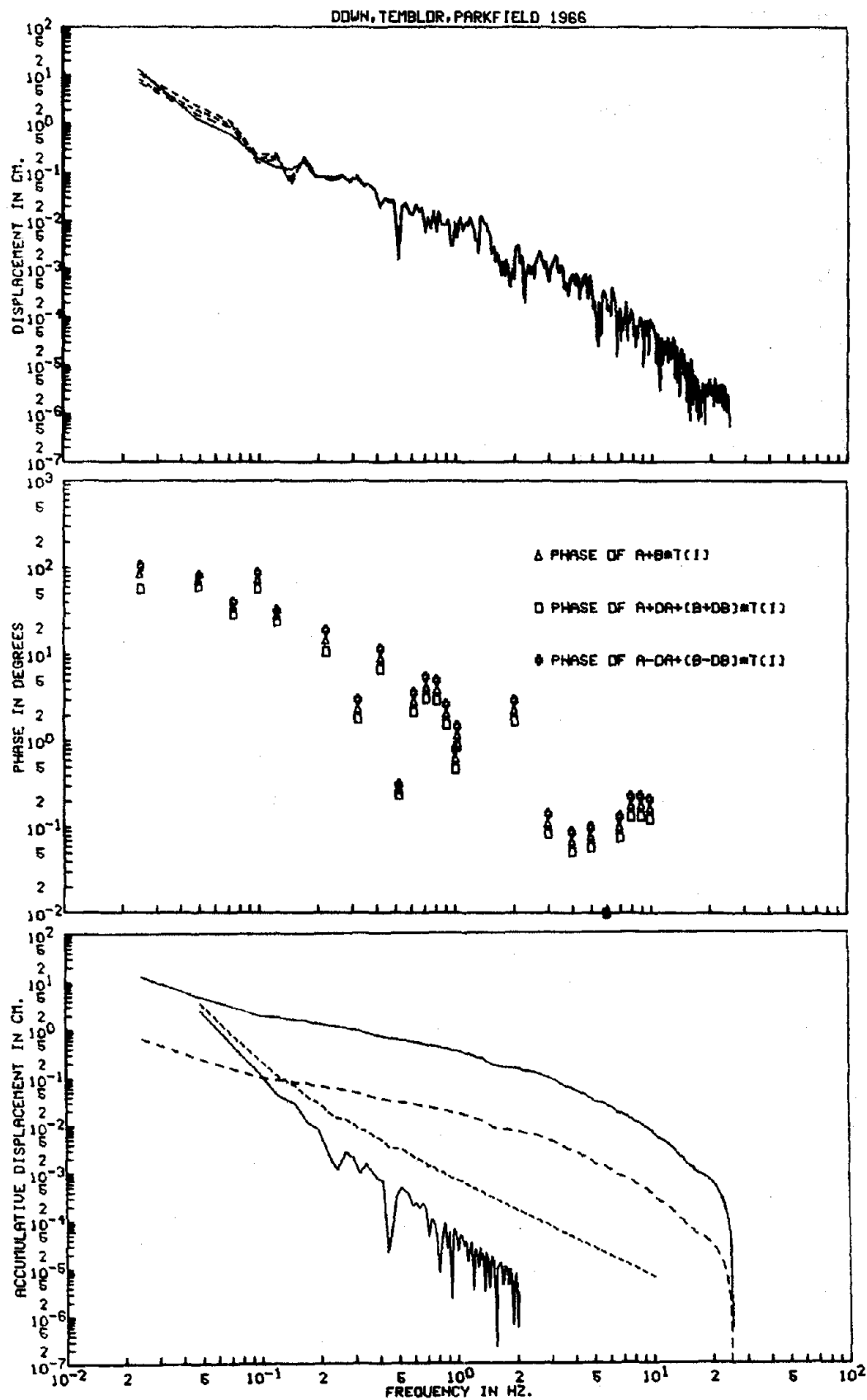


Fig. 3.7

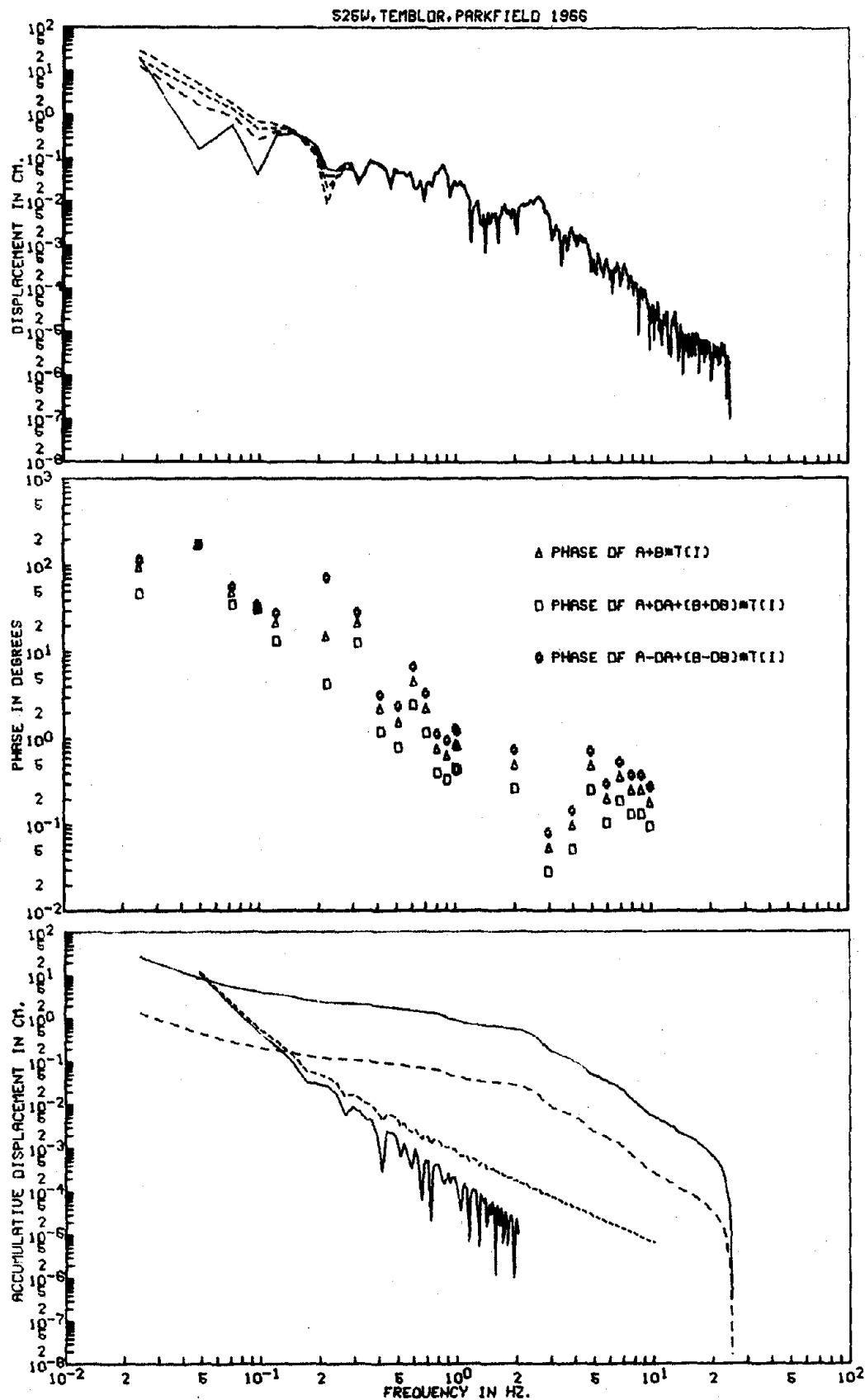


Fig. 3.8

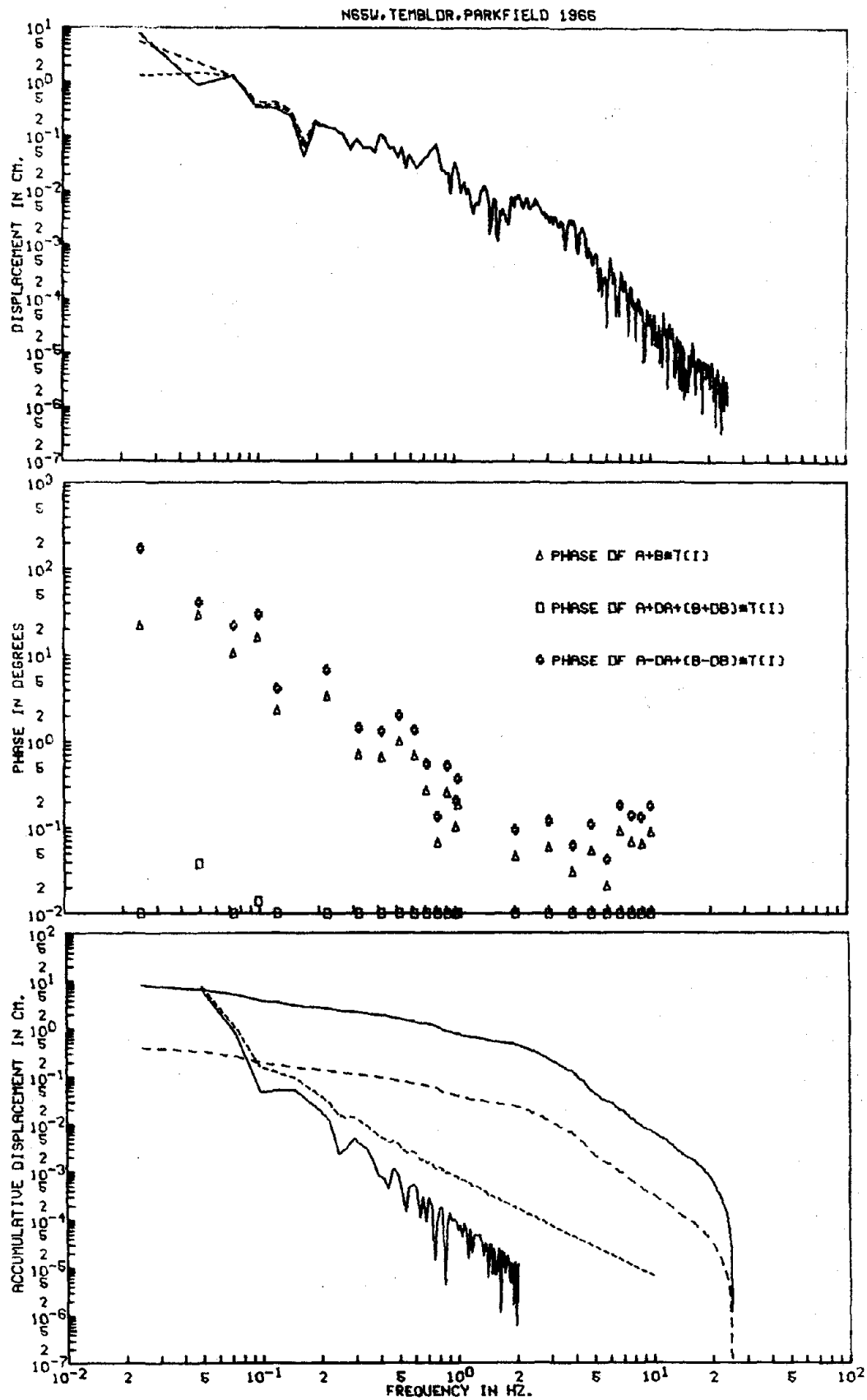


Fig. 3.9

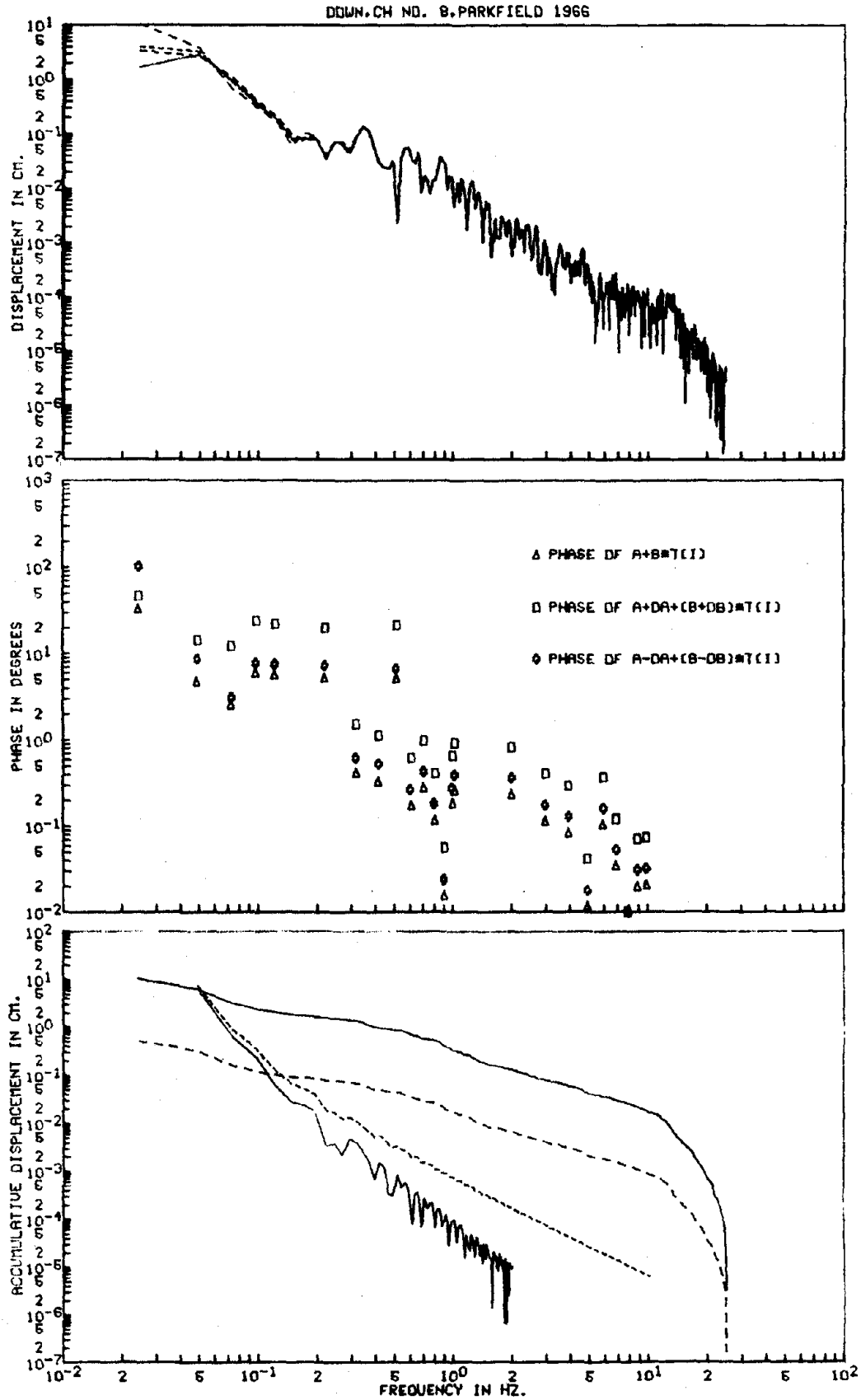


Fig. 3.10

N50E, CH NO. 9, PARKFIELD 1966

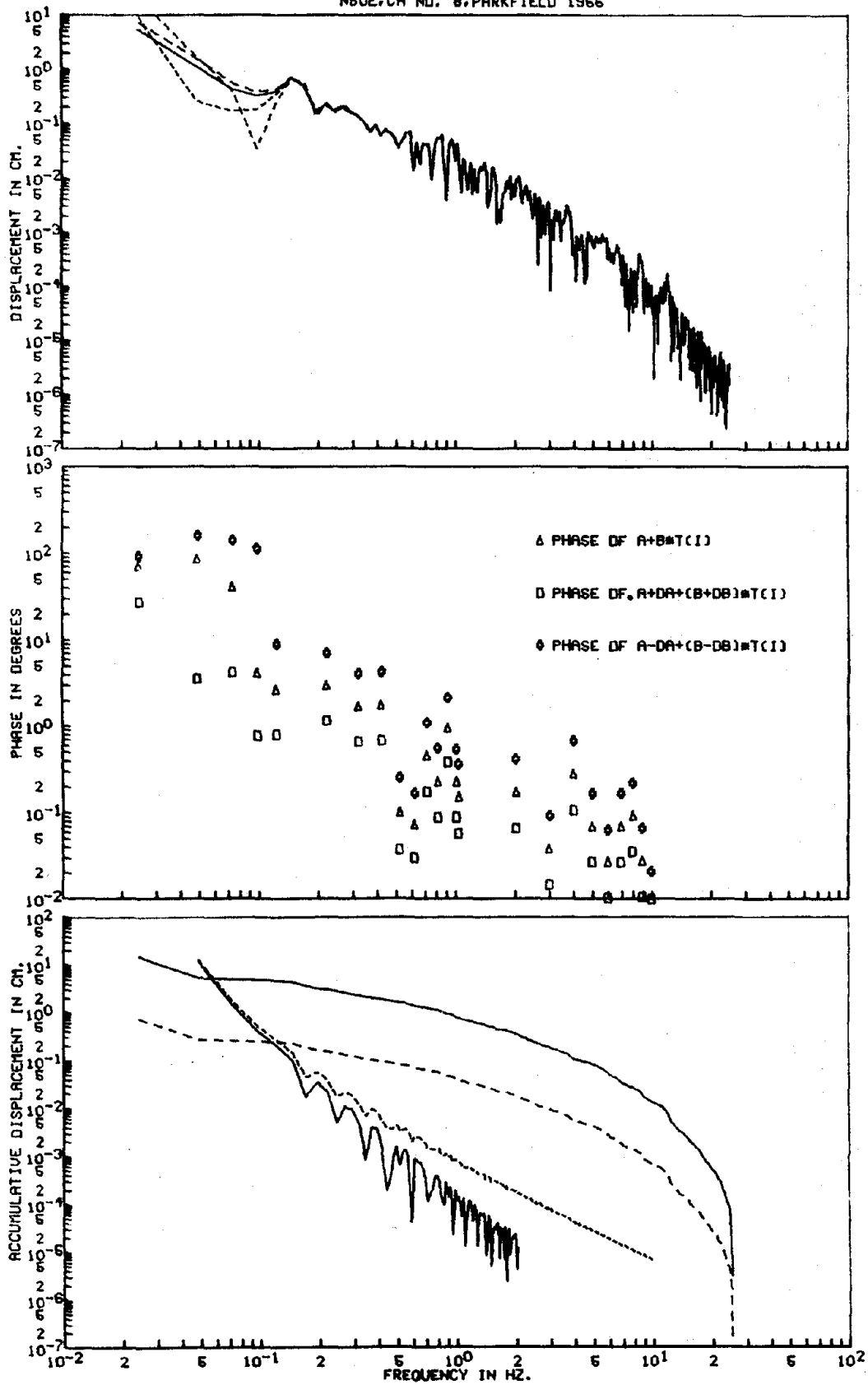


Fig. 3.11

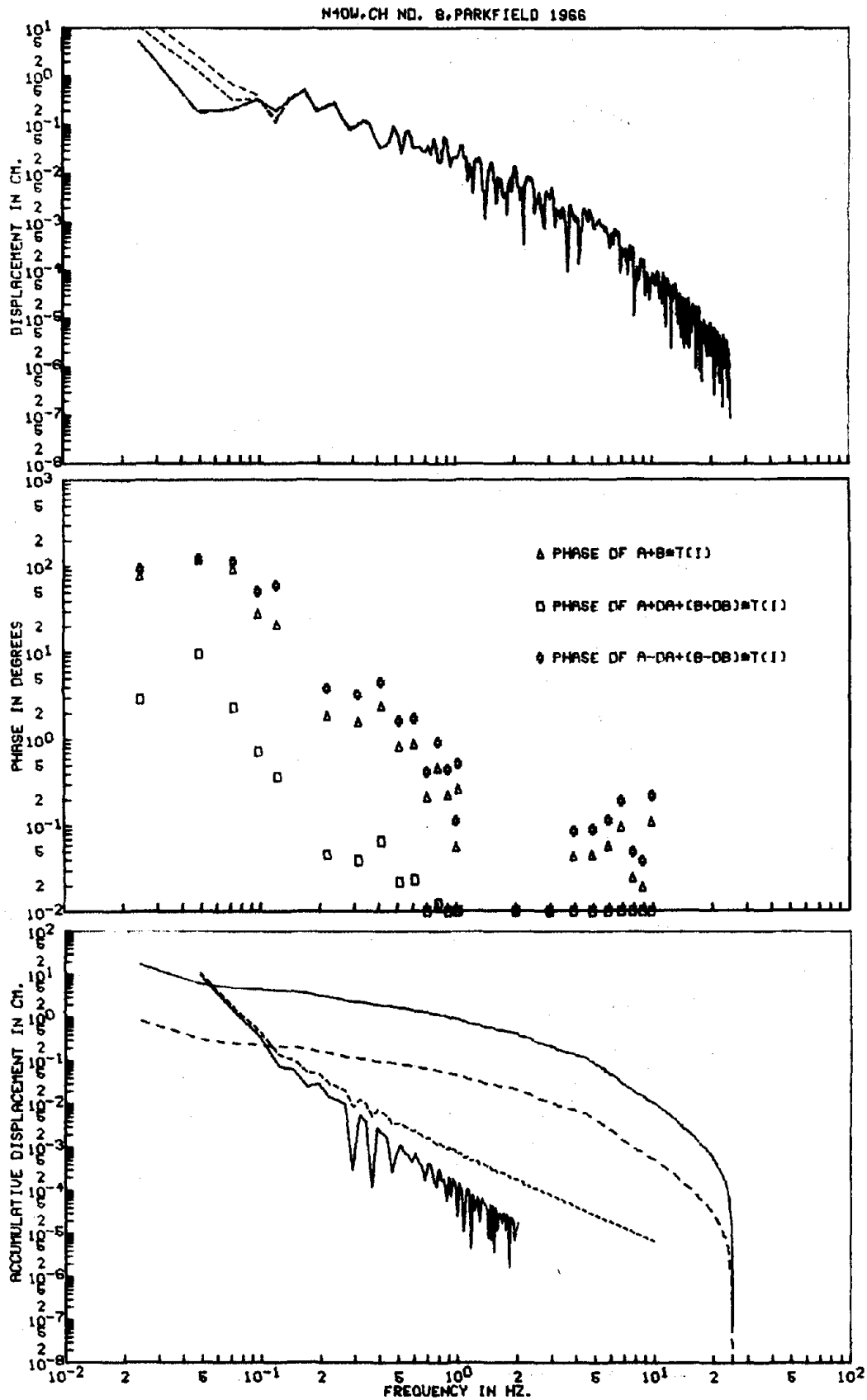


Fig. 3.12

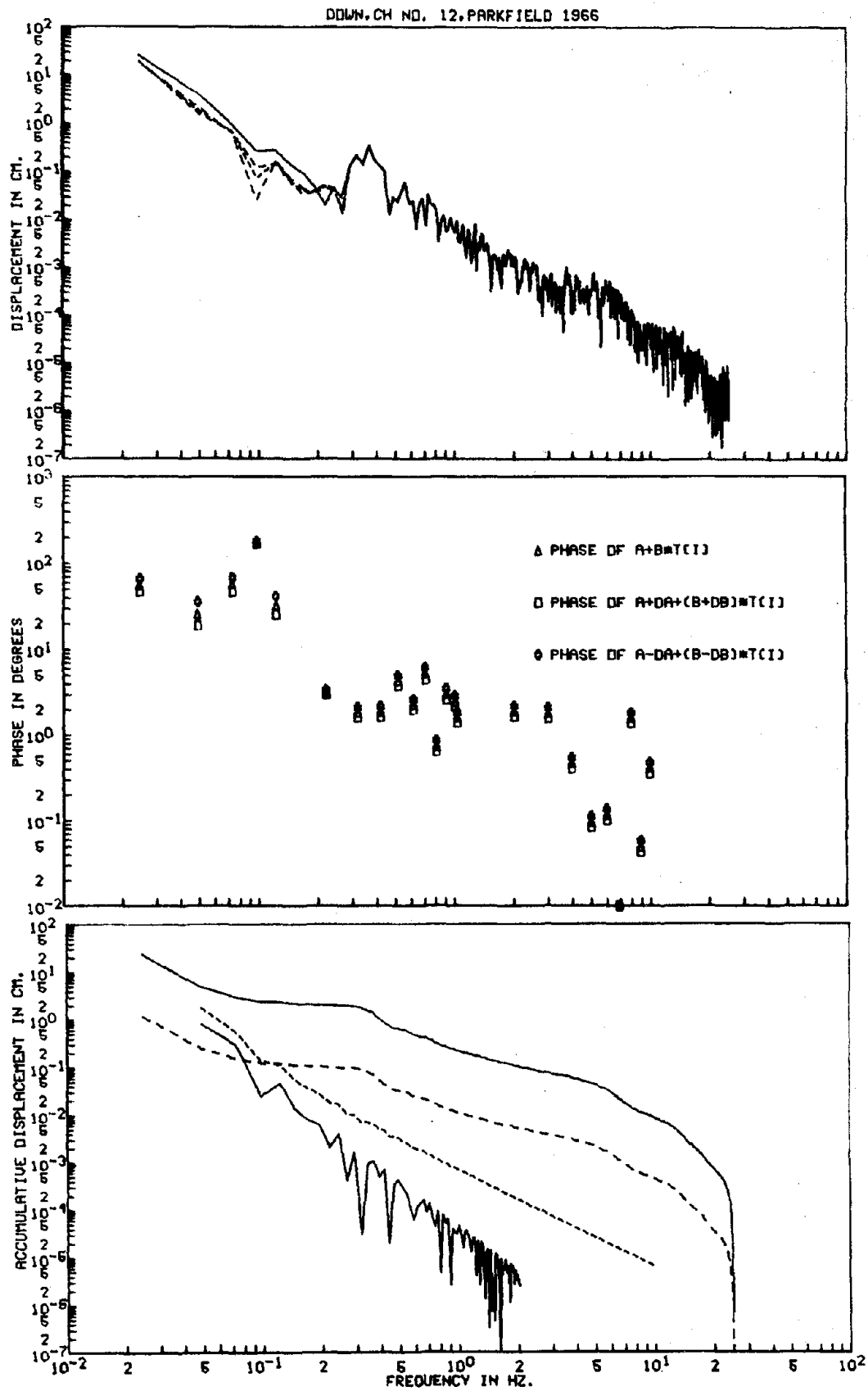


Fig. 3.13

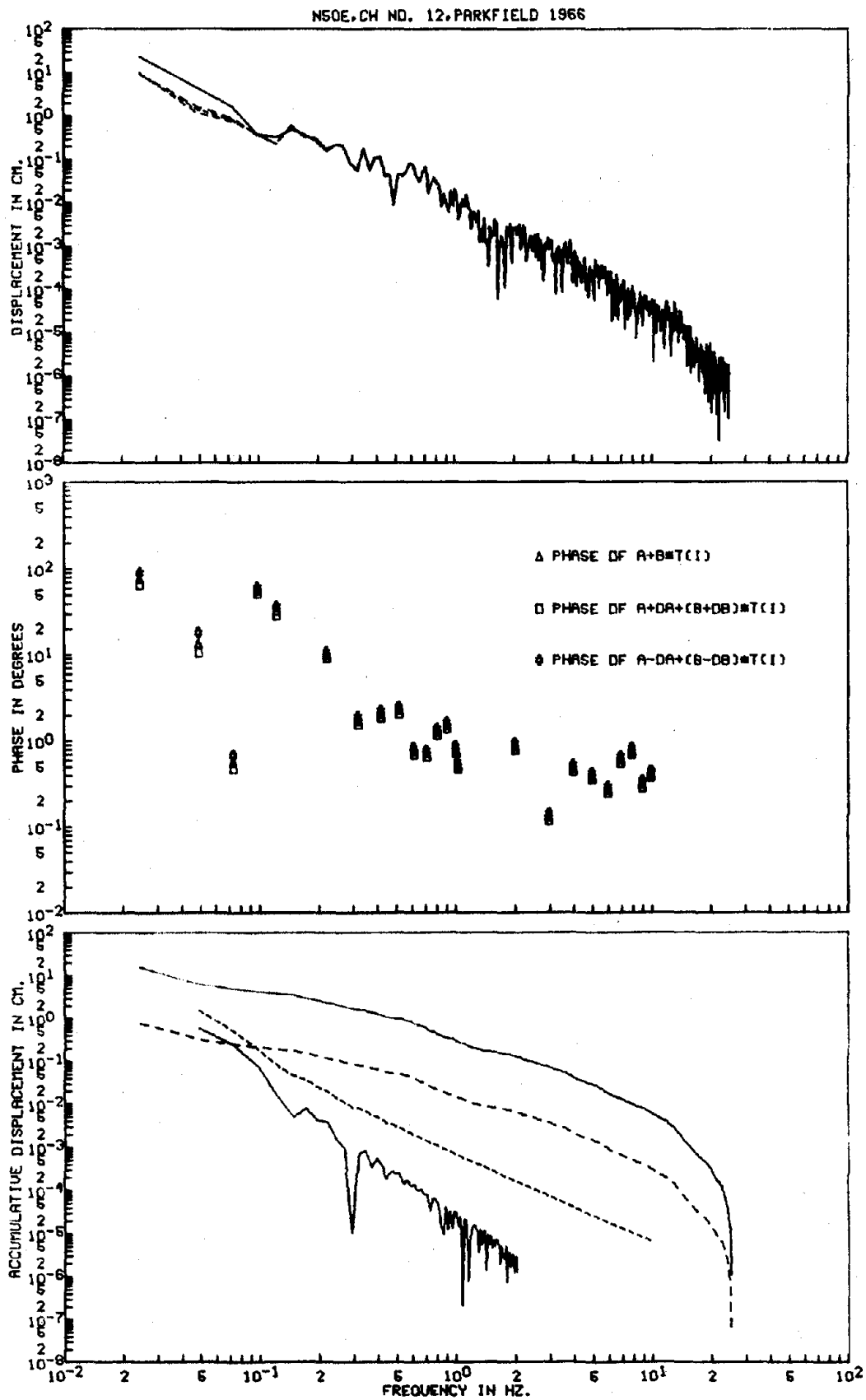


Fig. 3.14

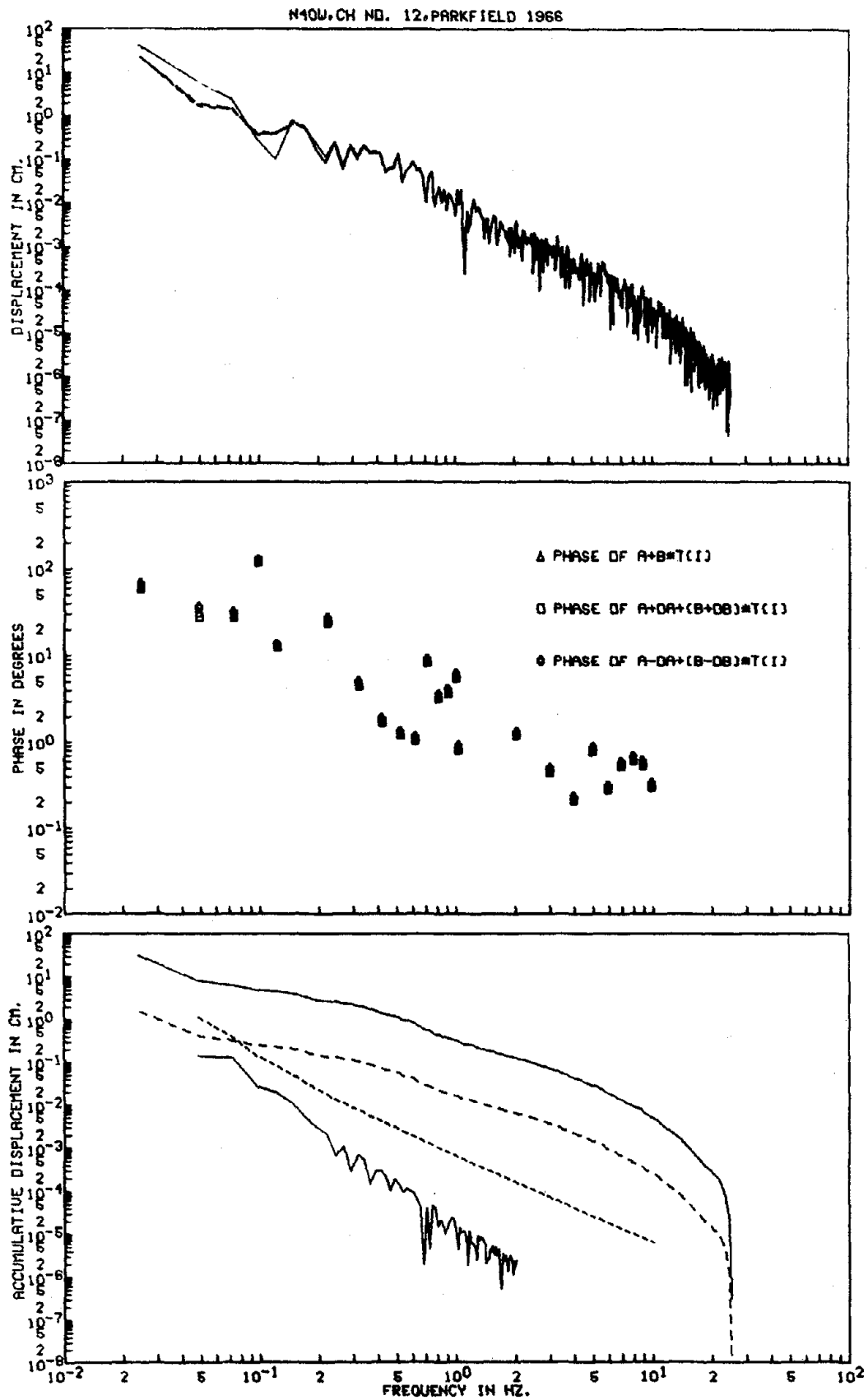


Fig. 3.15

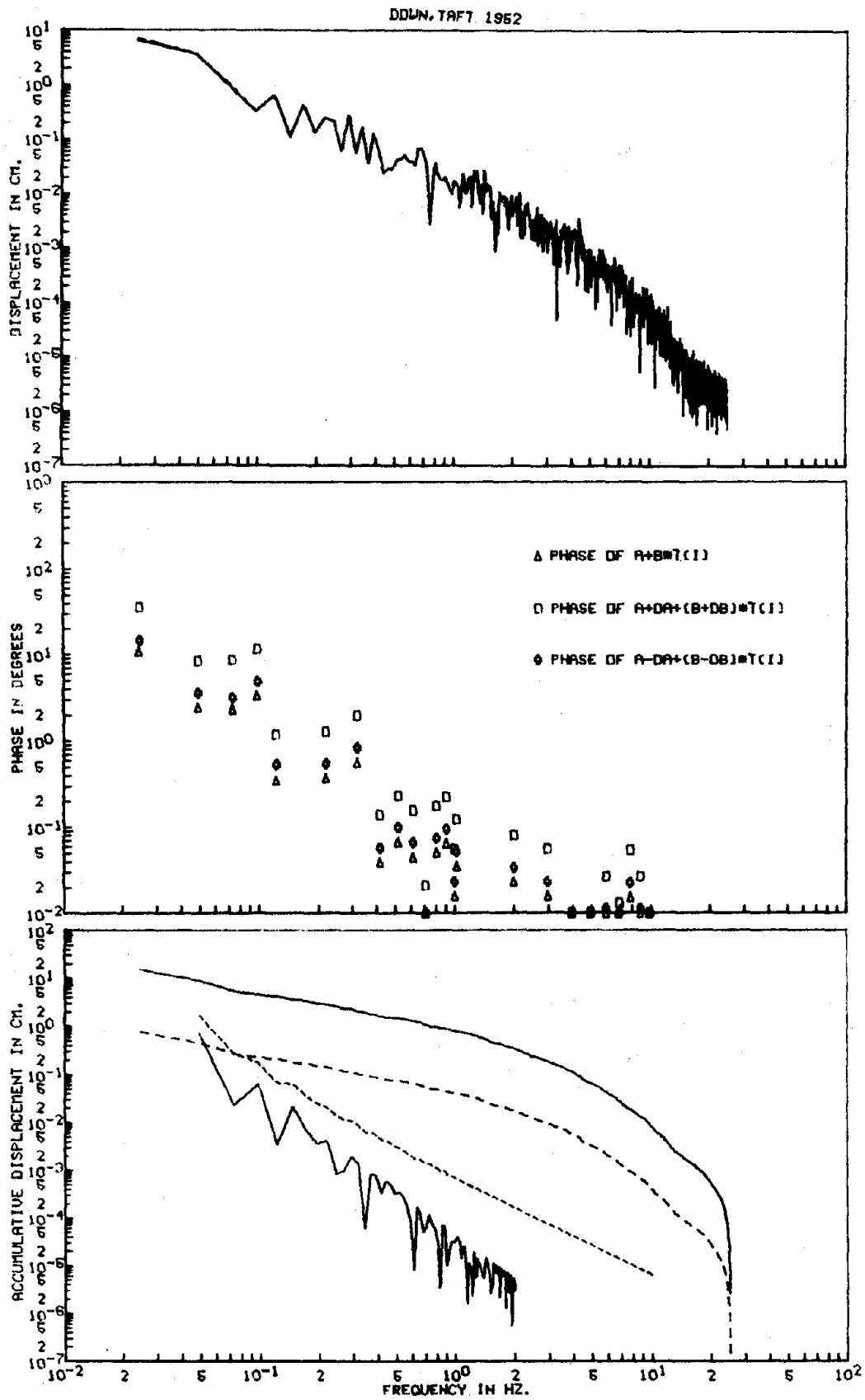


Fig. 3.16

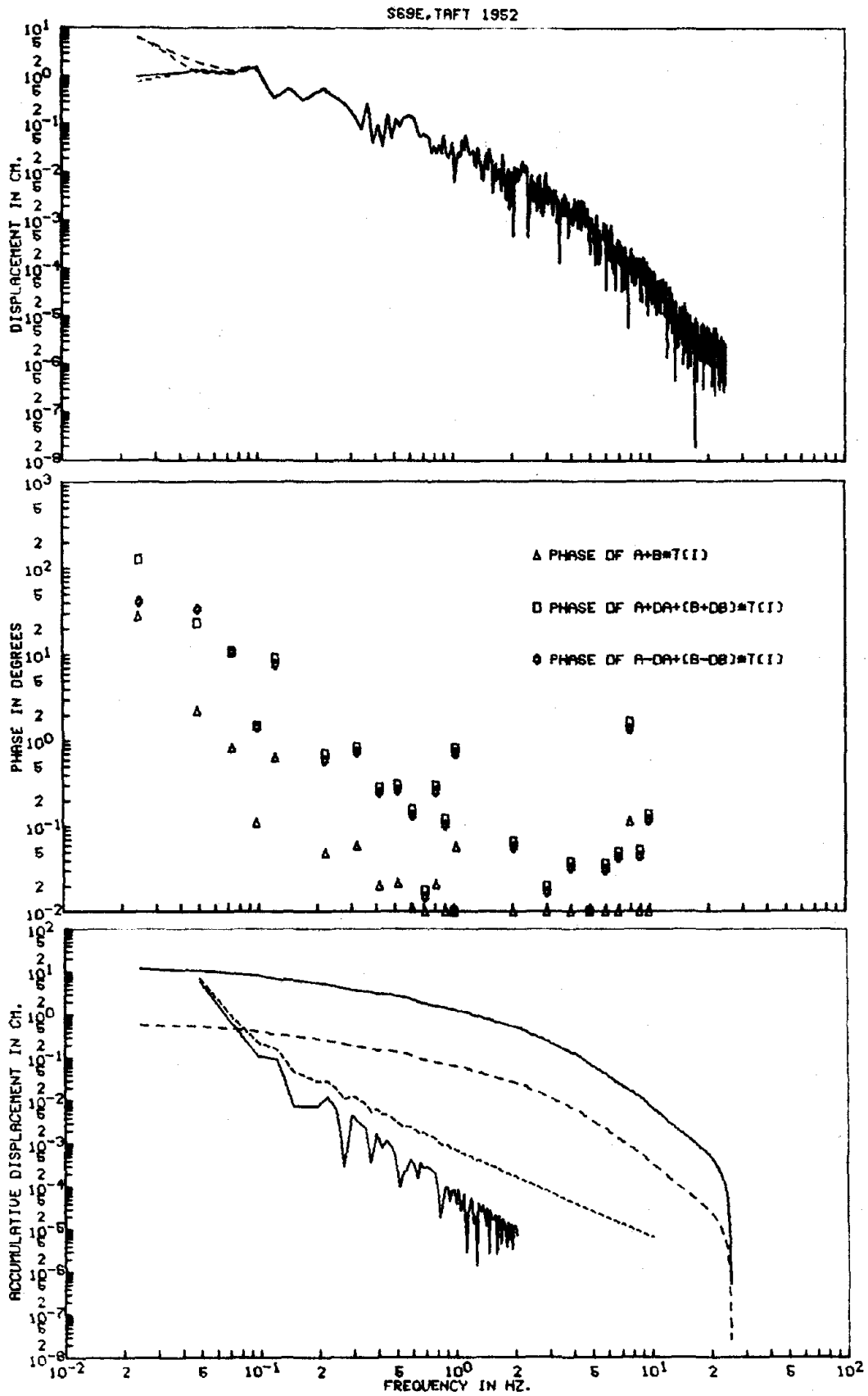


Fig. 3.17

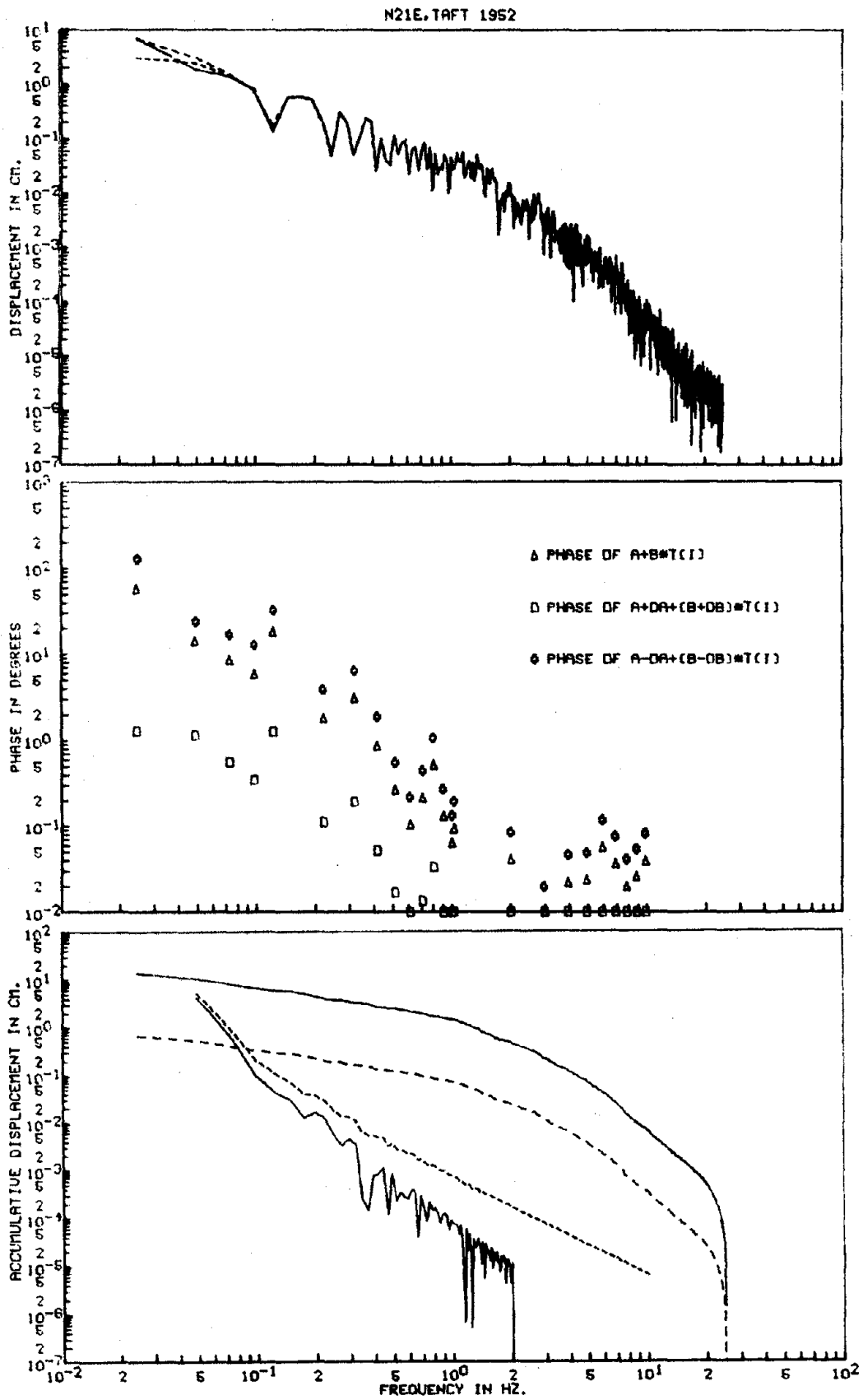


Fig. 3.18

CHAPTER IV

TIME INTEGRATION OF STRONG MOTION ACCELEROGRAMS BOTH IN THE TIME AND FREQUENCY DOMAIN. A NEW METHOD OF ACCURATE TIME INTEGRATION IN THE FREQUENCY DOMAIN4.1--Introduction

Integration of the digitized strong motion seismograms are, generally, carried out in the time domain using one or another form of the quadrature rules of approximate integration (Housner, 1947; Brady, 1966; Boyce, 1970; Trifunac, Brady and Hudson, 1973c). While these rules are generally more than adequate for smooth integrands, serious errors might arise for oscillatory functions (Davis and Rabinowitz, 1967).

Integration of a function can also be performed in the frequency domain. The application of this method of integration in the conventional form is, however, restricted because the expected discontinuity of the integral (periodic with period equal to record length) between the last point and the first point of the next oscillation either causes Gibb's phenomenon or distorts the general shape of the integral, depending on the relative amplitudes of the high-frequency components of the integral.

The aim of the present chapter is to compare critically these two methods of integration and, more importantly, to propose a modified version of the frequency domain integrations (and differentiation). It is believed that this version provides more reliable results of

integration and differentiation than methods previously used.

4.2--Integration of Strong Motion Accelerograms in the Time Domain

The quadrature formulas compute the approximate integral of discrete time or space functions. The accuracy of these formulas is, generally, proportional to higher derivatives of the integrand. For example, consider the two common integral formulas: trapezoidal and Simpson's. For the trapezoidal formula:

$$y_{n+1} = y_n + \frac{1}{2}h(x_{n+1} + x_n). \quad (4.1a)$$

The error terms calculated by Taylor's expansion of both sides of the formula are

$$\epsilon \approx -\frac{1}{12}h^3 x^{(2)}(t) - \frac{1}{480}h^5 x^{(4)}(t) - \dots \quad (4.1b)$$

where h is the time interval between successive points and $x^{(\cdot)}$ are time derivatives of the integrand. For Simpson's rule:

$$y_{n+2} = y_n + \frac{1}{3}h(x_n + 4x_{n+1} + x_{n+2}) \quad (4.2a)$$

the error is

$$\epsilon \approx -\frac{1}{90}h^5 x^{(5)}(t) - \frac{1}{420}h^7 x^{(6)}(t) - \dots; \quad (4.2b)$$

and the error of the Simpson's "half formula"

$$y_{n+1} = y_n + \frac{1}{12}h(5x_n + 8x_{n+1} - x_{n+2}) \quad (4.3a)$$

is

$$\epsilon \approx +\frac{1}{24}h^4 x^{(3)}(t) + \frac{13}{360}h^5 x^{(4)}(t) + \dots \quad (4.3b)$$

It is evident from (4.1b), (4.2b) and (4.3b) that the error introduced during integration by a quadrature formula depends not only on the formula used but also on the smoothness of the integrand. For an oscillatory integrand whose higher derivatives are not small, no quadrature rule seems capable of approximating the desired integration with sufficient accuracy without exceedingly close digitization. We can investigate this problem, using the trapezoid and the combination of both forms of Simpson's rule (the combined form is commonly used to avoid the high fluctuation of the resulting integral caused by (4.2a) (Hamming, 1973) to doubly y -integrate the strong motion accelerogram of the N65E component of CH #2 in the 1966 earthquake at Parkfield. Estimation of the errors introduced during integration is accomplished by prolonging this record by joining it to its mirror image so that the extended integrand is symmetric with respect to the center of its time length. This construction (see Figure 4.1) gives a symmetry property to the integrand which provides a mathematical basis for testing the degree of precision of the integration. This follows because an accurate integration of a symmetric integrand should result in a symmetric integral.

Figure 4.2 shows the double integral (displacement) of the Parkfield accelerogram (no base-line correction or high-passed filtering is carried out for the accelerograms used in this chapter). The upper and lower dashed-line curves are, respectively, the displacements calculated by the trapezoid and the combined Simpson rules. The middle curve (discussed later on in this chapter) is the computed displacement using integration in the frequency domain.

Figure 4.2 shows that the displacement curves calculated by

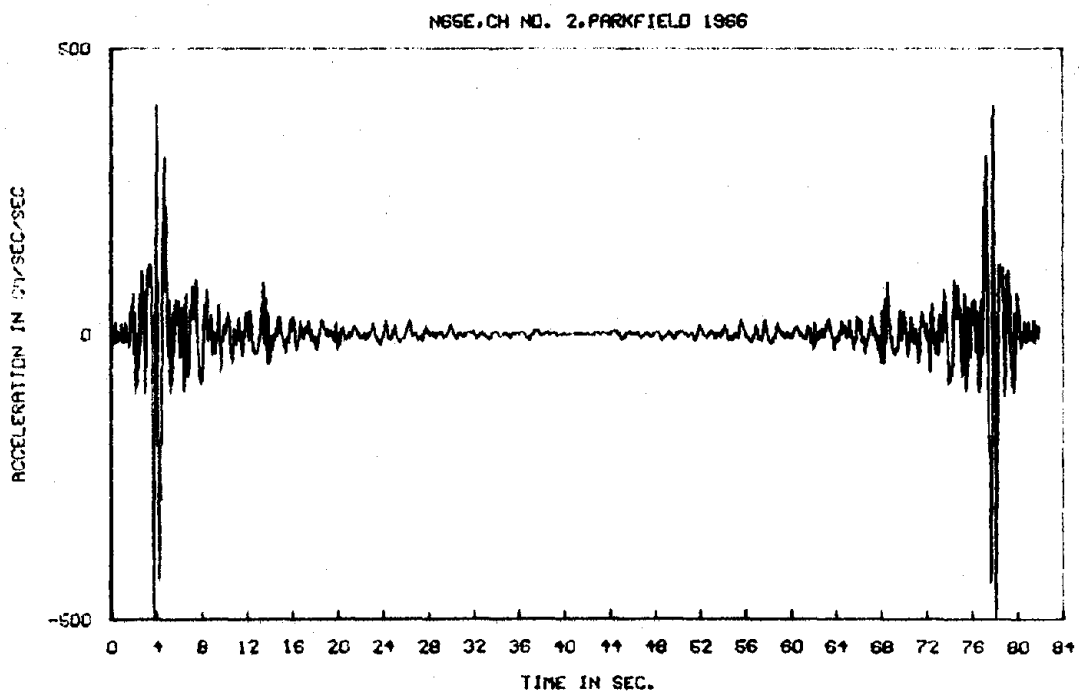


Fig. 4.1

Simpson and trapezoid rules are not precisely symmetric. This deviation reflects the accumulation of errors during integration. The question arises whether these errors merely originated from inadequate accuracies of the quadrature formulas, or are they introduced by truncation errors which arise from computation on the CDC 7600 used in this computation. In order to test whether or not truncation or rounding effects of the computing machine are significant, the calculations of Figure 4.2 were repeated in Figure 4.3 through 4.5 respectively, using single precision (14 digits) with round-off option, and double precision (28 digits) with and without round-off option. The resulting curves are essentially identical in these figures, which shows that the asymmetric features of the computed integrals by Simpson and trapezoid formulas result, definitely, from insufficient accuracy of the quadrature rules applied in the integration of the strong motion accelerogram.

Calculations similar to what are shown in Figure 4.2 were carried out for N85E component of CH #5, recorded during the 1966 earthquake of Parkfield and S16E component of Pacoima Dam, recorded during the 1971 earthquake of San Fernando. The results are illustrated in Figure 4.6 and 4.7 respectively. Again, asymmetry is produced by quadrature in the time domain.

The errors from quadrature formulas employed in integration of the oscillatory integrands such as normal seismograms do not necessarily decrease when higher derivatives are included. This point is demonstrated by noticing that the errors produced by Simpson's rule (4.2b and 4.3b) in Figure 4.2 through 4.7 are even greater than those of the trapezoid rule (4.1b).

Another illustration of this point is shown in Figure 4.8, in

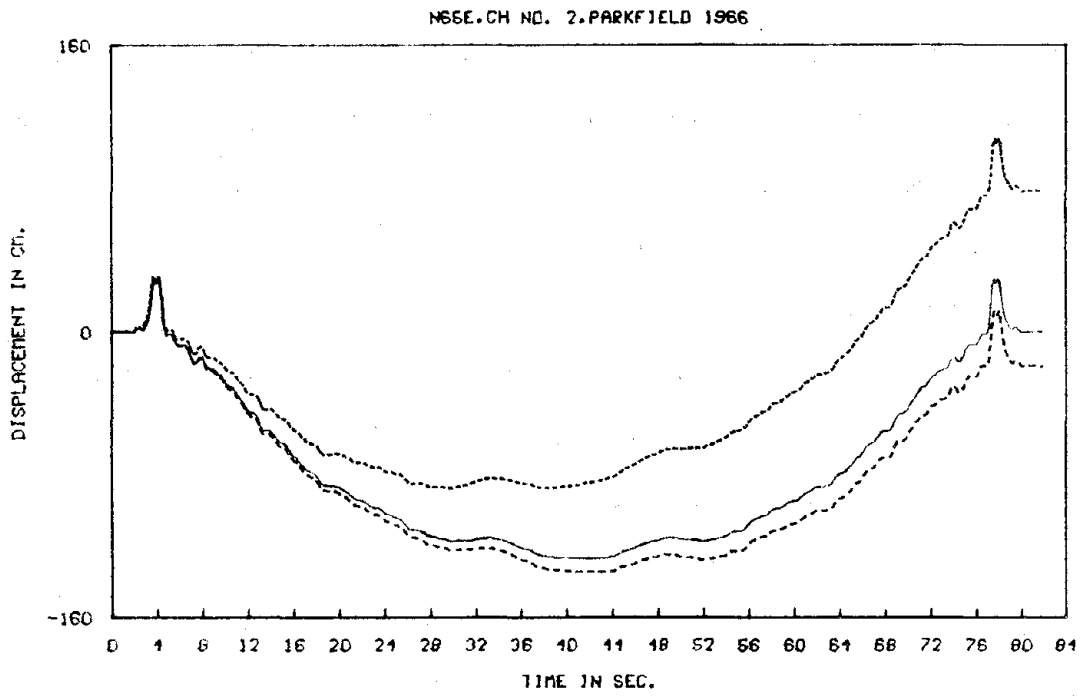


Fig. 4.2

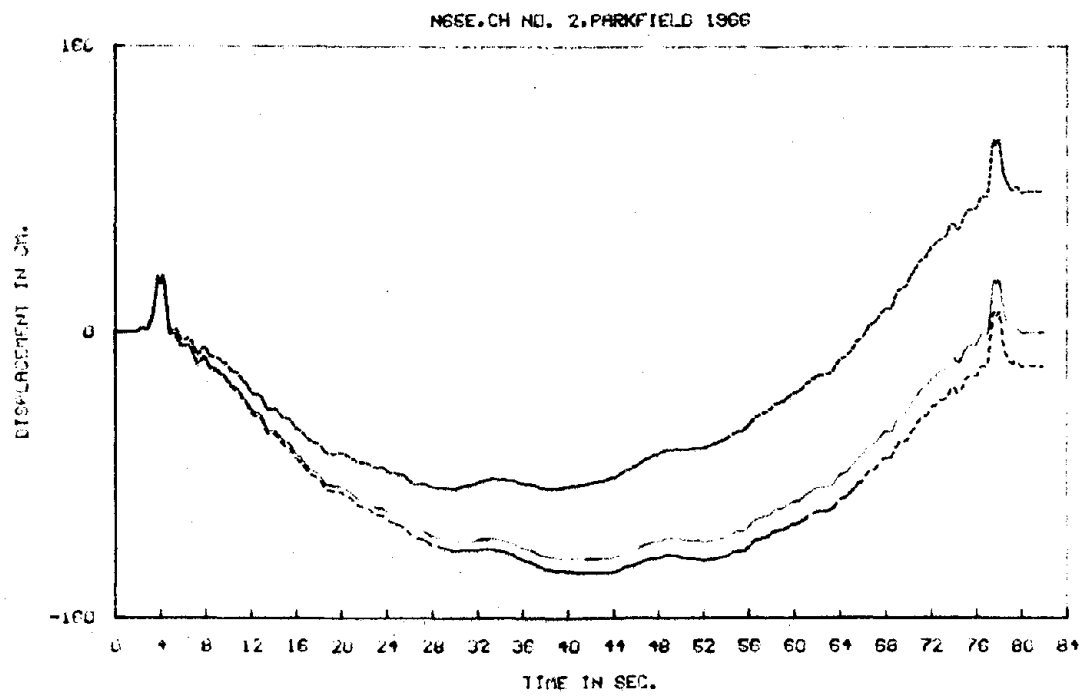


Fig. 4.3

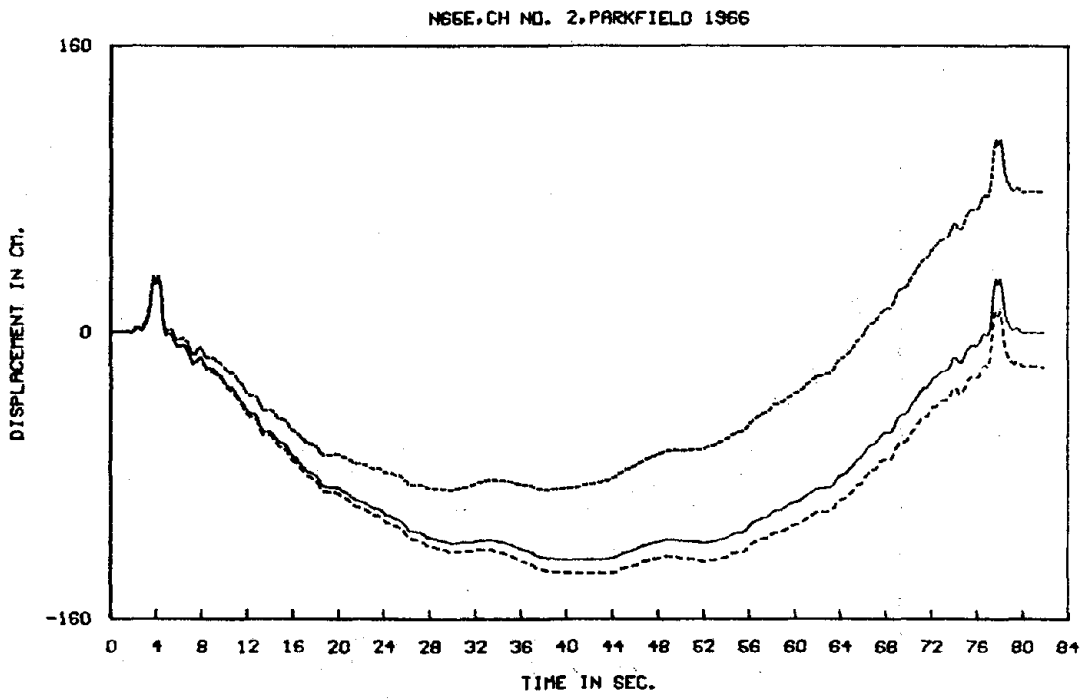


Fig. 4.4

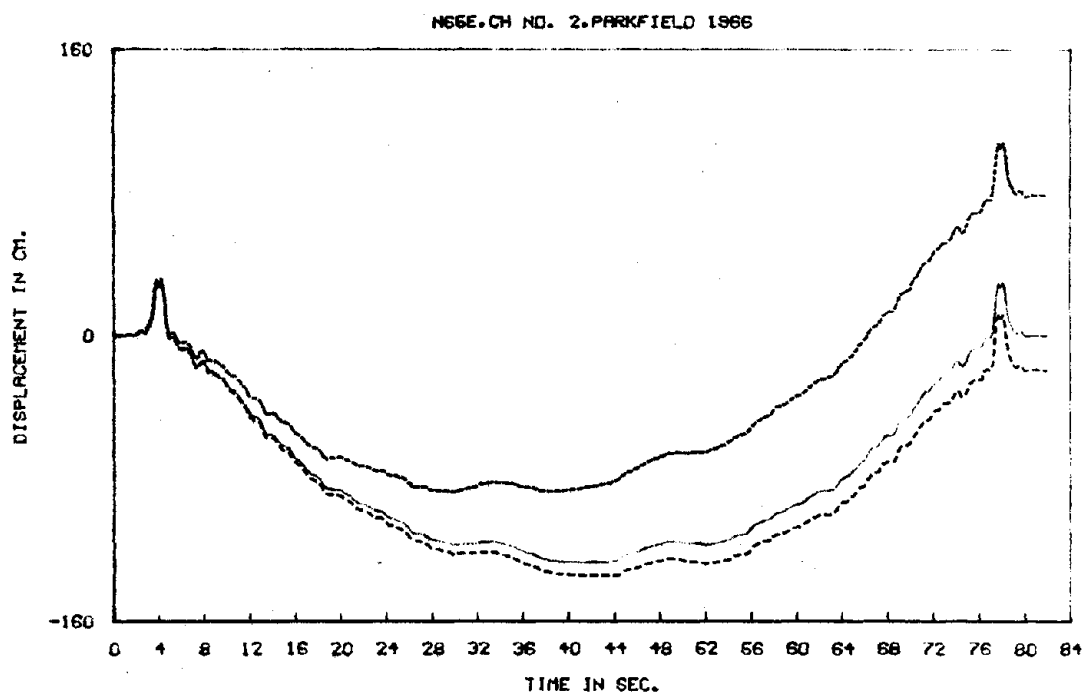


Fig. 4.5

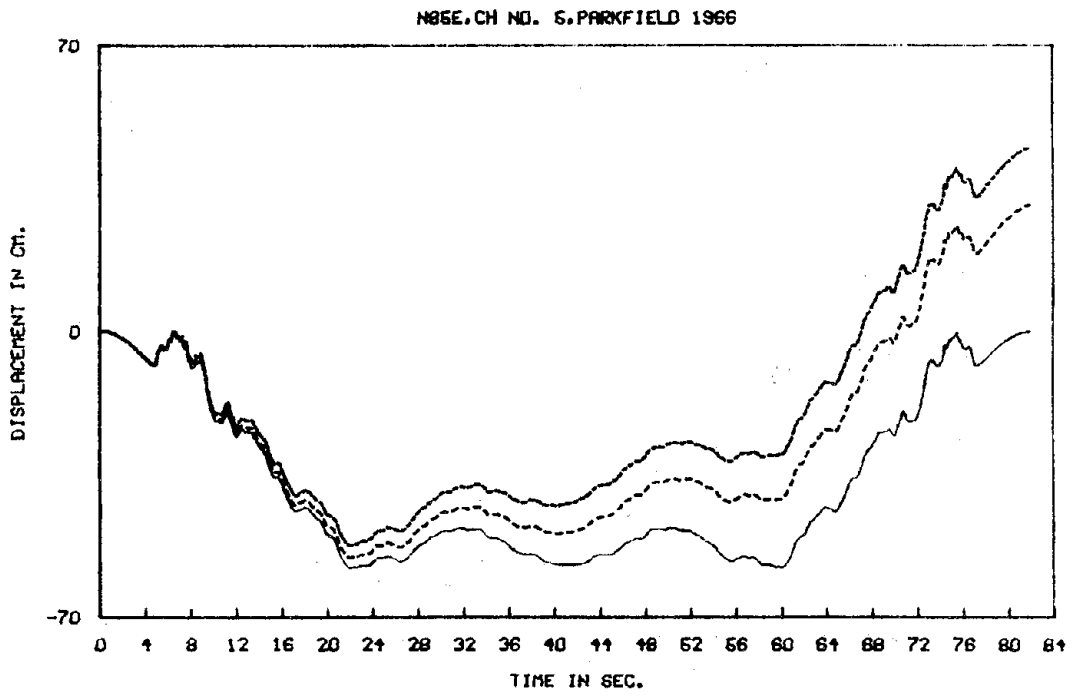


Fig. 4.6

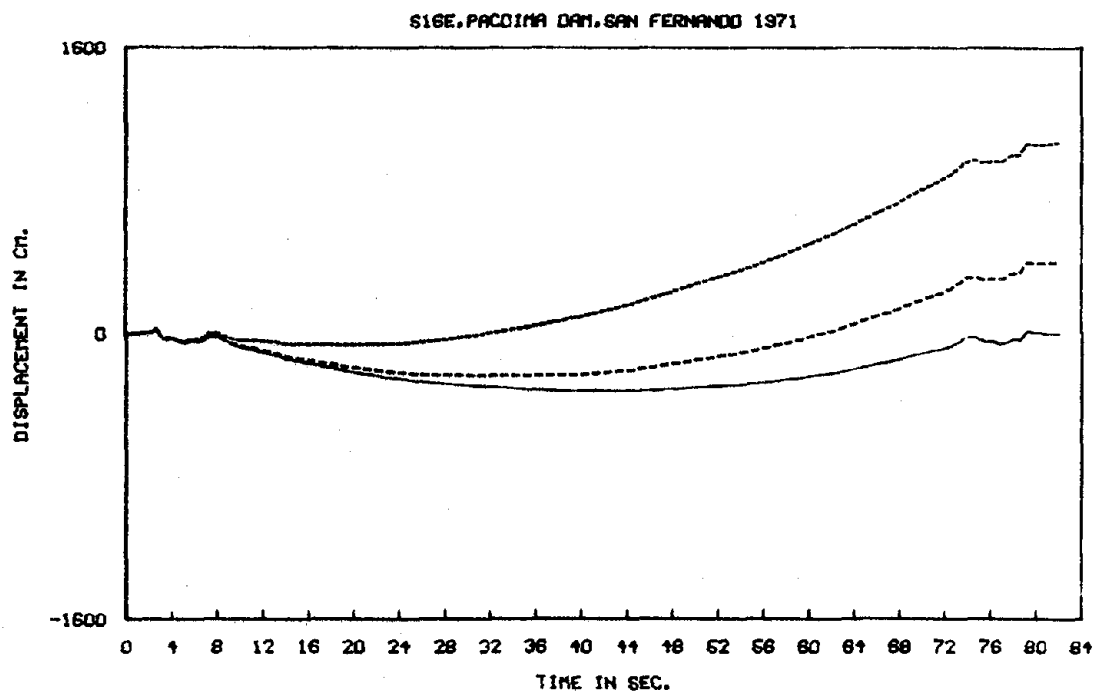


Fig. 4.7

which the double integration of N65E component of the CH #2 record is computed by the modified trapezoid rule in which the first error term of $\frac{1}{12} h^3 x^{(2)}$ is included. Comparison between this figure and the ones computed by non-modified form of this rule (Figure 4.2 through 4.5) also shows that the amount of error caused by imperfection of the quadrature rules might even grow from higher derivative terms when the integrands have oscillatory characteristics.

4.3--Integration of Strong Motion Accelerograms in Frequency Domain

The finite Fourier transform of the discrete time function, $f(T)$, consisting of a set of N equally spaced points, is

$$F(\omega) = \sum_{T=0}^{N-1} f(T) e^{-i\omega T/N} \quad (4.4)$$

The function $f(T)$ may be calculated by the inverse Fourier transform

$$f(T) = \frac{1}{T} \sum_{\omega=0}^{N-1} F(\omega) e^{i\omega T/N} \quad (4.5)$$

The recovery of $f(T)$ from (4.5) is exact since it consists of a set of orthogonal functions (Hamming, 1973; Kanasewich, 1973). This exact recovery of $f(T)$ using (4.5) forms a firm theoretical basis for accurate integration and differentiation of time functions in the frequency domain.

The time derivatives of $f(T)$ may be calculated by differentiating (4.5) with respect to time:

$$f^{(n)}(T) = b \sum_{\omega=0}^{N-1} (i\omega)^n F(\omega) e^{i\omega T} \quad (4.6)$$

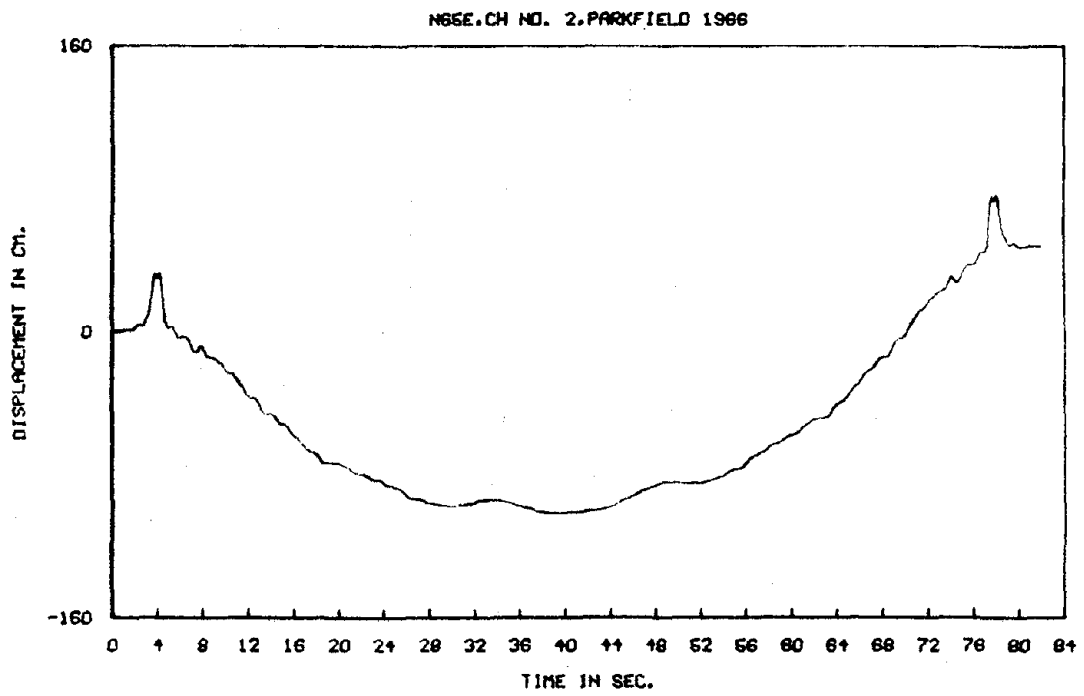


Fig. 4.8

where $f^{(n)}(T)$ is the n th derivative of $f(T)$, and $b = \frac{1}{N}$. Now let $f(T)$ and $v(T)$ be respectively the strong motion displacement and velocity which are to be calculated from the recorded strong motion acceleration $a(T)$. From (4.6), the Fourier transform, $A(\omega)$, of $a(T)$ in terms of the Fourier transform, $V(\omega)$, of $v(T)$, and the Fourier transform $F(\omega)$, is given by

$$A(\omega) = (ib\omega)V(\omega) \quad (4.7a)$$

and

$$A(\omega) = (ib\omega)^2 F(\omega) \quad (4.7b)$$

or

$$V(\omega) = \frac{1}{ib\omega} A(\omega) \quad (4.7c)$$

$$F(\omega) = -\frac{1}{(b\omega)^2} A(\omega) \quad (4.7d)$$

$V(\omega)$ and $F(\omega)$ are then employed in (4.5) to calculate respectively the exact values of $v(T)$ and $f(T)$.

Rapid computation of both direct and inverse discrete Fourier transforms by the method of Fast Fourier transform (FFT) introduced by Cooley and Tukey (1965) makes the frequency domain integration (and differentiation) economically feasible. For N samples, the direct calculation would involve approximately N^2 multiplications and N^2 additions. The FFT has, under suitable circumstances, reduced the number of operations to something like $N \log_2 N$.

It is, however, important to notice that the frequency domain integration suffers from the two following major restrictions which may lead to unreliable results unless special modifications are

undertaken:

First, it follows from (4.7c) and (4.7d) that the Fourier transforms of $V(\omega)$ and $F(\omega)$ for zero frequency are indeterminate. Secondly, the expected discontinuity of the periodic inverse Fourier transform, (4.5), between the last point and the first point of the next period causes distortion of the shape of the calculated functions. This is especially noticeable for the smooth functions such as strong motion displacements and velocities where high-frequency components are not large enough to recover the expected discontinuity between the last point and the first point of the next period.

Figure 4.9 illustrates the displacement curves of N65E component of CH #2 of the 1966 earthquake at Parkfield, calculated using the frequency domain algorithm. The upper dashed curve is computed, for comparison, using $N = 2048$ data points. The lower dashed curve is computed, for comparison, after the length of the accelerogram is doubled by adding to its end 2048 data points with zero values. The solid curves are computed after the length of the record is doubled by adding to the end the mirror image construction of the function.

For each curve, the indeterminate value of the Fourier transform, $F(\omega)$, at zero frequency, is arbitrarily replaced by zero value; hence from (4.4),

$$\sum_{T=0}^{N-1} f(T) = 0 \quad (4.8)$$

Accordingly, the base-line in each curve suffers a certain amount of vertical translation. In Figure 4.9 the base-line translation in each curve is corrected by subtracting the amplitude of the first point from

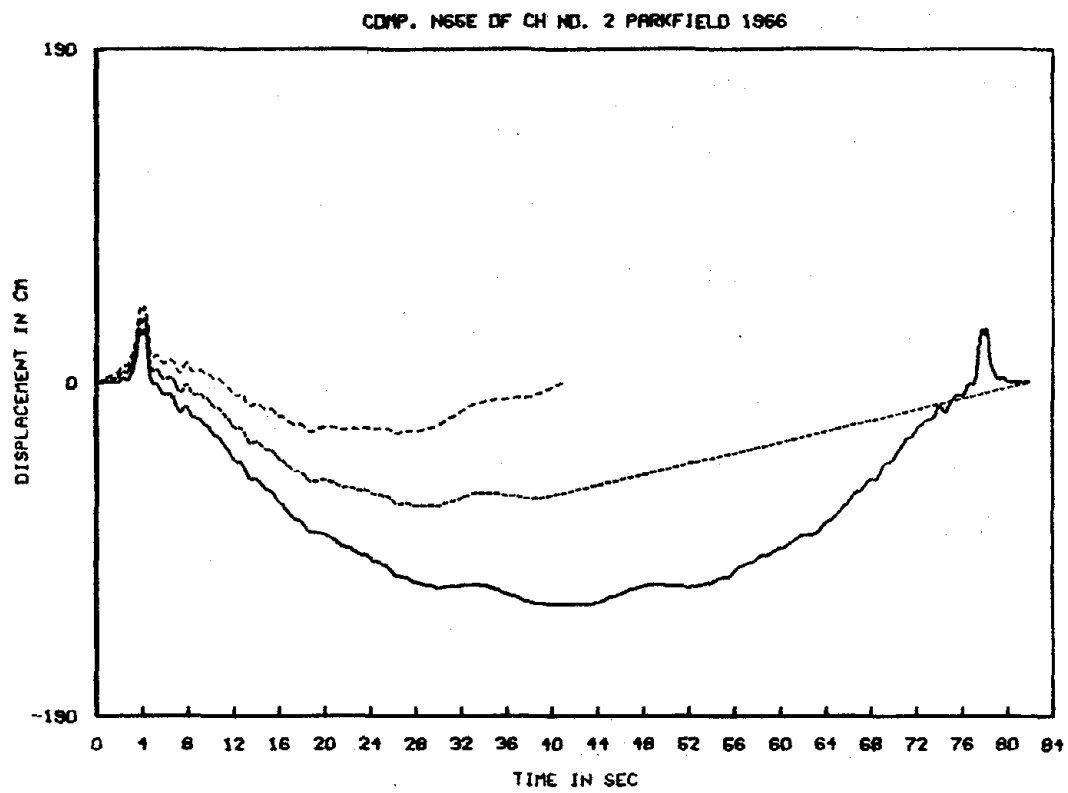


Fig. 4.9

the amplitude of all N points.

4.4--Accurate Time Integration and Differentiation of a Function in Frequency Domain

Although in principle the frequency domain, due to orthogonality properties of (4.4) and (4.5), offers a powerful tool for accurate integration and differentiation, the considerable differences observed among the curves in Figure 4.9 reveal that exact integration (and differentiation) requires the elimination, in an appropriate manner, of the distorting effects caused by the continuity imposed between the last point and the first point of the next period (see section 4.3).

The present research has shown, perhaps for the first time, that the most accurate results from integration of a strong motion record are attainable in the frequency domain if the record is first symmetrized by simply joining the corresponding mirror image to its end. The solid curves in Figure 4.2 through 4.9 illustrate the displacement records computed by applying the proposed algorithm.

The symmetry of the integrand constrains the computed displacement and its first and second derivatives to be continuous at the extreme ends. These continuities are essential in preventing distortion in the computed displacement. The exact symmetry of the displacement curves (solid curves) in Figure 4.2 through 4.9 confirms the accuracy of the method. Furthermore, the very close agreement existing between the beginning portions of these curves and the corresponding dashed curves (computed by trapezoid and Simpson's formulas) indicate that the shape of the solid curves (which are periodic) near the two ends remains unaffected by the functions in the neighboring periods. Recovery of zero frequency information of the computed integral

or differential curves is attainable by this method. This result is achieved by placing a sufficient number of zeros at the ends of the function which is to be integrated or differentiated. The values at the ends of the actual integral or differential of such a function must be, therefore, equal to zero. Hence, recovery is obtained by subtracting the value of the first point (or last point) from values of all points of the calculated curve.

A further advantage of this method is realized when the computed functions undergo filter processing. Filtering of a discontinuous function causes undesirable distortion on the shape of a function near the discontinuities.

The computing time required by frequency domain integration is a few times longer (depending on the number of data points) than the corresponding time required by time domain integration. However, because filter processing (often needed during integration of the accelerograms) is considerably faster in the frequency domain than that in the time domain, the frequency domain method of integration (including filtering) seems to be faster and more economical than that of time domain integration.

The frequency domain method developed in this chapter is employed as a basic tool for integration and also during filter processing of strong motion records in the next chapter.

CHAPTER V

PARKFIELD, CALIFORNIA, EARTHQUAKE OF JUNE 1966: SEISMOLOGICAL INTERPRETATION OF THE STRONG MOTION RECORDS5.1--Introduction

A theoretical explanation of the behavior of earthquakes near the sources of energy release (a rupturing fault) is among the most important problems in seismology and has recently attracted the attention of many investigators in this field (e.g., Aki, 1968; Haskell, 1969; Trifunac and Brune, 1970; Bolt, 1972; Boore and Zoback, 1974; Trifunac, 1974). The present scarcity of strong ground motion recordings together with the complexities introduced by geological variations and faulting mechanisms limit the observational data which are needed to test the theoretical models. However, the major social concerns regarding the problem of earthquake hazards have led many of the seismic prone countries (e.g., USA, Japan, USSR, Iran, Turkey) to install more strong motion instruments in active zones. The speedier collection of the strong motion observations together with the development of understanding of the detailed mechanism of earthquakes should lead in the next decade to major advances in strong motion seismology.

The culmination of the present study of strong motions, aimed at a better understanding of energy release and source mechanism, was an analysis of strong motion records of the Parkfield 1966 earthquake. An attempt is made in what follows to interpret these records in terms of a simple model of faulting (Bolt, 1972; Hanks, 1974; Boore et al.,

1974) and elementary seismic wave theory. Various results of the previous chapters were used in this final study.

5.2--Background

The main shock ($M_L = 5.5$, $m_b = 5.8$, $M_S = 6.4$) occurred on June 27, 1966 at 9:26 p.m. Pacific daylight time (04:26:13.4 GMT, June 28, 1966) following two light foreshocks (magnitudes 2-3) at 6:00 p.m. and 6:15 p.m., and a stronger foreshock of magnitude 5.1 at 9:09 p.m. on June 27 (McEvelly, 1966). The coordinates of the origin of the main shock were found to be $35^{\circ}57.3'N$ and $120^{\circ}29.9W$ (see Figure 5.1a). This earthquake was followed by a large number of aftershocks for several weeks (Eaton, O'Neill and Murdock, 1970).

The first field observation made along the San Andreas fault zone early the morning after the main shock (Allen and Smith, 1966) indicated that the white line on Highway 46 (see Figure 5.1a) at its intersection with the fault zone had been offset by 4.5 cm in the right lateral sense. But extrapolation of the offset curve back to the origin time of the main shock indicates that there was essentially no surface fault offset at the time of the main shock (Wallace and Roth, 1967).

On the basis of en echelon cracks exposed on the surface, the rupture length along the San Andreas fault may be estimated to be about 33 km (see Figure 5.1a). The overall distribution of the aftershocks, however, suggests a surface length of 27 km (McEvelly, Bakun and Casaday, 1967).

The accelerographs of Cholame approximately 30 km southeast along the trace fault from epicenter recorded several aftershocks during the first few minutes after the main shock (Murray, 1967). The S minus P of these events decreased from about 5 sec for the main shock

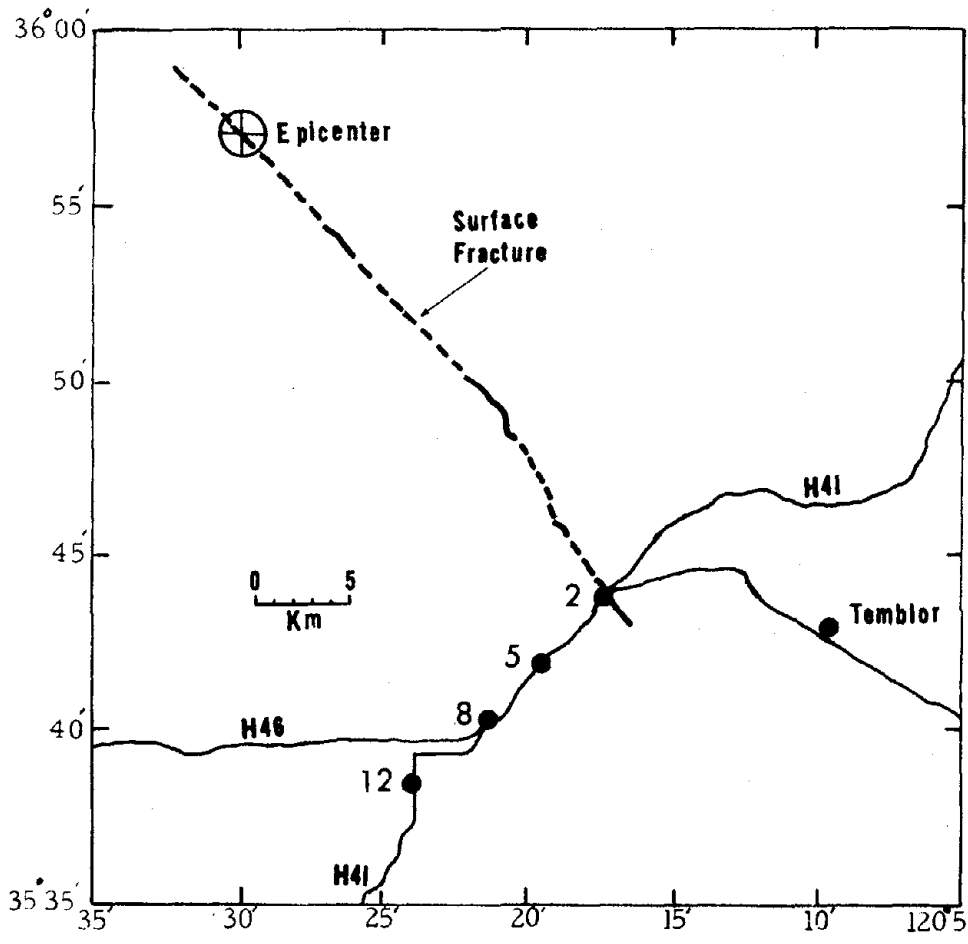


Fig. 5.1a

to about 2 sec or less for the aftershocks. This decrease indicates a smaller focal distance and hence that the fault propagated south-eastward from the epicenter for a distance of about 20 km.

Eaton et al. (1970) made a detailed analysis of the aftershocks which occurred between the 3rd and the 82nd day following the main shock. Using 474 well-located aftershocks, they found the strike and dip of the fault plane to be N39W and 86SW, respectively. Over 95 percent of these aftershocks had focal depths between 1 and 12 km, and none had a focal depth greater than 15 km. The foci of these aftershocks were highly concentrated between 2 and 4 km and also between 8 to 10 km.

The aftershocks south of $35^{\circ}50'N$ (see Table 2 of Eaton et al., 1970) show highest concentration between $35^{\circ}47.5'N$ and $35^{\circ}48.5'N$ (see Figure 5.1a).

Based on the P-wave polarities for the main shock, McEvelly et al. (1967) evaluated that the strike and dip angles range from N35W to N24W and 88NE to 85SW, respectively.

Eaton (1967) estimated the rupture velocity to be 2.2 km/sec by using the motion of a radio time recorder operated about 20 km down the fault from the epicenter. In addition, zeros of spectra from Love-waves recorded at Berkeley were found to be consistent with this rupture velocity (Filson and McEvelly, 1967).

Interpretation of the mechanism of the main shock by comparing observed and synthesized strong ground motion records has been carried out already by a number of investigators (e.g., Aki, 1968; Scholz, Wyss and Smith, 1969; Haskell, 1969; Anderson, 1973; Tsai and Patton, 1973). None of the studies provides explanation that is convincing in all

aspects. A recent investigation was made by Trifunac et al. (1974) by fitting a moving dislocation model to strong motion data obtained from five stations. The preferred resulting model (also consistent with geodetic data and fault creep measurements) has a zone of significant faulting about 20 km long in the northern section of the fault with a rupture velocity between 2.4 and 2.5 km/sec and a dislocation amplitude of 120 cm.

Eaton et al. (1970) have now conducted several short but detailed refraction profiles in the Parkfield-Cholame region to determine the structure in the upper crust. The P wave velocities of the upper 15 km of the crust for SW and NE sides of the fault are shown in Table 5.1.

TABLE 5.1

SW		NE	
(km)	(km/sec)	(km)	(km/sec)
0-0.28	1.70	0-0.18	2.36
0.28-1.55	2.80	0.18-1.24	3.34
1.55-3.74	5.00	1.24-2.76	4.62
3.74-15.00	6.00	2.76-4.40	5.62
		4.40-15.00	6.00

5.3--Interpretation of the Strong Motion Recordings

In the present section, the main shock of the Parkfield 1966 earthquake is analyzed by interpreting the recorded strong ground motion recordings using standard seismological theory on seismic waves;

ray theory arguments are applied to infer the rupture velocity during this earthquake. Further information on the source mechanism is drawn from studies of projections of particle velocities of the ground on three orthogonal planes (horizontal plane, and the planes parallel and normal to the fault plane).

The particle velocity traces have been chosen as the fundamental data against which the model of faulting is tested. The acceleration traces contain more information (because of higher frequency content), but they are too sensitive to minor details of faulting, geological heterogeneities, and surface topography. Furthermore, current theoretical models of source mechanisms (Brune, 1970) suggest that, in the near-field, particle velocity amplitude is directly proportional to the driving stress at the fault.

Displacement traces ^{are} used as supplementary data to test the gross features of the fault model inferred by the velocity traces and also to study the recorded surface waves.

For accurate calculation of velocity and displacement traces, the results of chapter 3 and 4 are employed. Each accelerogram is first high-pass filtered using Butterworth filter with four poles (Gold and Rader, 1969), and a corner frequency equivalent to the corresponding usable long-period limit in Table 3.1. The resulting filtered accelerogram is then integrated in the frequency domain, using the method developed in chapter 4, to calculate the corresponding velocity and displacement traces.

For modeling purposes, it is desirable to rotate the horizontal particle velocities and displacements into a coordinate system which corresponds to the components parallel and normal to the fault. The

directions of S33E and N57E are chosen (McEvelly, 1967) as the parallel and normal components to the fault. The fault plane is to be vertical. The recorded horizontal components of velocity and displacement of all sites, except CH #2 where only one horizontal component was recorded during the earthquake, were all rotated to the chosen coordinate system.

To convert the instrumentally recorded traces to the actual ground motions, all vertical and horizontal components (both velocity and displacement) were reversed. These records are shown in Figure 5.3a through 5.7a.

In order to enhance the extractable information on fault mechanisms, the velocity components were both high-pass and low-pass filtered using Butterworth filters with 4 poles and corner frequencies of 3 Hz. The high-pass and low-pass filtered velocity components are shown respectively on the upper half and lower half of Figure 5.3b through 5.7b.

The particle motion diagrams were constructed for consecutive one-second time windows on the three orthogonal planes (horizontal plane and the two vertical planes defined by the strike of the fault and its normal) using the low-passed velocity traces. The diagrams are illustrated in Figures 5.3c through 5.7c. In each plane, the time windows begin from the first diagram on the upper left corner and continue sequentially to the right. The beginning of each time window is designated by the plotted star. In each time window, the scale was arbitrarily chosen such that the peak would correspond to the half length of the area devoted for each window.

Using the crustal P velocity models given by Eaton et al. (1970; see Table 5.1) for southwest and northeast sides of the fault, the P and S travel times to each station were calculated for the main earthquake.

The focal depth was taken as 5 km, and Poisson's ratio was assumed to obtain S from P velocities so that $\sigma = 0.25$. The resulting travel times in upper layers from the source are as follows:

Station	T_P (sec)	T_S	T_{S-P}
2	6.2	10.7	4.5
5	6.3	10.8	4.6
8	6.6	11.4	4.8
12	6.9	12.0	5.1
Temblor	7.5	13.1	5.6

The absolute error may be on the order of 0.2 sec, judging from the standard errors in calculated origin times given for the aftershocks in Eaton et al. (1970). The average P velocities, for the main shock, resulting from the given crustal models, are as follows: 5.73 km/sec to station 2, 5.74 km/sec to station 5, 5.74 km/sec to station 8, 5.76 km/sec to station 12, and 5.69 km/sec to station Temblor.

The triggering device at station 5 was nearly in contact so that the accelerograph operated immediately after the calculated P wave arrived.

The observed arrival of the direct S wave at each station is shown by S_1 (Fig. 5.3a, b to Fig. 5.7a, b). Amplitudes as well as polarizations of S_1 in velocity components provide clear information on fault mechanism during the main shock. At all stations (except CH #2 where the parallel P component was not recorded) the velocity amplitudes on normal components N57E are larger than those for parallel components S33E. This is expected (because the epicentral distances, varying between 30 km to 40 km, are relatively larger than the fault

distances which vary between 80 m, for CH #2, and about 15 km for CH #12; see Fig. 5.1a) from the radiation pattern of a double-couple source (Savage, 1965b; Haskell, 1969; Boore et al., 1974). Polarization and amplitude of horizontal and vertical components at CH #5, 8, 12 (see Fig. 5.4b to Fig. 5.6b), which are on the SW side of the fault, generally indicate that the main shock had right-lateral strike-slip mechanism. At Temblor, which is on the NE side of the fault, the polarization of the S wave on N57E (see Fig. 5.7b) confirms the inferred mechanism by CH #5, 8, 12. But the polarization on vertical and S33E does not agree with this simple mechanism model. It should be noticed, however, that because the angle of epicentral azimuth of this station, with respect to the strike of the fault (see θ in Figure 5.2), is small (about 10°), the polarization of S waves on these components becomes quite sensitive (because of small amplitudes) to the details of faulting at the hypocenter, to the geological heterogeneities along the ray path and so on.

At CH #2, the direction of S wave recorded on S65E component (see Figure 5.3b) confirms the right-lateral direction of the fault, whereas the Down component does not imply such interpretation (perhaps for the same reason stated for Temblor station).

The particle velocity diagrams (Fig. 5.4c to Fig. 5.7c) of the S wave in the horizontal plane, at stations CH #5, 8, 12 and Temblor, are drawn in Figure 5.1b. The prograde elliptical patterns shown at CH #5, 8, 12 are expected from a double-couple right lateral mechanism. The unexpected prograde pattern of Temblor, for such a mechanism, is the result of polarization change of S wave (as discussed before) on the S33E component at this station. The arrows designated by S_1 s are drawn perpendicular to the major axes of the ellipses. In the absence

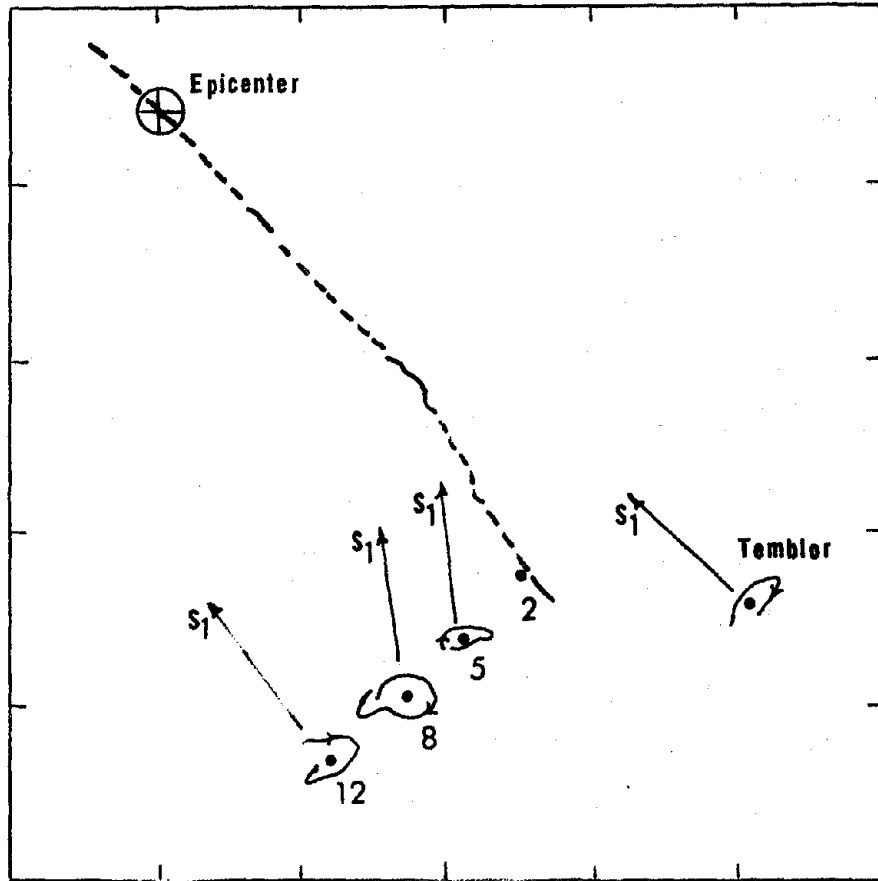


Fig. 5.1b

of geological and fault rupture complexities, these arrows would be directed toward the source. While the arrow at Temblor points approximately toward the epicenter, the directions of the arrows at CH #5, 8, 12 show rather large deviations from the expected directions.

There are two or three onsets shown prior to the arrival of the S wave (S_1) observed on the high-passed vertical component of velocity at CH #5. These arrivals are probably the P waves of small earthquakes that occurred immediately (within about 3 sec) after the main shock on the fractured fault. Since this chapter is mainly concerned with study of the gross mechanism of the main shock, these small shocks are not further discussed.

Next, let us consider the onsets designated by S_2 s in Figures 5.3a and 5.3b to Figures 5.7a and 5.7b. These onsets are related to the waves with peak accelerations recorded in the corresponding accelerograms (see Fig. 4.1 and Fig. 2.22b to 2.25b). From both engineering and seismological points of view, it is therefore vital to investigate the nature and also the possible source of generating these waves.

These seismic waves are not likely to be predominantly surface waves because they have short durations and non-dispersive features. The amplitudes decrease rather sharply with distance from the source of energy release (compare the amplitudes at CH #2, 5, 8, 12, and Temblor); for surface waves this is not plausible near to the source of energy release where production of surface waves should significantly increase with source distance. Furthermore, the arrival times are at least a few seconds earlier than expected if they are assumed to be surface waves (surface waves with such high frequency contents would travel only through a thin section, about 1 km, of the surface with a shear

velocity of 1 km/sec). The particle velocity diagrams of these waves are designated by S_2 in Figures 5.3c through 5.7c. The diagrams in the horizontal planes are drawn in Figure 5.1c. The arrows designated by S_2 in this figure are drawn perpendicular to the major axes of the ellipses.

The diagrams show that the particle motion of S_2 waves at all stations except CH #5 have opposite direction (retrograde) to those of S_1 waves which are originated from epicenter. It is difficult to infer any particular mechanism for the source of S_2 waves from these diagrams. The direction of S_2 arrows at CH #5, 8, and Tumbor (Fig. 5.1c) suggests that the source of these phases is located within a few km northwest of CH #2. The displacement N57E components at CH #2, 5, 8, 12, and Tumbor show that the displacement motions of S_2 waves have opposite directions to those of S_1 waves.

On the basis of these observations, the S_2 waves are interpreted as S waves generated by termination of the rupture (Savage, 1965a) within a few km northwest of CH #2.

A reasonable estimate of the location of the end of the fault rupture permits the determination of the average rupture velocity along the fault. As mentioned earlier in this chapter, the aftershocks' distribution suggests a fault length between 20 to 28 km.

Let us estimate the rupture velocity for two different rupture lengths: 28 km and 20 km, respectively. Since the aftershocks at the southeastern end of the rupture are highly concentrated at focal depths between 2 and 4 km, and also between 8 and 10 km (Eaton et al., 1970), for each assumed rupture length two different depths of 4 and 8 km are assigned to the depth at which rupture is terminated. It should be

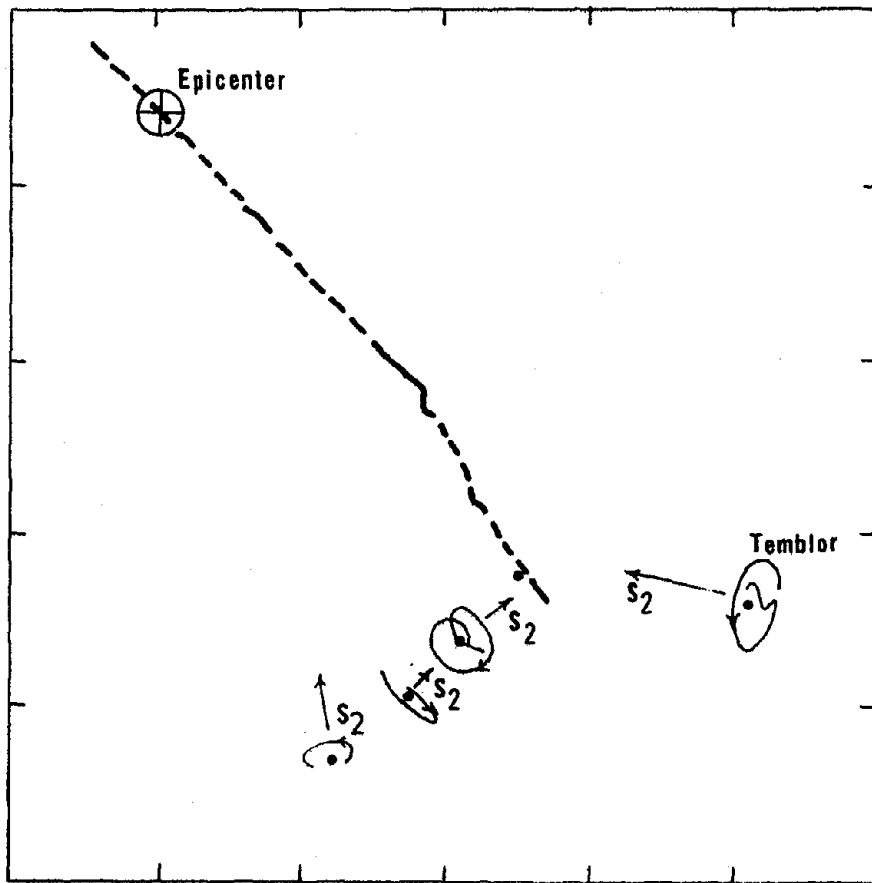


Fig. 5.1c

mentioned that because S wave travel times, from hypocenter to the station, are not too sensitive to variation of focal depth (change of focal depth from 5 km to 10 km introduces only about 0.1 sec variation in the travel times), only one focal depth of 5 km was assumed in estimation of rupture velocity. Table 5.2 shows the rupture velocities, estimated from arrival times of the S_1 and S_2 phases, and their standard deviations.

TABLE 5.2

Case	L(km)	H(km)	\bar{b} (km/sec)	Sd (from 5 observations)
1	28	4	3.13	0.53
2	28	8	3.11	0.30
3	20	4	2.48	0.11
4	20	8	2.42	0.07

In this table, L is the length assumed for rupture, H is the depth assumed for the termination of rupture, \bar{b} is the average of the rupture velocities estimated from CH #2, 5, 8, 12, and Temblor records, and Sd is the standard deviation of the rupture velocity for one observation.

Cases 1 and 2 with $L = 28$ result in a rupture velocity of about 3.1 km/sec and a relatively large standard deviation between 0.3 and 0.5 km/sec. This velocity is about 0.2 km/sec smaller than the average shear velocity along the ray paths between the initial source and the stations and about 0.5 km/sec larger than the average shear velocity along the ray path between the southern end of the rupture and the

stations. Cases 3 and 4 with $L = 20$ km result respectively in rupture velocities of about 2.5 km/sec and 2.4 km/sec with standard deviation of only 0.1 km/sec. These velocities are smaller than average shear velocities in the area.

The small standard error of 0.1 km/sec of the estimated rupture velocity corresponding to the rupture length of 20 km, together with the high concentration of aftershocks between $33^{\circ}47.5'N$ and $35^{\circ}48.5'N$ (see Table 2 of Eaton et al., 1970) suggest that the fault rupture during the main shock was about 20 km long. This conclusion is supported by considering the location of the aftershocks which occurred within a few minutes after the main shock.

The particle motion diagrams of the stopping phase (designated by S_2 in Fig. 5.3c to Fig. 5.7c) in vertical planes show considerable variation in both direction and pattern at different stations. However, the elongated pattern of these diagrams at CH #2, 5, and Temblor indicates that the dislocation at the southern end of the rupture was dominantly horizontal; this is, of course, clearly illustrated by the corresponding velocity traces.

Let us now consider the recorded surface waves and make some general remarks regarding their nature and their possible source of excitation. A significant portion of the total energy which arrived following the stopping ^{phase} in Fig. 5.3a, b to 5.7a, b can be shown to be contributed by surface waves (mainly Love waves because the amplitudes in horizontal components at each station are, generally, larger than those in the corresponding vertical component). The velocity components carry more detailed and thus less simply interpreted information on the properties of the recorded surface waves than those of corresponding

displacement records. For analysis of the gross features of these waves, it is therefore more appropriate to consider the recorded surface waves on displacement records. Love waves dominate the remaining portions of motion after the arrival of the stopping phase S_2 of the horizontal component N57E and S33E at CH #5, 8, 12. Similarity of the wave forms among these stations is clearly visible (see displacement components of N57E in Figures 5.4a to 5.6a). These waves suffer dispersion as they travel toward the further stations (e.g., CH #12). The rate of dispersion, estimated for different episodes of the recorded Love waves, indicates that dispersion is more rapid for the waves which are recorded within a few seconds (e.g., 5 sec) after arrival of the S_2 phases (see the AB intervals shown on displacement components N57E in Figures 5.4a to 5.6a) than for those which arrived later. From the observed rate of dispersion, it is interpreted that the Love waves arriving within a few seconds after the stopping phases originated from the southeastern part of the rupture, whereas the later arrivals are excited at the northwestern part of the rupture.

The late arrival of Love waves at different stations indicates that these waves propagate with quite small velocities (e.g., 1.0-1.5 km/sec). Such small velocities do not occur in the crustal model velocity estimated from refraction studies in this area (Eaton et al., 1970). The conflict may be resolved in part if a low-velocity zone of a few km thickness exists within the crust in this area; this possibility is not ruled out by the refraction studies, since the low-velocity zone cannot be detected by this method.

The N65E component of CH #2 also recorded the Love waves (see Figure 5.3a). The amplitudes are, in general, comparable with the

amplitudes of the corresponding waves recorded at CH #5, 8, 12.

It is interesting to note that the amplitudes of Love waves recorded at Temblor are considerably smaller than the amplitudes of those recorded at CH #5, 8, 12. The crust on the northeast side of the fault has more competent rocks and the upper crustal layers have smaller seismic velocity contrasts compared to those on the southwest side of the fault. These differences are perhaps responsible for the reduction of the amplitudes of Love waves at Temblor (on the northwest side of the fault). The diagrams of the particle velocities of the recorded Love waves show considerable scatter (Figures 5.4c through 5.7c). However, they have, in general, elliptical patterns with both prograde and retrograde directions. Because of the observed scatter no further interpretation on the recorded surface waves can be drawn from these diagrams. There is some indication that similar diagrams for particle displacements may offer more conclusive information. This was tested on the displacement components of CH #12 (see Figure 5.8). The diagrams were constructed for consecutive three-second time windows on the three orthogonal planes. The elliptical diagram designated by L_1 in the horizontal plane corresponds to the surface waves (dominantly Love waves) which arrived 4 seconds after the S_2 waves (see Figures 5.6a, b) and recorded for three seconds afterward. The diagrams designated by L_2 s are the Love waves recorded in the later portion of the records. The elongated L_2 diagrams are nearly parallel to each other. Comparison between orientation of L_2 diagrams and that of the L_1 diagram indicates that the source of L_2 diagrams is possibly located on the northwest of the source of the L_1 diagram.

The vertical displacement at CH #5, 8, 12 (see Figs. 5.4a to

5.6a) shows that Rayleigh waves have shorter periods than the corresponding Love waves recorded on the horizontal components. On the vertical component at CH #2, the Rayleigh waves are superimposed as a single harmonic wave with a period of about 10 sec.

It is interesting to note (see Figures 5.3a to 5.7a) that Rayleigh waves at CH #2, 5, 8, 12 are noticeably less energetic than Love waves. By comparison, the recorded Rayleigh waves at Temblor seem to carry more energy than Love waves.

The vertical component of displacement at Temblor illustrates, clearly (see Figure 5.7a), the reversed dispersion of the recorded Rayleigh waves. The reversal of dispersion together with late arrival for the Rayleigh waves require a crustal structure with low-velocity zones. The reversed dispersion of these waves may be, partly, explained if one assumes that the early portion of the surface waves originated from the epicentral area, whereas those of the late portion are excited from the area near the southeastern end of the rupture.

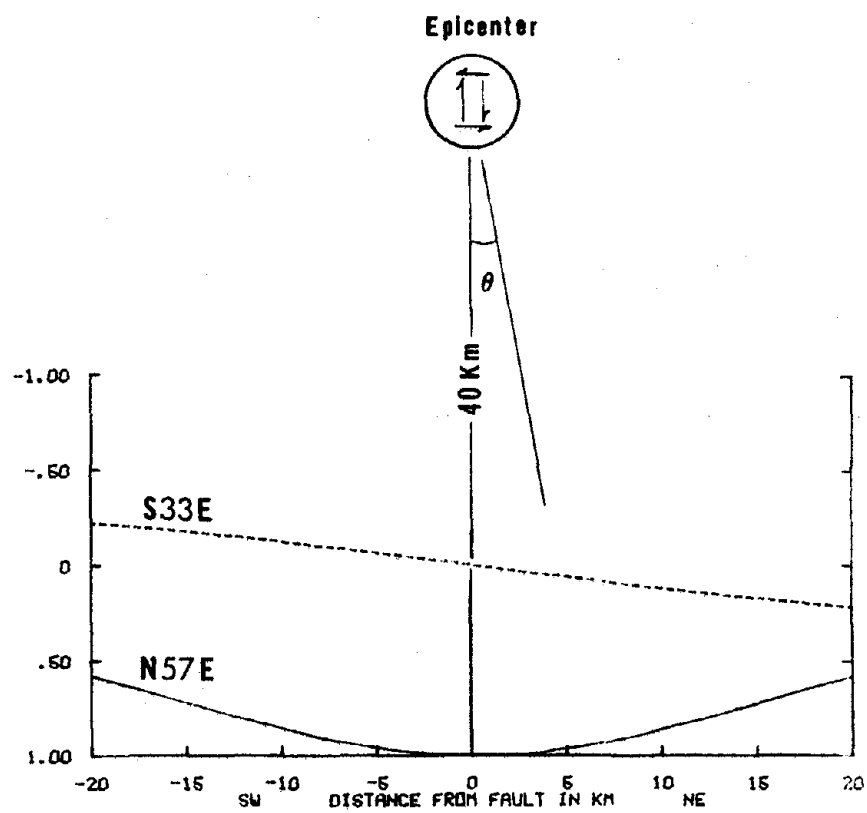


Fig. 5.2

The variation of peak amplitudes with distance to the fault.
 Amplitudes are normalized to the corresponding maximum motion
 at the fault surface.

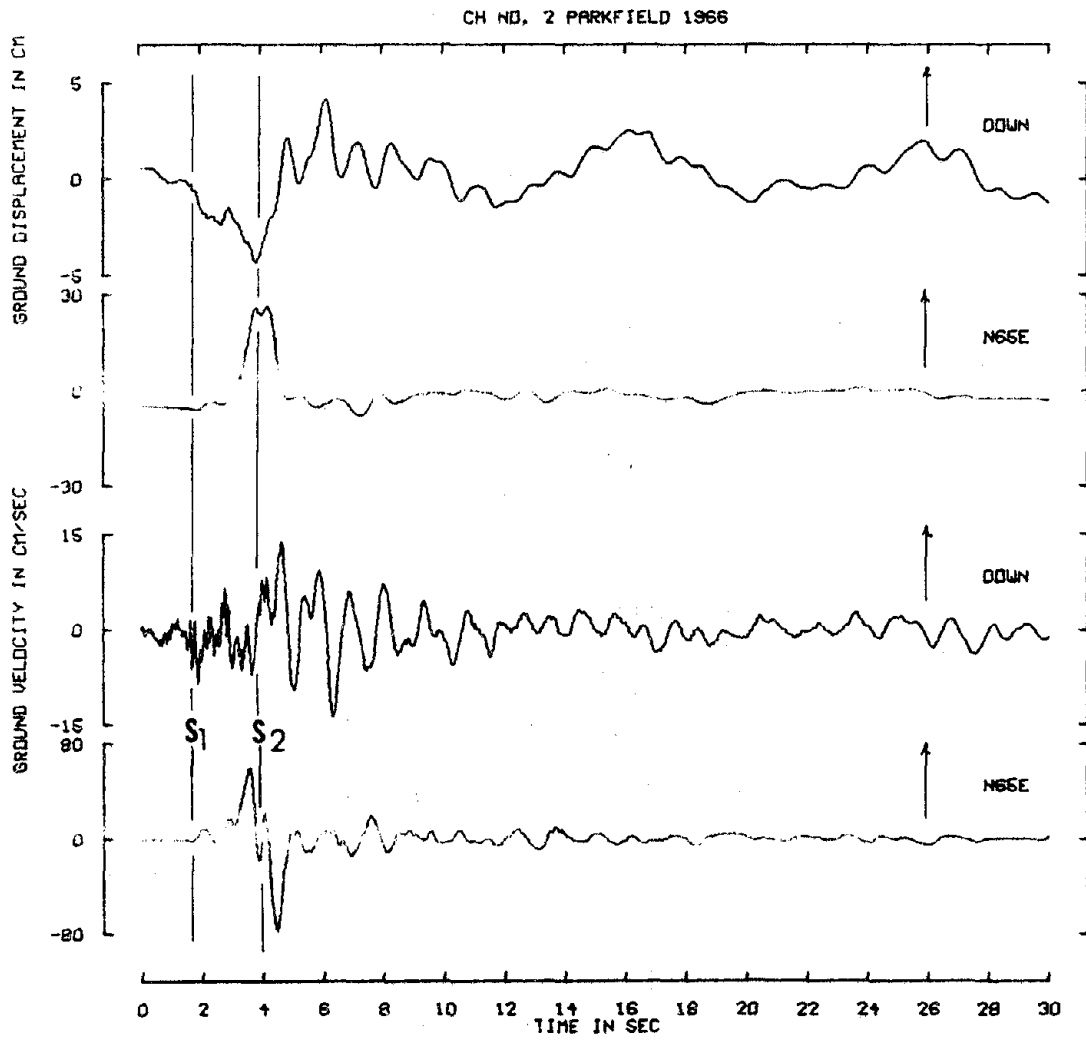


Fig. 5.3a

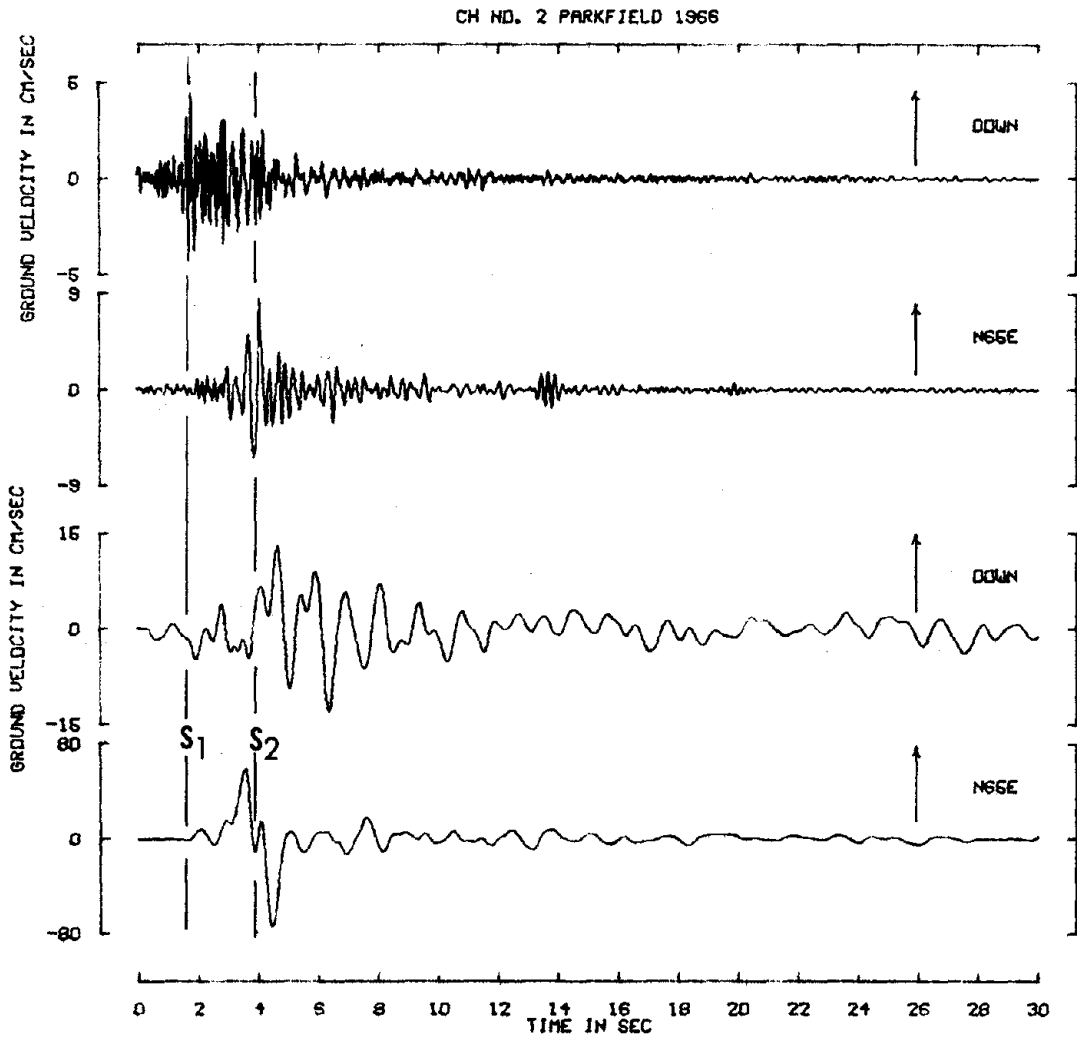


Fig. 5.3b

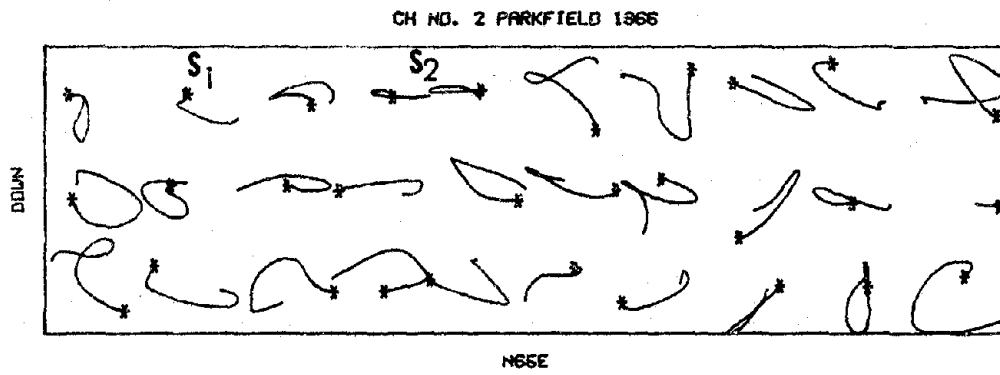


Fig. 5.3c

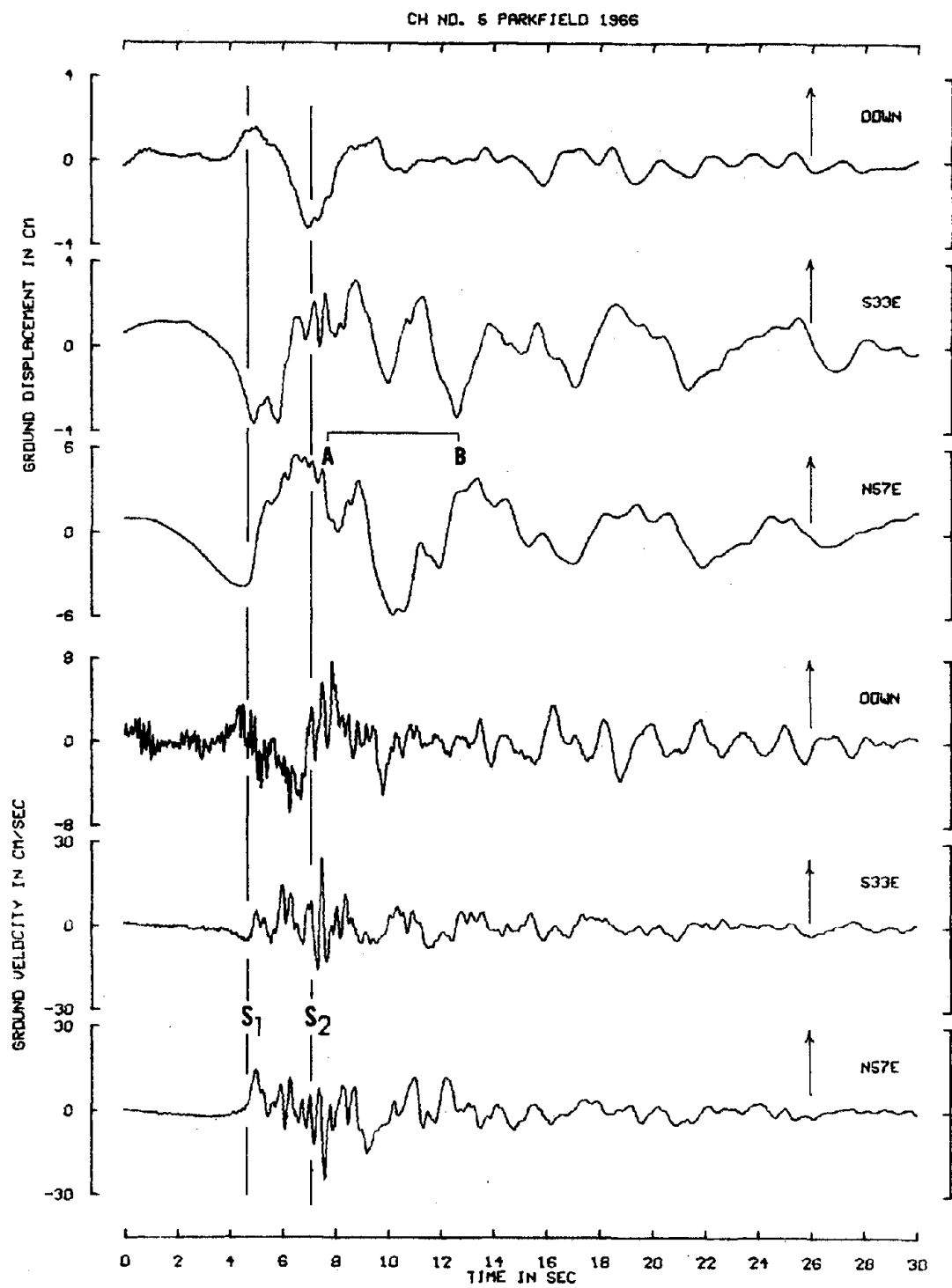


Fig. 5.4a

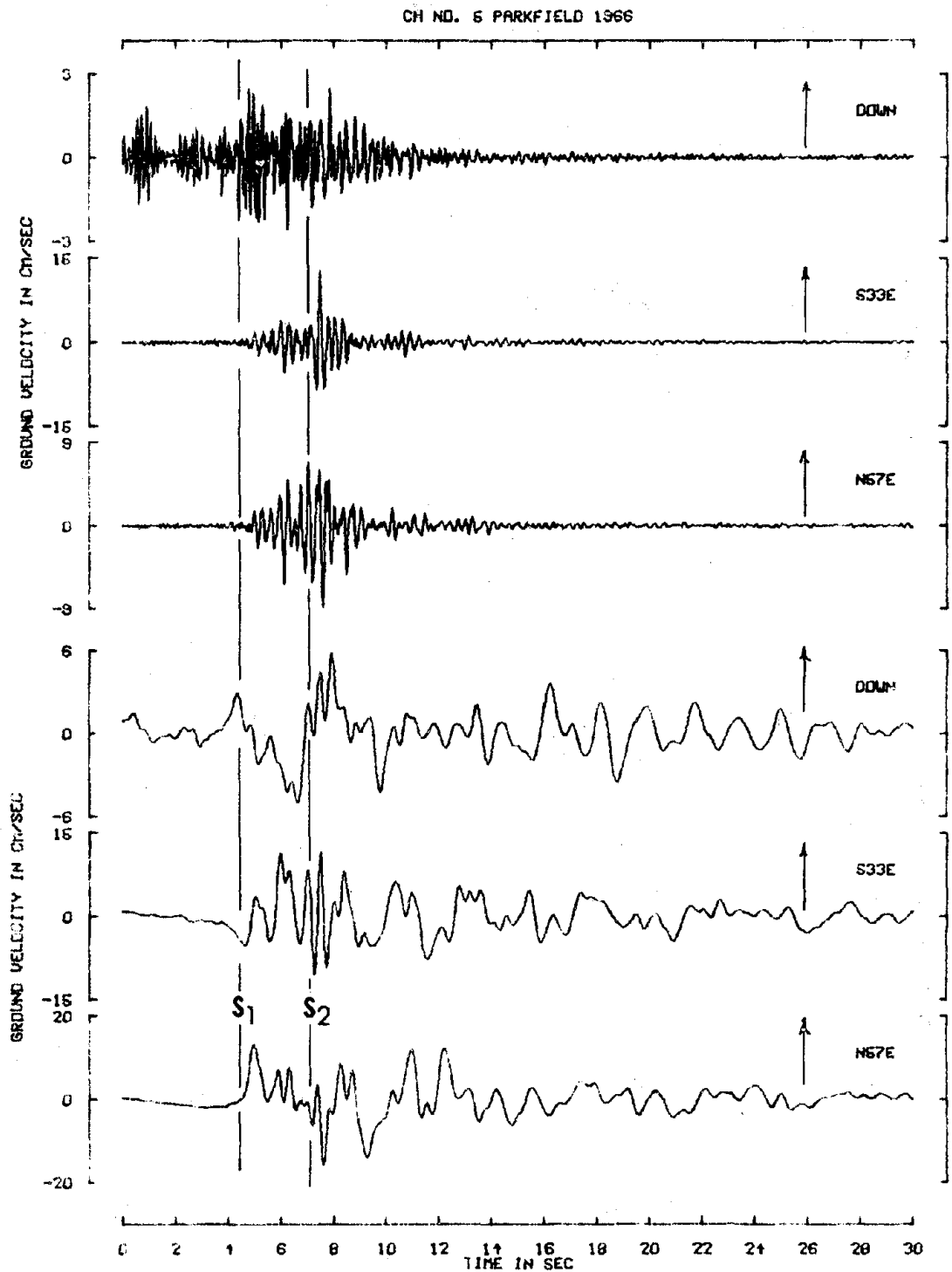
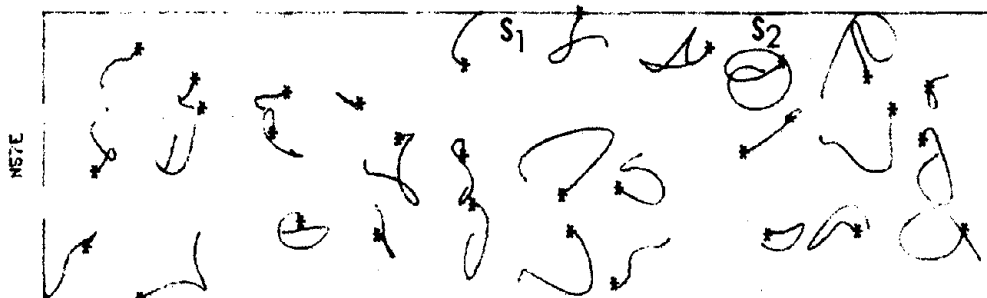
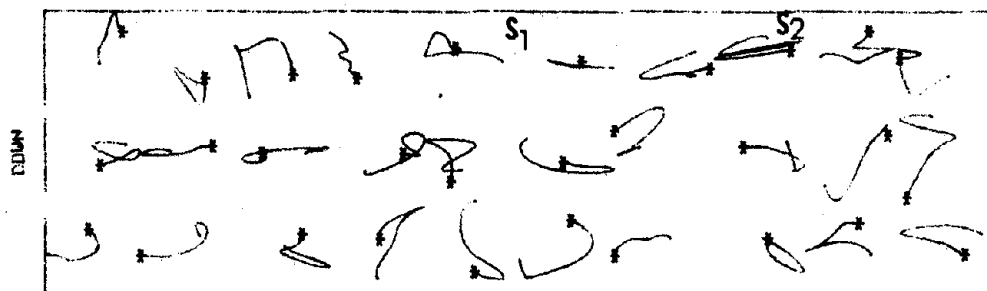


Fig. 5.4b

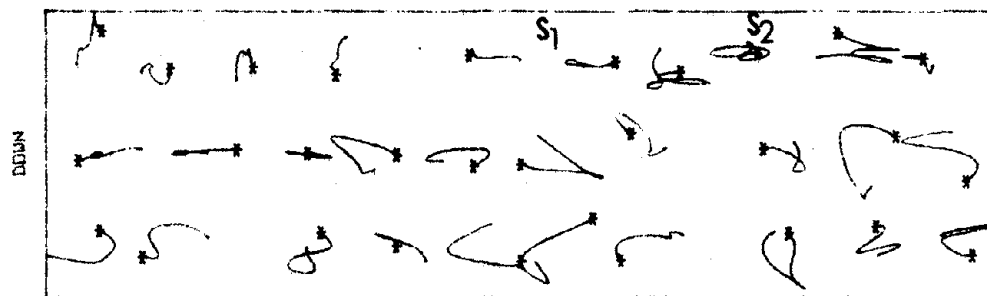
CH NO. 5 PARKFIELD 1966



S33E



S33E



N67E

Fig. 5.4c

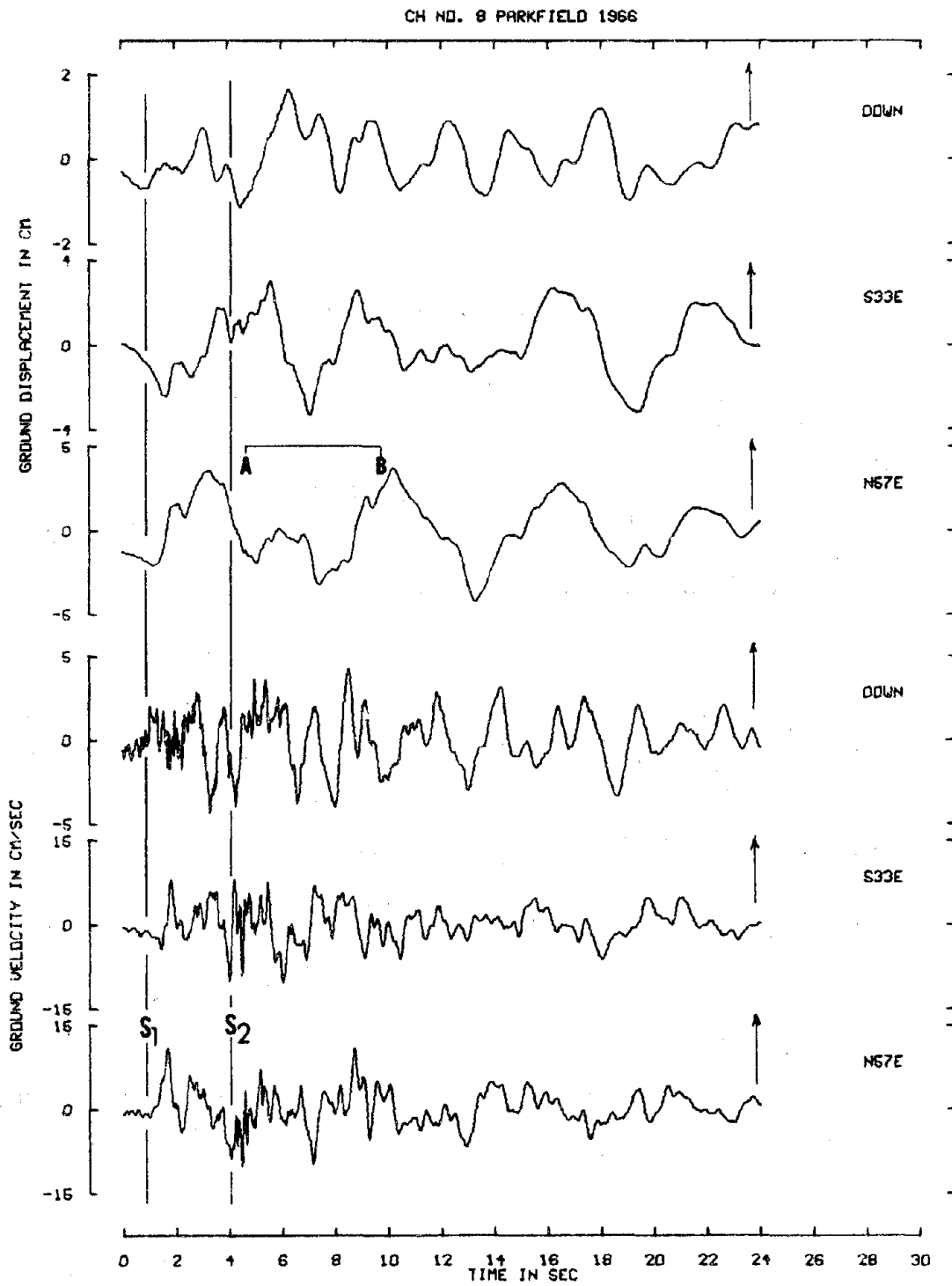


Fig. 5.5a

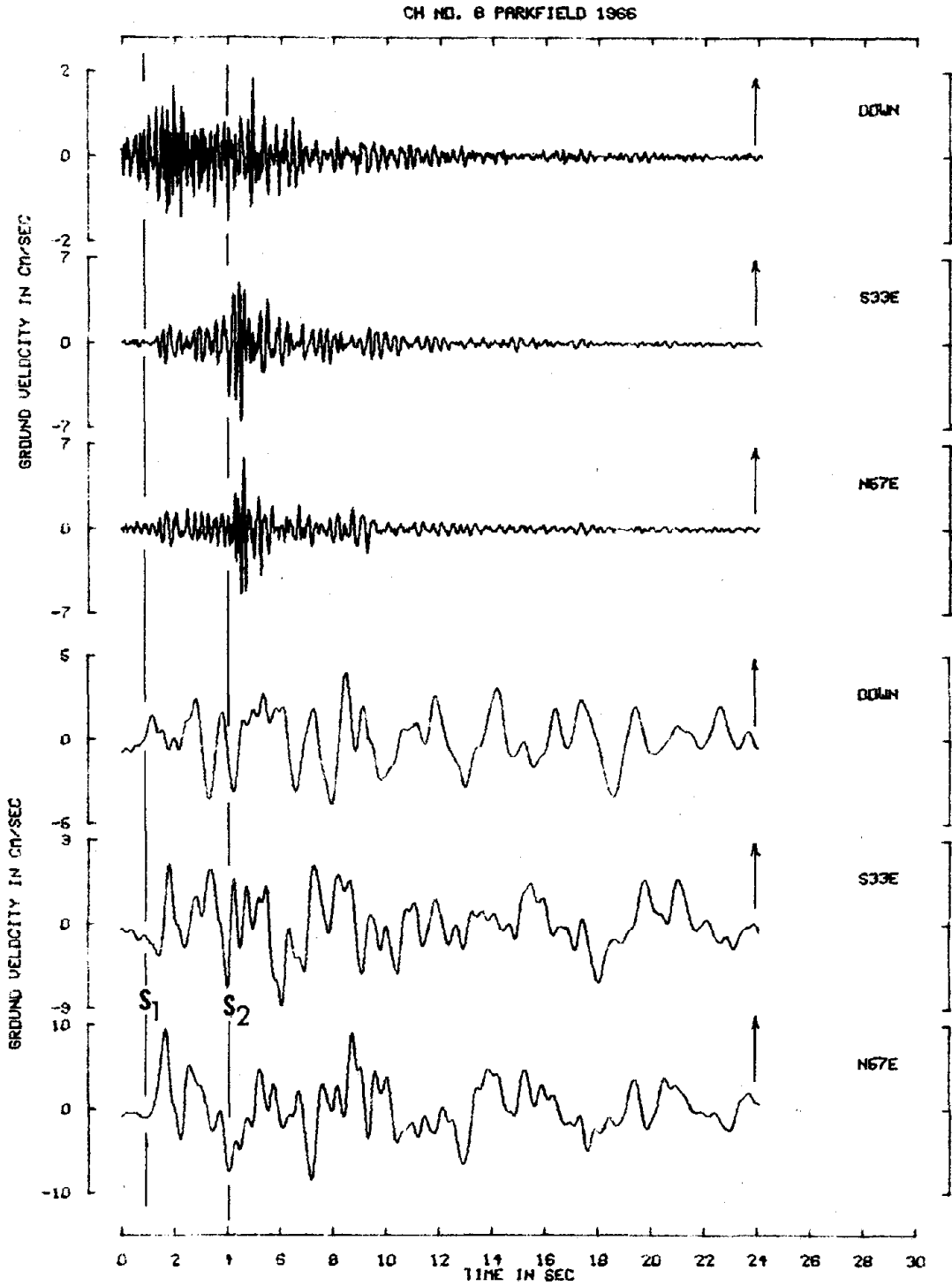


Fig. 5.5b

CH NO. 8 PARKFIELD 1966

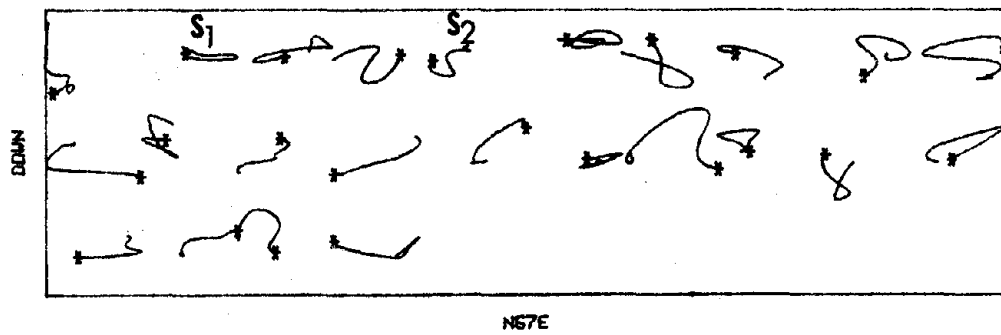
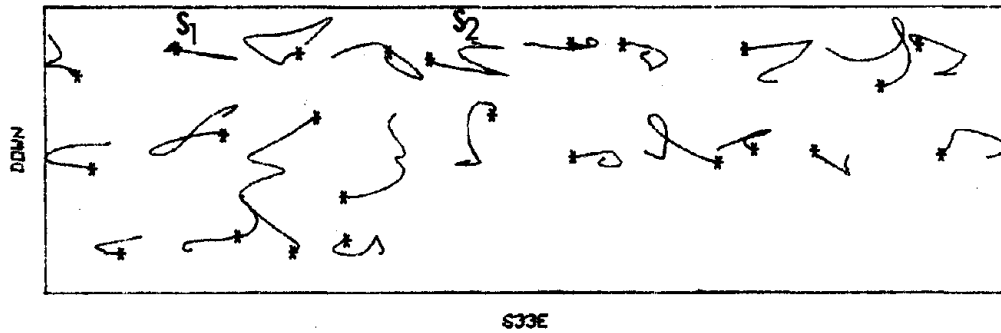
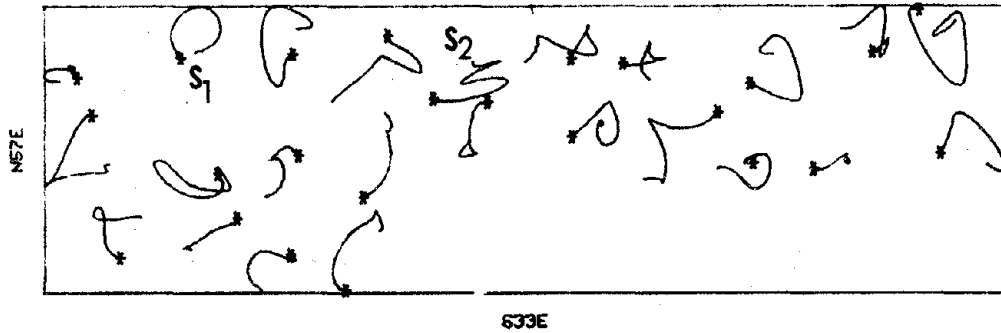


Fig. 5.5c

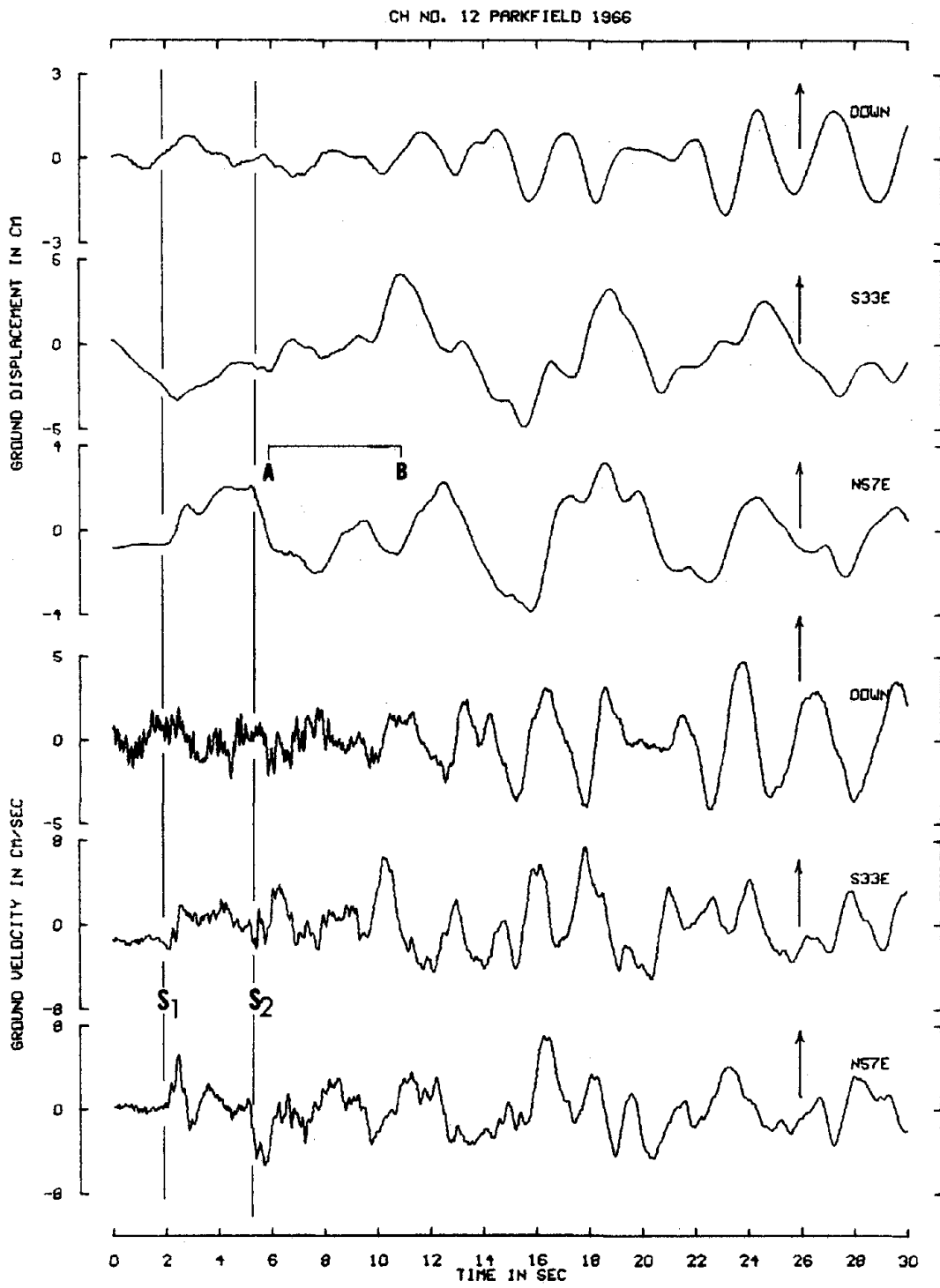


Fig. 5.6a

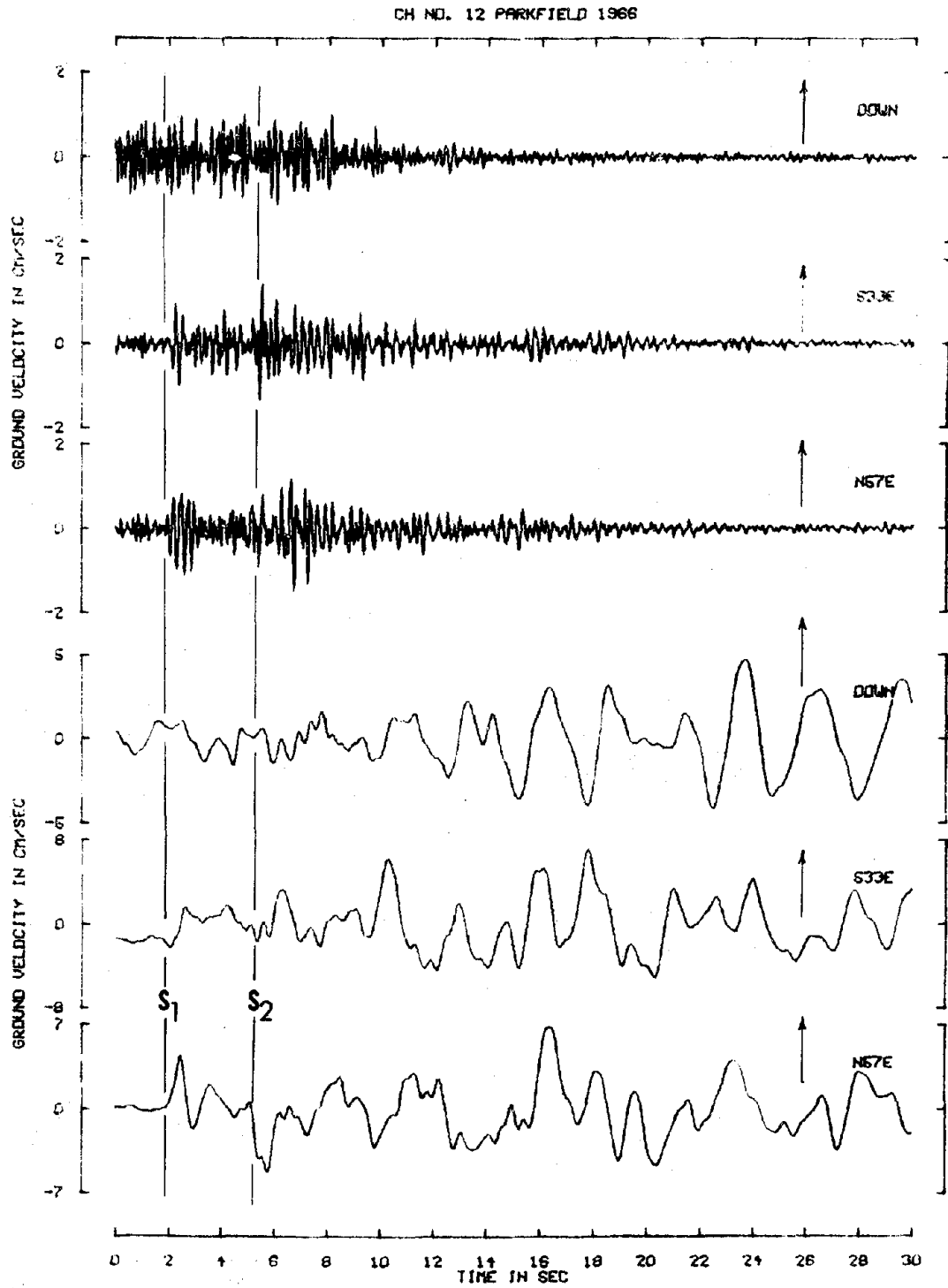


Fig. 5.6b

CH NO. 12 PARKFIELD 1966

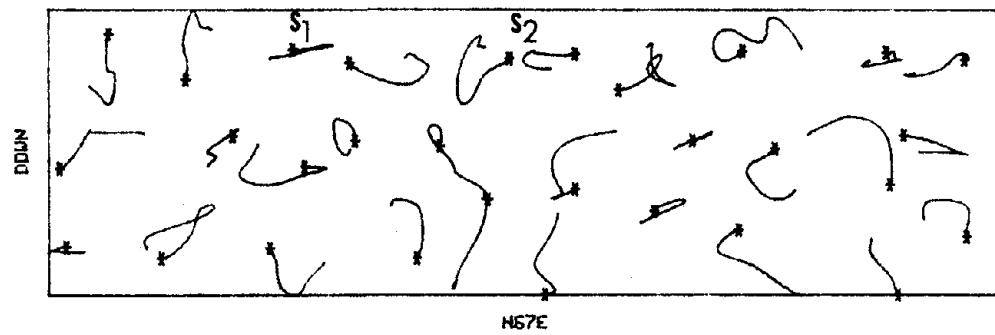
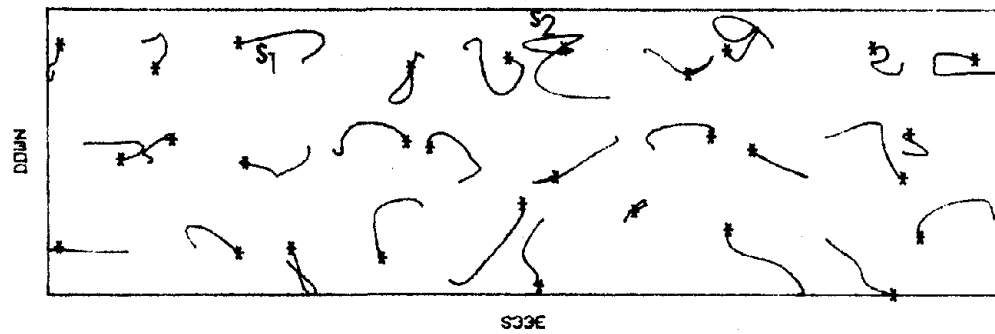
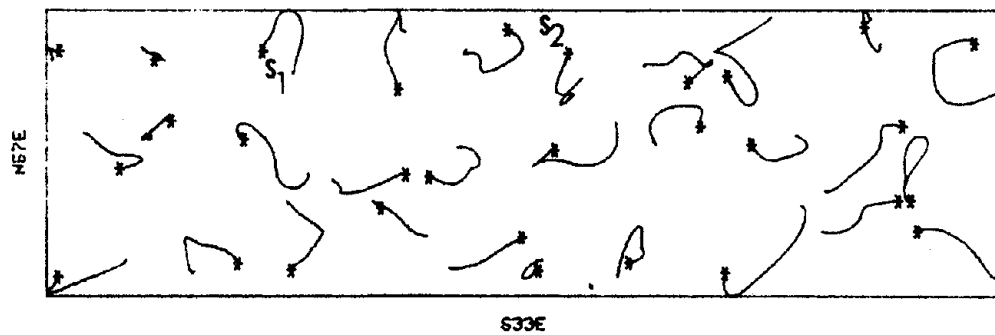


Fig. 5.6c

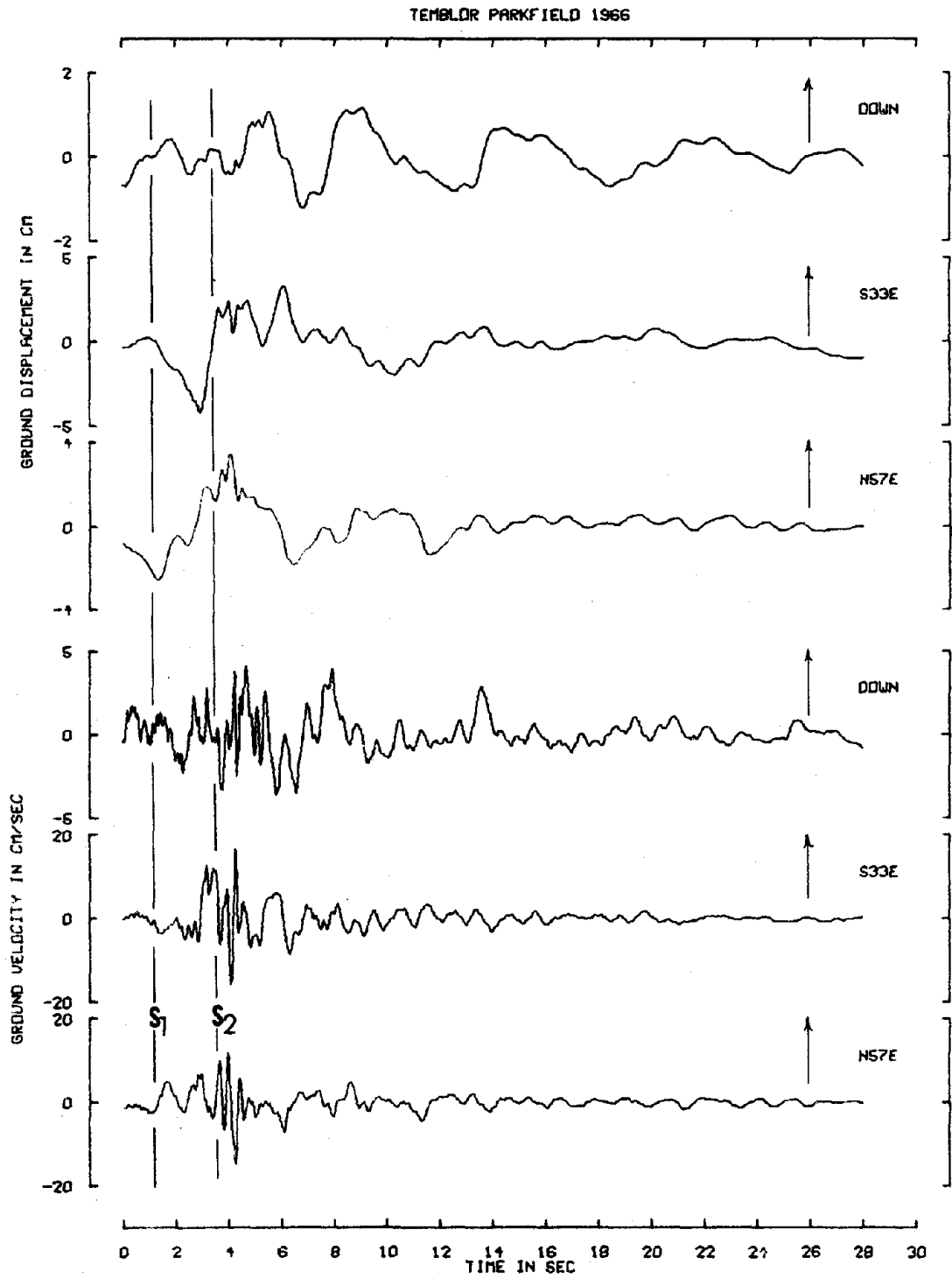


Fig. 5.7a

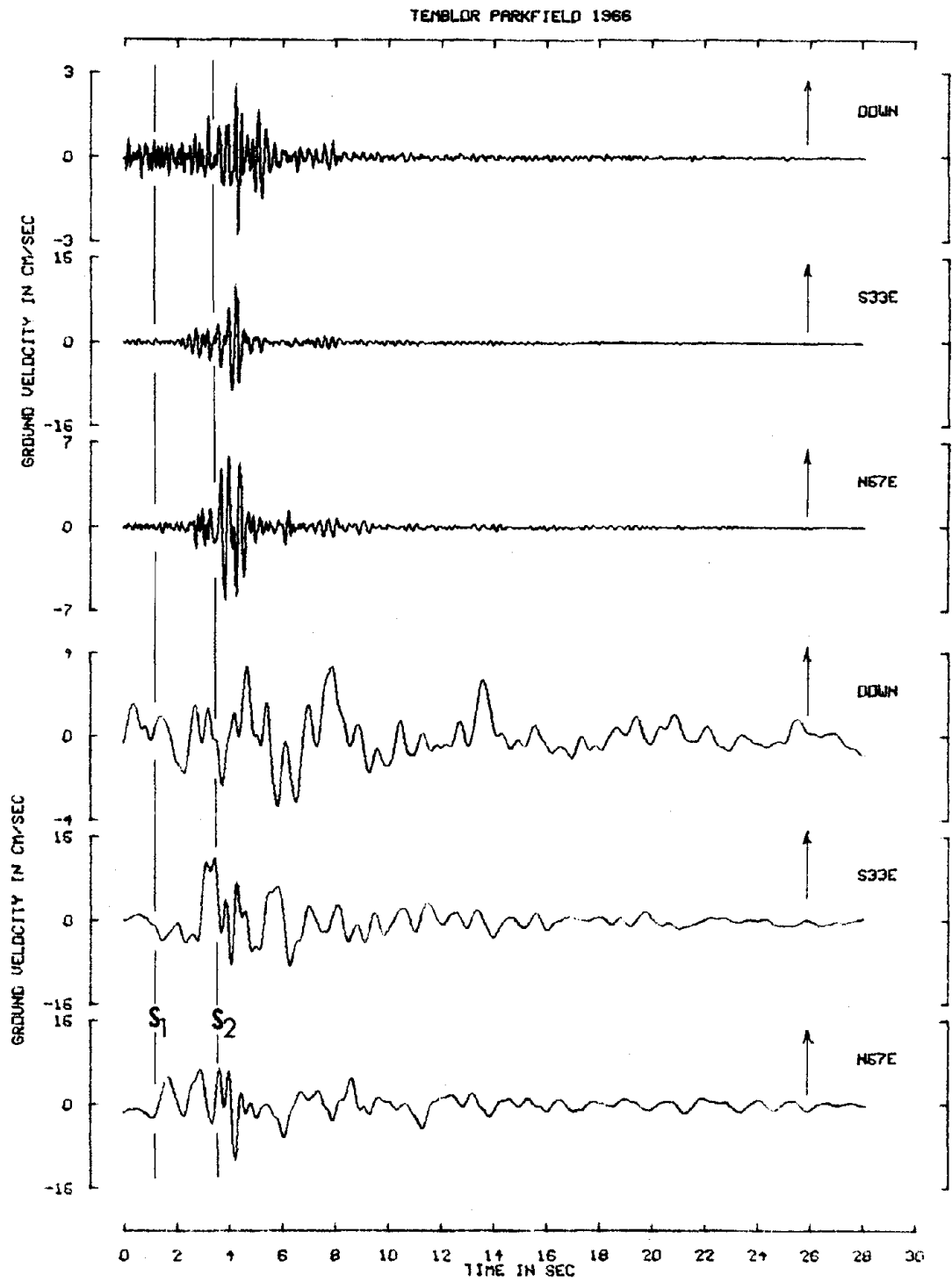


Fig. 5.7b

TEMLOR PARKFIELD 1966

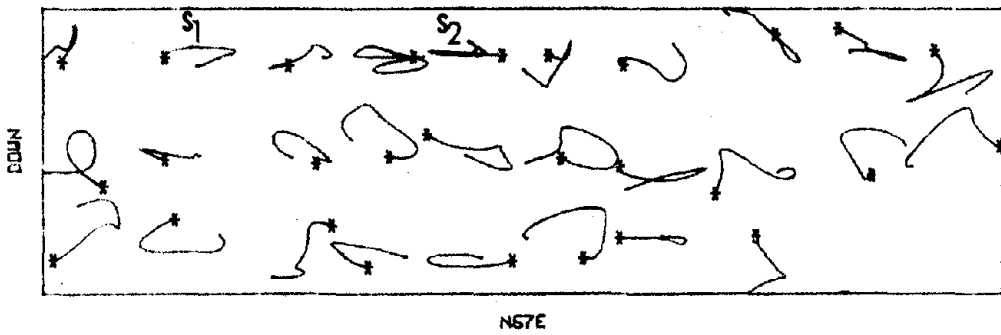
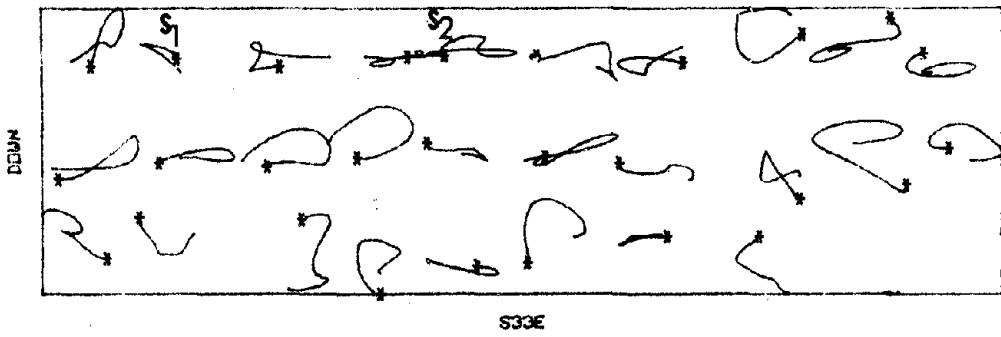
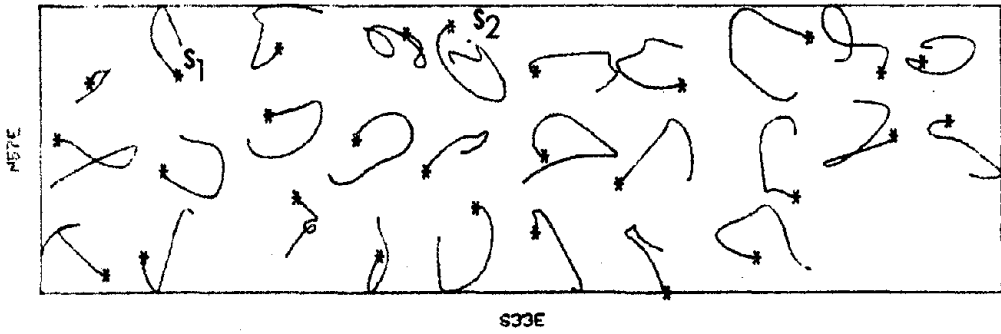
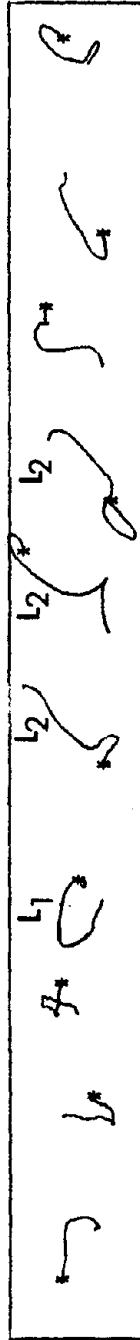


Fig. 5.7c

CH NO. 12 PARKFIELD 1966



NS7E

S33E



DOWN

S33E



DOWN

NS7E

Fig. 5.8

CHAPTER VI

CONCLUSIONS

In this thesis a number of problems pertinent to both engineering and seismological concepts of strong ground motions in earthquakes were studied. The basis of the work was a study of 33 accelerograms recorded by strong motion instruments around the world. First a new method was developed by which more robust estimates of earthquake design parameters (peak acceleration, duration, etc.) can be inferred. Secondly, in order to throw more light on understanding of the mechanism of energy release during an earthquake, the Parkfield earthquake of 1966 was specially analyzed by detailed seismological interpretation of the velocity and displacement records calculated from integration of corresponding accelerograms. The integration of accelerograms was carried out by a new and more precise method of integration developed in the present thesis. The following paragraphs summarize the main results obtained in this thesis.

1) A new method of combining individual recorded components of strong ground motion was devised. Combination is accomplished in the frequency domain by spectral maximization at each frequency. The corresponding spectra and accelerograms (Spectrally Maximized Records) appear to have valuable averaging properties in representing the complex shaking at a site. Nowadays, the response of certain large structures, such as dams, is calculated based on seismological estimates of likely ground motion. It is suggested that an SMR would provide

a more representative and prudent test of ground motions than any one single component of recorded motion.

In particular, SMRs allow a clear demonstration of the importance of taking account of the frequency dependence of strong motion parameters. Indeed, a physically advantageous procedure in selecting peak acceleration as a design parameter for a given structure is to use SMR accelerograms with frequency components restricted to the broad spectral band within which the structure has significant response.

The method also allows the prediction of an expected maximum acceleration for any given acceleration amplitude spectrum. At least for the frequency range 4 to 7 Hz, the average peak acceleration and the gross level of shaking seem closely related.

Use of the recent records from New Guinea adds to the evidence available from other seismic areas that attenuation laws are in general not strongly dependent upon earthquake magnitude (at least above 6.5). Use of this quantity as a strong scaling parameter on acceleration is not supported by the present analysis.

2) Statistical analysis of two major sources of error (human reading and base-line correction) in strong motion records was carried out. These errors limit the usable long period of ground displacements obtained from double integration of accelerogram records. All accelerograms of the Parkfield earthquake of 1966 and also of the Taft earthquake of 1952 were studied in estimating where noise contamination overwhelms the displacement signal.

In the range of the lowest frequency components ($0 < \omega < 0.1$ Hz) of displacement amplitude spectra, errors due to uncertainty in base-line parameters are more pronounced than those of human reading

errors. They have, therefore, a significant weight in controlling the usable long period limits. These errors become, however, considerably smaller than recording errors in intermediate and high-frequency components.

The usable long period limits of the displacement records analyzed in this thesis vary widely between 7 to 14 sec.

At a period of about 16 sec, the combined errors in the majority of cases exceed 25 percent of the accumulative displacement amplitude spectrum. In 35 percent of the cases, the combined errors at this period exceed 50 percent of the accumulative displacement spectrum. Therefore, the period of 16 sec suggested by Trifunac et al. (1973) is likely to be an overestimate of the usable long period limits of displacement records.

The usable long period limits estimated in this study were adopted as guidelines in chapter 5, where the Parkfield earthquake of 1966 was studied.

It is suggested that the most unbiased estimate of the long period limit of a given strong motion record can probably be obtained by analyzing a set of digitized records.

3) The general problem of the integration in the time domain of strong motion seismograms led to the following results.

Quadrature formulas lead to noticeable errors when they are employed in integration of ragged functions such as strong motion accelerograms. This is because the curvature terms of the quadrature formulas overcompensate for the long linear portions of the recorded wave forms and undercompensate for the sharp peaks. Under this circumstance, no form of the quadrature formula seems likely to yield accurate

integration.

Orthogonality of the discrete Fourier transform pairs offers a unique basis for accurate time integration, and perhaps differentiation, of the strong motion seismograms in the frequency domain. It should be noticed, however, that discontinuities expected near both ends of the computed integral functions (the functions are periodic during Fourier analysis) are reflected as distortions of the shape of these functions. These distortions, together with the indeterminacy of zero frequency information of the functions, reduce significantly the overall reliability of the frequency domain approach.

These deficiencies can be completely avoided by a new construction developed in this thesis. The construction extrapolates the integrand by joining its mirror image to the end. The zero frequency information is readily recovered if a sufficient number of zeros is added to the function at both ends. This method is also useful when a function has undergone filter processing. This new construction was employed as a basic tool during integration and filter processing of strong motion records in chapter 5.

4) The Parkfield earthquake of 1966 was analyzed by interpreting the velocity and displacement traces integrated from the corresponding recorded accelerograms. A double-couple right-lateral strike-slip mechanism (along the San Andreas fault) was inferred from the S waves originating from the hypocenter.

The high energy arrivals observed on velocity traces at CH #2, 5, 8, and Temblor (these arrivals also correspond to high amplitudes on the accelerograms) were interpreted as S waves originated at the termination of the rupture towards the southeast of the San Andreas

fault. Based on the reversed polarity of these waves, compared to those of hypocentral S waves observed on the N57E component of displacement at CH #2, 5, 8, 12, the rupture termination was probably established by a double-couple left-lateral mechanism (stopping phase).

From the overall distribution of aftershocks and also from particle velocity diagrams of the stopping phases in the horizontal plane, the rupture seemed to terminate within 10 km northwest of CH #2 (rupture length of about 20 to 28 km) at two possible depths of about 4 km or 8 km. For a depth of about 4 km, rupture velocities of 3.1 ± 0.5 km/sec and 2.5 ± 0.1 km/sec were estimated for two extreme rupture lengths of 28 km and 20 km, respectively. For a depth of 8 km, the estimated rupture velocities are 3.1 ± 0.3 km/sec and 2.4 ± 0.1 km/sec. The evidence gives a preferred length of fault rupture of about 20 km.

Love waves were more excited at the southwestern than the northeastern side of the fault. An explanation is the differences in geological structure of the crust between both sides of the fault. From the observed rate of dispersion, the Love waves that arrive within a few seconds after arrival of the stopping phases originated from the southern end of the rupture, whereas the later arrivals were excited at the northern end of the rupture.

The late arrival of Love waves of long period (e.g., 6 sec) at different stations indicates that these waves had propagated with small velocities (e.g., 1.0-1.5 km/sec). Such low values do not agree with the crustal velocity estimated from refraction studies in this area.

Rayleigh waves recorded at CH #2, 5, 8, 12 were less energetic than Love waves, whereas Rayleigh waves recorded at Temblor seemed to

carry more energy than the Love waves. The reversed dispersion together with the late arrivals of the long period (e.g., 6 sec) Rayleigh waves recorded at Temblor imply the existence of a low-velocity zone within the crust. The reversed dispersion of these waves may also be partly explained by assuming that the early portion of these waves originated from the hypocentral region, whereas those of the late portion originated from the area near the southeastern end of the rupture.

REFERENCES

- Aki, F. (1968). Seismic displacement near a fault, *J. Geophys. Res.*, 73, 5359-5376.
- Algermissen, S.T. and D. Perkins (1976). A probabilistic estimate of of maximum acceleration in rock in the contiguous United States, U.S. Geological Survey, Open File Report 76-416.
- Allen, C.R. and S.W. Smith (1966). Parkfield earthquake of June 27-29, 1966, pre-earthquake and post-earthquake surficial displacement, *Bull. Seism. Soc. Am.*, 56, 955-967.
- Amin, M. and A.H.S. Ang (1966). A nonstationary stochastic model for strong motion earthquakes, Structural Research Series No. 306, University of Illinois, Urbana.
- Anderson, T. (1973). A model source-time function for the Parkfield, California, earthquake (Abstract), 68th Annual National Meeting of the Seismological Society of America, Golden, Colorado.
- Berg, G.V. and G.W. Housner (1961). Integrated velocity and displacement of strong earthquake ground motion. *Bull. Seism. Soc. Am.*, 51, 175-189.
- Berg, G.V. (1963). A study of errors in response spectrum analysis, *Primera Jornadas Chilenas de Seismologia e Ingenieria Antisismica*, Santiago.
- Bolt, B.A. (1972). San Fernando rupture mechanism and the Pacoima strong motion record, *Bull. Seism. Soc. Am.*, 62, 1053-1061.
- _____ (1973). Duration of strong ground motion, Proc. Fifth World Conference on Earthquake Engineering, Rome, Italy.
- Boore, D.M. and M.D. Zoback (1974). Two-dimensional kinematic fault modeling of the Pacoima dam strong-motion recordings of the February 9, 1971, San Fernando earthquake, *Bull. Seism. Soc. Am.*, 64, 555-570.
- Boyce, W.H. (1970). Integration of accelerograms, *Bull. Seism. Soc. Am.*, 60, 261-263.
- Brady, A.G. (1966). Studies of response to earthquake ground motion, Earthquake Engineering Research Laboratory, California Institute of Technology, Pasadena.

- Brillinger, D.R. (1964). The asymptotic behaviour of Tukey's general method of setting approximate confidence limits (the jack knife) when applied to maximum likelihood estimates, *Rev. Inst. Statist.*, 32, 202-206.
- _____ (1966). The application of the jack knife to the analysis of sample surveys, *Commentary*, 8, 74-80.
- Brune, J.N. (1970). Tectonic stress and the spectra of seismic shear waves from earthquakes, *J. Geophys. Res.*, 75, 4997-5009.
- Cloud, W.K. and V. Perez (1969). Strong-motion records and acceleration, *Proc. Fourth World Conference on Earthquake Engineering*, Santiago, Chile.
- Cooley, J.W. and S.W. Tukey (1965). An algorithm for the machine calculation of complex Fourier series, *Mathematics of Computation*, 19, 297-301.
- Davis, P.J. and P. Rabinowitz (1967). Numerical integration, 230 pp., Blaisdell, Waltham, Massachusetts.
- Denham, D., G.R. Small, and I.B. Everingham (1973). Some strong motion seismic results from Papua, New Guinea 1967-1972, Bureau of Mineral Resources, Geology and Geophysics, Australia, Record 1973/13.
- Donovan, N.C. (1973). A statistical evaluation of strong motion data including the February 9, 1971 San Fernando earthquake, *Proc. Fifth World Conference on Earthquake Engineering*, Rome, Italy.
- Eaton, J.P. (1967). The Parkfield-Cholame, California, earthquakes of June-August 1966; Instrumental seismic studies, U.S. Geol. Surv. Prof. Paper 579.
- Eaton, J.P., M.E. O'Neill, and J.N. Murdock (1970). Aftershocks of the 1966 Parkfield-Cholame, California, earthquake: A detailed study, *Bull. Seism. Soc. Am.*, 60, 1151-1197.
- Filson, J. and T.V. McEvelly (1967). Love-wave spectra and the mechanism of the 1966 Parkfield sequence, *Bull. Seism. Soc. Am.*, 57, 1245-1257.
- Gold, B. and C.M. Rader (1969). Digital processing of signals, 269 pp., McGraw-Hill, New York.
- Hamming, R.W. (1973). Numerical methods for scientists and engineers, 721 pp., McGraw-Hill, New York.
- Hanks, T.C. (1974). The faulting mechanism of the San Fernando earthquake, *J. Geophys. Res.*, 79, 1215-1229.

- Hanks, T.C. (1975). Strong ground motion of the San Fernando, California, earthquake: Ground displacement, *Bull. Seism. Soc. Am.*, 65, 193-225.
- Haskell, N.A. (1969). Elastic displacements in the near-field of a propagating fault, *Bull. Seism. Soc. Am.*, 59, 865-908.
- Haskell, N.A. and K.C. Thomson (1972). Elasto-dynamic near-field of a finite propagating tensile fault, *Bull. Seism. Soc. Am.*, 62, 675-697.
- Hershberger, J. (1955). Recent developments in strong motion analysis, *Bull. Seism. Soc. Am.*, 45, 11-21.
- Housner, G.W. (1947). Ground displacement computed from strong motion accelerograms, *Bull. Seism. Soc. Am.*, 53, 419-437.
- _____, (1970). Strong ground motion, chapter IV in Earthquake engineering, R.L. Wiegel, ed., Englewood Cliffs, New Jersey.
- Hudson, D.E., N.C. Nigam, and M.D. Trifunac (1969). Analysis of strong motion accelerograph records, Fourth World Conference on Earthquake Engineering, Santiago, Chile.
- Jeffreys, H. and B.S. Jeffreys (1946). Methods of mathematical physics, Cambridge.
- Kanasewich, E.R. (1973). Time sequence analysis in geophysics, 352 pp., The University of Alberta Press, Edmonton.
- McComb, H.E., A.C. Ruge, and F. Neumann (1943). The determination of true ground motion: A symposium, *Bull. Seism. Soc. Am.*, 33, 1-63.
- McEvelly, T.V. (1966). Preliminary seismic data, June-July, 1966 in Parkfield earthquake of June 27-29, 1966, Monterey and San Luis Obispo counties, California--Preliminary report, *Bull. Seism. Soc. Am.*, 56, 967-971.
- McEvelly, T.V., W.H. Bakun, and K.B. Casaday (1967). The Parkfield, California, earthquakes of 1966, *Bull. Seism. Soc. Am.*, 57, 1221-1244.
- Murray, G.F. (1967). Note on strong motion records from the June 1966 Parkfield, California, earthquake sequence, *Bull. Seism. Soc. Am.*, 57, 1259-1266.
- Newmark, N.M. and E. Rosenblueth (1971). Fundamentals of earthquake engineering, Prentice-Hall, New Jersey.
- Penzin, J. and M. Watabe (1975). Characteristics of 3-dimensional earthquake ground motion, *Earthquake Engineering and Structural Dynamics*, 3, 365-373.

- Poppitz, J.V. (1968). Velocity and displacement of explosion-induced earth tremors derived from acceleration, *Bull. Seism. Soc. Am.*, 57, 857-874.
- Savage, J.C. (1965a). The stopping phase on seismograms, *Bull. Seism. Soc. Am.*, 55, 47-58.
- _____ (1965b). The effect of rupture velocity upon seismic first motions, *Bull. Seism. Soc. Am.*, 55, 263-275.
- Schiff, A. and J.L. Bogdanoff (1967). Laboratory evaluation and instrument corrections of strong motion accelerographs, Earthquake Engineering Research Laboratory, EERL 70-04, California Institute of Technology, Pasadena.
- Schnabel, P.B. and H.B. Seed (1973). Accelerations in rock for earthquakes in the western United States, *Bull. Seism. Soc. Am.*, 63, 501-576.
- Scholz, C.H., M. Wyss, and S.W. Smith (1969). Seismic and aseismic slip on the San Andreas fault, *J. Geophys. Res.*, 74, 2049-2069.
- Trifunac, M.D. and J. Brune (1970). Complexity of energy release during the Imperial Valley, California, earthquake of 1940, *Bull. Seism. Soc. Am.*, 60, 137-160.
- Trifunac, M.D. (1971). Zero base-line correction of strong motion accelerograms, *Bull. Seism. Soc. Am.*, 61, 1201-1211.
- Trifunac, M.D., F.E. Udawadia, and A.G. Brady (1973a). Analysis of errors in digitized strong-motion accelerograms, *Bull. Seism. Soc. Am.*, 63, 157-187.
- Trifunac, M.D., A.G. Brady, and D.E. Hudson (1973c). Strong-motion earthquake accelerograms, Vol. IIC, Corrected Accelerograms and Integrated Ground Velocity and Displacement Curves, EERL 73-51, Earthquake Eng. Res. Lab., Calif. Inst. of Tech., Pasadena.
- Trifunac, M.D. (1974a). A three-dimensional dislocation model for the San Fernando, California, earthquake of February 9, 1971, *Bull. Seism. Soc. Am.*, 64, 149-172.
- Trifunac, M.D. and F.E. Udawadia (1974b). Parkfield, California, earthquake of June 27, 1966: A three-dimensional moving dislocation, *Bull. Seism. Soc. Am.*, 64, 511-533.
- Trifunac, M.D. and V.W. Lee (1974). A note on the accuracy of computed ground displacements from strong-motion accelerograms, *Bull. Seism. Soc. Am.*, 64, 1209-1219.
- Trifunac, M.D. and A.G. Brady (1975). A study on the duration of strong earthquake ground motion, *Bull. Seism. Soc. Am.*, 65, 581-626.

- Tsai, Y.B. and H.J. Patton (1973). Interpretation of the strong-motion earthquake accelerograms using a moving dislocation model: The Parkfield, California, earthquake of June 28, 1966 (Abstract), 68th Annual National Meeting of the Seismological Society of America, Golden, Colorado.
- Tukey, J.W. (1958). Bias and confidence in not-quite large samples (Abstract), *Ann. Math. Statist.*, 29, 614.
- Wallace, R.E. and E.F. Roth (1967). The Parkfield-Cholame, California earthquakes of June-August, 1966--Rates and patterns of progressive deformation, *U.S. Geol. Surv. Prof. Paper* 579, 23-39.

EARTHQUAKE ENGINEERING RESEARCH CENTER REPORTS

- 189
- EERC 67-1 "Feasibility Study Large-Scale Earthquake Simulator Facility," by J. Penzien, J. G. Bouwkamp, R. W. Clough and D. Rea - 1967 (PB 187 905)
- EERC 68-1 Unassigned
- EERC 68-2 "Inelastic Behavior of Beam-to-Column Subassemblages Under Repeated Loading," by V. V. Bertero - 1968 (PB 184 888)
- EERC 68-3 "A Graphical Method for Solving the Wave Reflection-Refraction Problem," by H. D. McNiven and Y. Mengi - 1968 (PB 187 943)
- EERC 68-4 "Dynamic Properties of McKinley School Buildings," by D. Rea, J. G. Bouwkamp and R. W. Clough - 1968 (PB 187 902)
- EERC 68-5 "Characteristics of Rock Motions During Earthquakes," by H. B. Seed, I. M. Idriss and F. W. Kiefer - 1968 (PB 188 338)
- EERC 69-1 "Earthquake Engineering Research at Berkeley," - 1969 (PB 187 906)
- EERC 69-2 "Nonlinear Seismic Response of Earth Structures," by M. Dibaj and J. Penzien - 1969 (PB 187 904)
- EERC 69-3 "Probabilistic Study of the Behavior of Structures During Earthquakes," by P. Ruiz and J. Penzien - 1969 (PB 187 886)
- EERC 69-4 "Numerical Solution of Boundary Value Problems in Structural Mechanics by Reduction to an Initial Value Formulation," by N. Distefano and J. Schujman - 1969 (PB 187 942)
- EERC 69-5 "Dynamic Programming and the Solution of the Biharmonic Equation," by N. Distefano - 1969 (PB 187 941)
- EERC 69-6 "Stochastic Analysis of Offshore Tower Structures," by A. K. Malhotra and J. Penzien - 1969 (PB 187 903)
- EERC 69-7 "Rock Motion Accelerograms for High Magnitude Earthquakes," by H. B. Seed and I. M. Idriss - 1969 (PB 187 940)
- EERC 69-8 "Structural Dynamics Testing Facilities at the University of California, Berkeley," by R. M. Stephen, J. G. Bouwkamp, R. W. Clough and J. Penzien - 1969 (PB 189 111)
- EERC 69-9 "Seismic Response of Soil Deposits Underlain by Sloping Rock Boundaries," by H. Dezfulian and H. B. Seed - 1969 (PB 189 114)
- EERC 69-10 "Dynamic Stress Analysis of Axisymmetric Structures under Arbitrary Loading," by S. Ghosh and E. L. Wilson - 1969 (PB 189 026)

Note: Numbers in parenthesis are Accession Numbers assigned by the National Technical Information Service. Copies of these reports may be ordered from the National Technical Information Service, 5285 Port Royal Road, Springfield Virginia, 22161.

- EERC 69-11 "Seismic Behavior of Multistory Frames Designed by Different Philosophies," by J. C. Anderson and V. V. Bertero 1969 (PB 190 662)
- EERC 69-12 "Stiffness Degradation of Reinforcing Concrete Structures Subjected to Reversed Actions," by V. V. Bertero, B. Bresler and H. Ming Liao -1969 (PB 202 942)
- EERC 69-13 "Response of Non-Uniform Soil Deposits to Travel Seismic Waves," by H. Dezfulian and H. B. Seed - 1969 (PB 191 023)
- EERC 69-14 "Damping Capacity of A Model Steel Structure," by D. Rea, R. W. Clough and J. G. Bouwkamp - 1969 (PB 190 663)
- EERC 69-15 "Influence of Local Soil Conditions on Building Damage Potential during Earthquakes," by H. B. Seed and I. M. Idriss 1969 (PB 191 036)
- EERC 69-16 "The Behavior of Sands under Seismic Loading Conditions," by M. L. Silver and H. B. Seed - 1969 (AD 714 982)
- EERC 70-1 "Earthquake Response of Concrete Gravity Dams," by A. K. Chopra - 1970 (AD 709 640)
- EERC 70-2 "Relationships between Soil Conditions and Building Damage in the Caracas Earthquake of July 29, 1967," by H. B. Seed, I. M. Idriss and H. Dezfulian - 1970 (PB 195 762)
- EERC 70-3 "Cyclic Loading of Full Size Steel Connections," by E. P. Popov and R. M. Stephen - 1970 (PB 213 545)
- EERC 70-4 "Seismic Analysis of the Charaima Building, Caraballeda, Venezuela," by Subcommittee of the SEAONC Research Committee: V. V. Bertero, P. F. Fratessa, S. A. Mahin, J. H. Sexton, A. C. Scordelis, E. L. Wilson, L. A. Wyllie, H. B. Seed and J. Penzien, Chairman - 1970 (PB 201 455)
- EERC 70-5 "A Computer Program for Earthquake Analysis of Dams," by A. K. Chopra and P. Chakrabarti - 1970 (AD 723 994)
- EERC 70-6 "The Propagation of Love Waves Across Non-Horizontally Layered Structures," by J. Lysmer and L. A. Drake - 1970 (PB 197 896)
- EERC 70-7 "Influence of Base Rock Characteristics on Ground Response," by J. Lysmer, H. B. Seed and P. B. Schnabel - 1970 (PB 197 897)
- EERC 70-8 "Applicability of Laboratory Test Procedures for Measuring Soil Liquefaction Characteristics under Cyclic Loading," by H. B. Seed and W. H. Peacock - 1970 (PB 198 016)
- EERC 70-9 "A Simplified Procedure for Evaluating Soil Liquefaction Potential," by H. B. Seed and I. M. Idriss - 1970 (PB 198 009)

- EERC 70-10 "Soil Moduli and Damping Factors for Dynamic Response Analysis," by H. B. Seed and I. M. Idriss - 1970 (PB 197 869)
- EERC 71-1 "Koyna Earthquake and the Performance of Koyna Dam," by A. K. Chopra and P. Chakrabarti - 1971 (AD 731 496)
- EERC 71-2 "Preliminary In-Situ Measurements of Anelastic Absorption in Soils Using a Prototype Earthquake Simulator," by R. D. Borcherdt and P. W. Rodgers - 1971 (PB 201 454)
- EERC 71-3 "Static and Dynamic Analysis of Inelastic Frame Structures," by F. L. Porter and G. H. Powell - 1971 (PB 210 135)
- EERC 71-4 "Research Needs in Limit Design of Reinforced Concrete Structures," by V. V. Bertero - 1971 (PB 202 943)
- EERC 71-5 "Dynamic Behavior of a High-Rise Diagonally Braced Steel Building," by D. Rea, A. A. Shah and J. G. Bouwkamp - 1971 (PB 203 584)
- EERC 71-6 "Dynamic Stress Analysis of Porous Elastic Solids Saturated with Compressible Fluids," by J. Ghaboussi and E. L. Wilson 1971 (PB 211 396)
- EERC 71-7 "Inelastic Behavior of Steel Beam-to-Column Subassemblages," by H. Krawinkler, V. V. Bertero and E. P. Popov - 1971 (PB211 335)
- EERC 71-8 "Modification of Seismograph Records for Effects of Local Soil Conditions," by P. Schnabel, H. B. Seed and J. Lysmer - 1971 (PB 214 450)
- EERC 72-1 "Static and Earthquake Analysis of Three Dimensional Frame and Shear Wall Buildings," by E. L. Wilson and H. H. Dovey 1972 (PB 212 904)
- EERC 72-2 "Accelerations in Rock for Earthquakes in the Western United States," by P. B. Schnabel and H. B. Seed - 1972 (PB 213 100)
- EERC 72-3 "Elastic-Plastic Earthquake Response of Soil-Building Systems," by T. Minami - 1972 (PB 214 868)
- EERC 72-4 "Stochastic Inelastic Response of Offshore Towers to Strong Motion Earthquakes," by M. K. Kaul - 1972 (PB 215 713)
- EERC 72-5 "Cyclic Behavior of Three Reinforced Concrete Flexural Members with High Shear," by E. P. Popov, V. V. Bertero and H. Krawinkler - 1972 (PB 214 555)
- EERC 72-6 "Earthquake Response of Gravity Dams Including Reservoir Interaction Effects," by P. Chakrabarti and A. K. Chopra 1972 (AD 762 330)
- EERC 72-7 "Dynamic Properties on Pine Flat Dam," by D. Rea, C. Y. Liaw and A. K. Chopra - 1972 (AD 763 928)

- 192
- EERC 72-8 "Three Dimensional Analysis of Building Systems," by E. L. Wilson and H. H. Dovey - 1972 (PB 222 438)
- EERC 72-9 "Rate of Loading Effects on Uncracked and Repaired Reinforced Concrete Members," by S. Mahin, V. V. Bertero, D. Rea and M. Atalay - 1972 (PB 224 520)
- EERC 72-10 "Computer Program for Static and Dynamic Analysis of Linear Structural Systems," by E. L. Wilson, K.-J. Bathe, J. E. Peterson and H. H. Dovey - 1972 (PB 220 437)
- EERC 72-11 "Literature Survey - Seismic Effects on Highway Bridges," by T. Iwasaki, J. Penzien and R. W. Clough - 1972 (PB 215 613)
- EERC 72-12 "SHAKE-A Computer Program for Earthquake Response Analysis of Horizontally Layered Sites," by P. B. Schnabel and J. Lysmer - 1972 (PB 220 207)
- EERC 73-1 "Optimal Seismic Design of Multistory Frames," by V. V. Bertero and H. Kamil - 1973
- EERC 73-2 "Analysis of the Slides in the San Fernando Dams during the Earthquake of February 9, 1971," by H. B. Seed, K. L. Lee, I. M. Idriss and F. Makdisi - 1973 (PB 223 402)
- EERC 73-3 "Computer Aided Ultimate Load Design of Unbraced Multi-story Steel Frames," by M. B. El-Hafez and G. H. Powell 1973 (PB 248 315)
- EERC 73-4 "Experimental Investigation into the Seismic Behavior of Critical Regions of Reinforced Concrete Components as Influenced by Moment and Shear," by M. Celebi and J. Penzien 1973 (PB 215 884)
- EERC 73-5 "Hysteretic Behavior of Epoxy-Repaired Reinforced Concrete Beams," by M. Celebi and J. Penzien - 1973 (PB 239 568)
- EERC 73-6 "General Purpose Computer Program for Inelastic Dynamic Response of Plane Structures," by A. Kanaan and G. H. Powell 1973 (PB 221 260)
- EERC 73-7 "A Computer Program for Earthquake Analysis of Gravity Dams Including Reservoir Interaction," by P. Chakrabarti and A. K. Chopra - 1973 (AD 766 271)
- EERC 73-8 "Behavior of Reinforced Concrete Deep Beam-Column Subassemblies under Cyclic Loads," by O. Kustu and J. G. Bouwkamp 1973 (PB 246 117)
- EERC 73-9 "Earthquake Analysis of Structure-Foundation Systems," by A. K. Vaish and A. K. Chopra - 1973 (AD 766 272)
- EERC 73-10 "Deconvolution of Seismic Response for Linear Systems," by R. B. Reimer - 1973 (PB 227 179)
- EERC 73-11 "SAP IV: A Structural Analysis Program for Static and Dynamic Response of Linear Systems," by K.-J. Bathe, E. L. Wilson and F. E. Peterson - 1973 (PB 221 967)

- 193
- EERC 73-12 "Analytical Investigations of the Seismic Response of Long, Multiple Span Highway Bridges," by W. S. Tseng and J. Penzien - 1973 (PB 227 816)
- EERC 73-13 "Earthquake Analysis of Multi-Story Buildings Including Foundation Interaction," by A. K. Chopra and J. A. Gutierrez 1973 (PB 222 970)
- EERC 73-14 "ADAP: A Computer Program for Static and Dynamic Analysis of Arch Dams," by R. W. Clough, J. M. Raphael and S. Majtahedi 1973 (PB 223 763)
- EERC 73-15 "Cyclic Plastic Analysis of Structural Steel Joints," by R. B. Pinkney and R. W. Clough - 1973 (PB 226 843)
- EERC 73-16 "QUAD-4: A Computer Program for Evaluating the Seismic Response of Soil Structures by Variable Damping Finite Element Procedures," by I. M. Idriss, J. Lysmer, R. Hwang and H. B. Seed - 1973 (PB 229 424)
- EERC 73-17 "Dynamic Behavior of a Multi-Story Pyramid Shaped Building," by R. M. Stephen and J. G. Bouwkamp - 1973 (PB 240 718)
- EERC 73-18 "Effect of Different Types of Reinforcing on Seismic Behavior of Short Concrete Columns," by V. V. Bertero, J. Hollings, O. Kustu, R. M. Stephen and J. G. Bouwkamp - 1973
- EERC 73-19 "Olive View Medical Center Material Studies, Phase I," by B. Bresler and V. V. Bertero - 1973 (PB 235 986)
- EERC 73-20 "Linear and Nonlinear Seismic Analysis Computer Programs for Long Multiple-Span Highway Bridges," by W. S. Tseng and J. Penzien - 1973
- EERC 73-21 "Constitutive Models for Cyclic Plastic Deformation of Engineering Materials," by J. M. Kelly and P. P. Gillis - 1973 (PB 226 024)
- EERC 73-22 "DRAIN - 2D User's Guide," by G. H. Powell - 1973 (PB 227 016)
- EERC 73-23 "Earthquake Engineering at Berkeley - 1973," (PB 226 033)
- EERC 73-24 Unassigned
- EERC 73-25 "Earthquake Response of Axisymmetric Tower Structures Surrounded by Water," by C. Y. Liaw and A. K. Chopra - 1973 (AD 773 052)
- EERC 73-26 "Investigation of the Failures of the Olive View Stair-towers during the San Fernando Earthquake and Their Implications in Seismic Design," by V. V. Bertero and R. G. Collins 1973 (PB 235 106)
- EERC 73-27 "Further Studies on Seismic Behavior of Steel Beam-Column Subassemblages," by V. V. Bertero, H. Krawinkler and E. P. Popov 1973 (PB 234 172)

- 194
- EERC 74-1 "Seismic Risk Analysis," by C. S. Oliveira - 1974 (PB 235 920)
- EERC 74-2 "Settlement and Liquefaction of Sands under Multi-Directional Shaking," by R. Pyke, C. K. Chan and H. B. Seed - 1974
- EERC 74-3 "Optimum Design of Earthquake Resistant Shear Buildings," by D. Ray, K. S. Pister and A. K. Chopra - 1974 (PB 231 172)
- EERC 74-4 "LUSH - A Computer Program for Complex Response Analysis of Soil-Structure Systems," by J. Lysmer, T. Udaka, H. B. Seed and R. Hwang - 1974 (PB 236 796)
- EERC 74-5 "Sensitivity Analysis for Hysteretic Dynamic Systems: Applications to Earthquake Engineering," by D. Ray - 1974 (PB 233 213)
- EERC 74-6 "Soil-Structure Interaction Analyses for Evaluating Seismic Response," by H. B. Seed, J. Lysmer and R. Hwang - 1974 (PB 236 519)
- EERC 74-7 Unassigned
- EERC 74-8 "Shaking Table Tests of a Steel Frame - A Progress Report," by R. W. Clough and D. Tang - 1974 (PB 240 869)
- EERC 74-9 "Hysteretic Behavior of Reinforced Concrete Flexural Members with Special Web Reinforcement," by V. V. Bertero, E. P. Popov and T. Y. Wang - 1974 (PB 236 797)
- EERC 74-10 "Applications of Reliability-Based, Global Cost Optimization to Design of Earthquake Resistant Structures," by E. Vitiello and K. S. Pister - 1974 (PB 237 231)
- EERC 74-11 "Liquefaction of Gravelly Soils under Cyclic Loading Conditions," by R. T. Wong, H. B. Seed and C. K. Chan - 1974 (PB 242 042)
- EERC 74-12 "Site-Dependent Spectra for Earthquake-Resistant Design," by H. B. Seed, C. Ugas and J. Lysmer - 1974 (PB 240 953)
- EERC 74-13 "Earthquake Simulator Study of a Reinforced Concrete Frame," by P. Hidalgo and R. W. Clough - 1974 (PB 241 944)
- EERC 74-14 "Nonlinear Earthquake Response of Concrete Gravity Dams," by N. Pal - 1974 (A 006-583)
- EERC 74-15 "Modeling and Identification in Nonlinear Structural Dynamics, I - One Degree of Freedom Models," by N. Distefano and A. Rath - 1974 (PB 241 548)
- EERC 75-1 "Determination of Seismic Design Criteria for the Dumbarton Bridge Replacement Structure, Vol. I: Description, Theory and Analytical Modeling of Bridge and Parameters," by F. Baron and S.-H. Pang - 1975 (PB 259 407)
- EERC 75-2 "Determination of Seismic Design Criteria for the Dumbarton Bridge Replacement Structure, Vol. 2: Numerical Studies and Establishment of Seismic Design Criteria," by F. Baron and S.-H. Pang - 1975 (For the set of EERC 75-1 and 75-2 PB 259 406)

- 195
- EERC 75-3 "Seismic Risk Analysis for a Site and a Metropolitan Area," by C. S. Oliveira - 1975 (PB 248 134)
- EERC 75-4 "Analytical Investigations of Seismic Response of Short, Single or Multiple-Span Highway Bridges," by Ma-chi Chen and J. Penzien - 1975 (PB 241 454)
- EERC 75-5 "An Evaluation of Some Methods for Predicting Seismic Behavior of Reinforced Concrete Buildings," by Stephen A. Mahin and V. V. Bertero - 1975 (PB 246 306)
- EERC 75-6 "Earthquake Simulator Study of a Steel Frame Structure, Vol. I: Experimental Results," by R. W. Clough and David T. Tang - 1975 (PB 243 981)
- EERC 75-7 "Dynamic Properties of San Bernardino Intake Tower," by Dixon Rea, C.-Y. Liaw and Anil K. Chopra - 1975 (A 008 406)
- EERC 75-8 "Seismic Studies of the Articulation for the Dumbarton Bridge Replacement Structure, Vol. I: Description, Theory and Analytical Modeling of Bridge Components," by F. Baron and R. E. Hamati - 1975 (PB 251 539)
- EERC 75-9 "Seismic Studies of the Articulation for the Dumbarton Bridge Replacement Structure, Vol. 2: Numerical Studies of Steel and Concrete Girder Alternates," by F. Baron and R. E. Hamati - 1975 (PB 251 540)
- EERC 75-10 "Static and Dynamic Analysis of Nonlinear Structures," by Digambar P. Mondkar and Graham H. Powell - 1975 (PB 242 434)
- EERC 75-11 "Hysteretic Behavior of Steel Columns," by E. P. Popov, V. V. Bertero and S. Chandramouli - 1975 (PB 252 365)
- EERC 75-12 "Earthquake Engineering Research Center Library Printed Catalog," - 1975 (PB 243 711)
- EERC 75-13 "Three Dimensional Analysis of Building Systems (Extended Version)," by E. L. Wilson, J. P. Hollings and H. H. Dovey - 1975 (PB 243 989)
- EERC 75-14 "Determination of Soil Liquefaction Characteristics by Large-Scale Laboratory Tests," by Pedro De Alba, Clarence K. Chan and H. Bolton Seed - 1975 (NUREG 0027)
- EERC 75-15 "A Literature Survey - Compressive, Tensile, Bond and Shear Strength of Masonry," by Ronald L. Mayes and Ray W. Clough 1975 (PB 246 292)
- EERC 75-16 "Hysteretic Behavior of Ductile Moment Resisting Reinforced Concrete Frame Components," by V. V. Bertero and E. P. Popov 1975 (PB 246 388)
- EERC 75-17 "Relationships Between Maximum Acceleration, Maximum Velocity, Distance from Source, Local Site Conditions for Moderately Strong Earthquakes," by H. Bolton Seed, Ramesh Murarka, John Lysmer and I. M. Idriss - 1975 (PB 248 172)

- EERC 75-18 "The Effects of Method of Sample Preparation on the Cyclic Stress-Strain Behavior of Sands," by J. Paul Mulilis, Clarence K. Chan and H. Bolton Seed - 1975 (Summarized in EERC 75-28)
- EERC 75-19 "The Seismic Behavior of Critical Regions of Reinforced Concrete Components as Influenced by Moment, Shear and Axial Force," by B. Atalay and J. Penzien - 1975 (PB 258 842)
- EERC 75-20 "Dynamic Properties of an Eleven Story Masonry Building," by R. M. Stephen, J.P. Hollings, J. G. Bouwkamp and D. Jurukovski 1975 (PB 246 945)
- EERC 75-21 "State-of-the-Art in Seismic Strength of Masonry - An Evaluation and Review," by Ronald L. Mayes and Ray W. Clough - 1975 (PB 249 040)
- EERC 75-22 "Frequency Dependencies Stiffness Matrices for Viscoelastic Half-Plane Foundations," by Anil K. Chopra, P. Chakrabarti and Gautam Dasgupta - 1975 (PB 248 121)
- EERC 75-23 "Hysteretic Behavior of Reinforced Concrete Framed Walls," by T. Y. Wong, V. V. Bertero and E. P. Popov - 1975
- EERC 75-24 "Testing Facility for Subassemblages of Frame-Wall Structural Systems," by V. V. Bertero, E. P. Popov and T. Endo - 1975
- EERC 75-25 "Influence of Seismic History on the Liquefaction Characteristics of Sands," by H. Bolton Seed, Kenji Mori and Clarence K. Chan - 1975
- EERC 75-26 "The Generation and Dissipation of Pore Water Pressures during Soil Liquefaction," by H. Bolton Seed, Phillippe P. Martin and John Lysmer - 1975 (PB 252 648)
- EERC 75-27 "Identification of Research Needs for Improving a Seismic Design of Building Structures," by V. V. Bertero - 1975 (PB 248 136)
- EERC 75-28 "Evaluation of Soil Liquefaction Potential during Earthquakes," by H. Bolton Seed, I. Arango and Clarence K. Chan - 1975 (NUREG 0026)
- EERC 75-29 "Representation of Irregular Stress Time Histories by Equivalent Uniform Stress Series in Liquefaction Analyses," by H. Bolton Seed, I. M. Idriss, F. Makdisi and N. Banerjee - 1975 (PB 252 635)
- EERC 75-30 "FLUSH - A Computer Program for Approximate 3-D Analysis of Soil-Structure Interaction Problems," by J. Lysmer, T. Udaka, C.-F. Tsai and H. B. Seed - 1975
- EERC 75-31 "ALUSH - A Computer Program for Seismic Response Analysis of Axisymmetric Soil-Structure Systems," by E. Berger, J. Lysmer and H. B. Seed - 1975

- EERC 75-32 "TRIP and TRAVEL - Computer Programs for Soil-Structure Interaction Analysis with Horizontally Travelling Waves," by T. Udaka, J. Lysmer and H. B. Seed - 1975
- EERC 75-33 "Predicting the Performance of Structures in Regions of High Seismicity," by Joseph Penzien - 1975 (PB 248 130)
- EERC 75-34 "Efficient Finite Element Analysis of Seismic Structure - Soil - Direction," by J. Lysmer, H. Bolton Seed, T. Udaka, R. N. Hwang and C.-F. Tsai - 1975 (PB 253 570)
- EERC 75-35 "The Dynamic Behavior of a First Story Girder of a Three-Story Steel Frame Subjected to Earthquake Loading," by Ray W. Clough and Lap-Yan Li - 1975 (PB 248 841)
- EERC 75-36 "Earthquake Simulator Study of a Steel Frame Structure, Volume II - Analytical Results," by David T. Tang - 1975 (PB 252 926)
- EERC 75-37 "ANSR-I General Purpose Computer Program for Analysis of Non-Linear Structure Response," by Digambar P. Mondkar and Graham H. Powell - 1975 (PB 252 386)
- EERC 75-38 "Nonlinear Response Spectra for Probabilistic Seismic Design and Damage Assessment of Reinforced Concrete Structures," by Masaya Murakami and Joseph Penzien - 1975 (PB 259 530)
- EERC 75-39 "Study of a Method of Feasible Directions for Optimal Elastic Design of Framed Structures Subjected to Earthquake Loading," by N. D. Walker and K. S. Pister - 1975 (PB 257 781)
- EERC 75-40 "An Alternative Representation of the Elastic-Viscoelastic Analogy," by Gautam Dasgupta and Jerome L. Sackman - 1975 (PB 252 173)
- EERC 75-41 "Effect of Multi-Directional Shaking on Liquefaction of Sands," by H. Bolton Seed, Robert Pyke and Geoffrey R. Martin - 1975 (PB 258 781)
- EERC 76-1 "Strength and Ductility Evaluation of Existing Low-Rise Reinforced Concrete Buildings - Screening Method," by Tsuneo Okada and Boris Bresler - 1976 (PB 257 906)
- EERC 76-2 "Experimental and Analytical Studies on the Hysteretic Behavior of Reinforced Concrete Rectangular and T-Beams," by Shao-Yeh Marshall Ma, Egor P. Popov and Vitelmo V. Bertero - 1976 (PB 260 843)
- EERC 76-3 "Dynamic Behavior of a Multistory Triangular-Shaped Building," by J. Petrovski, R. M. Stephen, E. Gartenbaum and J. G. Bouwkamp 1976 ()
- EERC 76-4 "Earthquake Induced Deformations of Earth Dams," by Norman Serff and H. Bolton Seed - 1976 (PB 252 220)

- EERC 76-5 "Analysis and Design of Tube-Type Tall Building Structures," by H. de Clercq and G. H. Powell - 1976 (PB 252 220)
- EERC 76-6 "Time and Frequency Domain Analysis of Three-Dimensional Ground Motions, San Fernando Earthquake," by Tetsuo Kubo and Joseph Penzien - 1976 (PB 260 556)
- EERC 76-7 "Expected Performance of Uniform Building Code Design Masonry Structures," by R. L. Mayes, Y. Omote, S. W. Chen and R. W. Clough 1976
- EERC 76-8 "Cyclic Shear Tests on Concrete Masonry Piers, Part I - Test Results," by R. L. Mayes, Y. Omote and R. W. Clough - 1976
()
- EERC 76-9 "A Substructure Method for Earthquake Analysis of Structure - Soil Interaction," by Jorge Alberto Gutierrez and Anil K. Chopra - 1976 (PB 257 783)
- EERC 76-10 "Stabilization of Potentially Liquefiable Sand Deposits using Gravel Drain Systems," by H. Bolton Seed and John R. Booker - 1976 (PB 258 820)
- EERC 76-11 "Influence of Design and Analysis Assumptions on Computed Inelastic Response of Moderately Tall Frames," by G. H. Powell and D. G. Row - 1976
- EERC 76-12 "Sensitivity Analysis for Hysteretic Dynamic Systems: Theory and Applications," by D. Ray, K. S. Pister and E. Polak - 1976 (PB 262 859)
- EERC 76-13 "Coupled Lateral Torsional Response of Buildings to Ground Shaking," by Christopher L. Kan and Anil K. Chopra - 1976
()
- EERC 76-14 "Seismic Analyses of the Banco de America," by V. V. Bertero, S. A. Mahin and J. A. Hollings - 1976
- EERC 76-15 "Reinforced Concrete Frame 2: Seismic Testing and Analytical Correlation," by Ray W. Clough and Jawahar Gidwani 1976 (PB 261 323)
- EERC 76-16 "Cyclic Shear Tests on Masonry Piers, Part II - Analysis of Test Results," by R. L. Mayes, Y. Omote and R. W. Clough - 1976 ()
- EERC 76-17 "Structural Steel Bracing Systems: Behavior Under Cyclic Loading," by E. P. Popov, K. Takanashi and C. W. Roeder 1976 (PB 260 715)
- EERC 76-18 "Experimental Model Studies on Seismic Response of High Curved Overcrossings," by David Williams and William G. Godden - 1976
- EERC 76-19 "Effects of Non-Uniform Seismic Disturbances on the Dumbarton Bridge Replacement Structure," by Frank Baron and Raymond E. Hamati - 1976

- EERC 76-20 "Investigation of the Inelastic Characteristics of a Single Story Steel Structure using System Identification and Shaking Table Experiments," by Vernon C. Matzen and Hugh D. McNiven - 1976 (PB 258 453)
- EERC 76-21 "Capacity of Columns with Splice Imperfections," by E. P. Popov, R. M. Stephen and R. Philbrick - 1976 (PB 260 378)
- EERC 76-22 "Response of the Olive View Hospital Main Building during the San Fernando Earthquake," by Stephen A. Mahin, Robert Collins, Anil K. Chopra and Vitelmo V. Bertero - 1976
()
- EERC 76-23 "A Study on the Major Factors Influencing the Strength of Masonry Prisms," by N. M. Mostaghel, R. M. Mayes, R. W. Clough and S. W. Chen - 1976
- EERC 76-24 "GADFLEA - A Computer Program for the Analysis of Pore Pressure Generation and Dissipation during Cyclic or Earthquake Loading," by J. R. Booker, M. S. Rahman and H. Bolton Seed - 1976
- EERC 76-25 "Rehabilitation of an Existing Building: A Case Study," by B. Bresler and J. Axley - 1976
- EERC 76-26 "Correlative Investigations on Theoretical and Experimental Dynamic Behavior of a Model Bridge Structure," by Kazuhiko Kawashima and Joseph Penzien - 1976
- EERC 76-27 "Earthquake Response of Coupled Shear Wall Buildings," by Thirawat Srichatrapimuk - 1976
- EERC 76-28 "Tensile Capacity of Partial Penetration Welds," by Egor P. Popov and Roy M. Stephen - 1976
- EERC 76-29 "Analysis and Design of Numerical Integration Methods in Structural Dynamics," by Hans M. Hilber - 1976
- EERC 76-30 "Contribution of a Floor System to the Dynamic Characteristics of Reinforced Concrete Buildings," by L. J. Edgar and V. V. Bertero - 1976
- EERC 76-31 "The Effects of Seismic Disturbances on the Golden Gate Bridge," by Frank Baron, Metin Arikan and Raymond E. Hamati - 1976
- EERC 76-32 "Infilled Frames in Earthquake Resistant Construction," by R. E. Klinger and V. V. Bertero - 1976
- UCB/EERC-77/01 "PLUSH - A Computer Program for Probabilistic Finite Element Analysis of Seismic Soil-Structure Interaction," by Miguel P. Romo Organista, John Lysmer and H. Bolton Seed - 1977

- UCB/EERC-77/02 "Soil-Structure Interaction Effects at the Humbolt Bay Power Plant in the Ferndale Earthquake of June 7, 1975," by J. E. Valera, H. Bolton Seed, C. F. Tsai and J. Lysmer 1977
- UCB/EERC-77/03 "Influence of Sample Disturbance on Sand Response to Cyclic Loading," by Kenji Mori, H. Bolton Seed and Clarence K. Chan - 1977
- UCB/EERC-77/04 "Seismological Studies of Strong Motion Records," by Jafar Shoja-Taheri - 1977

